Extending Intermittent Search Strategy Models and Modeling Opioid Use Disorder using Stochastic Networking

A Dissertation Presented for the

Doctor of Philosophy

Degree

The University of Tennessee, Knoxville

Ryan Campbell

May 2026

© by Ryan Campbell, 2026
All Rights Reserved.

To my parents Billy and Lisa, my friend William, and my wife Jackie, who have been steady sources of encouragement.

Acknowledgements

I would like to begin by expressing my sincere gratitude to the University of Tennessee, Oak Ridge National Laboratory, and the Department of Veteran Affairs for their financial support throughout my graduate studies. Their support made it possible for me to pursue this work while providing for my family and avoiding additional debt.

I am grateful to my advisor, Dr. Christopher Strickland, for his guidance, patience, and steady encouragement. His patience and direction were invaluable, particularly when my tendency to pursue multiple avenues threatened to derail my efforts rather than move them forward. I also thank my committee members, Dr. Suzanne Lenhart, Dr. Tadele Mengesha, and Dr. Adam Spannaus, for their time and thoughtful feedback.

To my family - both biological and church - I am deeply grateful for their constant encouragement, prayers, and understanding throughout this process. Their support has been a continual source of strength.

Finally, I thank my wife, Jaqueline Campbell, for her unwavering love and patience. She carried more than her share when this dissertation demanded sacrifices of my time and attention, and I could not have completed this work without her support.

"There are a dozen views about everything until you know the answer. Then there's never more than one."

- C.S. Lewis, That Hideous Strength

Abstract

The ability to successfully forage for food or prey is essential to many species. Although Lévy flights have received substantial attention as a modeling framework, intermittent search strategy, an alternating between a detection (scanning) phase and a motion (relocation) phase, can offer a more plausible description in certain settings.

This dissertation studies two extensions of the classic intermittent search model. In Chapter 1, we assume the searcher's speed during the motion phase is allowed to vary according to an arbitrary distribution; within this generalization, we determine the optimal average durations of the detection and motion phases that minimize the overall mean search time. In Chapter 2, we introduce an additional detection zone in which the searcher has a rate of finding the target. We then characterize parameter regimes under which intermittence yields a smaller average search time than diffusion alone.

Motivated by a different application area, this dissertation also addresses the worsening opioid crisis. Opioid-related mortality has risen over the past three decades, and the U.S. Department of Health and Human Services has maintained a nationwide public health emergency since 2017. In Chapter 3, we present a stochastic, individual-based network model built from Kimberlyn Eversman's community/population compartmental framework to investigate how variation in individual connections can shape population-level dynamics.

Table of Contents

1 Extending Intermittent Search to Arbitrarily Distributed Velocity Magnitudes 1

1.1 Background . . . 2

1.1.1 Static One-Dimensional Case . . . 5

1.1.2 Static Two-Dimensional Case . . . 9

1.1.3 Static Three-Dimensional Case . . . 11

1.2 Our Model Extensions . . . 14

1.3 General Framework for Intermittent Search Strategy Model Extensions . . . 15

1.4 Extension Models with Arbitrarily-Distributed Velocities . . . 19

1.4.1 Three-Dimensional Case . . . 19

1.4.2 Two-Dimensional Case . . . 29

1.4.3 One-Dimensional Case . . . 32

1.4.4 Summary for Chapter 1 . . . 43

2 Modeling Intermittent Search Strategy with a 2nd Detection Zone 45

2.1 Background . . . 46

2.1.1 Diffusive One-Dimensional Case . . . 46

2.1.2 Diffusive Two-Dimensional Case . . . 47

2.2 Extension Models with 2nd Detection Zone . . . 50

2.2.1 One-Dimensional Case . . . 51

2.2.2 Two-Dimensional Case . . . 81

2.2.3 Summary for Chapter 2 . . . 116

3 Modeling Opioid Use Disorder using Stochastic Networking **118**

3.1 Background . . . 119

3.1.1 Previous Models . . . 121

3.1.2 Our Model . . . 131

3.2 Methods . . . 134

3.2.1 Establishing the initial graph . . . 138

3.2.2 Running the model . . . 142

3.2.3 Model with Connection Preferences . . . 147

3.2.4 Parameter Estimation . . . 154

3.3 Results . . . 165

3.3.1 Testing ℓ_a values . . . 167

3.3.2 Testing ℓ_i values . . . 172

3.4 Conclusion . . . 172

Bibliography **177**

Appendix **186**

A Appendices for Chapter 1 . . . 186

A.1 Further Details on the Solutions for Chapter 1.4.1 . . . 186

B Appendices for Chapter 2 . . . 187

B.1 Further Details on the Solutions for Chapter 2.2.1 . . . 187

B.2 Further Details on the Solutions for Chapter 2.2.2 . . . 192

Vita **198**

List of Tables

2.1 Results of comparing intermittence with diffusion-alone. F represents when intermittence is favorable and N represents when it is not. 71

2.2 Summary statistics for four parameter tests: sample mean $\bar{x}$, sample standard deviation s and sample size n, together with the corresponding 95% confidence Intervals (CIs). The resulting CIs are compared against the mean search time predicted by our formula and by the authors' formula. 74

2.3 Ranges of the mean search time approximations t_m in Equation (2.14) and t_{diff} in Equation (2.3) obtained by varying each of D, V, and K over the set $\{0.01, 0.1, 1, 10, 100\}$ (one parameter at a time), with all remaining parameters fixed at their baseline parameters. 76

2.4 Results of comparing intermittence with diffusion-alone. F represents when intermittence is favorable and N represents when it is not. 104

2.5 Ranges of the mean search time approximations t_m in Equation (2.37) and t_{diff} in Equation (2.38) obtained by varying each of D, V, and K over the set $\{0.01, 0.1, 1, 10, 100\}$ (one parameter at a time), with all remaining parameters fixed at their baseline parameters. 110

3.1 Definition of each drug class as described by Eversman [1]. 127

3.2 Definition of the drug classes from the general population G, the focal community C, and the out-community O. 136

3.3 Descriptions of the likelihood of any two vertices forming an edge respect to their community and their cluster. 149

3.4 Estimations for universal parameters involved in general population, focal community, and out-community, determined by Eversman [1]. 156
3.5 Parameter estimations specific for the general population determined by Eversman [1]. 156
3.6 Parameter estimations specific for focal community parameters determined by Eversman [1]. 157
3.7 The estimations of the parameters used in the out-community. 158
3.8 The distribution of individuals by loneliness levels and their reported use of heroin or nonprescription opioids in the past month. These values were calculated based on percentages provided by Polenick et al. [2]. 164
3.9 The distribution of individuals by age over a three-year period, calculated based on percentages provided by Roy et al. [3]. Data was collected, aggregated, and converted into counts from Supplementary Tables 1–4. Due to the presence of connections that neither formed nor decayed, the overall connection count in each column exceeds the sum of connections formed and decayed. 164
3.10 Directional sign of the one-sided two-sample KS test statistic when comparing the baseline $\ell_a = 1$ against each tested ℓ_a. "+" indicates the comparison is evaluated using Equation (3.13) and "−" means it is evaluated using Equation (3.12). 169
3.11 *P*-values of the one-sided two-sample KS tests using significance level $\alpha = 0.05$ for comparisons of the baseline case $\ell_a = 1$ against each tested ℓ_a. . . . 169
3.12 Directional sign of the one-sided two-sample KS test statistic when comparing the baseline $\ell_i = 1$ against each tested ℓ_i. "+" indicates the comparison is evaluated using Equation (3.13) and "−" means it is evaluated using Equation (3.12). 173
3.13 *P*-values of the one-sided two-sample KS tests using significance level $\alpha = 0.05$ for comparisons of the baseline case $\ell_i = 1$ against each tested ℓ_i. . . . 173

List of Figures

1.1 Static model in 1D designed by Loverado et al. [4] illustrating how a searcher find its target through time. 6

1.2 The static model in one dimension, as designed by Loverado et al. [4], incorporated graphs with fixed parameters $V = 1$ and $k = 1$. The visual representation utilized green squares for $b/a = 10$, red circles for $b/a = 100$, and blue crosses for $b/a = 1000$. Lines depicted the exact expression of t_m [Eqn (1.1)], while symbols represented the approximation of t_m [Eqn (1.3)]. To highlight the minimum values, the graphs were rescaled using both t_m^{opt} [Eqn (1.6)] and τ_1^{opt} [Eqn (1.4)] or τ_2^{opt} [Eqn (1.5)] as appropriate. 8

1.3 A static model in 2D, developed by Loverado et al. [4], illustrated the process by which a "static" searcher identified a target over time. 10

1.4 Static model in 3D designed by Loverado et al. [4] illustrating how a "static" searcher finds its target through time. 12

1.5 The static model in three dimensions, as designed by Loverado et al. [4], incorporated graphs with fixed parameters $V = 1$ and $k = 1$. Each graph plots $\ln(t_m)$ as a function of $\ln(\tau_2)$, using different values for τ_1, a, and b. Lines utilized the analytical expression of t_m [Eqn (1.8)], while small dots represented the $b \gg a$ approximation of t_m [Eqn (1.3)] and the dotted line denoted the $b \gg a$ and small α [Eqn (1.10)]. The optimal $\tau_1^{opt} = 0.74\sqrt{\frac{aV}{k}}$ [Eqn (1.11)], denoted as blue crosses, was compared with one smaller $\tau_1 = 0.25\sqrt{\frac{aV}{k}}$ as red circles and one larger $\tau_1 = 2.5\sqrt{\frac{aV}{k}}$ as green squares. . . . 13

2.1 Dynamic model in 1D designed by Loverado et al. [4] illustrating how a searcher found the target through time. 46

2.2 Diffusive model in 2D designed by Loverado et al. [4] illustrating how a "diffusive" searcher found the target through time. 48

2.3 Diagram of the one-dimensional domain with two detection zones. 51

2.4 Diagram of the two-dimensional domain with two detection zones. 81

2.5 The line represents the minimum detection rate K threshold for intermittence favorability in the limit $a \to 0$. 109

3.1 Flow diagram by Phillips et al. [5] illustrating the transitions between drug classes of individuals and ultimately visualizing a system of ordinary differential equations (ODEs). 123

3.2 Visual representations of how individuals from both the community in Figure 3.2a and subcommunity in Figure 3.2b. These diagrams were created by Eversman [1]. 130

3.3 Graphs by Pearcy [6] illustrating $\hat{\beta}_i(n)$ for varying shaping parameters r, m, and k. Subscripts here simply determined which isolation function was being considered; here, it is $\hat{\beta}_i(n)$. Each graph was generated with $\beta_i = 0.001$ on a network size of $N = 20$. As shown, r scaled the maximum susceptibility of isolated individuals, m shifted the midpoint of the curve, and k adjusted the steepness of the declining slope. 133

3.4 Visual representations of how individuals from both the focal community in Figure 3.4a and out-community in Figure 3.4b. 139
3.5 Overlapping histograms of the sampled outcomes. The values for $\ell_a = 10$ are stochastically larger than those of $\ell_a = 1$. 170
3.6 Overlapping histograms of the sampled outcomes for all outcomes that reject H_0 whenever $H_1 : F(x) < G(x)$ for some x. 171
3.7 Overlapping histograms of the sampled outcomes for all outcomes that reject H_0 whenever $H_1 : F(x) > G(x)$ for some x. 174
3.8 Overlapping histograms of the sampled outcomes for all outcomes that reject H_0 whenever $H_1 : F(x) < G(x)$ for some x. 175

Chapter 1

Extending Intermittent Search to Arbitrarily Distributed Velocity Magnitudes

1.1 Background

Searching is a fundamental behavior observed throughout the natural world, encompassing a wide range of organisms and contexts. From microorganisms seeking nutrients to deer foraging for food, shelter, and potential mates, and even humans searching for misplaced items such as keys or remotes, the act of searching is essential for survival. The process of searching inherently involves navigating critical trade-offs: speed versus accuracy [7], exploration versus exploitation* [8], and energy expenditure versus efficiency [9] are just a few. Given the complexity and importance of these considerations, mathematicians have developed models to describe and analyze the search process.

One of the earliest recorded models was the concept of the random walk, named by Karl Pearson in 1905 [10]. In this model, Pearson envisioned an individual starting at a fixed point, walking a distance of l yards in a straight line, then turning in a random direction to walk another l yards, repeating this process multiple times. While the random walk represented a significant foundational step in understanding stochastic processes, applying the model to real-world scenarios exposed several limitations that necessitated the development of more sophisticated models.

One notable limitation of the random walk model lied in the inherent trade-off between exploration and exploitation. Large step lengths enabled coverage of extensive domains but reduced the ability to focus on smaller areas. Conversely, small step lengths improved the searcher's capacity to concentrate on local regions but hindered broader exploration.

Another significant limitation of the random walk was the assumption that movement occurred in constant step lengths, a premise that lacked biological realism. Organisms naturally demonstrate variability in their movement patterns. Developing a more advanced model that incorporates variable step lengths would address both limitations and provide a framework more closely aligned with the complexities of real-world behaviors.

*In this context, exploration refers to a broad and wide-ranging survey characterized by movement across new and unfamiliar areas, whereas exploitation denotes a focused and deliberate mode of search, in which hunters concentrate on thoroughly examining known areas to optimize resource gain.

Lévy flights served as a prominent example of random walks with variable step lengths. In these walks, the step lengths are drawn from a probability distribution following a power-law pattern [11]. This distribution results in most steps being relatively short, interspersed with occasional longer steps. Such movement patterns had been documented across various species, including albatrosses [11], bumblebees [12], deer [12], spider monkeys [13], and even humans [14]. For a significant period, Lévy flights were widely regarded by the statistical and biological communities as the optimal search strategy for organisms [15]. However, later studies questioned this view, casting doubt on the universality of Lévy flights as the ideal approach to search behavior.

In 2007, Andrew Edwards and colleagues revisited several studies that had previously supported Lévy flight behavior and identified inconsistencies [16]. Specifically, they reexamined the data collection methods employed in earlier analyses of albatross flight patterns [11]. By utilizing satellite transmitter data that was unavailable to the original researchers, Edwards et al. revealed that many trips previously recorded as long-distance movements were, in fact, shorter trips interspersed with extended resting periods. Further analysis, supplemented by additional data collected in 2004, demonstrated that the observed movement patterns did not align with Lévy flights but instead followed a gamma distribution. These findings, along with other studies, began to cast doubt on the universality of Lévy flights as the optimal search strategy [15, 17, 18], leading researchers to investigate alternate models for understanding search behaviors.

One model of particular relevance to our research was the *intermittent search strategy*, first introduced by Bénichou, Coppey, Moreau, Suet, and Voituriez [19]. This strategy described a searcher, initially positioned at a random location, alternating between two distinct behavioral phases: a **slow phase**, during which the target could be detected, and a **fast phase**, during which detection was not possible. The searcher continued switching between these two phases until the target is located. This framework was further expanded and refined by Bénichou, Loverdo, Moreau, and Voituriez in their work "Intermittent search strategies" [20], which provided a comprehensive synthesis of several articles previously

authored by the researchers. Given the direct relevance of this framework to our research objectives, we explore the details of several models in greater depth.

The following three models presented were fundamentally identical, differing solely in the dimensionality of their respective domains, which were defined as one-, two-, and three-dimensional spheres. Across all models, a searcher alternated between two phases while attempting to locate an immobile target positioned at the origin of a d-dimensional spherical domain with radius b and reflective boundaries.[†] During Phase 1, the searcher was able to detect the target whenever the distance between them was at most a. Although three methods for detecting the target were proposed during this phase, only one holds particular relevance for the extensions discussed in this chapter. In the "static mode," the searcher remained stationary and detected the target at a fixed rate k whenever within the detection zone. During Phase 2, ballistic movement occurred at a constant speed V in a randomly chosen direction, with each transition into Phase 2 involving a new random direction for movement.

Transitions between the phases were regulated by time-independent Poisson processes with switching rates defined as λ_1 for transitions from Phase 1 to Phase 2 and λ_2 for transitions from Phase 2 to Phase 1. The searcher exhibited no memory of previous states, meaning that the probability of transitioning between phases depended exclusively on the current state. Additionally, the duration of each phase i adhered to an exponential distribution with the mean duration expressed as $\tau_i = 1/\lambda_i$.

Building upon these search behaviors, the authors developed mathematical models to characterize intermittent search strategies across the dimensions. The derivation of mean first-passage time equations, $t_i(\vec{r})$, provided a quantitative framework for determining the average duration needed to locate the target when search began in Phase i from position $\vec{r}$. The mean detection time, beginning in Phase 1, was then uniformly expressed across the entire domain through $t_1(\vec{r})$:

$$t_m = \frac{1}{V(\Omega_d)} \int_{\Omega_d} t_1(\vec{r}) d\vec{r},$$

[†]This discussion focuses on Section IV, Intermittent Search: A Robust Strategy [20].

where Ω_d represented the d-dimensional sphere of radius b, and $V(\Omega_d)$ denoted its volume. To optimize the time required for target discovery, the authors minimized t_m with respect to the mean durations τ_1 and τ_2 of each phase. The analysis revealed the optimal allocation of time for each phase. Notably, since the searcher remained stationary while detecting, target discovery was only possible if phase switching occurred or if the searcher started within the detection zone surrounding the target. This emphasized the essential role of intermittence in achieving successful target discovery.

Since our research builds upon these models, the subsequent sections provide a detailed summary of the authors' models before elaborating on our proposed extensions. The summary incorporates additional insights provided by Loverado et al. [4].

1.1.1 Static One-Dimensional Case

In the one-dimensional "static" model, the domain was defined as a line segment $[-b,b]$, where the target was positioned at $x=0$. During Phase 1, the stationary searcher demonstrated a fixed reaction rate k for detecting the target when located within a distance a. Transitioning to Phase 2, the searcher moved ballistically along the line segment in either direction, with motion to the right described by a positive velocity V and motion to the left described by a negative velocity $-V$. The mean first-passage times for searches initiated in these respective directions were denoted as t_2^+ and t_2^-. Figure 1.1 visually represents the one-dimensional static model. The system of backward equations governing this process for mean first-passage times was expressed as follows:

$$\begin{cases} \dfrac{1}{\tau_1}\left(\dfrac{t_2^+ + t_2^-}{2} - t_1\right) - kI_a(x)t_1 = -1 \\ V\dfrac{dt_2^+}{dx} + \dfrac{1}{\tau_2}\left(t_1 - t_2^+\right) = -1 \\ -V\dfrac{dt_2^-}{dx} + \dfrac{1}{\tau_2}\left(t_1 - t_2^-\right) = -1, \end{cases}$$

where the indicator function $I_a(x)$ was defined as

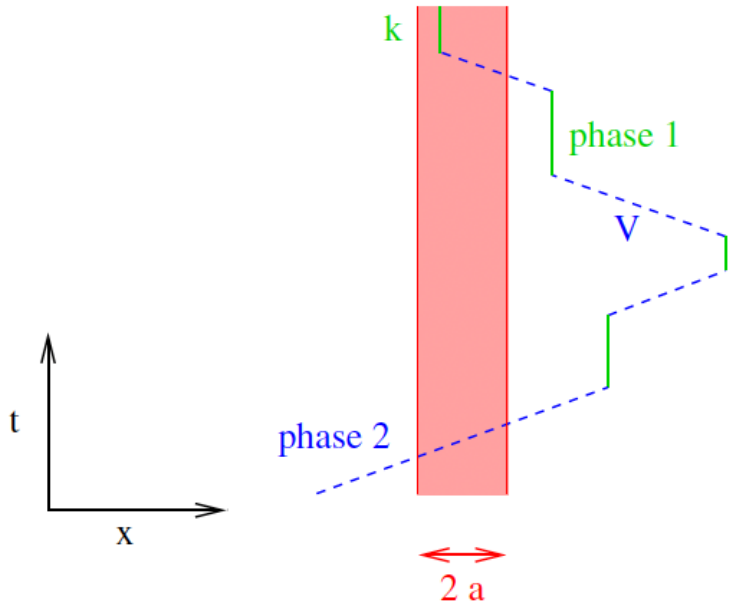

Figure 1.1: Static model in 1D designed by Loverado et al. [4] illustrating how a searcher find its target through time.

$$I_a(x) = \begin{cases} 1 \text{ if } x \leq a \\ 0 \text{ if } x > a. \end{cases}$$

Introducing $t_2 = (t_2^+ + t_2^-)/2$ and $t_2^d = (t_2^+ - t_2^-)/2$ the equations were reformulated into the following system:

$$\begin{cases} \dfrac{1}{\tau_1}(t_2 - t_1) - kI_a(x)t_1 = -1 \\ V^2\tau_2 \dfrac{d^2t_2}{dx^2} + \dfrac{1}{\tau_2}(t_1 - t_2) = -1^{\ddagger} \\ t_2^d = V\tau_2 \dfrac{dt_2}{dx}. \end{cases}$$

During Phase 1, detection occurred whenever the searcher was within a distance a from the target. Consequently, the domain was divided into two distinct regions: the region *inside* the detection zone ($x \leq a$) and the region *outside* the detection zone ($x > a$). Utilizing the

[‡]This amendment addresses a typographical error in the original publication, where the equation was incorrectly reported as $V^2\tau_2 \frac{d^2t_2}{dx^2} + \frac{1}{\tau_2}(t_1 - t_2) = 0$.

symmetry of $x \leftrightarrow -x$, the boundaries were analyzed within the nonnegative region $[0, b]$:

$$\frac{dt_2^{in}}{dx}(0) = 0, \qquad \frac{dt_2^{out}}{dx}(b) = 0, \qquad t_2^{in}(a) = t_2^{out}(a), \qquad \frac{dt_2^{in}}{dx}(a) = \frac{dt_2^{out}}{dx}.$$

The authors solved the system without giving the results. However, assuming the searcher began in the detection phase, the authors used their solved t_1 equation to calculate the overall mean first-passage time across the entire spatial domain:

$$t_m = \frac{(\tau_1 + \tau_2)}{b}\left[\frac{b}{k\tau_1} + \frac{(b-a)^3}{3V^2\tau_2^2} + \frac{\beta(b-a)^2}{V\tau_2}\coth\left(\frac{a}{V\tau_2\beta}\right) + (b-a)\beta^2\right] \tag{1.1}$$

The authors then assumed a low target density where $a \ll b$, simplifying Equation (1.1) to the following form:

$$t_m = (\tau_1 + \tau_2)\left[\frac{1}{k\tau_1} + \frac{b^2}{3V^2\tau_2^2} + \frac{\beta b}{V\tau_2}\coth\left(\frac{a}{V\tau_2\beta}\right) + \beta^2\right]. \tag{1.2}$$

For further simplification, the authors assumed that $\frac{a}{V\tau_2} \ll 1$ and used the fact that $\beta > 1$ and $\beta > 1/(k\tau_1)$ to get the final reduced form:

$$t_m = (\tau_1 + \tau_2)\left[\frac{b^2}{3V^2\tau_2^2} + \left(\frac{1}{k\tau_1} + 1\right)\frac{b}{a}\right]. \tag{1.3}$$

By minimizing Equation (1.3) with respect to τ_1 and τ_2, the authors derived the optimal search times for each stage as followed:

$$\tau_1^{opt} = \sqrt{\frac{a}{Vk}}\left(\frac{b}{12a}\right)^{1/4} \tag{1.4}$$

$$\tau_2^{opt} = \frac{a}{V}\sqrt{\frac{b}{3a}}. \tag{1.5}$$

Substituting the optimal values of τ_1^{opt} and τ_2^{opt} into Equation (1.3), the authors calculated the minimal value of the search time, which was expressed as follows:

$$t_m^{opt} = \frac{b}{ak}\left(\frac{b}{3a}\right)^{1/4}\left[\sqrt{\frac{2bk}{3V}}\left(\frac{3a}{b}\right)^{1/4} + 1\right]\left[\sqrt{\frac{2ka}{V}} + \left(\frac{3a}{b}\right)^{1/4}\right]. \tag{1.6}$$

The authors concluded that Equation (1.3) provided a reliable and practical approximation for the mean first-passage time. Figure 1.2 presented four graphs to illustrate this analysis. In the top row, τ_2 was set to τ_2^{opt}, and the relationship between τ_1/τ_1^{opt} and t_m/t_m^{opt} was plotted. In the bottom row, τ_1 was set to τ_1^{opt}, and the relationship between τ_2/τ_2^{opt} and t_m/t_m^{opt} was graphed. This approach ensured that the minimum value was normalized to $(1,1)$ across all graphs, regardless of the ratio between a and b.

As previously discussed, intermittence was revealed to led to favorable outcomes. The optimal strategy was achieved when $\tau_1^{opt} = \sqrt{\frac{a}{Vk}}\left(\frac{b}{12a}\right)^{1/4}$ and $\tau_2^{opt} = \frac{a}{V}\sqrt{\frac{b}{3a}}$. Additionally, the optimal duration of the motion phase, τ_2^{opt}, was independent of k, the detection rate during the detection phase.

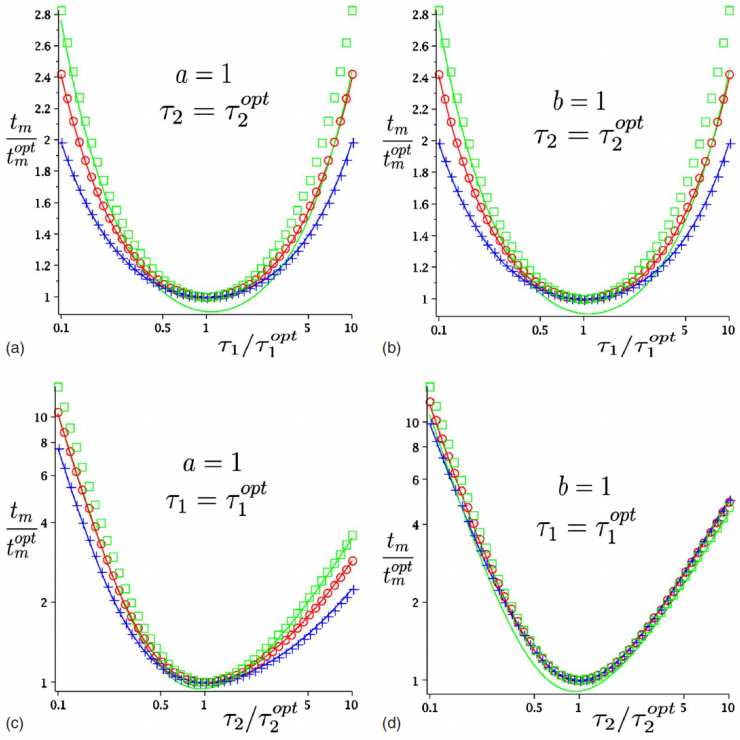

Figure 1.2: The static model in one dimension, as designed by Loverado et al. [4], incorporated graphs with fixed parameters $V = 1$ and $k = 1$. The visual representation utilized green squares for $b/a = 10$, red circles for $b/a = 100$, and blue crosses for $b/a = 1000$. Lines depicted the exact expression of t_m [Eqn (1.1)], while symbols represented the approximation of t_m [Eqn (1.3)]. To highlight the minimum values, the graphs were rescaled using both t_m^{opt} [Eqn (1.6)] and τ_1^{opt} [Eqn (1.4)] or τ_2^{opt} [Eqn (1.5)] as appropriate.

1.1.2 Static Two-Dimensional Case

In the two-dimensional "static" model, the domain was a circle of radius b, where the target was positioned at the origin $\vec{r} = (0,0)$. During Phase 2, the searcher traveled ballistically at a constant speed $V > 0$ in a direction $\theta_{\vec{V}}$ chosen uniformly at random, where $V = |\vec{V}| = \sqrt{V_1^2 + V_2^2}$. Upon entering the motion phase, a new direction was randomly selected. Figure 1.3 provides a visual representation of the two-dimensional static model. The system of backward equations for the mean first-passage times took the following form:

$$\begin{cases} \dfrac{1}{2\pi\tau_1}\displaystyle\int_0^{2\pi}(t_2 - t_1)d\theta_{\vec{V}} - kI_a(\vec{r})t_1 = -1 \\ \vec{V}\cdot\nabla t_2 - \dfrac{1}{\tau_2}(t_2 - t_1) = -1, \end{cases}$$

where the indicator function $I_a(\vec{r})$ was defined as

$$I_a(\vec{r}) = \begin{cases} 1 \text{ if } |\vec{r}| \leq a \\ 0 \text{ if } |\vec{r}| > a. \end{cases}$$

The authors observed that the current integro-differential equations appeared to lack an exact solution. In their detailed analysis, Bénichou, et al. [21] utilized a decoupling assumption

$$\langle V_i V_j t_2 \rangle_{\theta_{\vec{V}}} \simeq \langle V_i V_j \rangle_{\theta_{\vec{V}}} \langle t_2 \rangle_{\theta_{\vec{V}}}, \text{ for } i, j \in \{1,2\}$$

and proposed the transformation $s = \langle t_2 \rangle_{\theta_{\vec{V}}} = \frac{1}{2\pi}\int_0^{2\pi} t_2 d\theta_{\vec{V}}$ to express the system of equations in polar form:

$$\begin{cases} \dfrac{1}{\tau_1}[s(r) - t_1(r)] - kI_a(r)t_1(r) = -1 \\ \dfrac{V^2\tau_2}{2}\Delta s(r) - \dfrac{1}{\tau_2}[s(r) - t_1(r)] = -1, \end{cases}$$

where $V = |\vec{V}| = \sqrt{V_1^2 + V_2^2}$ and $r = |\vec{r}| = \sqrt{r_1^2 + r_2^2}$.

The domain, analogous to the one-dimensional scenario, was divided into two distinct regions: inside the detection zone ($r \leq a$) and outside the detection zone ($r > a$). Assuming

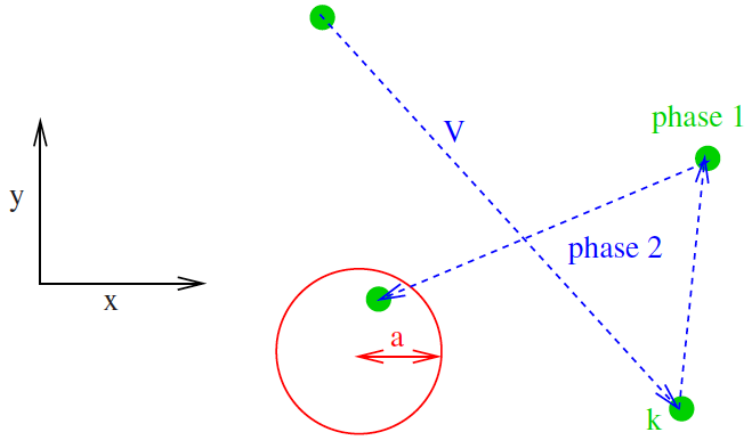

Figure 1.3: A static model in 2D, developed by Loverado et al. [4], illustrated the process by which a "static" searcher identified a target over time.

reflecting boundaries, the continuity of t_2 and its first derivative across these regions, as well as the finiteness of solutions within the domain, the authors established the following boundary conditions:

$$\frac{ds^{out}}{dr}(b)=0, \quad s^{out}(a)=s^{in}(a), \quad \frac{ds^{out}}{dr}(a)=\frac{ds^{in}}{dr}(a), \quad \lim_{r\to 0^+} s^{in}(r) \text{ remains finite.}$$

Again, though the solutions to the system were not given, the mean search time was calculated as follows:

$$t_m=\frac{\tau_1+\tau_2}{2k\tau_1 y^2}\left[\begin{array}{c}\frac{1}{x}(1+k\tau_1)\left(y^2-x^2\right)^2\frac{I_0(x)}{I_1(x)}\\ +\frac{1}{4}\left[8y^2+(1+k\tau_1)\left(4y^4\ln\frac{y}{x}+\left(y^2-x^2\right)\left(x^2-3y^2+8\right)\right)\right]\end{array}\right] \tag{1.7}$$

where

$$x=\frac{a}{V\tau_2}\sqrt{\frac{2k\tau_1}{1+k\tau_1}}, \qquad \text{and} \qquad y=\frac{b}{V\tau_2}\sqrt{\frac{2k\tau_1}{1+k\tau_1}}.$$

In the low target density limit $a \ll b$, the authors derived the optimal search times for each phase as follows:

$$\tau_1^{opt}=\left(\frac{a}{Vk}\right)^{1/2}\left(\frac{2\ln(b/a)-1}{8}\right)^{1/4}, \qquad \tau_2^{opt}=\frac{a}{V}\sqrt{\ln\frac{b}{a}-\frac{1}{2}}.$$

Once again, the authors concluded that intermittence was always favorable, where the optimal strategy was achieved when $\tau_1^{opt} = \left(\frac{a}{Vk}\right)^{1/2}\left(\frac{2\ln(b/a)-1}{8}\right)^{1/4}$ and $\tau_2^{opt} = \frac{a}{V}\sqrt{\ln\frac{b}{a}-\frac{1}{2}}$. Again, the optimal duration of the motion phase, τ_2^{opt}, did not depend on the discovery rate k of the detection phase.

1.1.3 Static Three-Dimensional Case

In the three-dimensional "static" model, the domain was a sphere of radius b with the target positioned at the origin $\vec{r} = (0,0,0)$. During Phase 2, the searcher traveled ballistically at a constant speed $V > 0$ in a horizontal direction $\theta_{\vec{V}} \in [0,\pi]$ and vertical direction $\phi_{\vec{V}} \in [0,2\pi)$ selected uniformly at random, where $V = |\vec{V}| = \sqrt{V_1^2+V_2^2+V_3^2}$. Upon entering the motion phase, new horizontal θ_V and vertical ϕ_V directions were chosen. A visual representation of the one-dimensional static mode is found in Figure 1.4. The system of backward equations for the mean first-passage times took the following form:

$$\begin{cases} \frac{1}{\tau_1}\left(\frac{1}{4\pi}\int_0^{2\pi}\int_0^{\pi}\left(t_{2,\theta_{\vec{V}},\phi_{\vec{V}}}-t_1\right)\sin\theta_{\vec{V}}\,d\theta_{\vec{V}}\,d\phi_{\vec{V}}\right) - kI_a(\vec{r})t_1 = -1 \\ \vec{V}\cdot\nabla t_{2,\theta_{\vec{V}},\phi_{\vec{V}}} + \frac{1}{\tau_2}\left(t_1 - t_{2,\theta_{\vec{V}},\phi_{\vec{V}}}\right) = -1, \end{cases}$$

where the indicator function $I_a(\vec{r})$ was defined as

$$I_a(\vec{r}) = \begin{cases} 1 \text{ if } |\vec{r}| \le a \\ 0 \text{ if } |\vec{r}| > a. \end{cases}$$

Utilizing the same decoupling assumption as the two-dimensional model, the authors assigned $t_2 = \frac{1}{4\pi}\int_0^{\pi}\int_0^{2\pi} t_{2,\theta_{\vec{V}},\phi_{\vec{V}}}\sin\theta_{\vec{V}}\,d\phi_{\vec{V}}\,d\theta_{\vec{V}}$ to express the system of equations in polar form:

$$\begin{cases} \frac{1}{\tau_1}\left[t_2(r)-t_1(r)\right] - kI_a(r)t_1(r) = -1 \\ \frac{V^2\tau_2}{3}\Delta t_2(r) + \frac{1}{\tau_2}\left[t_1(r)-t_2(r)\right] = -1, \end{cases}$$

where $V = |\vec{V}| = \sqrt{V_1^2+V_2^2+V_3^2}$ and $r = |\vec{r}| = \sqrt{r_1^2+r_2^2+r_3^2}$.

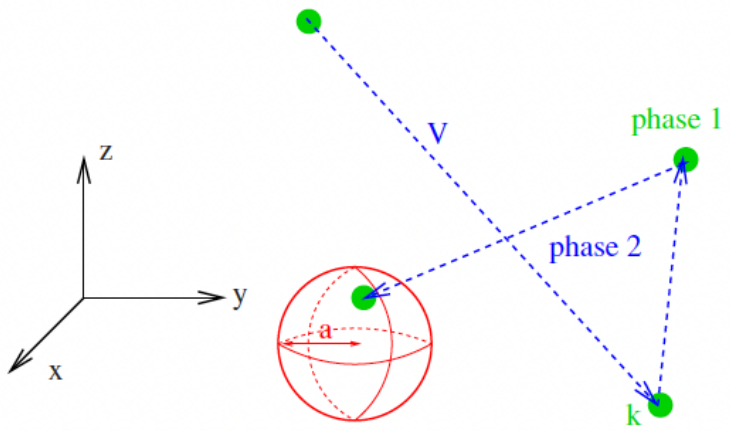

Figure 1.4: Static model in 3D designed by Loverado et al. [4] illustrating how a "static" searcher finds its target through time.

Similar to the one- and two-dimensional cases, the domain was naturally partitioned into two regions, ensuring analogous boundary conditions:

$$\frac{dt_2^{out}}{dr}(b) = 0, \qquad t_2^{out}(a) = t_2^{in}(a), \qquad \frac{dt_2^{out}}{dr}(a) = \frac{dt_2^{in}}{dr}(a), \qquad \lim_{r\to 0} t_2(r) \text{ remains finite.}$$

Without giving the solutions to the system, the mean searcher time was determined to be the following:

$$t_m = (\tau_1+\tau_2)\left[\frac{1}{k\tau_1} + \frac{1}{b^3V^2\tau_2^2}\left[\begin{array}{c} -2b^3\left(b^2-a^2\right)+\left(b^3-a^3\right)\left(3\dfrac{a^2}{\alpha^2}+\beta\right) \\ +\dfrac{1}{5}\left(b^5-a^5\right)\end{array}\right]\right] \tag{1.8}$$

where

$$\alpha = \frac{a}{V\tau_2}\sqrt{\frac{3k\tau_1}{1+k\tau_1}}, \qquad \text{and} \qquad \beta = \frac{-a^3\sinh\alpha + b^3\alpha\cosh\alpha}{a\left(-\sinh\alpha+\alpha\cosh\alpha\right)}.$$

Once again, under the assumption of a low target density limit, where $a \ll b$, the authors derived a simplified form of the mean search time, as expressed in Equation (1.8):

$$t_m \approx (\tau_1+\tau_2)\left[\frac{1}{k\tau_1} + \frac{1}{V^2\tau_2^2}\left(-\frac{9}{5}b^2 + 3\frac{a^2}{\alpha^2}+\beta\right)\right] \tag{1.9}$$

To achieve further simplification, the analysis proceeded under the assumption of a small α, leading to an additional reduction of the average search time Equation (1.9) into the

following form:

$$t_m \approx \frac{b^3(\tau_1+\tau_2)}{a}\left[\frac{1+k\tau_1}{a^2 k\tau_1}+\frac{6}{5V^2\tau_2^2}\right] \tag{1.10}$$

By minimizing Equation (1.10) with respect to τ_1 and τ_2, the authors determined that the optimal search times for each stage were

$$\tau_1^{opt} = \left(\frac{3}{10}\right)^{1/4}\sqrt{\frac{a}{Vk}}, \tag{1.11}$$

$$\tau_2^{opt} = \frac{a}{V}\sqrt{\frac{6}{5}}. \tag{1.12}$$

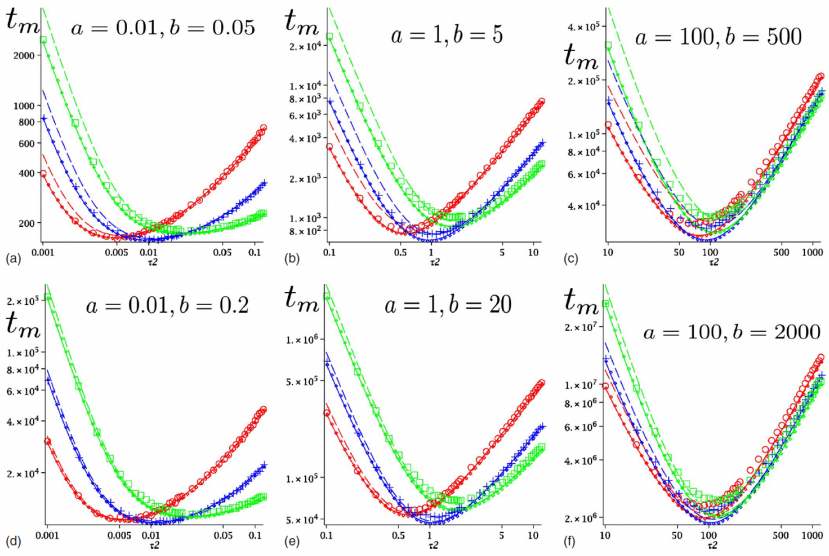

Figure 1.5: The static model in three dimensions, as designed by Loverado et al. [4], incorporated graphs with fixed parameters $V = 1$ and $k = 1$. Each graph plots $\ln(t_m)$ as a function of $\ln(\tau_2)$, using different values for τ_1, a, and b. Lines utilized the analytical expression of t_m [Eqn (1.8)], while small dots represented the $b \gg a$ approximation of t_m [Eqn (1.3)] and the dotted line denoted the $b \gg a$ and small α [Eqn (1.10)]. The optimal $\tau_1^{opt} = 0.74\sqrt{\frac{aV}{k}}$ [Eqn (1.11)], denoted as blue crosses, was compared with one smaller $\tau_1 = 0.25\sqrt{\frac{aV}{k}}$ as red circles and one larger $\tau_1 = 2.5\sqrt{\frac{aV}{k}}$ as green squares.

The authors concluded from numerical simulations and Figure 1.5 that the analytical expression Equation (1.8) was a good approximation. The figure presented six graphs to illustrate some of their analysis, each changing the ratios and values of a and b.

Additionally, except for small τ_2 or b, the fully simplified form of the average search time (Equation 1.10 represented in the graphs as dotted lines) was also determined to have fit the numerical data.

Again, intermittence was favorable. The optimal strategy was achieved when $\tau_1^{opt} = \left(\frac{3}{10}\right)^{1/4} \sqrt{\frac{a}{Vk}}$ and $\tau_2^{opt} = \frac{a}{V}\sqrt{\frac{6}{5}}$. As in the one- and two-dimensional models, the optimal duration of the motion phase, τ_2^{opt}, was independent of k, the discovery rate during the detection phase. However, in this model, the authors noted that τ_2^{opt} also did not depend on the radius b of the domain. Additionally, in all three models, there is a relation between the two optimal phase durations, where $\tau_1^{opt} = \sqrt{\tau_2^{opt}/(2k)}$.

1.2 Our Model Extensions

The original intermittent search strategy proposed by Bénichou et al. [20] sought the phase durations that optimized search performance: specifically, they identified the optimal mean times spent in the detection and motion phases that minimized the overall mean search time where intermittence outperformed purely diffusion exploration. The next two chapters develop and analyze two extensions of this baseline model: (i) arbitrarily distribution motion speeds and (ii) the presence of a second detection zone.

Chapter 1.4 generalizes the classical setting by allowing the searcher's speed to vary for each motion phase. Rather than moving at a fixed velocity magnitude, the searcher redraws a new speed from a prescribed arbitrary distribution at each entry into the motion phase. The main objective is to characterize how speed variability alters the optimal phase durations that minimize the overall mean search time in one, two, and three spatial dimensions.

Chapter 2.2 extends the detection mechanism by introducing an additional spatial zone in which the target can be detected at a specified rate. Because the resulting expressions for the mean search time become substantially more complex, the focus in this chapter is on establishing in one and two dimensions an intermittence criterion, i.e., conditions under which intermittent switching remains advantageous compared to diffusion alone.

Throughout the derivations of the models, a common structural pattern emerges across all model variants. For this reason, we begin by deriving a general governing equation in $d \in \{1,2,3\}$ spatial dimensions, which provides a unified foundation for the analyses developed in the subsequent chapters.

1.3 General Framework for Intermittent Search Strategy Model Extensions

Let $\mathscr{Y}$ and $\mathscr{J}$ denote the spatial and state domains, respectively. In all model variations, the spatial domain $\mathscr{Y}$ is taken to be the d-dimensional sphere of radius $b > 0$ with $d \in \{1,2,3\}$, and the target is fixed at the origin $\vec{0} \in \mathscr{Y}$. The state domain $\mathscr{J}$ encodes the searcher's phase within the search process and may be either discrete or continuous, depending on the particular model. Thus, the precise specifications of $\mathscr{Y}$ and $\mathscr{J}$ are given within each model's formulation.

The search dynamics are described by a process that alternates between two active phases - **detection** and **motion** - and ends upon entry into the **termination** phase. For notational convenience (and for reasons discussed later), the detection and termination phases are each represented by a single distinguished state in $\mathscr{J}$, denoted as $j = \mathbf{0}$ and $j = \mathbf{A}$, respectively. All remaining states $j \in \mathscr{J} \setminus \{\mathbf{0}, \mathbf{A}\}$ are collectively categorized as the motion phase. Since detection can only occur while $j = \mathbf{0}$, phase changes occur via instantaneous jumps from the detection phase into either the motion phase or the termination phase.

We may view the searcher's trajectory as a stochastic process (Y_t, J_t) defined on a probability space $(\Omega, \mathscr{F}, \mathbb{P})$ defined as follows:

- the sample space $\Omega = \Omega_Y \times \Omega_J$, where Ω_Y represents the set of all continuous paths $Y_t : [0,\infty) \to \mathscr{Y}$, and Ω_J represents the set of all càdlàg (right-continuous with left limits), piecewise constant functions $J_t : [0,\infty) \to \mathscr{J}$ that alternate exclusively between $J_t = \mathbf{0}$ and either $J_t = \mathbf{A}$ or $J_t \in \mathscr{J} \setminus \{\mathbf{0}, \mathbf{A}\}$.

- the event space $\mathscr{F} = \sigma(\Omega_Y) \otimes \sigma(\Omega_J)$, where $\sigma(\Omega_Y)$ and $\sigma(\Omega_J)$ are the usual Borel σ-algebras on Ω_Y and Ω_J, respectively.

- the probability measure $\mathbb{P}((Y_t, J_t) \in B | Y_0 = y_0, J_0 = j_0)$ is defined for a measurable set $B \subseteq \mathscr{Y} \times \mathscr{J}$.

Having established the underlying probability space, we proceed to describe the phase-switching dynamics.

Switching between detection and motion phases is driven by two independent Poisson processes $N_D(t)$ for transitions from detection to motion and $N_M(t)$ for transitions from motion to detection, with constant rates

$$\lambda_D = \frac{1}{\tau_D}, \qquad \lambda_M = \frac{1}{\tau_M}.$$

Consequently, the times spent in the detection and motion phases are exponentially distributed with means $\tau_D > 0$ and $\tau_M > 0$, respectively.

Switching from the detection phase to the termination phase occurs through one of two mechanisms. First, the search may end upon the searcher entering an absorbing set

$$A = \left\{ (Y, \mathbf{0}) \in \mathscr{Y} \times \mathscr{J} : \vec{0} \in Y \right\},$$

where the definition of Y depends on the particular model. The corresponding absorption (first-passage) time is

$$\tau_A = \inf \{ t \geq t_0 | (Y_t, J_t) \in A \}.$$

Second, outside the absorbing set, the target may be detected at a constant rate K, modeled by an independent Poisson process $N_K(t)$ with rate K. We define the associate detection time

$$\tau_K = \inf \{ t \geq t_0 | N_K(t) \geq 1 \}$$

so that $\tau_K \sim \exp(K)$.

In either case, upon entry into the termination phase, the search process ends. In particular, if

$$\tau = \tau_A \wedge \tau_K$$

denotes the overall termination time, then the process is stopped at τ. Specifically, $(Y_t, J_t) = (Y_\tau, \mathbf{A})$ for all $t \geq \tau$. We assume that the searcher eventually locates the target so that $\tau < \infty$ almost surely.

We assume the stochastic process (Y_t, J_t) is characterized by the Markov property and time homogenity. At any time t, the searcher is described by the position $y = y(t) = Y_t \in \mathscr{Y}$ and the state $j = j(t) = J_t \in \mathscr{J}$. We assume that the continuous process Y_t satisfies the stochastic differential equation:

$$dY_t = \mu_Y(t, Y_t, J_t)dt + \sigma_Y(t, Y_t, J_t)dW_t$$

where $\mu_Y(t, Y_t, J_t) \in \mathbb{R}^d$ represents the continuous drift, $\sigma_Y(t, Y_t, J_t) \in \mathbb{R}^{dxm}$ denotes the diffusion matrix, and W_t is an m-dimensional Wiener process for some m.

Additionally, recall that the discontinuous process J_t is càdlàg (with left limits) and piecewise constant. Let J_{t-} denote the left limit and, for a Poisson process N, consider $\Delta N(t) := N(t) - N(t-)$ for the jump at time t. The dynamics of J_t are specified by the following transition rules:

1) If $J_{t-} = \mathbf{0}$ and $\Delta N_D(t) = 1$, then $J_t \in \mathscr{J} \setminus \{\mathbf{0}, \mathbf{A}\}$.

2) If $J_{t-} = \mathbf{0}$ and $\Delta N_K(t) = 1$, then $J_t = \mathbf{A}$.

3) If $J_{t-} \in \mathscr{J} \setminus \{\mathbf{0}, \mathbf{A}\}$ and $\Delta N_M(t) = 1$, then $J_t = \mathbf{0}$.

4) If $J_{t-} = \mathbf{A}$, then $J_t = \mathbf{A}$ for all subsequent times.

Define $S(t|t_0, x, i)$ as the survival probability such that starting in position x and state i, the target is *not* found. This implies that the searcher has not entered the absorbing set, which can be expressed as

$$S(t \mid t_0, x, i) = \mathbb{P}\left(t < \tau_A \mid Y_{t_0} = x, J_{t_0} = i\right).$$

The survival probability S satisfies the Backward Chapman-Kolmogorov Differential Equation [22, 23]:

$$
\begin{aligned}
-\frac{\partial}{\partial t_0} S(t \mid t_0, x, i) &= \mu_Y(t_0, x, i) \cdot \nabla_x S(t \mid t_0, x, i) \\
&\quad + \frac{1}{2} \sigma_Y(t_0, x, i) \sigma_Y(t_0, x, i)^T : \nabla_x^2 S(t \mid t_0, x, i) \\
&\quad + \int_{\varsigma \neq i} \Lambda(t_0, x, \varsigma | x, i) \left[S(t | t_0, x, \varsigma) - S(t | t_0, x, i) \right] d\varsigma,
\end{aligned} \tag{1.13}
$$

where $\Lambda(t_0, x, \varsigma | x, i)$ represents the transition rate *out of state* i. The notation ":" is defined for matrices $A, B \in \mathbb{R}^{d \times d}$ as $A : B = \sum_{k,\ell} A_{k\ell} B_{k\ell}$ and $\nabla_x^2 S$ represents the Hessian matrix of S.

Time homogeneity is a property of S, which allows for the following conversion:

$$
S(t | t_0, x, i) = S(t - t_0 | 0, x, i).
$$

Using this property, differentiation with respect to t_0 simplifies as follows:

$$
\begin{aligned}
-\frac{\partial}{\partial t_0} S(t | t_0, x, i) &= -\frac{\partial}{\partial t_0} S(t - t_0 | 0, x, i) \\
&= -\frac{\partial S(t - t_0 | 0, x, i)}{\partial t} \frac{\partial (t - t_0)}{\partial t_0} \qquad \text{by chain rule} \\
&= \frac{\partial S(t - t_0 | 0, x, i)}{\partial t} \\
&= \frac{\partial S(t | t_0, x, i)}{\partial t}.
\end{aligned}
$$

When defining the initial time at $t_0 = 0$, Equation (1.13) simplifies to

$$
\begin{aligned}
\frac{\partial}{\partial t} S(t \mid 0, x, i) &= \mu_Y(0, x, i) \cdot \nabla_x S(t \mid 0, x, i) \\
&\quad + \frac{1}{2} \sigma_Y(0, x, i) \sigma_Y(0, x, i)^T : \nabla_x^2 S(t \mid 0, x, i) \\
&\quad + \int_{\varsigma \neq i} \Lambda(0, x, \varsigma | x, i) \left[S(t | 0, x, \varsigma) - S(t | 0, x, i) \right] d\varsigma.
\end{aligned} \tag{1.14}
$$

Lastly, the primary objective of most search strategies is to locate the target in the shortest possible time. So, we now convert these to the mean first-passage times (MFPT), defined as the expected durations required for the searcher to reach the target for the first time. Since the survival probability $S(t|0, x, i)$ represents the cumulative probability that the target has not been found by time t, $1 - S(t|0, x, i)$ corresponds to the cumulative probability that the target has been found by time t. The first-passage probability density function,

which describes the likelihood of finding the target at a specific time t, is given by:

$$\frac{\partial}{\partial t}(1-S_i) = -\frac{\partial S_i}{\partial t}.$$

The MFPT is calculated as the average of the first-passage times, using the following expression:

$$t_i(x) = \int_0^\infty t\left(-\frac{\partial S_i}{\partial t}\right)dt = -[tS_i]_0^\infty + \int_0^\infty S_i dt = \int_0^\infty S_i dt$$

since $\lim_{t\to\infty} S_i(t|0,x,i) = 0$, ensuring that the target is eventually located.

Integrating Equation (1.14) over all ending time simplifies the general equation to

$$\begin{aligned} -1 = \mu_Y(0,x,i)\cdot\nabla_x t_i(x) + \frac{1}{2}\sigma_Y(0,x,i)\sigma_Y(0,x,i)^T : \nabla_x^2 t_i(x) \\ + \int_{\varsigma\neq i} \Lambda(0,x,\varsigma|x,i)\left[t_\varsigma(x) - t_i(x)\right]d\varsigma. \end{aligned} \tag{1.15}$$

1.4 Extension Models with Arbitrarily-Distributed Velocities

The original intermittent search strategy, developed by Bénichou et al. [20], identified the optimal durations for the detection and motion phases. Our first extension relaxes the assumption that the searcher travels at a constant speed V during the motion phase. Specifically, upon entering each motion phase, the searcher draws a random speed from an arbitrary probability distribution. Our analysis quantifies how the resulting speed distribution modifies the optimal phase durations τ_D and τ_M in one, two, and three spatial dimensions. For clarity of presentation, we present the results in the reverse order of dimension.

1.4.1 Three-Dimensional Case

Our first model extends the original static three-dimensional setting described in Chapter 1.1.3. The immobile target is located at the origin within a spherical domain of radius b. During the detection phase, the searcher remains stationary and detects the

target at a constant reaction rate K whenever lying within a detection radius a of the target. During the motion phase, the searcher relocates ballistically with a random velocity vector $\mathbf{V} = (V, \Theta_V, \Phi_V)$, where $V \in [R_1, R_2]$ for $0 < R_1 < R_2$ denotes the speed, $\Theta_V \in (0, 2\pi]$ represents the horizontal direction and $\Phi_V \in [0, \pi]$ is the vertical direction. The random variable angles Θ_V and Φ_V are taken to be uniformly distributed, while V is selected from an arbitrary distribution with density f. At the start of each motion phase, a new independent random velocity vector $\mathbf{V}$ is chosen according to the specified distributions.

Let $\mathscr{Y} = \left\{(y_1, y_2, y_3) : y_1^2 + y_2^2 + y_3^2 \leq b\right\}$ define the spatial domain. We next specify the state domain $\mathscr{J}$. Since the motion phase is determined by the random velocity vector $\mathbf{V}$, we label the states $j \in \mathscr{J}$ within this phase as $j = \mathbf{V}$, where $\mathbf{V} = (V, \Theta_V, \Phi_V)$. Additionally, since there exists only one state in each of the detection and terminal phases, we denote these distinguished states by $j = \mathbf{0}$ and $j = \mathbf{A}$, respectively. Thus, we define the state domain as

$$\mathscr{J} = \{\mathbf{0}\} \cup \{\mathbf{V} : V \in [R_1, R_2], \Theta_V \in (0, 2\pi], \Phi_V \in [0, \pi]\} \cup \{\mathbf{A}\}.$$

Finally, we take the absorbing set to be $A = \left\{(\vec{0}, \mathbf{0}) \in \mathscr{Y} \times \mathscr{J}\right\}$, meaning that the absorption occurs when the searcher is at the target location in the detection state.

We now describe how transitions occur between phases. While seeking the target, the searcher alternates exclusively between the detection and motion phases. These transitions are governed by independent Poisson processes with constant switching rates $\lambda_D = \frac{1}{\tau_D}$ and $\lambda_M = \frac{1}{\tau_M}$. Consequently, the time spent in each phase follows an exponential distribution with means τ_D an τ_M, respectively. When the target is found, this event corresponds to a transition from the detection phase to the termination phase. This transition is controlled by an additional Poisson process with a rate of K. Upon reaching the termination phase, the searcher remains there permanently, effectively concluding the search process.

By applying the arguments presented in Chapter 1.3, we utilize the three-dimensional version of Equation (1.15) to derive the equations characterizing each phase, namely:

$$
\begin{aligned}
-1 = \mu_Y(0,\vec{x},i)\cdot\left(\frac{\partial t_i}{\partial x_1},\frac{\partial t_i}{\partial x_2},\frac{\partial t_i}{\partial x_3}\right) \\
+\frac{1}{2}\sigma_Y(0,\vec{x},i)\sigma_Y(0,\vec{x},i)^T : \begin{pmatrix} \frac{\partial^2 t_i}{\partial x_1^2} & \frac{\partial^2 t_i}{\partial x_1 \partial x_2} & \frac{\partial^2 t_i}{\partial x_1 \partial x_3} \\ \frac{\partial^2 t_i}{\partial x_1 \partial x_2} & \frac{\partial^2 t_i}{\partial x_2^2} & \frac{\partial^2 t_i}{\partial x_2 \partial x_3} \\ \frac{\partial^2 t_i}{\partial x_1 \partial x_3} & \frac{\partial^2 t_i}{\partial x_2 \partial x_3} & \frac{\partial^2 t_i}{\partial x_3^2} \end{pmatrix} \\
+\int_{\varsigma \neq i} \Lambda(0,\vec{x},\varsigma|\vec{x},i)\left[t_\varsigma(\vec{x}) - t_i(\vec{x})\right] d\varsigma,
\end{aligned}
\tag{1.16}
$$

where the searcher begins in state i at location $\vec{x} = (x_1, x_2, x_3)$.

We first derive the equation for the **detection phase**. Represented by state $i = \mathbf{0}$, the static searcher detects the target with a rate K. Due to the absence of movement during this phase, the following parameters are defined:

$$
\mu_Y(0,\vec{x},\mathbf{0}) = (0,0,0) \quad \text{and} \quad \frac{1}{2}\sigma_Y(0,\vec{x},\mathbf{0})\,\sigma_Y(0,\vec{x},\mathbf{0})^T = \begin{pmatrix} 0 & 0 & 0 \\ 0 & 0 & 0 \\ 0 & 0 & 0 \end{pmatrix}.
$$

The jump (integral) term accounts for transitions out the detection phase, either through detection of the target or to a state in the motion phase. If the target is found, the searcher transitions to state $i = \mathbf{A}$ at a fixed rate of K, provided that the searcher is within a distance a of the target. This transition is governed by the following relationship:

$$
\Lambda(0,\vec{x},\mathbf{A}|\vec{x},\mathbf{0})\left[t_{\mathbf{A}}(\vec{x}) - t_{\mathbf{0}}(\vec{x})\right] = KI_a(\vec{x})\left[0 - t_{\mathbf{0}}\right] = -KI_a(\vec{x})\,t_{\mathbf{0}},
$$

where $I_a(\vec{x})$ denotes the indicator function

$$
I_a(\vec{x}) = \begin{cases} 1, & |\vec{x}| \leq a \\ 0, & |\vec{x}| > a. \end{cases}
$$

Since the process ends upon detecting the target, no additional time is spent in the termination phase $\mathbf{A}$, leading to $t_{\mathbf{A}}(\vec{x}) \equiv 0$.

In the case where the target is not found, the searcher transitions to a state $i = \mathbf{V}$ in the motion phase at a fixed rate of $\Lambda(0,\vec{x},\varsigma|\vec{x},\mathbf{0}) = 1/\tau_D$. The relationships governing these

transitions are expressed as follows:

$$\int_{\substack{\varsigma\neq\mathbf{0}\\ \varsigma\neq\mathbf{A}}} \Lambda\left(0,\vec{x},\varsigma|\vec{x},\mathbf{0}\right)\left(t_{\varsigma}-t_{\mathbf{0}}\right)d\varsigma = \frac{1}{4\pi\tau_D}\int_{R_1}^{R_2}\int_0^{2\pi}\int_0^{\pi}\left(t_{\mathbf{V}}-t_{\mathbf{0}}\right)f(v)\sin\phi_V d\phi_V d\theta_V dv.$$

Substituting these expressions into Equation (1.16) results in the equation for state $i=0$:

$$\frac{1}{4\pi\tau_D}\int_{R_1}^{R_2}\int_0^{2\pi}\int_0^{\pi}\left(t_{\mathbf{V}}-t_{\mathbf{0}}\right)f(v)\sin\phi_V d\phi_V d\theta_V dv - KI_a\left(\vec{x}\right)t_{\mathbf{0}} = -1. \tag{1.17}$$

Now, we derive the equations for the states in the **motion phase**. Since the motion phase consists of an infinite number of states, we consider an arbitrary $\mathbf{V}=(V,\theta_V,\phi_V)$. Since $\mathbf{V}$ is in polar coordinates, we can rewrite the vector into cartesian coordinates (V_1,V_2,V_3), where

$$V_1 = V\cosh\Theta_V\sin\Phi_V, \qquad V_2 = V\sinh\Theta_V\sinh\Phi_V, \qquad V_3 = V\cosh\Phi_V.$$

The absence of diffusion and the velocity $\vec{V}=(V_1,V_2,V_3)$ define the following parameters:

$$\frac{1}{2}\sigma_Y\left(0,\vec{x},\mathbf{V}\right)\sigma_Y\left(0,\vec{x},\mathbf{V}\right)^T = \begin{pmatrix}0&0&0\\0&0&0\\0&0&0\end{pmatrix} \qquad \text{and} \qquad \mu_Y\left(0,\vec{x},\mathbf{V}\right)=\vec{V}.$$

Transitions from states in the motion phase occur exclusively to the detection phase at a fixed rate of $1/\tau_M$. This relationship is expressed as:

$$\Lambda\left(0,\vec{x},\mathbf{0}|\vec{x},\mathbf{V}\right) = \frac{1}{\tau_M}.$$

Substituting these values into Equation (1.16) provides the equation for state $i=\mathbf{V}$:

$$\vec{V}\cdot\nabla t_{\mathbf{V}} + \frac{1}{\tau_M}\left[t_{\mathbf{0}}(\vec{x}) - t_{\mathbf{V}}(\vec{x})\right] = -1. \tag{1.18}$$

Since Equations (1.17) and Equations (1.18) do not appear to admit an exact solution, we adopt the method outlined by Bénichou et al. [24] to reformulate these equations into a solvable system. Given the assumption that the searcher begins in the detection phase, we only need to determine $t_{\mathbf{0}}$. To achieve this, we utilize the following proposed modifications of $t_{\mathbf{V}}$:

$$s(\vec{x}) = \left\langle t_{\mathbf{V}}\right\rangle_{V,\theta_V,\phi_V} \qquad \text{and} \qquad \vec{d}(\vec{x}) = \left\langle t_{\mathbf{V}}\vec{V}\right\rangle_{V,\theta_V,\phi_V},$$

where

$$\langle \cdot \rangle_{V,\theta_V,\phi_V} = \frac{1}{4\pi} \int_{R_1}^{R_2} \int_0^{2\pi} \int_0^{\pi} \cdot f(v) \sin\phi_V \, d\phi_V \, d\phi_V \, d\theta_V \, dv$$

Using these definitions, we restructure Equation (1.17) in polar coordinates as follows:

$$\frac{1}{\tau_D} [s(r) - t_{\mathbf{0}}(r)] - KI_a(r) t_{\mathbf{0}}(r) = -1,$$

where $r = |\vec{x}| = \sqrt{x_1^2 + x_2^2 + x_3^2}$.

We next reformulate the motion phase Equation (1.18) by considering all possible velocities V and directions θ_V, ϕ_V. We start by computing two averages: one involving the equation itself and another involving the equation multiplied by $\vec{V}$. These calculations give us the following expressions:

$$\nabla \cdot \vec{d}(\vec{r}) + \frac{1}{\tau_M} [t_{\mathbf{0}}(\vec{r}) - s(\vec{r})] = -1 \tag{1.19}$$

and

$$\vec{d}(\vec{r}) = \tau_M \left\langle \left(\vec{V} \cdot \nabla t_{\mathbf{V}} \right) \vec{V} \right\rangle_{V,\theta_V,\phi_V}, \tag{1.20}$$

respectively. By taking the divergence of Equation (1.20), we derive the following result:

$$\nabla \cdot \vec{d}(\vec{r}) = \tau_M \sum_{i,j=1}^{2} \frac{\partial^2}{\partial x_i \partial x_j} \left\langle V_i V_j t_{\mathbf{V}} \right\rangle_{V,\theta_V,\phi_V}. \tag{1.21}$$

By employing the following decoupling assumption

$$\left\langle V_i V_j t_{\mathbf{V}} \right\rangle_{V,\theta_V,\phi_V} \simeq \left\langle V_i V_j \right\rangle_{V,\theta_V,\phi_V} \left\langle t_{\mathbf{V}} \right\rangle_{V,\theta_V,\phi_V}, \tag{1.22}$$

we approximate Equation (1.21) as

$$\nabla \cdot \vec{d}(\vec{r}) = \frac{\mathbb{E}\left[V^2\right] \tau_M}{3} \Delta s,$$

where

$$\mathbb{E}[\,\cdot\,] = \int_{R_1}^{R_2} \cdot f(v) dv.$$

Substituting this approximation into Equation (1.19) leads to the following:

$$\frac{\mathbb{E}\left[V^2\right] \tau_M}{3} \Delta s + \frac{1}{\tau_M} [t_{\mathbf{0}}(\vec{r}) - s(\vec{r})] = -1. \tag{1.23}$$

Since the radial symmetry of each $t_{\mathbf{V}}$ implies s also has radial symmetry, we express Equation (1.23) in polar coordinates as follows:

$$\frac{\mathbb{E}\left[V^2\right]\tau_M}{3}\frac{d^2s}{dr^2}+\frac{\mathbb{E}\left[V^2\right]\tau_M}{3}\frac{2}{r}\frac{ds}{dr}+\frac{1}{\tau_M}\left[t_{\mathbf{0}}(r)-s(r)\right]=-1.$$

We next discuss the boundary conditions required. Considering reflective boundaries with respect to the motion phase, we have the boundary condition:

$$\frac{ds^{out}}{dr}(b)=\frac{d}{dr}\left\langle t_{\mathbf{V}}^{out}(b)\right\rangle_{V,\theta_V,\phi_V}=\left\langle\frac{dt_{\mathbf{V}}^{out}}{dr}(b)\right\rangle_{V,\theta_V,\phi_V}=\langle 0\rangle_{V,\theta_V,\phi_V}=0.$$

Additionally, as the searcher moves through the domain, we assume continuity of $t_{\mathbf{V}}$ and their first derivatives at $x=a$ such that

$$s^{in}(a)=\left\langle t_{\mathbf{V}}^{in}(a)\right\rangle_{V,\theta_V,\phi_V}=\left\langle t_{\mathbf{V}}^{out}(b)\right\rangle_{V,\theta_V,\phi_V}=s^{out}(a)$$

and

$$\frac{ds^{in}}{dx}(a)=\frac{d}{dx}\left[\left\langle t_{\mathbf{V}}^{in}(a)\right\rangle_{V,\theta_V,\phi_V}\right]=\frac{d}{dx}\left[\left\langle t_{\mathbf{V}}^{out}(a)\right\rangle_{V,\theta_V,\phi_V}\right]=\frac{ds^{out}}{dx}(a).$$

Lastly, we note that as $r\to 0^+$, we must have that $s^{in}(r)$ remains finite.

Putting these together, we have the following system of equations:

$$\begin{cases}\dfrac{1}{\tau_D}\left[s(r)-t_{\mathbf{0}}(r)\right]-KI_a(r)t_{\mathbf{0}}(r)=-1,\\ \dfrac{\mathbb{E}\left[V^2\right]\tau_M}{3}\dfrac{d^2s}{dr^2}+\dfrac{\mathbb{E}\left[V^2\right]\tau_M}{3}\dfrac{2}{r}\dfrac{ds}{dr}+\dfrac{1}{\tau_M}\left[t_{\mathbf{0}}(r)-s(r)\right]=-1,\\ \dfrac{ds^{out}}{dr}(b)=0,\qquad s^{in}(a)=s^{out}(a),\qquad \dfrac{ds^{in}}{dr}(a)=\dfrac{ds^{out}}{dr}(a),\\ \lim_{r\to 0^+}s^{in}(r)\text{ is finite.}\end{cases}$$

The solution to the system yields the following results:

$$t_{\mathbf{0}}^{in}(r)=\frac{(\tau_D+\tau_M)(b^3-a^3)}{\mathbb{E}\left[V^2\right]\tau_M^2(1+K\tau_D)\left(-\sinh\alpha+\alpha\cosh\alpha\right)}\sinh\left(r\sqrt{\frac{3K\tau_D}{\mathbb{E}\left[V^2\right]\tau_M^2(1+K\tau_D)}}\right)r^{-1}$$
$$+\frac{\tau_D+\tau_M}{K\tau_D},$$

$$
\begin{aligned}
s^{in}(r) &= \frac{(\tau_D+\tau_M)(b^3-a^3)}{\mathbb{E}[V^2]\,\tau_M^2\,(-\sinh\alpha+\alpha\cosh\alpha)}\sinh\left(r\sqrt{\frac{3K\tau_D}{\mathbb{E}[V^2]\,\tau_M^2(1+K\tau_D)}}\right)r^{-1} \\
&\quad + \frac{\tau_D+\tau_M}{K\tau_D} + \tau_M, \\
t_{\mathbf{0}}^{out}(r) &= \frac{(\tau_D+\tau_M)(r-a)\left(2b^3-r^2a-ra^2\right)}{2\mathbb{E}[V^2]\,\tau_M^2 ra} + \frac{(\tau_D+\tau_M)\left(b^3-a^3\right)\sinh\alpha}{\mathbb{E}[V^2]\,\tau_M^2 a\,(-\sinh\alpha+\alpha\cosh\alpha)} \\
&\quad + \frac{(\tau_D+\tau_M)(1+K\tau_D)}{K\tau_D}, \\
s^{out}(r) &= \frac{(\tau_D+\tau_M)(r-a)\left(2b^3-r^2a-ra^2\right)}{2\mathbb{E}[V^2]\,\tau_M^2 ra} + \frac{(\tau_D+\tau_M)\left(b^3-a^3\right)\sinh\alpha}{\mathbb{E}[V^2]\,\tau_M^2 a\,(-\sinh\alpha+\alpha\cosh\alpha)} \\
&\quad + \frac{(\tau_D+\tau_M)}{K\tau_D} + \tau_M,
\end{aligned}
$$

where

$$
\alpha = a\sqrt{\frac{3K\tau_D}{\mathbb{E}[V^2]\,\tau_M^2(1+K\tau_D)}}.
$$

Appendix A.1 provides a comprehensive justification for all denominators remaining strictly nonzero.

Assuming the searcher begins in the detection phase, the average search time across the entire spatial domain is given by the following:

$$
t_m = \frac{3}{4\pi b^3}\int_0^b\int_0^{2\pi}\int_0^{\pi} t_{\mathbf{0}} r^2\sin\phi_r\, d\phi_r\, d\theta_r\, dr = \frac{3}{b^3}\int_0^a t_{\mathbf{0}}^{in} r^2 dr + \frac{3}{b^3}\int_a^b t_{\mathbf{0}}^{out} r^2 dr
$$

$$
\begin{aligned}
t_m &= \frac{(\tau_D+\tau_M)}{b^3\mathbb{E}[V^2]\,\tau_M^2}\left[\frac{1}{5}\left(b^5-a^5\right)-2b^3\left(b^2-a^2\right)+\left(b^3-a^3\right)\left(3\frac{a^2}{\alpha^2}+\beta\right)\right] \\
&\quad + \frac{(\tau_D+\tau_M)}{K\tau_D}
\end{aligned}
\tag{1.24}
$$

where

$$
\alpha = a\sqrt{\frac{3K\tau_D}{\mathbb{E}[V^2]\,\tau_M^2(1+K\tau_D)}}, \qquad \beta = \frac{-a^3\sinh\alpha + b^3\alpha\cosh\alpha}{a\,(-\sinh\alpha+\alpha\cosh\alpha)}.
$$

Assuming a low target density regime, where $a \ll b$, we can simplify Equation (1.24) using the approximation $b - a \approx b$:

$$t_m \approx (\tau_D + \tau_M)\left[\frac{1}{K\tau_D} + \frac{1}{\mathbb{E}[V^2]\,\tau_M^2}\left(-\frac{9}{5}b^2 + 3\frac{a^2}{\alpha^2} + \beta\right)\right] \tag{1.25}$$

The following demonstrates the process for simplifying β. Firstly, since $\sinh\alpha \approx 0$ for small α, we see that

$$\begin{aligned}
\beta &= \frac{-a^3\sinh\alpha + b^3\alpha\cosh\alpha}{a(-\sinh\alpha + \alpha\cosh\alpha)} \\
&= \frac{-a^3\sinh\alpha + b^3\alpha\cosh\alpha}{a\alpha\cosh\alpha\left(1 - \frac{1}{\alpha}\tanh\alpha\right)} \\
&\approx \frac{b^3\alpha\cosh\alpha}{a\alpha\cosh\alpha\left(1 - \frac{1}{\alpha}\tanh\alpha\right)} \\
&= \frac{b^3}{a}\frac{1}{1 - \frac{1}{\alpha}\tanh\alpha}.
\end{aligned}$$

Since expanding $\tanh\alpha$ results in the following:

$$\tanh\alpha = \alpha - \frac{1}{3}\alpha^3 + \frac{2}{15}\alpha^5 + \mathcal{O}(\alpha^7)$$

we simplify β further:

$$\begin{aligned}
\beta &\approx \frac{b^3}{a}\frac{1}{1 - \frac{1}{\alpha}\left(\alpha - \frac{1}{3}\alpha^3 + \frac{2}{15}\alpha^5 + \mathcal{O}(\alpha^7)\right)} \\
&= \frac{b^3}{a}\frac{1}{\frac{1}{3}\alpha^2 - \frac{2}{15}\alpha^4 + \mathcal{O}(\alpha^6)} \\
&= \frac{3b^3}{a\alpha^2}\frac{1}{1 - \left(\frac{2}{5}\alpha^2 + \mathcal{O}(\alpha^4)\right)}.
\end{aligned}$$

Lastly, since for small x,

$$\frac{1}{1-x} = 1 + x + \mathscr{O}\left(x^2\right),$$

we simplify β to the following expression:

$$\beta \approx \frac{3b^3}{a\alpha^2}\left[1 + \left(\frac{2}{5}\alpha^2 + \mathscr{O}\left(\alpha^4\right)\right)\right] \approx \frac{b^3}{a}\left(\frac{3}{\alpha^2} + \frac{6}{5}\right).$$

Thus, the fully simplified form of the mean search time Equation (1.25) becomes

$$t_m \approx (\tau_D + \tau_M)\left[\frac{b^3}{a}\left(\frac{1 + K\tau_D}{a^2 K\tau_D} + \frac{6}{5\mathbb{E}\left[V^2\right]\tau_M^2}\right) - \frac{9}{5\mathbb{E}\left[V^2\right]\tau_M^2}b^2 + \frac{2 + K\tau_D}{K\tau_D}\right]$$

$$t_m \approx \frac{(\tau_D + \tau_M)b^3}{a}\left[\frac{1 + K\tau_D}{a^2 K\tau_D} + \frac{6}{5\mathbb{E}\left[V^2\right]\tau_M^2}\right]. \tag{1.26}$$

To determine the minimal value of Equation (1.26) with respect to (τ_D, τ_M), the critical value of (τ_D^*, τ_M^*) is calculated as:

$$(\tau_D^*, \tau_M^*) = \left(\left(\frac{3}{10}\right)^{1/4}\sqrt{\frac{a}{\sqrt{\mathbb{E}\left[V^2\right]}K}}, \frac{a}{\sqrt{\mathbb{E}\left[V^2\right]}}\sqrt{\frac{6}{5}}\right). \tag{1.27}$$

Additionally, the Hessian determinant is expressed as

$$D(\tau_D^*, \tau_M^*) = \frac{4b^6\mathbb{E}\left[V^2\right]\left(5 + \sqrt{aK}\left(\frac{3000}{\mathbb{E}\left[V^2\right]}\right)^{1/4}\right)}{3a^8} > 0,$$

and the second derivative with respect to τ_D is given by

$$\frac{\partial^2 t_m}{\partial \tau_D^2}(\tau_D^*, \tau_M^*) = \left(\frac{10\mathbb{E}\left[V^2\right]}{3}\right)^{1/4}\frac{4b^3}{a^3}\sqrt{\frac{K}{a}} > 0.$$

By applying the Second Derivative Test, (τ_D^*, τ_M^*) is identified as an approximate minimizer of t_m.

As in the original formulation, the mean duration τ_M^* of the motion phase is not dependent on K. By contrast, both τ_D^* and τ_M^* are dependent on the second moment of

the speed distribution, $\mathbb{E}\left[V^2\right]$. At first glance, this may seem counterintuitive, since one might expect the relevant scale to be the mean speed $\mathbb{E}[V]$. The appearance of $\mathbb{E}\left[V^2\right]$ is a direct consequence of our specific decoupling assumption used in Equation (1.22) when converting the random motion times $t_{\mathbf{V}}$ into the average function s. Under this assumption, the velocity appears only in second-order terms, and the resulting averages therefore reduce to $\mathbb{E}\left[V^2\right]$ rather than $\mathbb{E}[V]$.

To see why the alternative decoupling fails, suppose instead that we assume the following approximation:

$$\langle V_i t_{\mathbf{V}} \rangle_{V,\theta_V,\phi_V} \simeq \langle V_i \rangle_{V,\theta_V,\phi_V} \langle t_{\mathbf{V}} \rangle_{V,\theta_V,\phi_V} .$$

This estimation is not useful here because the symmetry of the velocity directions implies that each Cartesian component has zero mean, namely:

$$\langle V_i \rangle_{V,\theta_V,\phi_V} = 0, \qquad \forall i \in \{1,2,3\}.$$

Specifically, when using

$$v_1 = v\cos\theta_V \sin\phi_V, \qquad v_2 = v\sin\theta_V \sin\phi_V, \qquad v_3 = v\cos\phi_V,$$

we obtain the following:

$$\langle V_1 \rangle_{V,\theta_V,\phi_V} = \frac{1}{4\pi} \int_{R_1}^{R_2} v f(v) dv \int_0^{2\pi} \cos\theta_V d\theta_V \int_0^{\pi} \sin^2\phi_V d\phi_V = 0, \tag{1.28}$$

$$\langle V_2 \rangle_{V,\theta_V,\phi_V} = \frac{1}{4\pi} \int_{R_1}^{R_2} v f(v) dv \int_0^{2\pi} \sin\theta_V d\theta_V \int_0^{\pi} \sin^2\phi_V d\phi_V = 0, \tag{1.29}$$

and

$$\langle V_3 \rangle_{V,\theta_V,\phi_V} = \frac{1}{4\pi} \int_{R_1}^{R_2} v f(v) dv \int_0^{2\pi} d\theta_V \int_0^{\pi} \cos\phi_V \sin\phi_V d\phi_V = 0. \tag{1.30}$$

In Equations (1.28) and (1.29), the horizontal angular averages $\int_0^{2\pi} \cos\theta_V d\theta_V$ and $\int_0^{2\pi} \sin\theta_V d\theta_V$ evaluate to 0, whereas in Equation (1.30), the vertical angular average $\int_0^{\pi} \cos\phi_V \sin\phi_V d\phi_V$ is 0. Consequently, any approximation that relies on $\langle V_i \rangle$ becomes trivial and cannot contribute to the motion. This is precisely why the durations the minimal values τ_D^* and τ_M^* in Equation (1.27) are governed by the second moment $\mathbb{E}\left[V^2\right]$ rather than by the mean speed $\mathbb{E}[V]$.

Now that we have illustrated the three-dimensional model, we move to the corresponding two-dimensional case.

1.4.2 Two-Dimensional Case

Building upon the original static two-dimensional framework described in Chapter 1.1.2, we assume during the motion phase that the searcher moves ballistically with a random velocity vector $\mathbf{V} = (V, \Theta_V)$, where $V \in [R_1, R_2]$ for $0 < R_1 < R_2$ denotes the speed selected from an arbitrary distribution with density f and $\Theta_V \in (0, 2\pi]$ represents the direction chosen from a uniform distribution. Upon each transition into the motion phase, a new random velocity vector $\mathbf{V}$ is chosen from the specified distributions.

Using similar arguments to Chapter 1.4.1, we define the spatial domain as $\mathscr{Y} = \{(y_1, y_2) : y_1^2 + y_2^2 \leq b\}$ and the state domain as

$$\mathscr{J} = \{\mathbf{0}\} \cup \{\mathbf{V} : V \in [R_1, R_2], \Theta_V \in (0, 2\pi]\} \cup \{\mathbf{A}\},$$

where the detection phase corresponds to state $j = \mathbf{0}$, the motion phase consists of the collection of states $j = \mathbf{V}$, and the terminal phase is represented as state $j = \mathbf{A}$. Additionally, the absorbing set is $A = \{(\vec{0}, \mathbf{0}) \in \mathscr{Y} \times \mathscr{J}\}$. Using the two-dimensional version of Equation (1.15) as well as the arguments outlined in the Chapter 1.4.1, we have the following system of equations in polar form:

$$\begin{cases} \dfrac{1}{\tau_D}\left[s(r) - t_{\mathbf{0}}(r)\right] - KI_a(r)t_{\mathbf{0}}(r) = -1, \\ \dfrac{\mathbb{E}\left[V^2\right]\tau_M}{2}\dfrac{d^2 s}{dr^2} + \dfrac{\mathbb{E}\left[V^2\right]\tau_M}{2}\dfrac{1}{r}\dfrac{ds}{dr} + \dfrac{1}{\tau_M}\left[t_{\mathbf{0}}(r) - s(r)\right] = -1, \\ \dfrac{ds^{out}}{dr}(b) = 0, \qquad s^{in}(a) = s^{out}(a), \qquad \dfrac{ds^{in}}{dr}(a) = \dfrac{ds^{out}}{dr}(a), \\ \lim_{r \to 0^+} s^{in}(r) \text{ is finite}, \end{cases}$$

where

$$s(r) = \frac{1}{2\pi}\int_{R_1}^{R_2}\int_0^{2\pi} t_{\mathbf{V}} f(v)\, d\theta_V\, dv.$$

Solving the system yields the following results:

$$t_{\mathbf{0}}^{in}(r) = \frac{(\tau_D+\tau_M)\left(b^2-a^2\right)}{\mathbb{E}[V^2]\,\tau_M^2 a\alpha(1+K\tau_D)}\frac{I_0(r\alpha)}{I_1(a\alpha)} + \frac{\tau_D+\tau_M}{K\tau_D},$$

$$s^{in}(r) = \frac{(\tau_D+\tau_M)\left(b^2-a^2\right)}{\mathbb{E}[V^2]\,\tau_M^2 a\alpha}\frac{I_0(r\alpha)}{I_1(a\alpha)} + \frac{\tau_D+\tau_M}{K\tau_D} + \tau_M,$$

$$t_{\mathbf{0}}^{out}(r) = \frac{(\tau_D+\tau_M)\left(2b^2\ln\frac{r}{a}-r^2+a^2\right)}{2\mathbb{E}[V^2]\,\tau_M^2} + \frac{(\tau_D+\tau_M)\left(b^2-a^2\right)}{\mathbb{E}[V^2]\,\tau_M^2 a\alpha}\frac{I_0(a\alpha)}{I_1(a\alpha)} + \frac{(\tau_D+\tau_M)(1+K\tau_D)}{K\tau_D},$$

$$s^{out}(r) = \frac{(\tau_D+\tau_M)\left(2b^2\ln\frac{r}{a}-r^2+a^2\right)}{2\mathbb{E}[V^2]\,\tau_M^2} + \frac{(\tau_D+\tau_M)\left(b^2-a^2\right)}{\mathbb{E}[V^2]\,\tau_M^2 a\alpha}\frac{I_0(a\alpha)}{I_1(a\alpha)} + \frac{\tau_D+\tau_M}{K\tau_D} + \tau_M,$$

where

$$\alpha = \sqrt{\frac{2K\tau_D}{\mathbb{E}[V^2]\,\tau_M^2(1+K\tau_D)}}.$$

In each expression, we clearly see that all denominator terms are strictly nonzero.

Again, assuming the searcher begins in the detection phase, the average search time across the entire spatial domain:

$$t_m = \frac{1}{\pi b^2}\int_0^b\int_0^{2\pi} t_{\mathbf{0}}(r)\,d\theta_r dr = \frac{2}{b^2}\int_0^a t_{\mathbf{0}}^{in}(r)dr + \frac{2}{b^2}\int_a^b t_{\mathbf{0}}^{out}(r)dr$$

$$t_m = \frac{\tau_D+\tau_M}{2K\tau_D y^2}\left[\begin{array}{c}\frac{1}{x}(1+K\tau_D)\left(y^2-x^2\right)^2\frac{I_0(x)}{I_1(x)} \\ +\frac{1}{4}\left[8y^2+(1+K\tau_D)\left(4y^4\ln\frac{y}{x}+\left(y^2-x^2\right)\left(x^2-3y^2+8\right)\right)\right]\end{array}\right] \tag{1.31}$$

where

$$x = a\sqrt{\frac{2K\tau_D}{\mathbb{E}[V^2]\,\tau_M^2(1+K\tau_D)}}, \qquad y = b\sqrt{\frac{2K\tau_D}{\mathbb{E}[V^2]\,\tau_M^2(1+K\tau_D)}}.$$

Under the assumption of low target density, where $a \ll b$, we leverage the approximation $b-a \approx b$. Since $y = b\alpha$ and $x = a\alpha$, this also means $y-x \approx y$. We reduce Equation (1.31) as the following

$$t_m = \frac{(\tau_D+\tau_M)(1+K\tau_D)}{2K\tau_D}\left[y^2\left(\frac{1}{x}\frac{I_0(x)}{I_1(x)}+\ln\frac{y}{x}-\frac{3}{4}\right)+\frac{2}{(1+K\tau_D)}+\frac{1}{x^2}\right]$$

$$t_m = \frac{(\tau_D+\tau_M)(1+K\tau_D)y^2}{2K\tau_D}\left(\frac{1}{x}\frac{I_0(x)}{I_1(x)}+\ln\frac{y}{x}-\frac{3}{4}\right) \tag{1.32}$$

since the y^2-term dominates. Lastly, since for small x,

$$\frac{I_0(x)}{I_1(x)} = \frac{2}{x}\left(1+\frac{x^2}{8}+\mathscr{O}\left(x^4\right)\right),$$

Equation (1.32) is further simplified to the following:

$$t_m = \frac{(\tau_D+\tau_M)b^2\left[a^2K\tau_D\left(2\ln\left(b/a\right)-1\right)+2\mathbb{E}\left[V^2\right]\tau_M^2(1+K\tau_D)\right]}{2a^2K\tau_D\mathbb{E}\left[V^2\right]\tau_M^2}. \tag{1.33}$$

To identify the minimal value of Equation (1.33) with respect to (τ_D, τ_M), we determine the critical value of (τ_D^*, τ_M^*) as follows:

$$(\tau_D^*, \tau_M^*) = \left(\sqrt{\frac{a}{\sqrt{\mathbb{E}\left[V^2\right]}k}}\left(\frac{2\ln\left(b/a\right)-1}{8}\right)^{1/4}, \frac{a}{\sqrt{\mathbb{E}\left[V^2\right]}}\sqrt{\ln\left(\frac{b}{a}\right)-\frac{1}{2}}\right) \tag{1.34}$$

Given that $\frac{b}{a}$ is significantly large, allowing the assumption $\frac{b}{a} > e^{1/2} \approx 1.65$, the Hessian determinant is computed as

$$D(\tau_D^*, \tau_M^*) = \frac{16b^4\mathbb{E}\left[V^2\right]\left(1+\sqrt{ak}\left(\frac{4\ln\frac{b}{a}-2}{\mathbb{E}\left[V^2\right]}\right)^{1/4}\right)}{a^6\left(2\ln\frac{b}{a}-1\right)} > 0$$

and the second derivative with respect to τ_D is given by

$$\frac{\partial^2 t_m}{\partial\tau_D^2}(\tau_D^*, \tau_M^*) = \frac{4b^2}{a^2}\sqrt{\frac{k}{a}}\left(\frac{8\mathbb{E}\left[V^2\right]}{2\ln\frac{b}{a}-1}\right)^{1/4} > 0.$$

Thus, by applying the Second Derivative Test, (τ_D^*, τ_M^*) is confirmed as an approximate minimizer of t_m.

Again, as seen in the original derivation, the mean motion-phase duration τ_M^* is not dependent on K. Moreover, consistent with the three-dimensional case, the minimal

durations τ_D^* and τ_M^* depend on the second moment $\mathbb{E}\left[V^2\right]$ rather than on the mean speed $\mathbb{E}[V]$ by the same decoupling assumption and symmetry-based reasoning as in the three-dimensional case.

We now turn to our final, the one-dimensional model, where our analysis is necessarily more involved.

1.4.3 One-Dimensional Case

Our one-dimensional setting generalizes the static one-dimensional model introduced in Chapter 1.1.1. In the motion phase, the searcher travels ballistically along a line segment $[-b,b]$. At the start of each motion phase, a speed random variable $V \in [R_1,R_2]$ with $0 < R_1 < R_2$ is drawn from an arbitrary distribution with density f. The direction of travel is then selected with equal probability: the searcher moves to the right with velocity V or to the left with velocity $-V$, both having the same magnitude V.

Using arguments similar to those from the three-dimensional case in Chapter 1.4.1, we define $\mathscr{Y} = [-b,b]$ as the spatial domain and

$$\mathscr{J} = \{\mathbf{0}\} \cup \{-\mathbf{V} : V \in [R_1,R_2]\} \cup \{\mathbf{V} : V \in [R_1,R_2]\} \cup \{\mathbf{A}\}$$

as the state domain, where the detection phase corresponds to state $j = \mathbf{0}$, the motion phase consists of the collection of states $j = -\mathbf{V}$ and $j = \mathbf{V}$, and the termination phase is denoted by $j = \mathbf{A}$. Lastly, the absorbing set is $A = \{(0,\mathbf{0}) \in \mathscr{Y} \times \mathscr{J}\}$.

Following the method from Chapter 1.3, the one-dimensional version of Equation (1.15) is given by:

$$\mu_Y(0,x,i)\frac{dt_i(x)}{dx} + \frac{1}{2}\sigma_Y^2(0,x,i)\frac{d^2t_i(x)}{dx^2} + \int_{\varsigma \neq i} \Lambda(0,x,\varsigma|x,i)\left[t_\varsigma(x) - t_i(x)\right] d\varsigma = -1 \quad (1.35)$$

where $\Lambda(0,x,\varsigma|x,i)$ denotes the transition rate out of state i when starting at location x.

We first derive the equation for the **detection phase**. Represented by state $i = 0$, the searcher does not move, resulting in the following parameters:

$$\mu_Y(0,x,\mathbf{0}) = 0 \quad \text{and} \quad \frac{1}{2}\sigma_Y^2(0,x,\mathbf{0}) = 0.$$

The jump (integral) term accounts for transitions out the detection phase, either to a state in the motion phase or through detection of the target. If the target is not found, the searcher transitions to a state $i = -\mathbf{V}$ or $i = \mathbf{V}$ in the motion phase at a fixed rate of $1/\tau_D$. Assuming the searcher is equally likely to go left or right, each transition occurs with probability $\frac{1}{2}f$. The relationships governing these transitions are expressed as:

$$\Lambda(0,x,-\mathbf{V}|x,\mathbf{0}) = \frac{1}{\tau_D}\left(\frac{1}{2}f\right) \qquad \text{and} \qquad \Lambda(0,x,\mathbf{V}|x,\mathbf{0}) = \frac{1}{\tau_D}\left(\frac{1}{2}f\right).$$

In the case where the target is found, the searcher transitions to state $i = \mathbf{A}$ at a fixed rate of K, provided that the searcher is within a distance a of the target. This transition is governed by the following relationship:

$$\Lambda(0,x,\mathbf{A}|x,\mathbf{0})[t_{\mathbf{A}}(x) - t_{\mathbf{0}}(x)] = KI_a(x)[0 - t_{\mathbf{0}}(x)] = -KI_a(x)t_{\mathbf{0}}(x),$$

where $I_a(x)$ denotes the indicator function

$$I_a(x) = \begin{cases} 1, & x \le a \\ 0, & x > a. \end{cases}$$

Since the process ends upon detecting the target, no additional time is spent in state $\mathbf{A}$, leading to $t_{\mathbf{A}}(x) \equiv 0$.

Substituting these expressions into Equation (1.35) results in the equation for state $i = \mathbf{0}$:

$$\frac{1}{\tau_D}\int_{R_1}^{R_2}\left[\frac{t_{\mathbf{V}}(x) + t_{-\mathbf{V}}(x)}{2} - t_{\mathbf{0}}(x)\right] f(v)dv - KI_a(x)t_{\mathbf{0}}(x) = -1. \tag{1.36}$$

Now, we derive the equations for the states in the **motion phase**. The motion phase consists of an infinite number of states, each labeled as $i = -\mathbf{V}$ or $i = \mathbf{V}$ for any $V \in [R_1, R_2]$. Beginning with an arbitrary state $i = -\mathbf{V}$, the searcher exhibits ballistic movement at velocity $-V$, which corresponds to movement to the left with magnitude V. The absence of diffusion and the velocity $-V$ define the following parameters:

$$\frac{1}{2}\sigma_Y^2(0,x,-\mathbf{V}) = 0 \qquad \text{and} \qquad \mu_Y(0,x,-\mathbf{V}) = -V.$$

Transitions from states in the motion phase occur exclusively to the detection phase at a fixed rate of $1/\tau_M$. This relationship is expressed as:

$$\Lambda(0,x,\mathbf{0}|x,-\mathbf{V}) = \frac{1}{\tau_M}.$$

Substituting these values into Equation (1.35) provides the equation for state $i = -\mathbf{V}$:

$$-V\frac{dt_{-\mathbf{V}}(x)}{dx} + \frac{1}{\tau_M}\left[t_{\mathbf{0}}(x) - t_{-\mathbf{V}}(x)\right] = -1. \tag{1.37}$$

Similarly, for an arbitrary motion phase state $i = \mathbf{V}$ where $V \in [R_1, R_2]$, the searcher performs ballistic movement to the right with magnitude V. Substituting the corresponding values into Equation (1.35) results in the following equation for state $i = \mathbf{V}$:

$$V\frac{dt_{\mathbf{V}}}{dx} + \frac{1}{\tau_M}\left[t_{\mathbf{0}}(x) - t_{\mathbf{V}}(x)\right] = -1. \tag{1.38}$$

As in the two- and three-dimensional models, the coupled equations in the one-dimensional model are not directly solvable in their present form. In contrast to the higher-dimensional cases, however, two plausible decoupling choices emerge, which lead to distinct cases to be analyzed. We start by introducing the usual averaged motion phase function:

$$s(x) = \mathbb{E}\left[\frac{t_{\mathbf{V}} + t_{-\mathbf{V}}}{2}\right],$$

where

$$\mathbb{E}[\,\cdot\,] = \int_{R_1}^{R_2} \cdot\, f(v)dv.$$

With this notation, the detection phase Equation (1.36) can be rewritten as follows:

$$\frac{1}{\tau_D}\left[s(x) - t_{\mathbf{0}}(x)\right] - KI_a(x)t_{\mathbf{0}}(x) = -1. \tag{1.39}$$

Turning now to the motion phase equation, we consider two alternative decoupling assumptions and analyze each in turn:

1) First-moment decoupling:

$$\mathbb{E}[Vt_{\mathbf{V}}] \simeq \mathbb{E}[V]\,\mathbb{E}[t_{\mathbf{V}}], \qquad \mathbb{E}[Vt_{-\mathbf{V}}] \simeq \mathbb{E}[V]\,\mathbb{E}[t_{-\mathbf{V}}]$$

2) Second-moment decoupling:

$$\mathbb{E}\left[V^2 t_{\mathbf{V}}\right] \simeq \mathbb{E}\left[V^2\right]\mathbb{E}[t_{\mathbf{V}}], \qquad \mathbb{E}\left[V^2 t_{-\mathbf{V}}\right] \simeq \mathbb{E}\left[V^2\right]\mathbb{E}[t_{-\mathbf{V}}].$$

Case 1: First-Order Decoupling

Using the same values for V, we integrate the average of Equations (1.37) and (1.38) with respect to the speed and get the following:

$$\frac{d}{dx}\mathbb{E}\left[V\frac{t_{\mathbf{V}}(x)-t_{-\mathbf{V}}(x)}{2}\right]+\frac{1}{\tau_M}\left[t_{\mathbf{0}}(x)-s(x)\right]=-1. \tag{1.40}$$

Then we integrate the half difference of Equations (1.38) and (1.37) with respect to the speed to get the following:

$$\mathbb{E}\left[\frac{t_{\mathbf{V}}(x)-t_{-\mathbf{V}}(x)}{2}\right]=\tau_M\frac{d}{dx}\mathbb{E}\left[V\frac{t_{\mathbf{V}}(x)+t_{-\mathbf{V}}(x)}{2}\right]. \tag{1.41}$$

We now use the first-order decoupling assumptions:

$$\mathbb{E}\left[Vt_{\mathbf{V}}\right]\simeq\mathbb{E}\left[V\right]\mathbb{E}\left[t_{\mathbf{V}}\right],\qquad \mathbb{E}\left[Vt_{-\mathbf{V}}\right]\simeq\mathbb{E}\left[V\right]\mathbb{E}\left[t_{-\mathbf{V}}\right].$$

Using this approximation with Equation (1.40), we get

$$\mathbb{E}\left[V\right]\frac{d}{dx}\mathbb{E}\left[V\frac{t_{\mathbf{V}}(x)-t_{-\mathbf{V}}(x)}{2}\right]+\frac{1}{\tau_M}\left[t_{\mathbf{0}}(x)-s(x)\right]=-1. \tag{1.42}$$

Using the same approximation with Equation (1.41) gives us the following:

$$\mathbb{E}\left[\frac{t_{\mathbf{V}}(x)-t_{-\mathbf{V}}(x)}{2}\right]=\mathbb{E}[V]\tau_M\frac{ds}{dx}. \tag{1.43}$$

Plugging in Equation (1.43) into Equation (1.42) gives us our converted motion phase equation:

$$\mathbb{E}^2[V]\tau_M\frac{d^2s}{dx^2}+\frac{1}{\tau_M}\left(t_{\mathbf{0}}-s\right)=-1. \tag{1.44}$$

We next discuss the boundaries required. Because of the symmetry $x\leftrightarrow -x$, we can simply consider the nonnegative region $[0,b]$. This means that

$$s(-x)=\mathbb{E}\left[\frac{t_{\mathbf{V}}(-x)+t_{-\mathbf{V}}(-x)}{2}\right]=\mathbb{E}\left[\frac{t_{\mathbf{V}}(x)+t_{-\mathbf{V}}(x)}{2}\right]=s(x)$$

so that

$$-\frac{ds}{dx}(-x)=\frac{ds}{dx}(x).$$

Setting $x=0$ gives us the boundary condition:

$$\frac{ds^{in}}{dx}(0) = 0.$$

Using this and previous boundary conditions from Chapter 1.4.1 with Equations (1.39) and (1.44) gives us the following system of equations:

$$\begin{cases} \frac{1}{\tau_D}\left[s(x) - t_{\mathbf{0}}(x)\right] - KI_a(x)t_{\mathbf{0}}(x) = -1, \\ \mathbb{E}^2[V]\tau_M\frac{ds}{dx} + \frac{1}{\tau_M}\left[t_{\mathbf{0}}(x) - s(x)\right] = -1, \\ \frac{ds^{in}}{dx}(0) = 0, \qquad \frac{ds^{out}}{dx}(b) = 0, \\ s^{in}(a) = s^{out}(a), \qquad \frac{ds^{in}}{dx}(a) = \frac{ds^{out}}{dx}(a). \end{cases}$$

Solving the system gives us

$$t_{\mathbf{0}}^{in}(x) = \frac{(\tau_D+\tau_M)(b-a)\beta}{\mathbb{E}[V]\tau_M(1+K\tau_D)}\frac{\cosh\left(\frac{x}{\mathbb{E}[V]\tau_M\beta}\right)}{\sinh\left(\frac{a}{\mathbb{E}[V]\tau_M\beta}\right)} + \frac{\tau_D+\tau_M}{K\tau_D},$$

$$s^{in}(x) = \frac{(\tau_D+\tau_M)(b-a)\beta}{\mathbb{E}[V]\tau_M}\frac{\cosh\left(\frac{x}{\mathbb{E}[V]\tau_M\beta}\right)}{\sinh\left(\frac{a}{\mathbb{E}[V]\tau_M\beta}\right)} + \frac{\tau_D+\tau_M}{K\tau_D} + \tau_M,$$

$$t_{\mathbf{0}}^{out}(x) = \frac{\tau_D+\tau_M}{2\mathbb{E}^2[V]\tau_M^2}\left(2bx - x^2 - 2ab + a^2\right) + \frac{(\tau_D+\tau_M)(b-a)\beta}{\mathbb{E}[V]\tau_M}\coth\left(\frac{a}{\mathbb{E}[V]\tau_M\beta}\right) + \frac{(\tau_D+\tau_M)(1+K\tau_D)}{K\tau_D},$$

$$s^{out}(x) = \frac{\tau_D+\tau_M}{2\mathbb{E}^2[V]\tau_M^2}\left(2bx - x^2 - 2ab + a^2\right) + \frac{(\tau_D+\tau_M)(b-a)\beta}{\mathbb{E}[V]\tau_M}\coth\left(\frac{a}{\mathbb{E}[V]\tau_M\beta}\right) + \frac{(\tau_D+\tau_M)}{K\tau_D} + \tau_M,$$

where

$$\beta = \sqrt{\frac{1+K\tau_D}{K\tau_D}}.$$

We obviously see that all denominator terms are nonzero. Also, each function has symmetry such that

$$s(-a,-x,-b) = s(a,x,b) \qquad \text{and} \qquad t_{\mathbf{0}}(-a,-x,-b) = t_{\mathbf{0}}(a,x,b).$$

Assuming the searcher begins in the detection phase, the average search time across the entire spatial domain:

$$t_m = \frac{1}{2b}\int_{-b}^{b} t_{\mathbf{0}}dx = \frac{1}{2b}\cdot 2\int_{0}^{b} t_{\mathbf{0}}dx = \frac{1}{b}\int_{0}^{a} t_{\mathbf{0}}^{in}dx + \frac{1}{b}\int_{a}^{b} t_{\mathbf{0}}^{out}dx$$

$$t_m = \frac{(\tau_D+\tau_M)}{b}\left[\frac{b}{K\tau_D} + \frac{(b-a)^3}{3\mathbb{E}^2[V]\tau_M^2} + (b-a)\beta^2 + \frac{\beta(b-a)^2}{\mathbb{E}[V]\tau_M}\coth\left(\frac{a}{\mathbb{E}[V]\tau_M\beta}\right)\right]. \quad (1.45)$$

We now turn to the second decoupling case.

Case 2: Second-Order Decoupling

Starting with Equation (1.40), instead of integrating the half-difference of Equations (1.38) and (1.37) to get Equation (1.41), we integrate the half-difference times V to get the following:

$$\mathbb{E}\left[V\frac{t_{\mathbf{V}}(x)-t_{-\mathbf{V}}(x)}{2}\right] = \tau_M\frac{d}{dx}\mathbb{E}\left[V^2\frac{t_{\mathbf{V}}(x)+t_{-\mathbf{V}}(x)}{2}\right]$$

$$\frac{d}{dx}\mathbb{E}\left[V\frac{t_{\mathbf{V}}(x)-t_{-\mathbf{V}}(x)}{2}\right] = \tau_M\frac{d^2}{dx^2}\mathbb{E}\left[V^2\frac{t_{\mathbf{V}}(x)+t_{-\mathbf{V}}(x)}{2}\right]. \quad (1.46)$$

We now use the second-order decoupling assumptions:

$$\mathbb{E}\left[V^2 t_{\mathbf{V}}\right] \simeq \mathbb{E}\left[V^2\right]\mathbb{E}\left[t_{\mathbf{V}}\right], \qquad \mathbb{E}\left[V^2 t_{-\mathbf{V}}\right] \simeq \mathbb{E}\left[V^2\right]\mathbb{E}\left[t_{-\mathbf{V}}\right].$$

Using this approximation with Equation (1.46), we get

$$\frac{d}{dx}\mathbb{E}\left[V\frac{t_{\mathbf{V}}(x)-t_{-\mathbf{V}}(x)}{2}\right] = \mathbb{E}\left[V^2\right]\tau_M\frac{d^2s}{dx^2}.$$

Plugging this into Equation (1.40) gives us our converted motion phase equation:

$$\mathbb{E}\left[V^2\right]\tau_M\frac{d^2s}{dx^2} + \frac{1}{\tau_M}\left[t_{\mathbf{0}}(x)-s(x)\right] = -1.$$

Using the arguments from Case 1 gives us the following system of equations:

$$\begin{cases} \dfrac{1}{\tau_D}\left[s(x)-t_{\mathbf{0}}(x)\right]-KI_a(x)t_{\mathbf{0}}(x)=-1, \\ \mathbb{E}\left[V^2\right]\tau_M\dfrac{d^2s}{dx^2}+\dfrac{1}{\tau_M}\left[t_{\mathbf{0}}(x)-s(x)\right]=-1, \\ \dfrac{ds^{in}}{dx}(0)=0, \qquad \dfrac{ds^{out}}{dx}(b)=0, \\ s^{in}(a)=s^{out}(a), \qquad \dfrac{ds^{in}}{dx}(a)=\dfrac{ds^{out}}{dx}(a). \end{cases}$$

Solving the system gives us

$$t_{\mathbf{0}}^{in}(x)=\frac{(\tau_D+\tau_M)(b-a)\beta}{\sqrt{\mathbb{E}\left[V^2\right]}\tau_M(1+K\tau_D)}\frac{\cosh\left(\dfrac{x}{\sqrt{\mathbb{E}\left[V^2\right]}\tau_M\beta}\right)}{\sinh\left(\dfrac{a}{\sqrt{\mathbb{E}\left[V^2\right]}\tau_M\beta}\right)}+\frac{\tau_D+\tau_M}{K\tau_D},$$

$$s^{in}(x)=\frac{(\tau_D+\tau_M)(b-a)\beta}{\sqrt{\mathbb{E}\left[V^2\right]}\tau_M}\frac{\cosh\left(\dfrac{x}{\sqrt{\mathbb{E}\left[V^2\right]}\tau_M\beta}\right)}{\sinh\left(\dfrac{a}{\sqrt{\mathbb{E}\left[V^2\right]}\tau_M\beta}\right)}+\frac{\tau_D+\tau_M}{K\tau_D}+\tau_M,$$

$$\begin{aligned} t_{\mathbf{0}}^{out}(x)=&\frac{\tau_D+\tau_M}{2\mathbb{E}\left[V^2\right]\tau_M^2}\left(2bx-x^2-2ab+a^2\right)+\frac{(\tau_D+\tau_M)(b-a)\beta}{\sqrt{\mathbb{E}\left[V^2\right]}\tau_M}\coth\left(\frac{a}{\sqrt{\mathbb{E}\left[V^2\right]}\tau_M\beta}\right) \\ &+\frac{(\tau_D+\tau_M)(1+K\tau_D)}{K\tau_D}, \end{aligned}$$

$$\begin{aligned} s^{out}(x)=&\frac{\tau_D+\tau_M}{2\mathbb{E}\left[V^2\right]\tau_M^2}\left(2bx-x^2-2ab+a^2\right)+\frac{(\tau_D+\tau_M)(b-a)\beta}{\sqrt{\mathbb{E}\left[V^2\right]}\tau_M}\coth\left(\frac{a}{\sqrt{\mathbb{E}\left[V^2\right]}\tau_M\beta}\right) \\ &+\frac{(\tau_D+\tau_M)}{K\tau_D}+\tau_M, \end{aligned}$$

where

$$\beta=\sqrt{\frac{1+K\tau_D}{K\tau_D}}.$$

Assuming the searcher begins in the detection phase, the average search time across the entire spatial domain:

$$t_m = \frac{(\tau_D + \tau_M)}{b} \left[\begin{array}{l} \dfrac{b}{K\tau_D} + \dfrac{(b-a)^3}{3\mathbb{E}[V^2]\,\tau_M^2} + (b-a)\beta^2 \\ + \dfrac{\beta(b-a)^2}{\sqrt{\mathbb{E}[V^2]}\tau_M} \coth\left(\dfrac{a}{\sqrt{\mathbb{E}[V^2]}\tau_M \beta} \right) \end{array} \right]. \tag{1.47}$$

We now must assess which expression for the mean search time provides the more accurate description: Equation (1.45), derived under the first-order decoupling assumption or Equation (1.47), obtained from the second-order decoupling assumption.

Numerical Determination of Correct Decoupling Case

The purpose of this numerical study is to determine which of the two formulas for the mean search time provides the more correct approximation. Accordingly, for the remainder of this section, we relabel the first-order decoupling from Equation (1.45) as t_{m_1} and the second-order decoupling from Equation (1.47) as t_{m_2}.

We begin by implementing a basic simulation of the intermittent search process. One key feature of the code is the treatment of detection phase. Whenever the searcher is within the detection zone of radius a, the code compares two independent exponential random variables $T_D \sim \exp(\tau_D)$ (the remaining duration of the detection phase) and $T_K \sim \exp(1/K)$ (the detection time of the target). If $T_K < T_D$, then detection occurs before the detection phase ends, and the target is recorded as found at the current simulation time plus T_K.

A second key step occurs at the end of each detection phase. The code samples a new velocity magnitude from the prescribed probability distribution to be used in the subsequent motion phase. We next evaluate three distinct choices for the probability distribution in order to assess which decoupling assumption yields the more accurate approximation.

Our objective is to determine which approximation is consistent with the simulation outcomes by checking which predicted mean lies within a two-sided 95% confidence interval for the mean. Because the population variance is unknown, the construction uses the Student's t-distribution. For each candidate distribution, we run independent simulations and compute the sample mean $\bar{x}$ and sample standard deviation s. Letting

$t_{0.025,n-1}$ denote the upper 2.5% critical value of the t-distribution, the corresponding margin of error is

$$E = t_{0.025,n-1}\left(\frac{s}{\sqrt{n}}\right)$$

so that the 95% confidence interval for the simulated mean is $(\bar{x}-E, \bar{x}+E)$. Under this interpretation, a 95% confidence interval asserts that the true mean search time falls between this interval. Consequently, if one decoupling assumption's predicated mean is consistently inside these intervals while the other lies outside, we regard the former as the correct decoupling assumption supported by the simulations.

For the first distribution, we consider $V \sim \text{Uniform}[R_1, R_2]$. To ensure the two mean search times are well separated, we fix $a = 1$, $b = 101$, $K = 10^6$, $\tau_D = 1$, $\tau_M = 0.01$, $R_1 = 1$, and $R_2 = 100$ so that $t_{m_1} \approx 13,277.3$ and $t_{m_2} \approx 10,084.7$. We run $n = 1600$ independent simulations and obtain a sample mean $\bar{x} \approx 10652.08$ and sample standard deviation $s \approx 12801.31$, giving the 95% confidence interval $(10,023.9, 11,280.3)$. Since t_{m_2} falls within the interval whereas t_{m_1} does not, the second-order decoupling provides a more accurate approximation in this distribution, while the first-order overestimates the mean search time.

For the second distribution, we use a scaled beta distribution on $[R_1, R_2]$, defined by $V = R_1 + (R_2 - R_1)X$ for $X \sim \text{Beta}(\alpha_b, \beta_b)$. With parameter choices $a = 0.05$, $b = 1$, $K = 50$, $\tau_D = 0.02$, $\tau_M = 0.05$, $R_1 = 0.01$, $R_2 = 1$, $\alpha_b = 0.2$, and $\beta_b = 0.2$, the two mean search times are $t_{m_1} = 35.5773$ and $t_{m_2} = 22.2488$. Running 200 simulations, we obtain a sample mean $\bar{x} \approx 26.07$ and a sample standard deviation $s \approx 28.49$. This produces a 95% confidence interval of $(21.1, 31.1)$. Once again, since t_{m_2} lies within the interval whereas t_{m_1} exceeds the upper bound, the second-order decoupling again provides the more accurate approximation for this distribution, while the first-order decoupling overestimates the mean search time.

For the third choice of a probability distribution, we let V follow a symmetric triangular distribution on $[R_1, R_2]$, namely:

$$f(V) = \begin{cases} \dfrac{4(V-R_1)}{(R_2-R_1)^2}, & \text{if } R_1 \le V < \dfrac{R_2+R_1}{2} \\ \dfrac{4(R_2-V)}{(R_2-R_1)^2}, & \text{if } \dfrac{R_2+R_1}{2} < V \le R_2 \end{cases}$$

To assess the accuracy of the two decoupling approximations, we again perform a study of 200 simulations using the parameter set $a = 50$, $b = 2050$, $K = 10$, $\tau_D = 1$, $\tau_M = 1$, $R_1 = 1$, and $R_2 = 100$. For these values, the mean search times are calculated as $t_{m1} = 1132.45$ and $t_{m2} = 988.47$. The study provides a sample mean $\bar{x} \approx 918.77$ and a sample standard deviation $s \approx 892.46$, producing a 95% confidence interval of $(718.6, 1118.9)$. As in the previous distributions t_{m_2} lies within the confidence interval, whereas t_{m_1} exceeds the upper endpoint. This again indicates that the second-order decoupling provides the more accurate approximation of the mean search time for this distribution.

Taken together, all three distributions in this section consistently support the second-order decoupling assumption from Case 2. In view of this consistency and its agreement with the higher-dimensional models, we therefore conclude that Case 2 is the preferable approximation. We now turn to Equation (1.47) to derive approximate values for the minimal durations for the detection and motion phases.

Under the assumption of low target density, where $a \ll b$, and $\frac{a}{\sqrt{\mathbb{E}[V^2]}\tau_M} \ll 1$ for further simplification, we can reduce Equation (1.47) using the asymptotic approximation $b - a \approx b$:

$$t_m = (\tau_D + \tau_M)\left[\frac{1}{K\tau_D} + \frac{b^3}{3\mathbb{E}[V^2]\,\tau_M^2} + \beta^2 + \frac{\beta b^2}{\sqrt{\mathbb{E}[V^2]}\tau_M} \coth\left(\frac{a}{\sqrt{\mathbb{E}[V^2]}\tau_M\beta}\right)\right]. \quad (1.48)$$

We further simplify the hyperbolic cotangent. Considering $\frac{a}{\sqrt{\mathbb{E}[V^2]}\tau_M} \ll 1$, we see that

$$\beta = \sqrt{\frac{1 + K\tau_D}{K\tau_D}} = \sqrt{\frac{1}{K\tau_D} + 1} > 1$$

so that $\frac{a}{\sqrt{\mathbb{E}[V^2]}\tau_M\beta}$ is small. Since for small x, we know that

$$\coth x = \frac{1}{x} + \mathcal{O}(x),$$

we see that

$$\frac{1}{\sqrt{\mathbb{E}[V^2]}\tau_M} \coth\left(\frac{a}{\sqrt{\mathbb{E}[V^2]}\tau_M\beta}\right) \approx \frac{1}{\sqrt{\mathbb{E}[V^2]}\tau_M}\left[\frac{1}{a/\left(\sqrt{\mathbb{E}[V^2]}\tau_M\beta\right)}\right] = \frac{\beta}{a}.$$

Using this, we fully simplify Equation (1.48) to the following:

$$t_m = (\tau_D + \tau_M)\left[\frac{1}{K\tau_D} + \frac{b^3}{3\mathbb{E}[V^2]\,\tau_M^2} + \beta^2 + \frac{\beta^2 b^2}{a}\right]$$

$$t_m = (\tau_D + \tau_M)\left[\frac{b^3}{3\mathbb{E}[V^2]\,\tau_M^2} + \frac{\beta^2 b^2}{a}\right] \tag{1.49}$$

since the b-terms dominate.

To minimize Equation (1.49) with respect to (τ_D, τ_M), we compute the associated critical point and obtain the following:

$$(\tau_D^*, \tau_M^*) = \left(\sqrt{\frac{a}{\sqrt{\mathbb{E}[V^2]}k}}\left(\frac{b}{12a}\right)^{1/4}, \frac{a}{\sqrt{\mathbb{E}[V^2]}}\sqrt{\frac{b}{3a}}\right) \tag{1.50}$$

Additionally, since the Hessian determinant is

$$\begin{aligned} D(\tau_D^*, \tau_M^*) &= \left[\frac{\partial^2 t_m}{\partial \tau_D^2}\frac{\partial^2 t_m}{\partial \tau_M^2} - \left(\frac{\partial^2 t_m}{\partial \tau_D \partial \tau_M}\right)^2\right]_{\substack{\tau_D=\tau_D^* \\ \tau_M=\tau_M^*}} \\ &= \frac{2ab^5\left(3 + \sqrt{\frac{2ak}{\sqrt{\mathbb{E}[V^2]}}}\left(\frac{27b}{a}\right)^{1/4}\right)}{81k^2\tau_D^4\mathbb{E}^6[V]\,\tau_M^6} > 0 \end{aligned}$$

and

$$\frac{\partial^2 t_m}{\partial \tau_D^2} = 4\sqrt{\frac{2k\sqrt{\mathbb{E}[V^2]}}{a}}\left(\frac{3b^3}{a^3}\right)^{1/4} > 0,$$

we know (τ_D^*, τ_M^*) is an approximate minimizer of t_m by the Second Derivative Test.

As seen in the original derivation, the mean duration τ_M^* of the motion phase is not dependent on K, however the durations of each phase are dependent on the second moment $\mathbb{E}\left[V^2\right]$ rather than on the mean speed $\mathbb{E}[V]$.

1.4.4 Summary for Chapter 1

In this chapter, we extended the classical intermittent-search framework derived by Bénichou, et al. [20] in one, two, and three spatial dimensions by allowing the searcher's speed to vary. Rather than assuming a constant velocity magnitude V, we modeled V as a random variable chosen from an arbitrary distribution with density f. For each dimension, we derived and solved the governing equations for the detection and motion phases, used these solutions to obtain an expression for the mean search time over the domain, and then determined approximate phase durations (τ_D^*, τ_M^*) that minimized the mean search time. Although our results largely aligned with those reported in the original work, the distribution of velocity magnitudes provided additional insights into how the components of speed influences the optimal durations of each phase.

For example, we can interpret the constant velocity in the original model as a random variable V being chosen from a distribution with density $f(v) = \delta_V(v)$, where $\delta_V(v)$ is the Kronecker delta function

$$\delta_V(v) = \begin{cases} 1, & v = V \\ 0, & v \neq V. \end{cases}$$

Since V is the only possibility, the mean and variance of the distribution are $\mathbb{E}[V] = V$ and $\mathrm{Var}(V) = 0$ so that the first-order and second-order moments are equal:

$$\mathbb{E}\left[V^2\right] = \mathbb{E}^2[V] = V^2.$$

However, the original formulations do not make explicit which velocity moment governs the appearance of V^2 in the final expressions. Our analysis clarifies this point: in each dimension, the mean search time depends naturally on the second moment $\mathbb{E}\left[V^2\right]$, rather than solely on the first $\mathbb{E}[V]$, which might be the more immediate expectation.

Several directions for future work follow from some modeling assumptions we made. First, the directions of the motion phase could be treated more realistically. We assumed uniform angle selection in two and three dimensions and symmetric left-right motion in one dimension, and while analytically convenient, these assumptions may not accurately

represent biologically motivated search behavior. Incorporating preferences for specific direction would better reflect natural behaviors and prevent scenarios where a searcher could repeatedly move between two locations without broader exploration.

Second, future studies could relax the assumption that the velocity magnitude and direction are chosen independently. In many biological settings, these quantities are plausibly coupled. For example, a searcher may move more cautiously when traveling in a particular due to terrain or perceived risk and could move more quickly along directions associated with favorable cues such as familiarity. Introducing such statistical dependence between speed and direction could yield yet further understanding of the intermittent search dynamics.

Chapter 2

Modeling Intermittent Search Strategy with a 2nd Detection Zone

2.1 Background

In the Background Section 1.1 of Chapter 1, we discussed how the authors of "Intermittent Search Strategies" [20] introduced three distinct modes through which a searcher located a target during the detection phase. While our discussion previously centered on the "static mode," this model extension focuses on another. The "diffusive mode" involved the searcher walking continuously with a diffusion coefficient D. Additionally, the searcher detected the target instantaneously upon entering the detection zone.

Although the original study explored additional aspects, this analysis emphasizes intermittent search strategies within one- and two-dimensional spaces. The following sections recount how diffusion during the detection phase modifies these models, incorporating supplementary insights from Loverado et al. [4].

2.1.1 Diffusive One-Dimensional Case

In the one-dimensional "diffusive" model, the domain was represented as a line segment $[-b, b]$, where the target was positioned at $x = 0$. During the detection phase, the searcher exhibited a continuous random walk governed by a diffusion coefficient D. The search stopped upon entering a detection zone, defined as a circle with radius a centered around the target. A visual representation of this model is provided in Figure 2.1. The system

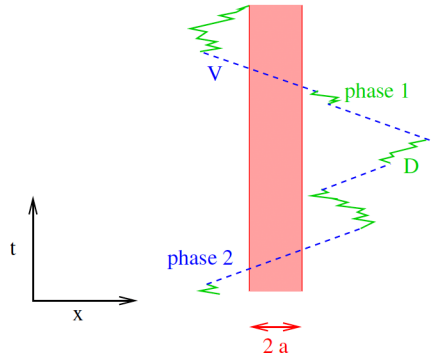

Figure 2.1: Dynamic model in 1D designed by Loverado et al. [4] illustrating how a searcher found the target through time.

of backward equations governing this process for mean first-passage times, along with the associated boundary conditions, was formulated as follows:

$$\begin{cases} D\dfrac{d^2t_1}{dx^2} + \dfrac{1}{\tau_1}(t_2 - t_1) = -1 \\ V^2\tau_2\dfrac{d^2t_2}{dx^2} + \dfrac{1}{\tau_2}(t_1 - t_2) = -1^* \\ t_1^{out}(a) = 0, \qquad \dfrac{dt_2^{in}}{dx}(0) = 0, \qquad \dfrac{dt_1^{out}}{dx}(b) = 0, \qquad \dfrac{dt_2^{out}}{dx}(b) = 0, \\ t_2^{in}(a) = t_2^{out}(a), \qquad \dfrac{dt_2^{in}}{dx}(a) = \dfrac{dt_2^{out}}{dx}(a). \end{cases}$$

Here, $t_2 = \frac{1}{2}\left(t_2^+ + t_2^-\right)$, where t_2^+ and t_2^- denoted the mean first-passage times for the motion phase when moving to the right with a positive velocity V and to the left with a negative velocity $-V$, respectively. Furthermore, t_1 represented the mean first-passage time associated with starting search in the detection phase. The notation t_1^{in} and t_2^{in} expressed the equations for scenarios where the search began inside the detection zone ($r \leq a$), while t_1^{out} and t_2^{out} were the equations corresponding to starting search outside the detection zone ($r > a$).

Although the authors solved the system without presenting the explicit results, they utilized the solved t_1^{out} equation to compute the overall mean first-passage time t_m across the entire spatial domain. Due to the length of the solution, this dissertation does not provide the full formulation, which can be found in Loverado et al. [4].

Through numerically studying the minimum of t_m, they determined that intermittence was favorable whenever $b > \frac{D}{V}$.

2.1.2 Diffusive Two-Dimensional Case

Again, in the "diffusive mode", the searcher operated under a diffusion coefficient D during the detection phase, instantly locating the target whenever entering the detection

*This amendment addresses another typographical error in the original publication, where the equation was incorrectly reported as $V^2\tau_2\dfrac{dt_2}{dx} + \dfrac{1}{\tau_2}(t_1 - t_2) = -1$.

zone. During the motion phase, the searcher moved ballistically with a velocity $\vec{V}$, where V was the magnitude and $\theta_{\vec{V}}$. A visual representation of the two-dimensional model is found in Figure 2.2. The system of backward equations for the mean first-passage times took the following form:

$$\begin{cases} D\Delta t_1(\vec{r}) + \dfrac{1}{2\pi\tau_1}\displaystyle\int_0^{2\pi} [t_2(\vec{r}) - t_1(\vec{r})]\, d\theta_{\vec{V}} = -1 \\ \vec{V}\cdot\nabla t_2(\vec{r}) + \dfrac{1}{\tau_2}\,[t_2(\vec{r}) - t_1(\vec{r})] = -1 \\ t_1(\vec{r}) = 0, \qquad |\vec{r}| \le a, \end{cases}$$

where t_1 and t_2 denoted the mean first-passage time associated when initiating search in the detection phase and motion phase, respectively. Since the primary objective was to compute the overall mean first-passage time across the entire domain starting in the *detection phase*, the authors ultimately did not need to determine t_2. To address the seemingly unsolvable system, Bénichou et al. [21] introduced an auxiliary function $s = \frac{1}{2\pi}\int_0^{2\pi} t_2 d\theta_{\vec{V}}$, converting the system into the following polar form:

$$\begin{cases} D\Delta t_1 + \dfrac{1}{\tau_1}(s - t_1) = -1, \\ \tilde{D}\Delta s + \dfrac{1}{\tau_2}\,(t_1 - s) = -1, \qquad \text{where } \tilde{D} = \dfrac{V^2\tau_2}{2}, \\ t_1(r) = 0, \qquad r \le a. \end{cases}$$

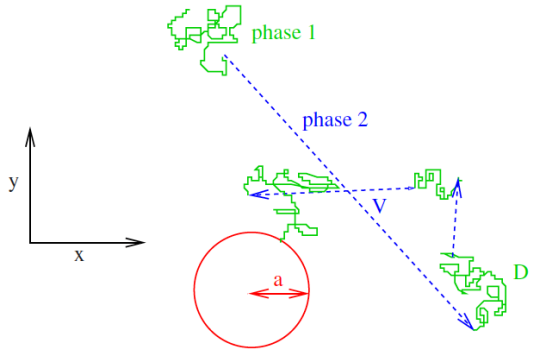

Figure 2.2: Diffusive model in 2D designed by Loverado et al. [4] illustrating how a "diffusive" searcher found the target through time.

The domain was naturally divided into two regions: inside the detection zone ($r \leq a$) and outside the target detection zone ($r > a$). The following boundary conditions were considered:

$$\lim_{r\to 0} s(r) \text{ remains finite}, \qquad \frac{dt_1^{out}}{dr}(b) = 0, \qquad \frac{ds^{out}}{dr}(b) = 0,$$

$$t_1^{out}(a) = t_1^{in}(a), \qquad s^{out}(a) = s^{in}(a), \qquad \frac{ds^{out}}{dr}(a) = \frac{ds^{in}}{dr}(a),$$

Although they did not present the final solutions explicitly, Bénichou et al. [21] did provide general solutions containing unknown constants:

$$t_1^{out}(r) = -\frac{1}{4}\frac{r^2(\tau_1+\tau_2)}{D\tau_1+\tilde{D}\tau_2} + A_1 + A_2\ln(r) + A_3 I_0(\alpha r) + A_4 K_0(\alpha r),$$

$$s^{out}(r) = \frac{\left(D-\tilde{D}\right)\tau_1\tau_2 - r^2(\tau_1+\tau_2)/4}{D\tau_1+\tilde{D}\tau_2} + A_1 + A_2\ln(r) - \frac{D\tau_1}{\tilde{D}\tau_2}\left(A_3 I_0(\alpha r) + A_4 K_0(\alpha r)\right),$$

$$t_1^{in}(r) \equiv 0,$$

$$s^{in}(r) = \tau_2 + A_5 I_0\left(\frac{r}{\sqrt{\tilde{D}\tau_2}}\right) + A_6 K_0\left(\frac{r}{\sqrt{\tilde{D}\tau_2}}\right),$$

where

$$\alpha = \sqrt{\frac{D\tau_1+\tilde{D}\tau_2}{D\tau_1\tilde{D}\tau_2}}, \qquad \tilde{D} = \frac{V^2\tau_2}{2}.$$

After applying the boundary conditions to solve for the six unknown constants, the authors successfully determined the mean search time across the entire domain:

$$t_m = \frac{(\tau_1+\tau_2)\left(1-\frac{a^2}{b^2}\right)}{(\alpha^2 D\tau_1)^2}\left[-\frac{\alpha^2 D\tau_1}{8\tilde{D}\tau_2}\frac{\left(3-4\ln\frac{b}{a}\right)b^4 - 4a^2b^2 + a^4}{b^2-a^2} + a\alpha\left(\frac{b^2}{a^2}-1\right)\frac{M}{2L_+} - \frac{L_-}{L_+}\right], \tag{2.1}$$

where

$$L_\pm = I_0\left(\frac{a}{\sqrt{\tilde{D}\tau_2}}\right)\left(I_1(b\alpha)K_1(a\alpha) - I_1(a\alpha)K_1(b\alpha)\right)$$
$$\pm\,\alpha\sqrt{\tilde{D}\tau_2}\, I_1\left(\frac{a}{\sqrt{\tilde{D}\tau_2}}\right)\left(I_1(b\alpha)K_0(a\alpha) + I_0(a\alpha)K_1(b\alpha)\right)$$

and

$$M = I_0\left(\frac{a}{\sqrt{\tilde{D}\tau_2}}\right)\left(I_1(b\alpha)K_0(a\alpha)+I_0(a\alpha)K_1(b\alpha)\right) - \frac{4a^2\sqrt{\tilde{D}\tau_2}}{\alpha\left(b^2-a^2\right)^2}I_1\left(\frac{a}{\sqrt{\tilde{D}\tau_2}}\right)\left(I_1(b\alpha)K_1(a\alpha)-I_1(a\alpha)K_1(b\alpha)\right).$$

Comparing this equation with the diffusion-alone, the authors determined that intermittence was only favorable whenever $b \gg \frac{D}{V}$.

2.2 Extension Models with 2nd Detection Zone

In the diffusion model of the original intermittent search strategy proposed by Bénichou et al. [20], detection of the target occurred through a single means: automatic identification when the searcher approached within a critical distance of the target. Biologically, this could represent visual recognition at a close range. However, in natural settings, animals rely on multiple sensory processes during searching, like olfaction or audition. These processes typically operate over longer ranges and introduce an element of uncertainty to detection.

To incorporate this added realism, we extend our model by introducing a second detection zone, allowing us to account for the effects of additional sensory input. The domain is now divided into three regions, each defined with respect to a stationary target:

1) **Inside first detection zone**: This region is located within a small distance from the target. Upon entering this zone during the detection phase, the searcher automatically detects the target.

2) **Intermediate, middle detection zone**: This region lies slightly farther from the target. Within this zone, the searcher detects the target through a Poisson process with a constant rate during the detection phase, representing the uncertain influence of long-range sensory cues.

3) **Outside any detection zones**: This region is located furthest from the target. The searcher has no capacity to detect the target.

This refinement enables the model to more accurately reflect the diverse sensory strategies employed in biological search behavior. We apply this to the one- and two–dimensional versions of the model. Our goal is to determine the conditions under which intermittence proves favorable compared to diffusion alone. To achieve this, we first establish the new models for diffusion alone.

2.2.1 One-Dimensional Case

The one-dimensional model has a line segment domain $[-b,b]$, where the searcher immediately finds the target when located within the first detection zone $[-a,a]$. Additionally, within the second detection zone $[-c,-a)\cup(a,c]$, the searcher can detect the target at a fixed rate K. The three regions are illustrated in Figure 2.3.

We consider both the diffusion-alone model and the intermittence model.

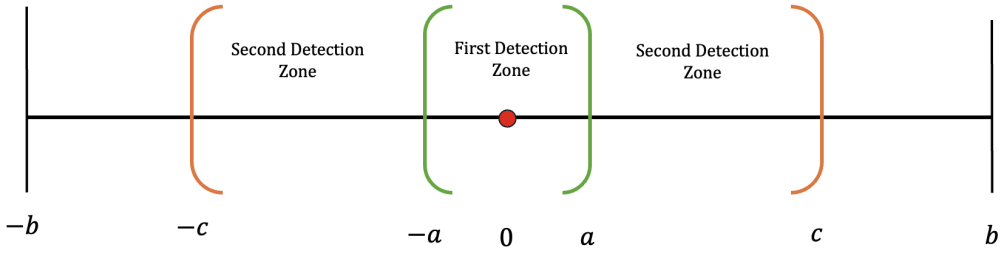

Figure 2.3: Diagram of the one-dimensional domain with two detection zones.

Diffusion Only: One-Dimensional Case

During the diffusion-only model, the searcher engages exclusively in a random walk characterized by a diffusion coefficient D until the target is located.

Let $\mathscr{Y} = [-b,b]$ denote the spatial domain. For the state domain, the searcher is either in the detection phase (labeled $j = \mathbf{0}$) or the termination phase (labeled $j = \mathbf{A}$); thus, we define the state domain as as $\mathscr{J} = \{\mathbf{0},\mathbf{A}\}$. Lastly, the absorbing set is $A = \{(y,\mathbf{0}) \in \mathscr{Y} \times \mathscr{J} \,|\, y \in [-a,a]\}$, corresponding to the searcher entering the first detection zone while in the detection phase.

We now derive the equation characterizing this process. Following the method from Chapter 1.3, the one-dimensional version of the general Equation (1.15) is given by:

$$\mu_Y(0,x,i)\frac{dt_i(x)}{dx}+\frac{1}{2}\sigma_Y^2(0,x,i)\frac{d^2t_i(x)}{dx^2}+\int_{\varsigma\neq i}\Lambda(0,x,\varsigma|x,i)\left[t_\varsigma(x)-t_i(x)\right]d\varsigma=-1 \quad (2.2)$$

where $\Lambda(0,x,\varsigma|x,i)$ denotes the transition rate out of the initial state i when starting search at location x.

With the lack of drift and diffusion coefficient D, the following parameters are defined:

$$\mu_Y(0,x,\mathbf{0})=0 \quad \text{and} \quad \frac{1}{2}\sigma_Y^2(0,x,\mathbf{0})=D.$$

The jump (integral) term accounts for transitions out the detection phase by detection of the target. In the case where the target is found, the searcher transitions to state $i=\mathbf{A}$ at a fixed rate of K, provided that the searcher is between the distance of a and c of the target. This transition is governed by the following relationship:

$$\Lambda(0,x,\mathbf{A}|x,\mathbf{0})[t_\mathbf{A}(x)-t_\mathbf{0}(x)]=K\left(I_c(x)-I_a(x)\right)\left[0-t_\mathbf{0}(x)\right]=-K\left(I_c(x)-I_a(x)\right)t_\mathbf{0}(x),$$

where $I_y(x)$ denotes the indicator function

$$I_y(x)=\begin{cases}1, & x\leq y\\ 0, & x>y.\end{cases}$$

Since the process ends upon detecting the target, no additional time is spent in the termination phase $i=\mathbf{A}$, leading to $t_\mathbf{A}(x)\equiv 0$. Substituting these expressions into Equation (2.2) results in the following equation:

$$D\frac{d^2t_\mathbf{0}(x)}{dx^2}-K\left(I_c(x)-I_a(x)\right)t_\mathbf{0}(x)=-1.$$

As previously stated, the function $t_\mathbf{0}$ can be partitioned into three distinct regions, defined as follows:

$$t_{\mathbf{0}}(x) = \begin{cases} t_{\mathbf{0}}^{in}(x), & \text{if } x \in [-a,a], \\ t_{\mathbf{0}}^{mid}(x), & \text{if } x \in [-c,a) \cup (a,c], \\ t_{\mathbf{0}}^{out}(x), & \text{if } x \in [-b,-c) \cup (c,b]. \end{cases}$$

To determine the boundary conditions, we leverage the symmetry $x \leftrightarrow -x$, allowing us to focus solely on the nonnegative region $[0,b]$. At the reflective boundary $x = b$, the derivative satisfies

$$\frac{dt_{\mathbf{0}}^{out}}{dx}(b) = 0.$$

Assuming continuity conditions of both $t_{\mathbf{0}}$ and $\frac{dt_{\mathbf{0}}}{dx}$ at $x = c$ yields

$$t_{\mathbf{0}}^{mid}(c) = t_{\mathbf{0}}^{out}(c), \qquad \frac{dt_{\mathbf{0}}^{mid}}{dx}(c) = \frac{dt_{\mathbf{0}}^{out}}{dx}(c).$$

Additionally, assuming continuity at $x = a$ imposes the following condition:

$$t_{\mathbf{0}}^{mid}(a) = t_{\mathbf{0}}^{in}(a) = 0,$$

highlighting that no time is spent hunting within the first detection zone. Solving this system gives us

$$\begin{aligned} t_{\mathbf{0}}^{in} &\equiv 0, \\ t_{\mathbf{0}}^{mid} &= \left(\frac{b-c}{\sqrt{DK}} - \frac{e^{-\sqrt{\frac{K}{D}}(c-a)}}{K} \right) \frac{\sinh\left(\sqrt{\frac{K}{D}}(x-a)\right)}{\cosh\left(\sqrt{\frac{K}{D}}(c-a)\right)} + \frac{1}{K}\left(1 - e^{-\sqrt{\frac{K}{D}}(x-a)}\right), \\ t_{\mathbf{0}}^{out} &= \left(\frac{b-c}{\sqrt{DK}} - \frac{e^{-\sqrt{\frac{K}{D}}(c-a)}}{K} \right) \tanh\left(\sqrt{\frac{K}{D}}(c-a)\right) - \frac{1}{2D}(2b-c-x)(c-x) \\ &\qquad + \frac{1}{K}\left(1 - e^{-\sqrt{\frac{K}{D}}(c-a)}\right). \end{aligned}$$

We use these functions to determine the mean search time over all space as follows:

$$t_{diff} = \frac{1}{2b}\int_{-b}^{b} t_{\mathbf{0}}dx = \frac{1}{2b}\cdot 2\int_{0}^{b} t_{\mathbf{0}}dx = \frac{1}{b}\int_{0}^{a} t_{\mathbf{0}}^{in}dx + \frac{1}{b}\int_{a}^{c} t_{\mathbf{0}}^{mid}dx + \frac{1}{b}\int_{c}^{b} t_{\mathbf{0}}^{out}dx$$

$$\begin{aligned} t_{diff} = {} & \frac{1}{bK}\left(2b - c - a + \frac{(b-c)^3 K}{3D}\right) - \frac{2(b-c)}{bK}\operatorname{sech}\left(\sqrt{\frac{K}{D}}(c-a)\right) \\ & + \frac{1}{bK}\left(\frac{(b-c)^2 K}{D} - 1\right)\sqrt{\frac{D}{K}}\tanh\left(\sqrt{\frac{K}{D}}(c-a)\right). \end{aligned} \tag{2.3}$$

Having established the diffusion-alone model, we now proceed to examine intermittence in one dimension.

Intermittence: One-Dimensional Case

During intermittence, the searcher continuously switches between a detection phase and motion phase before finding the target in the termination phase. The detection phase is characterized by the searcher performing a random walk with diffusion coefficient D while the motion phase has the searcher traveling ballistically with a constant velocity magnitude V, choosing the left or right direction with equal probability.

Let $\mathscr{Y} = [-b, b]$ and $\mathscr{J} = \{\mathbf{0}, -\mathbf{1}, \mathbf{1}, \mathbf{A}\}$ denote the spatial domain and state domain, respectively, where $j = \mathbf{0}$ represents the detection phase, $j = -\mathbf{1}$ and $j = \mathbf{1}$ correspond to the motion phase when moving to the left or right, respectively, and $j = \mathbf{A}$ denotes the termination phase. Lastly, the absorbing set is $A = \{(y, \mathbf{0}) \in \mathscr{Y} \times \mathscr{J} : y \in [-a, a]\}$, corresponding to the searcher entering the first detection zone while in the detection phase.

Following the method from Chapter 1.3, the one-dimensional version of Equation (1.15) is given by:

$$\mu_Y(0,x,i)\frac{dt_i(x)}{dx} + \frac{1}{2}\sigma_Y^2(0,x,i)\frac{d^2 t_i(x)}{dx^2} + \int_{\varsigma \neq i} \Lambda(0,x,\varsigma|x,i)\left[t_\varsigma(x) - t_i(x)\right] d\varsigma = -1 \tag{2.4}$$

where $\Lambda(0,x,\varsigma|x,i)$ denotes the transition rate out of the initial state i when starting search at location is x.

We first derive the equation for the **detection phase**. Represented by state $i = 0$, we define the drift and diffusive coefficients as the following:

$$\mu_Y(0,x,\mathbf{0}) = 0 \quad \text{and} \quad \frac{1}{2}\sigma_Y^2(0,x,\mathbf{0}) = D.$$

The jump (integral) term accounts for transitions out of the detection phase, either to a state within the motion phase or through discovering the target. When transitioning to the motion phase, the state switches to $i = -\mathbf{1}$ or $i = \mathbf{1}$ at a fixed rate $1/\tau_D$. Assuming equal likelihood of moving left or right, each transition occurs with a probability of $\frac{1}{2}$. The relationships governing these transitions are defined as follows:

$$\Lambda(0,x,-\mathbf{1}|x,\mathbf{0}) = \frac{1}{2}\frac{1}{\tau_D} \qquad \text{and} \qquad \Lambda(0,x,\mathbf{1}|x,\mathbf{0}) = \frac{1}{2}\frac{1}{\tau_D}.$$

In the case where the target is found, detection occurs at a fixed rate K, provided the searcher is within a distance $a \in (0,b)$ from the target. Since this process occurs within the detection phase, transition into the termination phase ($i = \mathbf{A}$) is governed by the following relationship:

$$\Lambda(0,x,\mathbf{A}|x,\mathbf{0})[t_{\mathbf{A}}(x) - t_{\mathbf{0}}(x)] = K\left(I_c(x) - I_a(x)\right)[0 - t_{\mathbf{0}}(x)] = -K\left(I_c(x) - I_a(x)\right)t_{\mathbf{0}}(x),$$

where $I_y(x)$ denotes the indicator function

$$I_y(x) = \begin{cases} 1, & x \le y \\ 0, & x > y. \end{cases}$$

Since the process ends upon detecting the target, no additional time is spent in state $i = \mathbf{A}$, leading to $t_{\mathbf{A}}(x) \equiv 0$.

Substituting these expressions into Equation (2.4) results in the detection phase equation for state $i = \mathbf{0}$:

$$D\frac{d^2 t_{\mathbf{0}}}{dx^2} + \frac{1}{\tau_D}\left(\frac{t_{-\mathbf{1}} + t_{\mathbf{1}}}{2} - t_{\mathbf{0}}\right) - K\left(I_c(x) - I_a(x)\right)t_{\mathbf{0}} = -1 \tag{2.5}$$

Now, we derive the equations for the states in the **motion phase**. Starting with state $i = \mathbf{1}$, we define the drift and diffusive coefficients as follows:

$$\mu_Y(0,x,\mathbf{1}) = V \quad \text{and} \quad \frac{1}{2}\sigma_Y^2(0,x,\mathbf{1}) = 0.$$

Since the motion phase can only transition into the detection phase at a fixed rate $1/\tau_M$, the jump term can be rewritten as follows:

$$\Lambda(0,x,\mathbf{0}|x,\mathbf{1})[t_{\mathbf{0}}(x)-t_{\mathbf{1}}(x)] = \frac{1}{\tau_M}[t_{\mathbf{0}}(x)-t_{\mathbf{1}}(x)].$$

Substituting these into Equation (2.4) gives us the motion phase equation for state $i=1$:

$$V\frac{dt_{\mathbf{1}}}{dx} + \frac{1}{\tau_M}(t_{\mathbf{0}}-t_{\mathbf{1}}) = -1. \tag{2.6}$$

By similar arguments, the motion phase equation for state $i=-1$ is as follows:

$$-V\frac{dt_{-\mathbf{1}}}{dx} + \frac{1}{\tau_M}(t_{\mathbf{0}}-t_{-\mathbf{1}}) = -1. \tag{2.7}$$

Recall that our goal is to determine the average search time whenever the searcher begins in the detection phase. This means we only need to solve $t_{\mathbf{0}}$. To simplify the equations, we follow the methodology outlined by Loverdo et al. [4]. We consider two new equations, namely, the average of both motion phase states and the half difference of both motion phase states:

$$s = \frac{t_{\mathbf{1}}+t_{-\mathbf{1}}}{2}, \qquad \text{and} \qquad \tilde{s} = \frac{t_{\mathbf{1}}-t_{-\mathbf{1}}}{2}.$$

Taking the half difference of Equations (2.6) and (2.7) results in the following:

$$\tilde{s} = V\tau_M\frac{ds}{dx}. \tag{2.8}$$

Then averaging Equations (2.6) and (2.7) gives us

$$V\frac{d\tilde{s}}{dx} + \frac{1}{\tau_M}(t_{\mathbf{0}}-s) = -1. \tag{2.9}$$

Substituting Equation (2.8) into Equation (2.9) results in the following:

$$V^2\tau_M\frac{d^2s}{dx^2} + \frac{1}{\tau_M}(t_{\mathbf{0}}-s) = -1.$$

As previously established, the domain is partitioned into three distinct regions: the area within the first detection zone $(x \le a)$, the region encompassing the second detection zone $(a < x \le c)$, and the area outside any detection zone $(x > c)$. For notation, we adopt superscripts *in*, *mid*, and *out* to denote these respective regions.

We now turn our attention to the boundary conditions. Owing to the inherent symmetry $x \leftrightarrow -x$, we only need to consider the nonnegative region $[0,b]$. Consequently, this implies that

$$s^{in}(-x) = \frac{t_{\mathbf{1}}^{in}(-x) + t_{-\mathbf{1}}^{in}(-x)}{2} = \frac{t_{\mathbf{1}}^{in}(x) + t_{-\mathbf{1}}^{in}(x)}{2} = s^{in}(x)$$

so that

$$-\frac{ds^{in}}{dx}(-x) = \frac{ds^{in}}{dx}(x).$$

Setting $x = 0$ gives us the boundary condition:

$$\frac{ds^{in}}{dx}(0) = 0.$$

Considering reflective boundaries with respect to the motion phase, we have the boundary condition:

$$\frac{dt_{\mathbf{0}}^{out}}{dr}(b) = 0$$

and

$$\frac{ds^{out}}{dr}(b) = \frac{1}{2}\frac{dt_{\mathbf{1}}^{out}}{dr}(b) + \frac{1}{2}\frac{dt_{-\mathbf{1}}^{out}}{dr}(b) = \frac{1}{2}(0) + \frac{1}{2}(0) = 0.$$

As the searcher moves through the domain, we desire continuity of the motion phase states $t_{\mathbf{1}}$ and $t_{-\mathbf{1}}$, along with their first derivatives, at $x = a$ and $x = c$ such that

$$s^{mid}(a) = \frac{t_{\mathbf{1}}^{mid}(a) + t_{-\mathbf{1}}^{mid}(a)}{2} = \frac{t_{\mathbf{1}}^{in}(a) + t_{-\mathbf{1}}^{in}(a)}{2} = s^{in}(a),$$

$$s^{mid}(c) = \frac{t_{\mathbf{1}}^{mid}(c) + t_{-\mathbf{1}}^{mid}(c)}{2} = \frac{t_{\mathbf{1}}^{out}(c) + t_{-\mathbf{1}}^{out}(c)}{2} = s^{out}(c),$$

$$\frac{ds^{mid}}{dr}(a) = \frac{1}{2}\frac{dt_{\mathbf{1}}^{mid}}{dr}(a) + \frac{1}{2}\frac{dt_{-\mathbf{1}}^{mid}}{dr}(a) = \frac{1}{2}\frac{dt_{\mathbf{1}}^{in}}{dr}(a) + \frac{1}{2}\frac{dt_{-\mathbf{1}}^{in}}{dr}(a) = \frac{ds^{out}}{dr}(a),$$

and

$$\frac{ds^{mid}}{dr}(c) = \frac{1}{2}\frac{dt_{\mathbf{1}}^{mid}}{dr}(c) + \frac{1}{2}\frac{dt_{-\mathbf{1}}^{mid}}{dr}(c) = \frac{1}{2}\frac{dt_{\mathbf{1}}^{out}}{dr}(c) + \frac{1}{2}\frac{dt_{-\mathbf{1}}^{out}}{dr}(c) = \frac{ds^{out}}{dr}(c).$$

Additionally, we desire continuity of the detection phase state $t_{\mathbf{0}}$ at $x = a$ and $x = c$ such that

$$t_{\mathbf{0}}^{mid}(c) = t_{\mathbf{0}}^{out}(c) \qquad \text{and} \qquad t_{\mathbf{0}}^{mid}(a) = t_{\mathbf{0}}^{in}(a) = 0.$$

Since discovering the target in the detection phase is automatic within the first detection zone, $t_{\mathbf{0}}^{in}(x) \equiv 0$ for all $x \leq a$. Lastly, since solving the system results in 10 unknown constants, we require an additional condition of continuity of the first derivative of t_0 at $x = c$:

$$\frac{dt_{\mathbf{0}}^{mid}}{dr}(c) = \frac{dt_{\mathbf{0}}^{out}}{dr}(c).$$

This gives us the following system of equations:

$$\begin{cases} D\dfrac{d^2t_{\mathbf{0}}}{dx^2} + \dfrac{1}{\tau_D}(s - t_{\mathbf{0}}) - K(I_c(x) - I_a(x))\,t_{\mathbf{0}} = -1, \\ V^2\tau_M\dfrac{d^2s}{dx^2} + \dfrac{1}{\tau_M}(t_{\mathbf{0}} - s) = -1, \\ \dfrac{ds^{in}}{dx}(0) = 0, \quad \dfrac{dt_{\mathbf{0}}^{out}}{dx}(b) = 0, \quad \dfrac{ds^{out}}{dx}(b) = 0, \\ t_{\mathbf{0}}^{mid}(a) = 0, \quad s^{mid}(a) = s^{in}(a), \quad \dfrac{ds^{mid}}{dx}(a) = \dfrac{ds^{in}}{dx}(a), \\ t_{\mathbf{0}}^{mid}(c) = t_{\mathbf{0}}^{out}(c), \quad \dfrac{dt_{\mathbf{0}}^{mid}}{dr}(c) = \dfrac{dt_{\mathbf{0}}^{out}}{dr}(c), \quad s^{mid}(c) = s^{out}(c), \quad \dfrac{ds^{mid}}{dx}(c) = \dfrac{ds^{out}}{dx}(c). \end{cases}$$

Solving the system yields

$$t_{\mathbf{0}}^{in} \equiv 0,$$

$$
\begin{aligned}
s^{in} = \tau_M &+ \frac{(\tau_D+\tau_M)(b-c)B_1B_4}{\phi_+\phi_-\left(D\tau_D+V^2\tau_M^2\right)L\mathscr{D}}\frac{\cosh\left(\frac{x}{V\tau_M}\right)}{\cosh\left(\frac{a}{V\tau_M}\right)} \\
&+ \frac{(\tau_D+\tau_M)(b-c)\left(K\tau_D-D\tau_D\phi_+^2\right)\left(K\tau_D-D\tau_D\phi_-^2\right)}{\phi_+\phi_-\left(D\tau_D+V^2\tau_M^2\right)L} \\
&\qquad\cdot\begin{pmatrix}\phi_+\sinh(\phi_-(c-a))\cosh(\phi_+(c-a)) \\ -\phi_-\cosh(\phi_-(c-a))\sinh(\phi_+(c-a))\end{pmatrix}\frac{\cosh\left(\frac{x}{V\tau_M}\right)}{\cosh\left(\frac{a}{V\tau_M}\right)} \\
&+ \frac{(\tau_D+\tau_M)D\tau_D\left(\phi_+^2-\phi_-^2\right)B_2B_4}{K\tau_DL\mathscr{D}}\frac{\cosh\left(\frac{x}{V\tau_M}\right)}{\cosh\left(\frac{a}{V\tau_M}\right)} \\
&+ \frac{(\tau_D+\tau_M)\left(K\tau_D-D\tau_D\phi_+^2\right)\left(K\tau_D-D\tau_D\phi_-^2\right)\begin{pmatrix}\cosh(\phi_-(c-a)) \\ -\cosh(\phi_+(c-a))\end{pmatrix}}{K\tau_DL}\frac{\cosh\left(\frac{x}{V\tau_M}\right)}{\cosh\left(\frac{a}{V\tau_M}\right)} \\
&+ \frac{(\tau_D+\tau_M)D\tau_DV^2\tau_M^2\left(\phi_+^2-\phi_-^2\right)B_3B_4}{\left(D\tau_D+V^2\tau_M^2\right)L\mathscr{D}}\frac{\cosh\left(\frac{x}{V\tau_M}\right)}{\cosh\left(\frac{a}{V\tau_M}\right)} \\
&- \frac{(\tau_D+\tau_M)D\tau_DV^2\tau_M^2\left(\phi_+^2-\phi_-^2\right)\cosh(\phi_+(c-a))\cosh(\phi_-(c-a))}{\left(D\tau_D+V^2\tau_M^2\right)L}\frac{\cosh\left(\frac{x}{V\tau_M}\right)}{\cosh\left(\frac{a}{V\tau_M}\right)},
\end{aligned}
$$

$$
\begin{aligned}
t_{\mathbf{0}}^{mid} = & \frac{(\tau_D+\tau_M)(b-c)}{D\tau_D\phi_+\phi_-\left(\phi_+^2-\phi_-^2\right)\left(D\tau_D+V^2\tau_M^2\right)L} \\
& \cdot \left[\begin{array}{c}
\phi_+\left(K\tau_D-D\tau_D\phi_+^2\right)^2\sinh\left(\phi_-(x-a)\right) \\
+\phi_-\left(K\tau_D-D\tau_D\phi_-^2\right)^2\sinh\left(\phi_+(x-a)\right) \\
+\phi_-\left(K\tau_D-D\tau_D\phi_+^2\right)\left(K\tau_D-D\tau_D\phi_-^2\right)\begin{pmatrix}\cosh\left(\phi_-(c-a)\right)\sinh\left(\phi_+(c-x)\right) \\ -\cosh\left(\phi_-(c-x)\right)\sinh\left(\phi_+(c-a)\right)\end{pmatrix} \\
+\phi_+\left(K\tau_D-D\tau_D\phi_+^2\right)\left(K\tau_D-D\tau_D\phi_-^2\right)\begin{pmatrix}\sinh\left(\phi_-(c-x)\right)\cosh\left(\phi_+(c-a)\right) \\ -\sinh\left(\phi_-(c-a)\right)\cosh\left(\phi_+(c-x)\right)\end{pmatrix}
\end{array}\right] \\
& + \frac{\tau_D+\tau_M}{K\tau_D} - \frac{(\tau_D+\tau_M)\begin{pmatrix}\left(K\tau_D-D\tau_D\phi_-^2\right)\cosh\left(\phi_+(c-x)\right) \\ -\left(K\tau_D-D\tau_D\phi_+^2\right)\cosh\left(\phi_-(c-x)\right)\end{pmatrix}}{K\tau_D L} \\
& + \frac{(\tau_D+\tau_M)V^2\tau_M^2\begin{pmatrix}\cosh\left(\phi_-(c-x)\right)\cosh\left(\phi_+(c-a)\right) \\ -\cosh\left(\phi_-(c-a)\right)\cosh\left(\phi_+(c-x)\right)\end{pmatrix}}{\left(D\tau_D+V^2\tau_M^2\right)L}
\end{aligned}
$$

$$
\begin{aligned}
& + \frac{(\tau_D+\tau_M)}{L\mathscr{D}}\left(\frac{(b-c)B_1}{D\tau_D\phi_+\phi_-\left(\phi_+^2-\phi_-^2\right)\left(D\tau_D+V^2\tau_M^2\right)}+\frac{B_2}{K\tau_D}+\frac{V^2\tau_M^2B_3}{\left(D\tau_D+V^2\tau_M^2\right)}\right) \\
& \cdot \left[\begin{array}{c}
-D^2\tau_D^2\phi_+\phi_-\varphi\left(\phi_+^2-\phi_-^2\right)\begin{pmatrix}\cosh\left(\phi_-(c-x)\right)\cosh\left(\phi_+(c-a)\right) \\ -\cosh\left(\phi_-(c-a)\right)\cosh\left(\phi_+(c-x)\right)\end{pmatrix}\cosh\left(\varphi(b-c)\right) \\
+\left(\begin{array}{c}
-\phi_-\left(K\tau_D+D\tau_D(\varphi^2-\phi_-^2)\right)\left(K\tau_D-D\tau_D\phi_-^2\right)\sinh\left(\phi_+(x-a)\right) \\
-\phi_+\left(K\tau_D+D\tau_D(\varphi^2-\phi_+^2)\right)\left(K\tau_D-D\tau_D\phi_+^2\right)\sinh\left(\phi_-(x-a)\right) \\
+\phi_-\left(K\tau_D-D\tau_D\phi_+^2\right)\begin{pmatrix}K\tau_D \\ +D\tau_D(\varphi^2-\phi_-^2)\end{pmatrix}\begin{pmatrix}\cosh\left(\phi_-(c-x)\right)\sinh\left(\phi_+(c-a)\right) \\ -\cosh\left(\phi_-(c-a)\right)\sinh\left(\phi_+(c-x)\right)\end{pmatrix} \\
+\phi_+\left(K\tau_D-D\tau_D\phi_-^2\right)\begin{pmatrix}K\tau_D \\ +D\tau_D(\varphi^2-\phi_+^2)\end{pmatrix}\begin{pmatrix}\sinh\left(\phi_-(c-a)\right)\cosh\left(\phi_+(c-x)\right) \\ -\sinh\left(\phi_-(c-x)\right)\cosh\left(\phi_+(c-a)\right)\end{pmatrix}
\end{array}\right) \\
\cdot\sinh\left(\varphi(b-c)\right)
\end{array}\right],
\end{aligned}
$$

$$
\begin{aligned}
s^{mid} = & \frac{(\tau_D+\tau_M)(b-c)}{D\tau_D\phi_+\phi_-\left(\phi_+^2-\phi_-^2\right)\left(D\tau_D+V^2\tau_M^2\right)L} \\
& \cdot\left[\begin{array}{c}
\left(1+K\tau_D-D\tau_D\phi_-^2\right)\left(K\tau_D-D\tau_D\phi_+^2\right) \\
\cdot\begin{pmatrix}
\phi_+\left(K\tau_D-D\tau_D\phi_+^2\right)\sinh\left(\phi_-(x-a)\right) \\
-\phi_-\left(K\tau_D-D\tau_D\phi_-^2\right)\cosh\left(\phi_-(c-x)\right)\sinh\left(\phi_+(c-a)\right) \\
+\phi_+\left(K\tau_D-D\tau_D\phi_-^2\right)\sinh\left(\phi_-(c-x)\right)\cosh\left(\phi_+(c-a)\right)
\end{pmatrix} \\
+\left(1+K\tau_D-D\tau_D\phi_+^2\right)\left(K\tau_D-D\tau_D\phi_-^2\right) \\
\cdot\begin{pmatrix}
\phi_-\left(K\tau_D-D\tau_D\phi_-^2\right)\sinh\left(\phi_+(x-a)\right) \\
-\phi_+\left(K\tau_D-D\tau_D\phi_+^2\right)\sinh\left(\phi_-(c-a)\right)\cosh\left(\phi_+(c-x)\right) \\
+\phi_-\left(K\tau_D-D\tau_D\phi_+^2\right)\cosh\left(\phi_-(c-a)\right)\sinh\left(\phi_+(c-x)\right)
\end{pmatrix}
\end{array}\right] \\
& +\frac{\tau_D+\tau_M}{K\tau_D}+\frac{(\tau_D+\tau_M)\begin{pmatrix}
\left(1+K\tau_D-D\tau_D\phi_-^2\right)\left(K\tau_D-D\tau_D\phi_+^2\right)\cosh\left(\phi_-(c-x)\right) \\
-\left(1+K\tau_D-D\tau_D\phi_+^2\right)\left(K\tau_D-D\tau_D\phi_-^2\right)\cosh\left(\phi_+(c-x)\right)
\end{pmatrix}}{K\tau_D L} \\
& +\tau_M-\frac{(\tau_D+\tau_M)V^2\tau_M^2\begin{pmatrix}
\left(1+K\tau_D-D\tau_D\phi_-^2\right)\cosh\left(\phi_-(c-x)\right)\cosh\left(\phi_+(c-a)\right) \\
-\left(1+K\tau_D-D\tau_D\phi_+^2\right)\cosh\left(\phi_-(c-a)\right)\cosh\left(\phi_+(c-x)\right)
\end{pmatrix}}{\left(D\tau_D+V^2\tau_M^2\right)L}
\end{aligned}
$$

$$
-\frac{(\tau_D+\tau_M)}{L\mathscr{D}}\left(\frac{(b-c)B_1}{D\tau_D\phi_+\phi_-\left(\phi_+^2-\phi_-^2\right)\left(D\tau_D+V^2\tau_M^2\right)}+\frac{B_2}{K\tau_D}+\frac{V^2\tau_M^2B_3}{\left(D\tau_D+V^2\tau_M^2\right)}\right)
$$

$$
\cdot\left[\begin{array}{c}
D^2\tau_D^2\phi_+\phi_-\varphi\left(\phi_+^2-\phi_-^2\right)\left(\begin{array}{c}\left(1+K\tau_D-D\tau_D\phi_-^2\right)\\ \cdot\cosh\left(\phi_-(c-x)\right)\cosh\left(\phi_+(c-a)\right)\\ -\left(1+K\tau_D-D\tau_D\phi_+^2\right)\\ \cdot\cosh\left(\phi_-(c-a)\right)\cosh\left(\phi_+(c-x)\right)\end{array}\right)\cosh\left(\varphi(b-c)\right)\\
+\left(\begin{array}{c}\phi_-\left(K\tau_D+D\tau_D(\varphi^2-\phi_-^2\right)\\ \cdot\left(\begin{array}{c}\left(K\tau_D-D\tau_D\phi_-^2\right)\left(1+K\tau_D-D\tau_D\phi_+^2\right)\sinh\left(\phi_+(x-a)\right)\\ +\left(K\tau_D-D\tau_D\phi_+^2\right)\left(1+K\tau_D-D\tau_D\phi_+^2\right)\cosh\left(\phi_-(c-a)\right)\sinh\left(\phi_+(c-x)\right)\\ -\left(K\tau_D-D\tau_D\phi_+^2\right)\left(1+K\tau_D-D\tau_D\phi_-^2\right)\cosh\left(\phi_-(c-x)\right)\sinh\left(\phi_+(c-a)\right)\end{array}\right)\\ +\phi_+\left(K\tau_D+D\tau_D(\varphi^2-\phi_+^2\right)\\ \cdot\left(\begin{array}{c}\left(K\tau_D-D\tau_D\phi_+^2\right)\left(1+K\tau_D-D\tau_D\phi_-^2\right)\sinh\left(\phi_-(x-a)\right)\\ +\left(K\tau_D-D\tau_D\phi_-^2\right)\left(1+K\tau_D-D\tau_D\phi_-^2\right)\sinh\left(\phi_-(c-x)\right)\cosh\left(\phi_+(c-a)\right)\\ -\left(K\tau_D-D\tau_D\phi_-^2\right)\left(1+K\tau_D-D\tau_D\phi_+^2\right)\sinh\left(\phi_-(c-a)\right)\cosh\left(\phi_+(c-x)\right)\end{array}\right)\end{array}\right)\\
\cdot\sinh\left(\varphi(b-c)\right)
\end{array}\right],
$$

$$
\begin{aligned}
t_{\mathbf{0}}^{out} &= \frac{(\tau_D+\tau_M)\left(2bx-x^2-2bc+c^2\right)}{2\left(D\tau_D+V^2\tau_M^2\right)} \\
&\quad + \frac{(\tau_D+\tau_M)(b-c)\begin{pmatrix}\phi_-(K\tau_D-D\tau_D\phi_-^2)\sinh(\phi_+(c-a))\\ -\phi_+(K\tau_D-D\tau_D\phi_+^2)\sinh(\phi_-(c-a))\end{pmatrix}}{\phi_+\phi_-\left(D\tau_D+V^2\tau_M^2\right)L} \\
&\quad + \frac{\tau_D+\tau_M}{K\tau_D} - \frac{(\tau_D+\tau_M)D\tau_D\left(\phi_+^2-\phi_-^2\right)}{K\tau_D L} + \frac{(\tau_D+\tau_M)V^2\tau_M^2\begin{pmatrix}\cosh(\phi_-(c-a))\\ -\cosh(\phi_+(c-a)\end{pmatrix}}{\left(D\tau_D+V^2\tau_M^2\right)L} \\
&\quad + \frac{(\tau_D+\tau_M)}{\varphi L\mathscr{D}}\left(\frac{(b-c)B_1}{\phi_+\phi_-\left(D\tau_D+V^2\tau_M^2\right)} + \frac{D\tau_D\left(\phi_+^2-\phi_-^2\right)B_2}{K\tau_D} + \frac{D\tau_D V^2\tau_M^2\left(\phi_+^2-\phi_-^2\right)B_3}{\left(D\tau_D+V^2\tau_M^2\right)}\right) \\
&\quad \cdot \begin{bmatrix}
\phi_+\varphi\left(K\tau_D+D\tau_D(\varphi^2-\phi_+^2)\right)\sinh(\phi_-(c-a))\sinh(\varphi(b-c)) \\
-\phi_-\varphi\left(K\tau_D+D\tau_D(\varphi^2-\phi_-^2)\right)\sinh(\phi_+(c-a))\sinh(\varphi(b-c)) \\
+\phi_+\phi_-\left(K\tau_D+D\tau_D(\varphi^2-\phi_+^2)\right)\cosh(\phi_-(c-a))\cosh(\varphi(b-c)) \\
-\phi_+\phi_-\left(K\tau_D+D\tau_D(\varphi^2-\phi_-^2)\right)\cosh(\phi_+(c-a))\cosh(\varphi(b-c)) \\
-\phi_+\phi_-\left(K\tau_D-D\tau_D\phi_+^2\right)\cosh(\phi_-(c-a))\cosh(\varphi(b-x)) \\
+\phi_+\phi_-\left(K\tau_D-D\tau_D\phi_-^2\right)\cosh(\phi_+(c-a))\cosh(\varphi(b-x))
\end{bmatrix},
\end{aligned}
$$

$$
\begin{aligned}
s^{out} = & \frac{(\tau_D+\tau_M)\left(2bx-x^2-2bc+c^2\right)}{2\left(D\tau_D+V^2\tau_M^2\right)} \\
& + \frac{(\tau_D+\tau_M)(b-c)\begin{pmatrix}\phi_-(K\tau_D-D\tau_D\phi_-^2)\sinh(\phi_+(c-a)) \\ -\phi_+(K\tau_D-D\tau_D\phi_+^2)\sinh(\phi_-(c-a))\end{pmatrix}}{\phi_+\phi_-\left(D\tau_D+V^2\tau_M^2\right)L} \\
& + \frac{\tau_D+\tau_M}{K\tau_D} - \frac{(\tau_D+\tau_M)D\tau_D\left(\phi_+^2-\phi_-^2\right)}{K\tau_D L} \\
& + \frac{(\tau_D+\tau_M)V^2\tau_M^2(\cosh(\phi_-(c-a))-\cosh(\phi_+(c-a))}{\left(D\tau_D+V^2\tau_M^2\right)L} + \frac{(\tau_D+\tau_M)D\tau_D}{\left(D\tau_D+V^2\tau_M^2\right)} - \tau_D \\
& + \frac{(\tau_D+\tau_M)}{\varphi L\mathscr{D}}\left(\frac{(b-c)B_1}{\phi_+\phi_-\left(D\tau_D+V^2\tau_M^2\right)} + \frac{D\tau_D\left(\phi_+^2-\phi_-^2\right)B_2}{K\tau_D} + \frac{D\tau_D V^2\tau_M^2\left(\phi_+^2-\phi_-^2\right)B_3}{\left(D\tau_D+V^2\tau_M^2\right)}\right) \\
& \cdot \begin{bmatrix}
\phi_+\varphi\left(K\tau_D+D\tau_D(\varphi^2-\phi_+^2)\right)\sinh(\phi_-(c-a))\sinh(\varphi(b-c)) \\
-\phi_-\varphi\left(K\tau_D+D\tau_D(\varphi^2-\phi_-^2)\right)\sinh(\phi_+(c-a))\sinh(\varphi(b-c)) \\
+\phi_+\phi_-\left(K\tau_D+D\tau_D(\varphi^2-\phi_+^2)\right)\cosh(\phi_-(c-a))\cosh(\varphi(b-c)) \\
-\phi_+\phi_-\left(K\tau_D+D\tau_D(\varphi^2-\phi_-^2)\right)\cosh(\phi_+(c-a))\cosh(\varphi(b-c)) \\
+\frac{D\tau_D}{V^2\tau_M^2}\phi_+\phi_-\left(K\tau_D-D\tau_D\phi_+^2\right)\cosh(\phi_-(c-a))\cosh(\varphi(b-x)) \\
-\frac{D\tau_D}{V^2\tau_M^2}\phi_+\phi_-\left(K\tau_D-D\tau_D\phi_-^2\right)\cosh(\phi_+(c-a))\cosh(\varphi(b-x))
\end{bmatrix},
\end{aligned}
$$

where

$$
\varphi = \sqrt{\frac{D\tau_D+V^2\tau_M^2}{D\tau_D V^2\tau_M^2}},
$$

$$
\phi_\pm = \sqrt{\frac{D\tau_D+V^2\tau_M^2+K\tau_D V^2\tau_M^2 \pm \sqrt{V^4\tau_M^4+2D\tau_D V^2\tau_M^2+2K\tau_D V^4\tau_M^4+(D-KV^2\tau_M^2)^2\tau_D^2}}{2D\tau_D V^2\tau_M^2}},
$$

$$
L = \left(K\tau_D-D\tau_D\phi_-^2\right)\cosh(\phi_+(c-a)) - \left(K\tau_D-D\tau_D\phi_+^2\right)\cosh(\phi_-(c-a)),
$$

$$
\begin{aligned}
\mathscr{D} = {} & D^2\tau_D^2\phi_+\phi_-\varphi\left(\phi_+^2-\phi_-^2\right) \\
& \cdot\begin{pmatrix}
\phi_+\left(1+K\tau_D-D\tau_D\phi_+^2\right)\cosh\left(\phi_-(c-a)\right)\sinh\left(\phi_+(c-a)\right) \\
-\phi_-\left(1+K\tau_D-D\tau_D\phi_-^2\right)\sinh\left(\phi_-(c-a)\right)\cosh\left(\phi_+(c-a)\right) \\
-\dfrac{D\tau_D}{V\tau_M}\left(\phi_+^2-\phi_-^2\right)\tanh\left(\dfrac{a}{V\tau_M}\right)\cosh\left(\phi_-(c-a)\right)\cosh\left(\phi_+(c-a)\right)
\end{pmatrix}\cosh\left(\varphi(b-c)\right) \\
& +\begin{pmatrix}
\phi_+\phi_-\begin{pmatrix}\left(K\tau_D-D\tau_D\phi_+^2\right)\left(1+K\tau_D-D\tau_D\phi_-^2\right)\left(K\tau_D+D\tau_D(\varphi^2-\phi_+^2)\right) \\ +\left(K\tau_D-D\tau_D\phi_-^2\right)\left(1+K\tau_D-D\tau_D\phi_+^2\right)\left(K\tau_D+D\tau_D(\varphi^2-\phi_-^2)\right)\end{pmatrix} \\
+\begin{pmatrix}\phi_-^2\left(K\tau_D-D\tau_D\phi_+^2\right)\left(1+K\tau_D-D\tau_D\phi_-^2\right)\left(K\tau_D+D\tau_D(\varphi^2-\phi_-^2)\right) \\ +\phi_+^2\left(K\tau_D-D\tau_D\phi_-^2\right)\left(1+K\tau_D-D\tau_D\phi_+^2\right)\left(K\tau_D+D\tau_D(\varphi^2-\phi_+^2)\right)\end{pmatrix} \\
\cdot\sinh\left(\phi_-(c-a)\right)\sinh\left(\phi_+(c-a)\right) \\
-\phi_+\phi_-\begin{pmatrix}\left(K\tau_D-D\tau_D\phi_+^2\right)\left(1+K\tau_D-D\tau_D\phi_+^2\right)\left(K\tau_D+D\tau_D(\varphi^2-\phi_-^2)\right) \\ +\left(K\tau_D-D\tau_D\phi_-^2\right)\left(1+K\tau_D-D\tau_D\phi_-^2\right)\left(K\tau_D+D\tau_D(\varphi^2-\phi_+^2)\right)\end{pmatrix} \\
\cdot\cosh\left(\phi_-(c-a)\right)\cosh\left(\phi_+(c-a)\right) \\
+\dfrac{D\tau_D}{V\tau_M}\phi_-\left(\phi_+^2-\phi_-^2\right)\tanh\left(\dfrac{a}{V\tau_M}\right)\left(K\tau_D-D\tau_D\phi_+^2\right)\left(K\tau_D+D\tau_D(\varphi^2-\phi_-^2)\right) \\
\cdot\cosh\left(\phi_-(c-a)\right)\sinh\left(\phi_+(c-a)\right) \\
-\dfrac{D\tau_D}{V\tau_M}\phi_+\left(\phi_+^2-\phi_-^2\right)\tanh\left(\dfrac{a}{V\tau_M}\right)\left(K\tau_D-D\tau_D\phi_-^2\right)\left(K\tau_D+D\tau_D(\varphi^2-\phi_+^2)\right) \\
\cdot\sinh\left(\phi_-(c-a)\right)\cosh\left(\phi_+(c-a)\right)
\end{pmatrix} \\
& \cdot\sinh\left(\varphi(b-c)\right),
\end{aligned}
$$

$$
\begin{aligned}
B_1 = {} & \phi_+ \left(1 + K\tau_D - D\tau_D\phi_+^2\right) \\
& \cdot \begin{pmatrix} \phi_- \left(K\tau_D - D\tau_D\phi_-^2\right)^2 \\ +\phi_+ \left(K\tau_D - D\tau_D\phi_+^2\right)\left(K\tau_D - D\tau_D\phi_-^2\right)\sinh\left(\phi_-(c-a)\right)\sinh\left(\phi_+(c-a)\right) \\ -\phi_- \left(K\tau_D - D\tau_D\phi_+^2\right)\left(K\tau_D - D\tau_D\phi_-^2\right)\cosh\left(\phi_-(c-a)\right)\cosh\left(\phi_+(c-a)\right) \end{pmatrix} \\
& + \phi_- \left(1 + K\tau_D - D\tau_D\phi_-^2\right) \\
& \cdot \begin{pmatrix} \phi_+ \left(K\tau_D - D\tau_D\phi_+^2\right)^2 \\ +\phi_- \left(K\tau_D - D\tau_D\phi_+^2\right)\left(K\tau_D - D\tau_D\phi_-^2\right)\sinh\left(\phi_-(c-a)\right)\sinh\left(\phi_+(c-a)\right) \\ -\phi_+ \left(K\tau_D - D\tau_D\phi_+^2\right)\left(K\tau_D - D\tau_D\phi_-^2\right)\cosh\left(\phi_-(c-a)\right)\cosh\left(\phi_+(c-a)\right) \end{pmatrix} \\
& - \frac{D\tau_D}{V\tau_M}\left(\phi_+^2 - \phi_-^2\right)\left(K\tau_D - D\tau_D\phi_+^2\right)\left(K\tau_D - D\tau_D\phi_-^2\right) \\
& \cdot \begin{pmatrix} \phi_+ \sinh\left(\phi_-(c-a)\right)\cosh\left(\phi_+(c-a)\right) \\ -\phi_- \cosh\left(\phi_-(c-a)\right)\sinh\left(\phi_+(c-a)\right) \end{pmatrix} \tanh\left(\frac{a}{V\tau_M}\right), \\
B_2 = {} & \phi_+ \left(1 + K\tau_D - D\tau_D\phi_+^2\right)\left(K\tau_D - D\tau_D\phi_-^2\right)\sinh\left(\phi_+(c-a)\right) \\
& - \phi_- \left(1 + K\tau_D - D\tau_D\phi_-^2\right)\left(K\tau_D - D\tau_D\phi_+^2\right)\sinh\left(\phi_-(c-a)\right) \\
& + \left(K\tau_D - D\tau_D\phi_+^2\right)\left(K\tau_D - D\tau_D\phi_-^2\right)\cosh\left(\phi_+(c-a)\right)\frac{1}{V\tau_M}\tanh\left(\frac{a}{V\tau_M}\right) \\
& - \left(K\tau_D - D\tau_D\phi_+^2\right)\left(K\tau_D - D\tau_D\phi_-^2\right)\cosh\left(\phi_-(c-a)\right)\frac{1}{V\tau_M}\tanh\left(\frac{a}{V\tau_M}\right), \\
B_3 = {} & -\phi_+ \left(1 + K\tau_D - D\tau_D\phi_+^2\right)\cosh\left(\phi_-(c-a)\right)\sinh\left(\phi_+(c-a)\right) \\
& + \phi_- \left(1 + K\tau_D - D\tau_D\phi_-^2\right)\sinh\left(\phi_-(c-a)\right)\cosh\left(\phi_+(c-a)\right) \\
& + \frac{D\tau_D}{V\tau_M}\left(\phi_+^2 - \phi_-^2\right)\tanh\left(\frac{a}{V\tau_M}\right)\cosh\left(\phi_-(c-a)\right)\cosh\left(\phi_+(c-a)\right),
\end{aligned}
$$

$$
\begin{aligned}
B_4 = &-D^2\tau_D^2\phi_+\phi_-\varphi\left(\phi_+^2-\phi_-^2\right)\cosh\left(\phi_-(c-a)\right)\cosh\left(\phi_+(c-a)\right)\cosh\left(\varphi(b-c)\right)\\
&-\phi_+\left(K\tau_D-D\tau_D\phi_-^2\right)\left(K\tau_D+D\tau_D(\varphi^2-\phi_+^2)\right)\\
&\quad\cdot\sinh\left(\phi_-(c-a)\right)\cosh\left(\phi_+(c-a)\right)\sinh\left(\varphi(b-c)\right)\\
&+\phi_-\left(K\tau_D-D\tau_D\phi_+^2\right)\left(K\tau_D+D\tau_D(\varphi^2-\phi_-^2)\right)\\
&\quad\cdot\cosh\left(\phi_-(c-a)\right)\sinh\left(\phi_+(c-a)\right)\sinh\left(\varphi(b-c)\right).
\end{aligned}
$$

For a comprehensive discussion regarding the guarantee that all denominators remain nonzero, refer to Appendix B.1. Notably, the solutions exhibit a symmetry such that

$$
s(-a,-c,-b,-x)=s(a,c,b,x)\qquad\text{and}\qquad t_{\mathbf{0}}(-a,-c,-b,-x)=t_{\mathbf{0}}(a,c,b,x).
$$

Leveraging this symmetry and assuming an initial detection phase, we determined the mean detection time averaged over the entire domain as follows:

$$
\begin{aligned}
t_m &= \frac{1}{2b}\int_{-b}^{b} t_{\mathbf{0}}dx = \frac{1}{2b}\cdot 2\int_0^b t_{\mathbf{0}}dx = \frac{1}{b}\int_0^a t_{\mathbf{0}}^{in}dx+\frac{1}{b}\int_a^c t_{\mathbf{0}}^{mid}dx+\frac{1}{b}\int_c^b t_{\mathbf{0}}^{out}dx\\
t_m &= \frac{(\tau_D+\tau_M)}{b}\left(\begin{array}{c}\dfrac{(b-c)^3}{3\left(D\tau_D+V^2\tau_M^2\right)}+\dfrac{(b-c)^2M_1}{\left(D\tau_D+V^2\tau_M^2\right)}+\dfrac{b-a}{K\tau_D}+\dfrac{(b-c)M_2}{K\tau_D}\\ +\dfrac{(b-c)M_3}{\left(D\tau_D+V^2\tau_M^2\right)}+\dfrac{M_4}{K\tau_D}+\dfrac{M_5}{\left(D\tau_D+V^2\tau_M^2\right)}\end{array}\right),
\end{aligned}
\tag{2.10}
$$

where

$$
M_1 = \frac{B_1B_6+\begin{pmatrix}-\phi_+\left(K\tau_D-D\tau_D\phi_+^2\right)\sinh\left(\phi_-(c-a)\right)\\ +\phi_-\left(K\tau_D-D\tau_D\phi_-^2\right)\sinh\left(\phi_+(c-a)\right)\end{pmatrix}\varphi\mathscr{D}}{\phi_+\phi_-\varphi L\mathscr{D}},
$$

$$
M_2 = \frac{D\tau_D\left(\phi_+^2-\phi_-^2\right)}{\varphi L\mathscr{D}}\left(B_2B_6-\varphi\mathscr{D}\right),
$$

$$M_3 = \frac{B_1 \sinh(\varphi(b-c))}{\varphi^2 \mathscr{D}} + \frac{V^2 \tau_M^2}{L} \left(\cosh(\phi_-(c-a)) - \cosh(\phi_+(c-a))\right)$$
$$+ \frac{D\tau_D V^2 \tau_M^2 \left(\phi_+^2 - \phi_-^2\right) B_3 B_6}{\varphi L \mathscr{D}} + \frac{B_1 B_5}{D\tau_D \phi_+^2 \phi_-^2 \left(\phi_+^2 - \phi_-^2\right) L \mathscr{D}}$$
$$+ \frac{\left[\begin{array}{c} \phi_+^2 \left(K\tau_D - D\tau_D \phi_+^2\right)^2 \left(\cosh(\phi_-(c-a)) - 1\right) \\ +\phi_-^2 \left(K\tau_D - D\tau_D \phi_-^2\right)^2 \left(\cosh(\phi_+(c-a)) - 1\right) \\ +\phi_- \left(K\tau_D - D\tau_D \phi_+^2\right)\left(K\tau_D - D\tau_D \phi_-^2\right) \begin{pmatrix} \phi_- \cosh(\phi_-(c-a)) \left(\cosh(\phi_+(c-a)) - 1\right) \\ -\phi_+ \sinh(\phi_-(c-a)) \sinh(\phi_+(c-a)) \end{pmatrix} \\ +\phi_+ \left(K\tau_D - D\tau_D \phi_+^2\right)\left(K\tau_D - D\tau_D \phi_-^2\right) \begin{pmatrix} \phi_+ \left(\cosh(\phi_-(c-a)) - 1\right) \cosh(\phi_+(c-a)) \\ -\phi_- \sinh(\phi_-(c-a)) \sinh(\phi_+(c-a)) \end{pmatrix} \end{array}\right]}{D\tau_D \phi_+^2 \phi_-^2 \left(\phi_+^2 - \phi_-^2\right) L},$$

$$M_4 = \frac{D\tau_D \phi_+ \phi_- \left(\phi_+^2 - \phi_-^2\right) \sinh(\varphi(b-c)) B_2}{\varphi^2 \mathscr{D}} + \frac{B_2 B_5}{\phi_+ \phi_- L \mathscr{D}}$$
$$- \frac{\begin{pmatrix} \phi_- \left(K\tau_D - D\tau_D \phi_-^2\right) \sinh(\phi_+(c-a)) \\ -\phi_+ \left(K\tau_D - D\tau_D \phi_+^2\right) \sinh(\phi_-(c-a)) \end{pmatrix}}{\phi_+ \phi_- L},$$

$$M_5 = \frac{D\tau_D V^2 \tau_M^2 \phi_+ \phi_- \left(\phi_+^2 - \phi_-^2\right) \sinh(\varphi(b-c)) B_2}{\varphi^2 \mathscr{D}} + \frac{V^2 \tau_M^2 B_3 B_5}{\phi_+ \phi_- L \mathscr{D}}$$
$$- \frac{V^2 \tau_M^2 \begin{pmatrix} \phi_- \left(K\tau_D - D\tau_D \phi_-^2\right) \sinh(\phi_+(c-a)) \\ -\phi_+ \left(K\tau_D - D\tau_D \phi_+^2\right) \sinh(\phi_-(c-a)) \end{pmatrix}}{\phi_+ \phi_- L},$$

$$B_5 = -D^2\tau_D^2\phi_+\phi_-\varphi\left(\phi_+^2-\phi_-^2\right)\begin{pmatrix}\phi_+\sinh\left(\phi_-(c-a)\right)\cosh\left(\phi_+(c-a)\right)\\ -\phi_-\cosh\left(\phi_-(c-a)\right)\sinh\left(\phi_+(c-a)\right)\end{pmatrix}\cosh\left(\varphi(b-c)\right)$$

$$+\begin{pmatrix}-\phi_-^2\left(K\tau_D+D\tau_D(\varphi^2-\phi_-^2)\right)\left(K\tau_D-D\tau_D\phi_-^2\right)\left(\cosh\left(\phi_+(c-a)\right)-1\right)\\ -\phi_+^2\left(K\tau_D+D\tau_D(\varphi^2-\phi_+^2)\right)\left(K\tau_D-D\tau_D\phi_+^2\right)\left(\cosh\left(\phi_-(c-a)\right)-1\right)\\ +\phi_-\left(K\tau_D-D\tau_D\phi_+^2\right)\begin{pmatrix}K\tau_D\\ +D\tau_D(\varphi^2-\phi_-^2)\end{pmatrix}\begin{pmatrix}\phi_+\sinh\left(\phi_-(c-a)\right)\sinh\left(\phi_+(c-a)\right)\\ -\phi_-\cosh\left(\phi_-(c-a)\right)\\ \cdot\left(\cosh\left(\phi_+(c-a)\right)-1\right)\end{pmatrix}\\ +\phi_+\left(K\tau_D-D\tau_D\phi_-^2\right)\begin{pmatrix}K\tau_D\\ +D\tau_D(\varphi^2-\phi_+^2)\end{pmatrix}\begin{pmatrix}\phi_-\sinh\left(\phi_-(c-a)\right)\sinh\left(\phi_+(c-a)\right)\\ -\phi_+\cosh\left(\phi_+(c-a)\right)\\ \cdot\left(\cosh\left(\phi_-(c-a)\right)-1\right)\end{pmatrix}\end{pmatrix}$$

$$\cdot\sinh\left(\varphi(b-c)\right),$$

$$B_6 = \begin{pmatrix}\phi_+\phi_-\left(K\tau_D+D\tau_D(\varphi^2-\phi_+^2)\right)\cosh\left(\phi_-(c-a)\right)\cosh\left(\varphi(b-c)\right)\\ -\phi_+\phi_-\left(K\tau_D+D\tau_D(\varphi^2-\phi_-^2)\right)\cosh\left(\phi_+(c-a)\right)\cosh\left(\varphi(b-c)\right)\\ +\phi_+\varphi\left(K\tau_D+D\tau_D(\varphi^2-\phi_+^2)\right)\sinh\left(\phi_-(c-a)\right)\sinh\left(\varphi(b-c)\right)\\ -\phi_-\varphi\left(K\tau_D+D\tau_D(\varphi^2-\phi_-^2)\right)\sinh\left(\phi_+(c-a)\right)\sinh\left(\varphi(b-c)\right)\end{pmatrix}.$$

The goal of this section is to determine the intermittence criterion, i.e., when intermittence is favorable to the diffusion-alone model. We begin by seeing how space affects each model. Recall that in the one detection zone model, the authors determined that intermittence was favorable whenever $b > \frac{D}{V}$. We check to see if this is true for our model.

Starting wth baseline parameters $a = 1$, $c = 3$, $b = 10$, and $K = 1$, we evaluate the mean search time formulas for intermittence in Equation (2.10) and diffusion-alone in Equation (2.3) using all pair combinations of D and V within the set $\{0.01, 0.1, 1, 10, 100\}$. In every case where $b > \frac{D}{V}$, there exists a pair (τ_D, τ_M) such that intermittence is less than diffusion-alone. By contrast, in every case with $b \leq \frac{D}{V}$, the intermittent strategy does not outperform the diffusion-only strategy.

We next investigate how the detection rate K affects the intermittence criterion. Throughout this comparison, we fix the baseline parameters $a = 1$, $b = 10$, $D = 1$, and $V = 1$. Because K is only meaningful relative to the region between a and c, we examine a range of (c, K) pairs with $c \in \{2, 3, ..., 8, 9\}$ and $K = \{10^{-7}, 10^{-6}, ..., 10^{6}, 10^{7}\}$.

For each (c, K), we compare the diffusion-only mean search time in Equation (2.3) with the intermittent mean search time in Equation (2.10). To evaluate the intermittent expression, we perform evaluations of (τ_D, τ_M) using a 100×100 uniform mesh on $[0, T_{diff}] \times [0, T_{diff}]$, where T_{diff} denotes the diffusion-only mean search time at (c, K). The outcomes are reported in Table 2.1. We mark an entry **F** if there exists at least one choice (τ_D, τ_M) for which intermittence achieves a strictly smaller mean search time than diffusion alone, and **N** otherwise.

In a small subset of parameter combinations, the numerical evaluation triggered overflow-related `RuntimeWarning` messages; these cases are denoted by **N***. Because such overflow may obscure the true minimum of the intermittence expression, the corresponding **N*** classifications should be interpreted cautiously. In particular, intermittence could still be favorable in some of these cases, especially if Equation (2.10) is further simplified.

The results reveal a pattern: intermittence is typically advantageous when the detection rate K is small, whereas the diffuion-only strategy tends to be preferable for large K. This contrast becomes more pronounced as the outer boundary of the second detection zone c increases from a towards b.

This behavior aligns with interpreting detection in the second zone as a Poisson process with rate K. Under this assumption, the waiting time to detect the target while in the second detection zone is exponentially distributed with mean $\frac{1}{K}$. Consequently, as $K \to 0^+$, detection in the second zone becomes effectively negligible: a searcher spends time in a "detection-capable" phase but has essentially no chance of success, making relocation via intermittence increasingly beneficial. In contrast, as $K \to \infty$, detection in the second zone becomes nearly instantaneous, substantially improving detection performance and eliminating any advantage gained from intermittence.

Table 2.1: Results of comparing intermittence with diffusion-alone. F represents when intermittence is favorable and N represents when it is not.

	$c=2$	$c=3$	$c=4$	$c=5$	$c=6$	$c=7$	$c=8$	$c=9$
$K=10^{-7}$	F	F	F	F	F	F	F	F
$K=10^{-6}$	F	F	F	F	F	F	F	F
$K=10^{-5}$	F	F	F	F	F	F	F	F
$K=10^{-4}$	F	F	F	F	F	F	F	F
$K=10^{-3}$	F	F	F	F	F	F	F	F
$K=10^{-2}$	F	F	F	F	F	F	F	F
$K=10^{-1}$	F	F	F	F	N	N	N	N
$K=10^{0}$	F	F	F	N	N	N	N	N
$K=10^{1}$	F	F	F	N	N	N	N	N
$K=10^{2}$	F	F	F	F	F	F	F	N*
$K=10^{3}$	F	F	F	N	N	F	F	N*
$K=10^{4}$	F	F	F	N	N*	N*	N*	N*
$K=10^{5}$	F	N*	N	N	N	N	N*	N
$K=10^{6}$	N*	N	N	N	N	N	N	N
$K=10^{7}$	N	N	N	N	N	N	N	N

However, while Table 2.1 confirms this overall trend, the table also shows an "island" of intermittence favorability for some middling rates of K. For instance, for $c=5$, the classification switches from **N** at moderate rates $K=10^{0}-10^{1}$ back to **F** at $K=10^{2}$ and before returning again to **N** at $K\geq 10^{3}$. Thus, although there is an overall pattern of small K promoting intermittence and large K suppressing it, the boundary is not strictly monotone. While this "island" of favorability is evident numerically, deriving a clean analytical characterization of the corresponding threshold(s) is prohibitively complicated for our purposes.

To better understand how each spatial region contributes to the full (and otherwise analytically cumbersome) model, we study a set of limiting regimes in which one region is effectively removed. This reduction serves as a controlled way to isolate mechanisms and build intuition: by simplifying the geometry, we can more clearly interpret how the first

detection zone, the second detection zone, and the exterior no-detection region interact. Accordingly, we analyze the following three limits:

1) $c \to a$

2) $a \to 0$

3) $b \to c$

Case 1: $c \to a$ During this case, the second detection zone collapses, and the model reduces to the single-detection zone setting studied by Loverdo et al. [4]. In examining this limiting case as well as the original article, we also identify an inconsistency in the mean search time expression reported in [4]. Specifically, by (i) reproducing the authors' derivation step by step and (ii) independently taking the limit $c \to a$ in our two detection zone formula, we obtain a potential corrected mean search time expression as follows:

$$t_m = \frac{(\tau_D+\tau_M)(b-a)^3}{3b\left(D\tau_D+V^2\tau_M^2\right)} + \frac{(\tau_D+\tau_M)V^4\tau_M^4\begin{pmatrix}(b-a)\\ +V\tau_M\tanh\left(\dfrac{a}{V\tau_M}\right)\end{pmatrix}\begin{pmatrix}\varphi(b-a)\cosh(\varphi(b-a))\\ -\sinh(\varphi(b-a))\end{pmatrix}}{b\left(D\tau_D+V^2\tau_M^2\right)^2\left(V\tau_M\varphi\cosh(\varphi(b-a))\tanh\left(\dfrac{a}{V\tau_M}\right)+\sinh(\varphi(b-a))\right)}. \tag{2.11}$$

By evaluating the equations with the same parameters, we determine that the resulting formula is not a simplification of the one reported by the authors; rather, Equation (2.11) defines a distinct formula.

To assess which mean search-time expression is accurate, we evaluate both formulas against Monte Carlo simulations of the search process under several parameter choices. For each parameter set, we estimate the mean search time from the simulation output and construct a two-sided 95% confidence intervals for the true mean using the Student's t-distribution. In particular, we compute the margin of error:

$$E = t_{0.025,n-1}\left(\frac{s}{\sqrt{n}}\right),$$

where n is the number of simulations, $\bar{x}$ is the sample mean, s is the sample standard deviation, and $t_{0.025,n-1}$ denotes the upper 2.5% critical value of the t-distribution. The resulting confidence interval is $(\bar{x}-E, \bar{x}+E)$, which we interpret as the range in which the true mean search time lies with 95% confidence.

We then evaluate each candidate mean search-time expression at the same parameter values and compare these predictions to the simulated confidence intervals. If one expression falls inside the interval while the other falls outside, we treat the former as consistent with the simulations and the latter as an under- or overestimate.

The results of these comparisons are summarized in Table 2.2. Across all parameter settings tested, our predicted mean search time lies within the corresponding confidence interval, whereas the value given by the authors' expression falls below the interval. We therefore conclude that our formula correctly gives the mean search time for the 1D original intermittence model and that the discrepancy with the expression reported by Loverdo et.al [4] is most likely due to a typographical error in their equation.

While our expression may be different, intermittent criterion is the similar. Taking the limit $c \to a$ reduces the diffusion-alone Equation (2.3) to the following:

$$t_{diff} = \frac{(b-a)^3}{3bD}.$$

Once again, we begin our numerical study comparing the two equations with baseline parameters $a = 1$ and $b = 10$. Evaluating both mean search time equations for intermittent and diffusion-alone using all pair combinations of D and V within the set $\{0.01, 0.1, 1, 10, 100\}$ result in intermittence only being disadvantageous whenever $b \leq \frac{D}{V}$.

Case 2: $a \to 0$ During this case, the first detection zone collapses to the target's location so that the searcher effectively encounters a single detection region with fixed detection rate K. Relative to Equation (2.10), the only modification is that the term $\frac{b-a}{K\tau_D}$ reduces to $\frac{b}{K\tau_D}$ and that every instance of $\phi_{\pm}(c-a)$ is replaced by $\phi_{\pm}c$ in the following hyperbolic functions:

Table 2.2: Summary statistics for four parameter tests: sample mean $\bar{x}$, sample standard deviation s and sample size n, together with the corresponding 95% confidence Intervals (CIs). The resulting CIs are compared against the mean search time predicted by our formula and by the authors' formula.

Parameters	Test 1	Test 2	Test 3	Test 4
a	10	5	15	20
b	30	50	60	40
D	2	2	5	2
V	3	5	2	5
τ_D	1	4	10	10
τ_M	2	5	5	5
$\bar{x}$	13.18	58.13	66.35	11.72
s	18.30	63.05	98.03	19.17
n	1500	3500	1000	3000
95% CI	$(12.25, 14.11)$	$(56.04, 60.22)$	$(60.27, 72.43)$	$(11.04, 12.41)$
Our formula	13.16	56.37	66.52	11.12
Authors' formula	12.19	55.26	60.21	10.79

$$\sinh(\phi_\pm(c-a)) \to \sinh(c\phi_\pm), \qquad \cosh(\phi_\pm(c-a)) \to \cosh(c\phi_\pm)$$

throughout the expression. For the diffusion-alone model, Equation (2.3) simplifies to the following:

$$\begin{aligned} t_{diff} = \frac{1}{bK}\left(2b - c + \frac{(b-c)^3 K}{3D}\right) - \frac{2(b-c)}{bK}\operatorname{sech}\left(c\sqrt{\frac{K}{D}}\right) \\ + \frac{1}{bK}\left(\frac{(b-c)^2 K}{D} - 1\right)\sqrt{\frac{D}{K}}\tanh\left(c\sqrt{\frac{K}{D}}\right). \end{aligned} \tag{2.12}$$

Since the limit $a \to 0$ does not alter the domain radius b, the spatial intermittence criterion is unaffected: intermittence remains advantageous whenever $b > \frac{D}{V}$. We now must assess whether the detection rate K influences the favorability of intermittence.

Intuitively, we expect that K should not modify the intermittence criterion. As $K \to \infty$, detection within the existing detection zone becomes effectively instantaneous, mirroring the model designed in the original article [4]. Since this criterion is unaffected by a K-value

in the original model, we naturally expect that reducing an infinite K to finite values also would not alter the criterion. Indeed, our numerical study confirms our suspicion.

Fixing $c = 1$ and $b = 10$, we evaluate each mean search time formula using all triple combinations of D, V, and K within the set $\{0.01, 0.1, 1, 10, 100\}$. In every parameter set satisfying $b \leq \frac{D}{V}$, intermittence was unfavorable. Conversely, whenever $b > \frac{D}{V}$, we observed the existence of (τ_D, τ_M) for which the intermittence mean search time t_m is smaller than the diffusion-only mean search time t_{diff}.

Case 3: $b \to c$ During this case, the space outside the target decreases so that the searcher always has a chance of finding the target throughout the entire domain. By taking the limit $b \to c$, we reduce the mean search time formula for diffusion-alone in Equation (2.3) to

$$t_{diff} = \frac{1}{cK}\left(c - a - \sqrt{\frac{D}{K}}\tanh\left(\sqrt{\frac{K}{D}}(c-a)\right)\right) \tag{2.13}$$

and the mean search time formula for intermittence in Equation (2.10) to

$$\begin{aligned} t_m = {} & \frac{(\tau_D+\tau_M)(c-a)}{cK\tau_D} \\ & - \frac{(\tau_D+\tau_M)\begin{pmatrix} V\tau_M\left(\phi_+^2-\phi_-^2\right)\left(1+K\tau_D-D\tau_D\left(\phi_+^2+\phi_-^2\right)\right)S_-S_+ \\ +\phi_+\left(K\tau_D-D\tau_D\phi_+^2\right)\tanh\left(\frac{a}{V\tau_M}\right)S_-C_+ \\ -\phi_-\left(K\tau_D-D\tau_D\phi_-^2\right)\tanh\left(\frac{a}{V\tau_M}\right)C_-S_+ \end{pmatrix}}{K\tau_D V\tau_M c\phi_+\phi_-\begin{pmatrix} \phi_+\left(1+K\tau_D-D\tau_D\phi_+^2\right)C_-S_+ \\ -\phi_-\left(1+K\tau_D-D\tau_D\phi_-^2\right)S_-C_+ \\ -\frac{D\tau_D}{V\tau_M}\left(\phi_+^2-\phi_-^2\right)\tanh\left(\frac{a}{V\tau_M}\right)C_-C_+ \end{pmatrix}} \end{aligned} \tag{2.14}$$

where

$$C_- = \cosh\left(\phi_-(c-a)\right), \qquad C_+ = \cosh\left(\phi_+(c-a)\right),$$

$$S_- = \sinh\left(\phi_-(c-a)\right), \qquad S_+ = \sinh\left(\phi_+(c-a)\right).$$

To assess the intermittence criterion, we first test whether the previous conclusion, namely intermittence is favorable whenever domain radius c is greater than $\frac{D}{V}$. In this case, this implication fails. For example, when $a = 1$, $c = 10$, $K = 1$, $D = 0.01$, $V = 0.1$, we did not find any pair of times (τ_D, τ_M) for which the intermittence mean search time Equation (2.14) is smaller than the diffusion-only mean search time Equation (2.13). More broadly, we discover that variations in D and V have only a modest effect on these mean search time expressions, whereas changes in the detection rate K can alter the times by larger orders of magnitude.

To quantify this sensitivity, we perform a numerical study by setting the baseline parameters $a = 1$, $c = 10$, $\tau_D = 10$, $\tau_M = 10$, $D = 1$, $V = 1$, and $K = 1$. We then vary a single parameter D, V, or K, over the set $\{0.01, 0.1, 1, 10, 100\}$ while holding all remaining parameters at their baseline values. For each variation, we evaluate the corresponding mean search time formulas and record the minimum and maximum values in Table (2.3). The resulting comparisons confirm that K exerts a substantially stronger influence on the mean search times than either D or V.

Table 2.3: Ranges of the mean search time approximations t_m in Equation (2.14) and t_{diff} in Equation (2.3) obtained by varying each of D, V, and K over the set $\{0.01, 0.1, 1, 10, 100\}$ (one parameter at a time), with all remaining parameters fixed at their baseline parameters.

Varying Parameter	t_m Ranges	t_{diff} Ranges
D	$(0.3654, 1.7622)$	$(0.1837, 0.8900)$
V	$(1.5785, 1.5999)$	$(0.8000, 0.8000)$
K	$(0.0178, 24.6524)$	$(0.0089, 18.3702)$

This behavior is a direct consequence of the interpretation of K as a detection rate. Specifically in this case, detection outside the first detection zone is modeled by a Poisson process with constant rate K, so that the associated detection waiting time is exponential with mean $\frac{1}{K}$. Hence, when $K \leq 1$, the expected detection time is at most one time unit. This makes detection sufficiently fast that the diffusion-only strategy is expected to dominate because adding motion phases needlessly interrupts detection.

In contrast, whenever $K \to 0^+$, detection outside the first detection zone becomes exceptionally slow, and the model effectively reduces to the 1D diffusive model from the original article [4] discussed in Chapter 2.1.1. In that model, intermittence favorability exists. Therefore, it is natural to expect the existence of a transition threshold $K \ll 1$ such that intermittence may improve the mean search time.

To determine the threshold $K \ll 1$, we start by determining the asymptotic diffusion-alone equation. Assuming $K \ll 1$ such that

$$\sqrt{\frac{K}{D}}(c-a) \ll 1, \tag{2.15}$$

Equation (2.3) reduces to the following:

$$t_{diff} \approx \frac{(c-a)^3}{3cD} \tag{2.16}$$

since for small x,

$$\tanh(x) \approx x - \frac{x^3}{3}.$$

We next consider the asymptotic approximation for the intermittence equation. Assuming $K \ll 1$ such that

$$\frac{2K\tau_D V^2 \tau_M^2 (V^2\tau_M^2 - D\tau_D)}{(D\tau_D + V^2\tau_M^2)^2} \ll 1 \tag{2.17}$$

we can reduce $\phi_\pm$ to the following:

$$\phi_\pm \approx \frac{\left(D\tau_D + V^2\tau_M^2 + K\tau_D V^2\tau_M^2 - \left(D\tau_D + V^2\tau_M^2\right)\left(1 + \frac{1}{2}\frac{2K\tau_D V^2\tau_M^2(V^2\tau_M^2 - D\tau_D)}{\left(D\tau_D + V^2\tau_M^2\right)^2}\right)\right)}{\sqrt{2D\tau_D V^2\tau_M^2}}$$

using

$$\sqrt{1+x} \approx 1 + \frac{x}{2}$$

for small x. Continuing the calculations,

$$\phi_- \approx \frac{\sqrt{K\tau_D}}{\sqrt{D\tau_D + V^2\tau_M^2}}$$

and

$$\phi_+ \approx \frac{\sqrt{\left(D\tau_D + V^2\tau_M^2\right)^2 + K\tau_D V^4 \tau_M^4}}{\sqrt{D\tau_D V^2 \tau_M^2 \left(D\tau_D + V^2\tau_M^2\right)}}. \tag{2.18}$$

Since the approximation for ϕ_- is dependent on K, we can reduce the hyperbolic functions $\cosh(\phi_-(c-a))$ and $\sinh(\phi_-(c-a))$ by assuming $K \ll$ such that

$$\phi_-(c-a) \ll 1 \tag{2.19}$$

so that

$$\cosh(\phi_-(c-a)) \approx 1 + \frac{\phi_-^2(c-a)^2}{2}, \qquad \sinh(\phi_-(c-a)) \approx \phi_-(c-a) + \frac{\phi_-^3(c-a)^3}{6}.$$

However, the hyperbolic terms involving ϕ_+ cannot be simplified in the same way. The essential obstruction is that varying K does not drive ϕ_+ to a sufficiently small value. This can be seen from the following simplification of Equation 2.18:

$$\phi_+ \approx \varphi \sqrt{1 + \frac{K\tau_D V^4 \tau_M^4}{(D\tau_D + V^2\tau_M^2)^2}}.$$

where

$$\varphi = \sqrt{\frac{D\tau_D + V^2\tau_M^2}{D\tau_D V^2 \tau_M^2}}.$$

Assuming $K \ll 1$ such that

$$\frac{K\tau_D V^4 \tau_M^4}{(D\tau_D + V^2\tau_M^2)^2} \ll 1, \tag{2.20}$$

ϕ_+ reduces to the following

$$\phi_+ \approx \varphi + \frac{K\tau_D V^3 \tau_M^3}{2\sqrt{D\tau_D}(D\tau_D + V^2\tau_M^2)^{3/2}}.$$

when using $\sqrt{1+x} \approx 1 + \frac{1}{2}x$. Thus, linearizing the required hyperbolic functions yield the following:

$$\sinh(\phi_+(c-a)) \approx \sinh(\varphi(c-a)) + \frac{K\tau_D V^3 \tau_M^3 (c-a)}{2\sqrt{D\tau_D}\left(D\tau_D + V^2\tau_M^2\right)^{3/2}} \cosh(\varphi(c-a))$$

and

$$\cosh(\phi_+(c-a)) \approx \cosh(\varphi(c-a)) + \frac{K\tau_D V^3 \tau_M^3 (c-a)}{2\sqrt{D\tau_D}\left(D\tau_D + V^2\tau_M^2\right)^{3/2}} \sinh(\varphi(c-a)).$$

Plugging these approximations into the intermittence formula in Equation (2.14) and using the inequality $t_m < t_{diff}$ representing when intermittence is favorable, we arrive at the following inequality:

$$D(\tau_D + \tau_M)(R_1 + R_2) < (c-a)^3 (D\tau_D + V^2\tau_M^2)^2 (R_3 + R_4) \tag{2.21}$$

where

$$R_1 = \cosh(\varphi(c-a))\sqrt{D\tau_D}$$
$$\cdot \begin{pmatrix} -3V^2\tau_M^3(c-a)^2\left(K\tau_D V^4\tau_M^4 - 2(D\tau_D + V^2\tau_M^2)(D\tau_D + V^2\tau_M^2 + K\tau_D V^2\tau_M^2)\right) \\ +2K\tau_D V^3\tau_M^3(D\tau_D + V^2\tau_M^2)(c-a)^4 \\ -3V^4\tau_M^4\left(K\tau_D V^4\tau_M^4 - 2(D\tau_D + V^2\tau_M^2)^2\right)(c-a)\tanh\left(\frac{a}{V\tau_M}\right) \\ +(D\tau_D + V^2\tau_M^2)\begin{pmatrix} K\tau_D V^2\tau_M^2(3V^2\tau_M^2 - 2D\tau_D) \\ +2(D\tau_D + V^2\tau_M^2)^2 \end{pmatrix}(c-a)^3\tanh\left(\frac{a}{V\tau_M}\right) \end{pmatrix},$$

$$R_2 = \sinh(\varphi(c-a))\sqrt{D\tau_D + V^2\tau_M^2}$$

$$\cdot \begin{pmatrix} -6D\tau_D V^4\tau_M^4(D\tau - S + V^2\tau_M^2 + K\tau_D V^2\tau_M^2)(c-a) \\ +\left(2D\tau_D(D\tau_D + V^2\tau_M^2)^2 + K\tau_D V^2\tau_M^2(V^2\tau_M^2 - D\tau_D)(2D\tau_D + 3V^2\tau_M^2)\right)(c-a)^3 \\ -6D\tau_D V^5\tau_M^5(D\tau_D + V^2\tau_M^2)\tanh\left(\dfrac{a}{V\tau_M}\right) \\ +3K\tau_D V^5\tau_M^5(V^2\tau_M^2 - D\tau_D)(c-a)^2\tanh\left(\dfrac{a}{V\tau_M}\right) \\ +K\tau_D V^3\tau_M^3(D\tau_D + V^2\tau_M^2)(c-a)^4\tanh\left(\dfrac{a}{V\tau_M}\right) \end{pmatrix},$$

$$R_3 = \cosh(\varphi(c-a))\sqrt{D\tau_D}\begin{pmatrix} 3K\tau_D V^3\tau_M^3(c-a) + K\tau_D(D\tau_D + V^2\tau_M^2)(c-a)^2\tanh\left(\dfrac{a}{V\tau_M}\right) \\ +2\left((D\tau_D + V^2\tau_M^2)^2 + K\tau_D V^2\tau_M^2(V^2\tau_M^2 - D\tau_D)\right)\tanh\left(\dfrac{a}{V\tau_M}\right) \end{pmatrix},$$

$$R_4 = \sinh(\varphi(c-a))\sqrt{D\tau_D + V^2\tau_M^2}\begin{pmatrix} 2D\tau_D(D\tau_D + V^2\tau_M^2 - K\tau_D V^2\tau_M^2) \\ +KD\tau_D^2(c-a)^2 + K\tau_D V^3\tau_M^3(c-a)\tanh\left(\dfrac{a}{V\tau_M}\right) \end{pmatrix}.$$

Therefore, our threshold for $K \ll 1$ exists whenever the conditions from Equations (2.17), (2.20), and (2.21) hold. We confirm numerically by using various choices for the parameters a, c, D, V, τ_D, and τ_M and by varying K over the set $\left\{10^{-3}, 10^{-4}, ..., 10^{-9}, 10^{-10}\right\}$. In every case where the three conditions held, intermittence was deemed as favorable. Additionally, there were several cases where two of the previously discussed conditions (Equations (2.15) and (2.19)) were not met and yet intermittence was still favorable, one being the following:

$$a = 1, \quad c = 100, \quad D = 1.2, \quad V = 1.3, \quad \tau_D = 10, \quad \tau_M = 5, \quad K = 10^{-3}.$$

However, we also have several examples where intermittence was unfavorable where only the inequality condition from Equation (2.21) did not hold, one being the following:

$$a = 1, \quad c = 100, \quad D = 12, \quad V = 1.3, \quad \tau_D = 10, \quad \tau_M = 60, \quad K = 10^{-10}.$$

This confirms that Equations (2.17), (2.20), and (2.21) are the important for intermittence criterion, with Equation (2.21) possibly being the most important.

2.2.2 Two-Dimensional Case

For the two-dimensional model, we consider the circular domain of radius b, where the target is positioned at the origin. The first detection zone is defined as the circle of radius a centered at the target. The second detection zone is represented by an annulus also centered at the target and spanning radii a and c. The three regions are illustrated in Figure 2.4.

We consider both the diffusion-only and intermittence models.

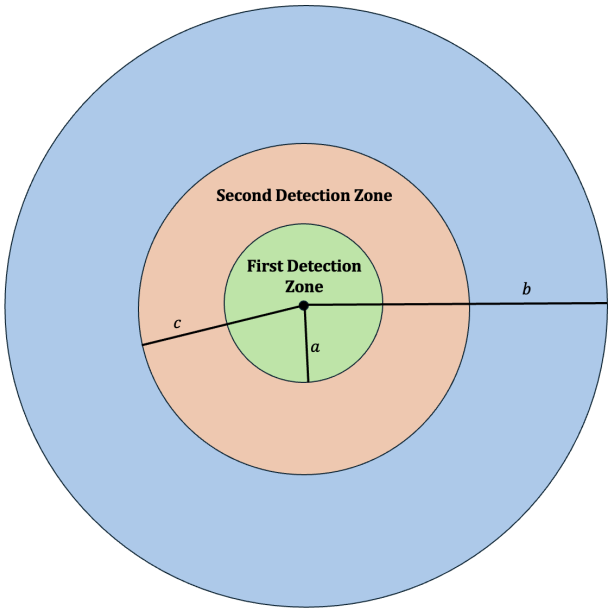

Figure 2.4: Diagram of the two-dimensional domain with two detection zones.

Diffusion Only: Two-Dimensional Case

During the diffusion-only model, the searcher exclusively performs a random walk with diffusion coefficient D until locating the target. Let $\mathscr{Y} = \{(y_1, y_2) : y_1^2 + y_2^2 \leq b\}$ denote the spatial domain, and $\mathscr{J} = \{\mathbf{0}, \mathbf{A}\}$, where $j = \mathbf{0}$ represents the detection phase and $j = \mathbf{A}$ denotes the termination phase. Again, we label the state corresponding to scanning as

$j = \mathbf{0}$, representing diffusion alone. Lastly, the absorbing set is $A = \{(\vec{y}, \mathbf{0}) \in \mathscr{Y} \times \mathscr{J} : |\vec{y}| = y_1^2 + y_2^2 \leq a\}$, which represents the searcher entering the first detection zone while in the detection phase.

To formulate the equation governing the process, we apply the methodology described in Chapter 1.3 and utilize the general Equation (1.15) to derive its two-dimensional representation:

$$-1 = \mu_Y(0,\vec{x},i) \cdot \left(\frac{\partial t_i}{\partial x_1}, \frac{\partial t_i}{\partial x_2} \right) + \frac{1}{2} \sigma_Y(0,\vec{x},i) \sigma_Y(0,\vec{x},i)^T : \begin{pmatrix} \frac{\partial^2 t_i}{\partial x_1^2} & \frac{\partial^2 t_i}{\partial x_1 \partial x_2} \\ \frac{\partial^2 t_i}{\partial x_1 \partial x_2} & \frac{\partial^2 t_i}{\partial x_2^2} \end{pmatrix} \tag{2.22}$$
$$+ \int_{\varsigma \neq i} \Lambda(0,\vec{x},\varsigma|\vec{x},i) \left[t_\varsigma(\vec{x}) - t_i(\vec{x}) \right] d\varsigma,$$

where $\Lambda(0,\vec{x},\varsigma|\vec{x},i)$ denotes the transition rate out of the initial state i when starting search at location $\vec{x} = (x_1, x_2)$. We set the drift and diffusion parameters as the following:

$$\mu_Y(0,\vec{x},\mathbf{0}) = 0 \quad \text{and} \quad \frac{1}{2}\sigma_Y^2(0,\vec{x},\mathbf{0}) = \begin{pmatrix} D & 0 \\ 0 & D \end{pmatrix}.$$

Similar to the one-dimensional case in Chapter 2.2.1, the jump (integral) term is written as follows:

$$\Lambda(0,\vec{x},\mathbf{A}|\vec{x},\mathbf{0})[t_\mathbf{A}(\vec{x}) - t_\mathbf{0}(\vec{x})] = -K\left(I_c(\vec{x}) - I_a(\vec{x})\right) t_\mathbf{0}(\vec{x}),$$

where $I_y(\vec{x})$ denotes the indicator function

$$I_y(\vec{x}) = \begin{cases} 1, & |\vec{x}| \leq y, \\ 0, & |\vec{x}| > y. \end{cases}$$

Substituting these expressions into Equation (2.22) results in the following equation:

$$D\Delta t_\mathbf{0}(\vec{x}) - K\left(I_c(\vec{x}) - I_a(\vec{x})\right) t_\mathbf{0}(\vec{x}) = -1.$$

As we have seen in Chapter 1, since the searcher's random walk does not favor any direction, $t_\mathbf{0}$ exhibits radial symmetry so that $t_\mathbf{0}(\vec{x}) = t_\mathbf{0}(r)$, where $r = |\vec{x}| = \sqrt{x_1^2 + x_2^2}$. Using the boundary conditions derived from the one-dimensional model presented in

Chapter 2.2.1, the new system is formulated as follows in polar form:

$$\begin{cases} D\dfrac{d^2t_{\mathbf{0}}}{dr^2}+D\dfrac{1}{r}\dfrac{d^2t_{\mathbf{0}}}{dr^2}-K\left(I_c(r)-I_a(r)\right)t_{\mathbf{0}}(r)=-1, \\ \dfrac{dt_{\mathbf{0}}^{out}}{dr}(b)=0, \qquad t_{\mathbf{0}}^{mid}(a)=0, \\ \dfrac{dt_{\mathbf{0}}^{mid}}{dr}(c)=\dfrac{dt_{\mathbf{0}}^{out}}{dr}(c), \qquad t_{\mathbf{0}}^{mid}(c)=t_{\mathbf{0}}^{out}(c). \end{cases}$$

Solving the system gives us

$$\begin{aligned} t_{\mathbf{0}}^{in} &\equiv 0, \\ t_{\mathbf{0}}^{mid} &= \frac{\left(b^2-c^2\right)}{2DcJ_2}\sqrt{\frac{D}{K}}\left[I_0\left(r\sqrt{\frac{K}{D}}\right)K_0\left(a\sqrt{\frac{K}{D}}\right)-I_0\left(a\sqrt{\frac{K}{D}}\right)K_0\left(r\sqrt{\frac{K}{D}}\right)\right] \\ &\quad -\frac{1}{KJ_2}\left[I_1\left(c\sqrt{\frac{K}{D}}\right)K_0\left(r\sqrt{\frac{K}{D}}\right)+I_0\left(r\sqrt{\frac{K}{D}}\right)K_1\left(c\sqrt{\frac{K}{D}}\right)-J_2\right], \\ t_{\mathbf{0}}^{out} &= \frac{1}{4D}\left(2b^2\ln\frac{r}{c}-r^2+c^2\right)+\frac{\left(b^2-c^2\right)J_1}{2DcJ_2}\sqrt{\frac{D}{K}}+\frac{1}{K}\left(1-\frac{1}{cJ_2}\sqrt{\frac{D}{K}}\right), \end{aligned}$$

where

$$\begin{aligned} J_1 &= I_0\left(c\sqrt{\frac{K}{D}}\right)K_0\left(a\sqrt{\frac{K}{D}}\right)-I_0\left(a\sqrt{\frac{K}{D}}\right)K_0\left(c\sqrt{\frac{K}{D}}\right), \\ J_2 &= I_1\left(c\sqrt{\frac{K}{D}}\right)K_0\left(a\sqrt{\frac{K}{D}}\right)+I_0\left(a\sqrt{\frac{K}{D}}\right)K_1\left(c\sqrt{\frac{K}{D}}\right). \end{aligned}$$

This leads to the mean search time as follows:

$$t_{diff}=\frac{1}{\pi b^2}\int_0^b\int_0^{2\pi}t_{\mathbf{0}}rd\theta_r dr=\frac{2}{b^2}\int_0^b t_{\mathbf{0}}rdr=\frac{2}{b^2}\int_0^a t_{\mathbf{0}}^{in}rdr+\frac{2}{b^2}\int_a^c t_{\mathbf{0}}^{mid}rdr+\frac{2}{b^2}\int_c^b t_{\mathbf{0}}^{out}rdr$$

$$\begin{aligned} t_{diff} &= -\frac{\left(3-4\ln\frac{b}{c}\right)b^4-4b^2c^2+c^4}{8b^2D}+\frac{b^2-a^2}{b^2K}-\frac{b^2-c^2+2caJ_3}{b^2cKJ_2} \\ &\quad +\frac{\left(\left(b^2-c^2\right)^2KJ_1+2\left(b^2-c^2\right)\left(cKJ_2-D\right)\right)}{2b^2cKDJ_2}\sqrt{\frac{D}{K}}, \end{aligned} \tag{2.23}$$

where

$$J_3 = I_1\left(c\sqrt{\frac{K}{D}}\right)K_1\left(a\sqrt{\frac{K}{D}}\right) - I_1\left(a\sqrt{\frac{K}{D}}\right)K_1\left(c\sqrt{\frac{K}{D}}\right).$$

Having established the diffusion-only models, we next discuss the intermittence model.

Intermittence: Two-Dimensional Case

Similar to the diffusion-only Chapter 2.2.2, we consider a circular domain with radius b, where the target is positioned at the origin. Within this domain, two distinct detection zones are defined. The first detection zone is defined as a circle with radius a centered at the origin, where the target. The second, also centered at the origin, is an annulus spanning radii a and c.

The searcher operates within this domain through two distinct phases. The motion phase is described by ballistic motion, where the velocity magnitude is fixed at $V > 0$ and the direction θ_V is uniformly distribution within $(0, 2\pi]$. The detection phase involves a random walk characterized by a diffusion coefficient D. During this phase, the searcher automatically finds the target upon entering the first detection zone and detects the target at a fixed rate of $K > 0$ when within the second detection zone.

Let $\mathscr{Y} = \{(y_1, y_2) : y_1^2 + y_2^2 \leq b\}$ denote the spatial domain. We now consider the state domain $\mathscr{J}$. Since the motion phase is determined by the direction $\theta_V \in (0, 2\pi]$, we label the states within the phase as $j = \theta_{\mathbf{V}}$. For notation clarity, we then label the single states of the detection and termination phase as $i = \mathbf{0}$ and $j = \mathbf{A}$, respectively. Thus, the state domain is

$$\mathscr{J} = \{\mathbf{0}\} \cup \{\theta_{\mathbf{V}} : \theta_V \in (0, 2\pi]\} \cup \{\mathbf{A}\}.$$

Lastly, the absorbing set is $A = \left\{(\vec{y}, \mathbf{0}) \in \mathscr{Y} \times \mathscr{J} : |\vec{y}| = y_1^2 + y_2^2 \leq a\right\}$, corresponding to the searcher entering the first detection zone while in the detection phase.

Following the method from Chapter 1.3, the two-dimensional version of Equation (1.15) is given by:

$$-1 = \mu_Y(0,\vec{x},i)\cdot\left(\frac{\partial t_i}{\partial x_1},\frac{\partial t_i}{\partial x_2}\right)+\frac{1}{2}\sigma_Y(0,\vec{x},i)\sigma_Y(0,\vec{x},i)^T : \begin{pmatrix} \frac{\partial^2 t_i}{\partial x_1^2} & \frac{\partial^2 t_i}{\partial x_1 \partial x_2} \\ \frac{\partial^2 t_i}{\partial x_1 \partial x_2} & \frac{\partial^2 t_i}{\partial x_2^2} \end{pmatrix} \tag{2.24}$$
$$+\int_{\varsigma\neq i}\Lambda(0,\vec{x},\varsigma|\vec{x},i)\left[t_\varsigma(\vec{x})-t_i(\vec{x})\right]d\varsigma,$$

where $\Lambda(0,\vec{x},\varsigma|\vec{x},i)$ denotes the transition rate out of the initial location $\vec{x}=(x_1,x_2)$ and state i.

We first derive the equation for the **detection phase**, labeled as $i=\mathbf{0}$. With no motion and diffusion coefficient D, we define the following parameters:

$$\mu_Y(0,\vec{x},\mathbf{0})=0 \quad \text{and} \quad \frac{1}{2}\sigma_Y(0,\vec{x},\mathbf{0})\sigma_Y(0,\vec{x},\mathbf{0})^T=\begin{pmatrix} D & 0 \\ 0 & D \end{pmatrix}.$$

The jump (integral) term represents transitions out of the detection phase, either to a state in the motion phase or through locating the target. When the target is found, the searcher transitions to the termination phase $i=\mathbf{A}$ at a fixed rate K within the second detection zone. This transition is expressed as follows:

$$\Lambda(0,\vec{x},\mathbf{A}|\vec{x},\mathbf{0})[t_\mathbf{A}(\vec{x})-t_\mathbf{0}(\vec{x})]=-K\left(I_c(\vec{x})-I_a(\vec{x})\right)t_\mathbf{0}(\vec{x}),$$

where $I_y(x)$ denotes the indicator function:

$$I_y(\vec{x})=\begin{cases}1, & |\vec{x}|\leq y \\ 0, & |\vec{x}|>y.\end{cases}$$

If the target is not located, the search transitions to a state $i=\theta_\mathbf{V}$ within the motion phase at a fixed rate of $1/\tau_D$. Since this transition occurs with a uniformly random distribution over $(0,2\pi]$, we express the relationship as follows:

$$\int_{\substack{\varsigma\neq\mathbf{0}\\ \varsigma\neq\mathbf{A}}}\Lambda(0,\vec{x},\varsigma|\vec{x},\mathbf{0})\left[t_\varsigma(\vec{x})-t_\mathbf{0}(\vec{x})\right]d\varsigma=\frac{1}{2\pi}\int_0^{2\pi}\frac{1}{\tau_D}\left[t_{\theta_\mathbf{V}}(\vec{x})-t_\mathbf{0}(\vec{x})\right]d\theta_V.$$

Combining these components yields the complete expression for the jump term:

$$\int_{\varsigma\neq\mathbf{0}} \Lambda(0,\vec{x},\varsigma|\vec{x},\mathbf{0})\left[t_\varsigma(\vec{x})-t_{\mathbf{0}}(\vec{x})\right]d\varsigma$$
$$= \frac{1}{2\pi\tau_D}\int_0^{2\pi}\left(t_{\theta_\mathbf{V}}(\vec{x})-t_{\mathbf{0}}(\vec{x})\right)d\theta_V - K\left[I_c(\vec{x})-I_a(\vec{x})\right]t_{\mathbf{0}}.$$

Substituting these expressions into Equation (2.24) results in the equation for state $i=\mathbf{0}$:

$$D\Delta t_{\mathbf{0}} + \frac{1}{2\pi\tau_D}\int_0^{2\pi}\left(t_{\theta_\mathbf{V}}-t_{\mathbf{0}}\right)d\theta_V - K\left[I_c(\vec{x})-I_a(\vec{x})\right]t_{\mathbf{0}} = -1. \tag{2.25}$$

Now, we derive the states within the **motion phase**. We consider an arbitrary state $i=\theta_\mathbf{V}$. With no diffusion and constant drift velocity $\vec{V}=(V_1,V_2)$ in Cartesian coordinates, we define the following parameters:

$$\mu_Y(0,\vec{x},\theta_\mathbf{V})=\vec{V} \quad \text{and} \quad \frac{1}{2}\sigma_Y(0,\vec{x},\theta_\mathbf{V})\sigma_Y(0,\vec{x},\theta_\mathbf{V})^T = \begin{pmatrix} 0 & 0 \\ 0 & 0 \end{pmatrix}.$$

Since the searcher is only allowed to transition out of the motion phase to the single state $i=\mathbf{0}$ of the detection phase at a rate of $1/\tau_M$, the jump term represents as follows:

$$\int_{\varsigma\neq\theta_\mathbf{V}} \Lambda(0,\vec{x},\varsigma|\vec{x},\theta_\mathbf{V})\left[t_\varsigma(\vec{x})-t_{\theta_\mathbf{V}}(\vec{x})\right]d\varsigma = \frac{1}{\tau_M}\left[t_{\mathbf{0}}(\vec{x})-t_{\theta_\mathbf{V}}(\vec{x})\right].$$

Substituting these expressions into Equation (2.24) results in the motion phase equation for state $i=\theta_\mathbf{V}$:

$$\vec{V}\cdot\nabla t_{\theta_\mathbf{V}}(\vec{x}) + \frac{1}{\tau_M}\left[t_{\mathbf{0}}(\vec{x})-t_{\theta_\mathbf{V}}(\vec{x})\right] = -1. \tag{2.26}$$

Since our goal is to determine the average search time whenever the searcher starts in the detection phase, we only need to solve $t_{\mathbf{0}}$. As such, we follow the methodology outlined by Bénichou et al. [21] to help simplify the system of Equations (2.25) and (2.26). We consider the functions representing the average and the average times the velocity vector $\vec{V}$ of all motion phase states:

$$s(\vec{x}) = \left\langle t_{\theta_\mathbf{V}}\right\rangle_{\theta_V} \qquad \text{and} \qquad \vec{d}(\vec{x}) = \left\langle t_{\theta_\mathbf{V}}\vec{V}\right\rangle_{\theta_V},$$

where

$$\langle\cdot\rangle_{\theta_V} = \frac{1}{2\pi}\int_0^{2\pi}\cdot\, d\theta_V.$$

Using these definitions, we restructure Equation (2.25) in polar coordinates as follows:

$$D\Delta t_{\mathbf{0}} + \frac{1}{\tau_D}(s - t_{\mathbf{0}}) - K\left[I_c(\vec{x}) - I_a(\vec{x})\right] t_{\mathbf{0}} = -1. \tag{2.27}$$

We next reformulate the motion phase Equation (2.26). By computing two averages, one involving the equation itself and another involving the equation multiplied by $\vec{V}$, we obtain the following expressions:

$$\nabla \cdot \vec{d}(\vec{x}) + \frac{1}{\tau_M}\left[t_{\mathbf{0}}(\vec{x}) - s(\vec{x})\right] = -1 \tag{2.28}$$

and

$$\vec{d}(\vec{x}) = \tau_M \left\langle \left(\vec{V} \cdot \nabla t_{\theta_{\mathbf{V}}}\right) \vec{V} \right\rangle_{\theta_V}, \tag{2.29}$$

respectively. By taking the divergence of Equation (2.29), we derive the following result:

$$\nabla \cdot \vec{d}(\vec{x}) = \tau_M \sum_{i,j=1}^{2} \frac{\partial^2}{\partial x_i \partial x_j} \left\langle V_i V_j t_{\theta_{\mathbf{V}}} \right\rangle_{\theta_V}. \tag{2.30}$$

By employing the following decoupling assumption

$$\left\langle V_i V_j t_{\theta_{\mathbf{V}}} \right\rangle_{\theta_V} \simeq \left\langle V_i V_j \right\rangle_{\theta_V} \left\langle t_{\theta_{\mathbf{V}}} \right\rangle_{\theta_V},$$

we approximate Equation (2.30) as

$$\nabla \cdot \vec{d}(\vec{x}) = \frac{V^2 \tau_M}{2} \Delta s. \tag{2.31}$$

Substituting this approximation into Equation (2.28) leads to the following:

$$\frac{V^2 \tau_M}{2} \Delta s + \frac{1}{\tau_M}\left[t_{\mathbf{0}}(\vec{x}) - s(\vec{x})\right] = -1 \tag{2.32}$$

As described in the diffusion-only Chapter 2.2.2, the state $t_{\mathbf{0}}$ of the diffusion phase and each state $t_{\theta_{\mathbf{V}}}$ of the motion phase have radial symmetry so that $t_{\mathbf{0}}(\vec{x}) = t_{\mathbf{0}}(r)$ and $t_{\theta_{\mathbf{V}}}(\vec{x}) = t_{\theta_{\mathbf{V}}}(r)$, where $r = \sqrt{x_1^2 + x_2^2}$. This implies that s also has radial symmetry. We use the same boundary conditions as the one-dimensional case in Chapter 2.2.1, excluding $\frac{ds^{in}}{dr}(0)$, mainly because solving the system results in 9 unknown constants instead of 10. Thus, the

new system of equations in polar form results in the following:

$$\begin{cases} D\Delta t_{\mathbf{0}} + \dfrac{1}{\tau_D}(s - t_{\mathbf{0}}) - K\left[I_c(\vec{x}) - I_a(\vec{x})\right] t_{\mathbf{0}} = -1, \\ \dfrac{V^2 \tau_M}{2} \Delta s + \dfrac{1}{\tau_M}(t_{\mathbf{0}} - s) = -1, \\ \dfrac{dt_{\mathbf{0}}^{out}}{dx}(b) = 0, \quad \dfrac{ds^{out}}{dx}(b) = 0, \\ t_{\mathbf{0}}^{mid}(a) = 0, \quad s^{mid}(a) = s^{in}(a), \quad \dfrac{ds^{mid}}{dx}(a) = \dfrac{ds^{in}}{dx}(a), \\ t_{\mathbf{0}}^{mid}(c) = t_{\mathbf{0}}^{out}(c), \quad \dfrac{dt_{\mathbf{0}}^{mid}}{dr}(c) = \dfrac{dt_{\mathbf{0}}^{out}}{dr}(c), \\ s^{mid}(c) = s^{out}(c), \quad \dfrac{ds^{mid}}{dx}(c) = \dfrac{ds^{out}}{dx}(c). \end{cases}$$

Solving the system gives us the following:

$$t_{\mathbf{0}}^{in} \equiv 0,$$

$$
\begin{aligned}
s^{in} = \tau_M &- \frac{(\tau_D+\tau_M)V\tau_M\phi_+\phi_-I_0\left(\frac{r\sqrt{2}}{V\tau_M}\right)}{\sqrt{2}K\tau_D\mathscr{D}I_1\left(\frac{a\sqrt{2}}{V\tau_M}\right)}\begin{pmatrix}\left(\phi_+^2-\varphi^2\right)I_1(a\phi_-)L_3\\ +c\phi_-\left(\phi_+^2-\varphi^2\right)I_0(c\phi_-)L_3M_5\\ +c\phi_+\left(\varphi^2-\phi_-^2\right)I_1(c\phi_-)L_3M_8\\ +c\varphi\left(\phi_+^2-\phi_-^2\right)I_1(c\phi_-)L_4M_5\end{pmatrix}\\
&+\frac{(\tau_D+\tau_M)cV\tau_ML_3I_0\left(\frac{r\sqrt{2}}{V\tau_M}\right)}{\sqrt{2}a\phi_+\left(2D\tau_D+V^2\tau_M^2\right)\mathscr{D}I_1\left(\frac{a\sqrt{2}}{V\tau_M}\right)}\begin{pmatrix}\left(2-V^2\tau_M^2\phi_+^2\right)\phi_-\left(\varphi^2-\phi_-^2\right)I_1(c\phi_-)\\ +\left(2-V^2\tau_M^2\phi_-^2\right)a\phi_+^2\left(\phi_+^2-\varphi^2\right)I_0(a\phi_-)M_5\\ +\left(2-V^2\tau_M^2\phi_+^2\right)a\phi_+\phi_-\left(\phi_+^2-\varphi^2\right)I_1(a\phi_-)M_6\end{pmatrix}\\
&-\frac{(\tau_D+\tau_M)\left(b^2-c^2\right)V\tau_MI_0\left(\frac{r\sqrt{2}}{V\tau_M}\right)}{2\sqrt{2}a\phi_+\varphi D\tau_DV^2\tau_M^2\mathscr{D}I_1\left(\frac{a\sqrt{2}}{V\tau_M}\right)}\begin{pmatrix}-\left(2-V^2\tau_M^2\phi_+^2\right)\phi_-^2\left(\varphi I_0(c\phi_-)L_3+\phi_-I_1(c\phi_-)L_4\right)\\ +\left(2-V^2\tau_M^2\phi_-^2\right)a\phi_+^3I_0(a\phi_-)\left(\varphi L_3M_8+\phi_+L_4M_5\right)\\ +\left(2-V^2\tau_M^2\phi_+^2\right)a\phi_+^2\phi_-I_1(a\phi_-)\left(\varphi L_3M_7+\phi_+L_4M_6\right)\end{pmatrix}\\
&-\frac{(\tau_D+\tau_M)V\tau_MI_0\left(\frac{r\sqrt{2}}{V\tau_M}\right)A}{2\sqrt{2}a\phi_+\mathscr{D}I_1\left(\frac{a\sqrt{2}}{V\tau_M}\right)}\begin{pmatrix}\left(2-V^2\tau_M^2\phi_-^2\right)\phi_+^2\begin{pmatrix}\left(\phi_+^2-\varphi^2\right)L_3\\ +ca\phi_-^2\left(\phi_+^2-\varphi^2\right)L_3M_5N_7\\ +ca\phi_+\phi_-\left(\varphi^2-\phi_-^2\right)L_3M_8N_6\\ +ca\phi_-\varphi\left(\phi_+^2-\phi_-^2\right)L_4M_5N_6\end{pmatrix}\\ -\left(2-V^2\tau_M^2\phi_+^2\right)\phi_-^2\begin{pmatrix}\left(\varphi^2-\phi_-^2\right)L_3\\ +ca\phi_+\phi_-\left(\phi_+^2-\varphi^2\right)L_3M_6N_8\\ +ca\phi_+^2\left(\varphi^2-\phi_-^2\right)L_3M_7N_5\\ +ca\phi_+\varphi\left(\phi_+^2-\phi_-^2\right)L_4M_6N_5\end{pmatrix}\end{pmatrix},
\end{aligned}
$$

$$t_{\mathbf{0}}^{mid} = \frac{(\tau_D+\tau_M)}{2K\tau_D\mathscr{D}} \begin{pmatrix} -\left(2-V^2\tau_M^2\phi_-^2\right)\phi_+\left(\phi_+^2-\varphi^2\right)\left(I_0(r\phi_-)-I_0(a\phi_-)\right)L_3 \\ +\left(2-V^2\tau_M^2\phi_+^2\right)c\phi_-^2\left(\phi_+^2-\varphi^2\right)I_0(c\phi_-)L_3\left(F_6(r)-M_6\right) \\ +\left(2-V^2\tau_M^2\phi_+^2\right)c\phi_+\phi_-\left(\varphi^2-\phi_-^2\right)I_1(c\phi_-)L_3\left(F_7(r)-M_7\right) \\ +\left(2-V^2\tau_M^2\phi_+^2\right)c\phi_-\varphi\left(\phi_+^2-\phi_-^2\right)I_1(c\phi_-)L_4\left(F_6(r)-M_6\right) \end{pmatrix}$$

$$+\frac{(\tau_D+\tau_M)\left(2-V^2\tau_M^2\phi_+^2\right)cL_3}{2\phi_+\left(2D\tau_D+V^2\tau_M^2\right)\mathscr{D}} \cdot \begin{pmatrix} \left(2-V^2\tau_M^2\phi_-^2\right)\phi_+\left(\phi_+^2-\varphi^2\right)\left(I_0(r\phi_-)M_6-I_0(a\phi_-)F_6(r)\right) \\ +\left(2-V^2\tau_M^2\phi_+^2\right)\phi_-\left(\varphi^2-\phi_-^2\right)I_1(c\phi_-)F_1(r) \end{pmatrix}$$

$$+\frac{(\tau_D+\tau_M)\left(b^2-c^2\right)\left(2-V^2\tau_M^2\phi_+^2\right)}{4D\tau_DV^2\tau_M^2\phi_+\varphi\mathscr{D}} \cdot \begin{pmatrix} -\left(2-V^2\tau_M^2\phi_-^2\right)\phi_+^2I_0(r\phi_-)\left(\varphi L_3M_7+\phi_+L_4M_6\right) \\ +\left(2-V^2\tau_M^2\phi_-^2\right)\phi_+^2I_0(a\phi_-)\left(\varphi L_3F_7(r)+\phi_+L_4F_6(r)\right) \\ +\left(2-V^2\tau_M^2\phi_+^2\right)\phi_-^2\left(\varphi I_0(c\phi_-)L_3+\phi_-I_1(c\phi_-)L_4\right)F_1(r) \end{pmatrix}$$

$$+\frac{(\tau_D+\tau_M)A}{4\phi_+\mathscr{D}} \cdot \begin{pmatrix} -\left(2-V^2\tau_M^2\phi_-^2\right)^2\phi_+^2\left(\phi_+^2-\varphi^2\right)L_3G_1(r) \\ +\left(2-V^2\tau_M^2\phi_+^2\right)^2\phi_-^2\left(\varphi^2-\phi_-^2\right)L_3F_1(r) \\ +\left(2-V^2\tau_M^2\phi_+^2\right)\left(2-V^2\tau_M^2\phi_-^2\right)c\phi_+^2\phi_-\left(\varphi^2-\phi_-^2\right)L_3\left(F_7(r)N_6-M_7G_6(r)\right) \\ +\left(2-V^2\tau_M^2\phi_+^2\right)\left(2-V^2\tau_M^2\phi_-^2\right)c\phi_+\phi_-^2\left(\phi_+^2-\varphi^2\right)L_3\left(F_6(r)N_7-M_6G_7(r)\right) \\ +\left(2-V^2\tau_M^2\phi_+^2\right)\left(2-V^2\tau_M^2\phi_-^2\right)c\phi_+\phi_-\varphi\left(\phi_+^2-\phi_-^2\right)L_4\left(F_6(r)N_6-M_6G_6(r)\right) \end{pmatrix},$$

$$
\begin{aligned}
s^{mid} = \tau_M + \frac{(\tau_D+\tau_M)}{2K\tau_D\mathscr{D}} & \begin{pmatrix} -\phi_+\left(\phi_+^2-\varphi^2\right)\left(2I_0(r\phi_-)-\left(2-V^2\tau_M^2\phi_-^2\right)I_0(a\phi_-)\right)L_3 \\ +c\phi_-^2\left(\phi_+^2-\varphi^2\right)I_0(c\phi_-)L_3\left(2F_6(r)-\left(2-V^2\tau_M^2\phi_+^2\right)M_6\right) \\ +c\phi_+\phi_-\left(\varphi^2-\phi_-^2\right)I_1(c\phi_-)L_3\left(2F_7(r)-\left(2-V^2\tau_M^2\phi_+^2\right)M_7\right) \\ +c\phi_-\varphi\left(\phi_+^2-\phi_-^2\right)I_1(c\phi_-)L_4\left(2F_6(r)-\left(2-V^2\tau_M^2\phi_+^2\right)M_6\right) \end{pmatrix} \\
+\frac{(\tau_D+\tau_M)cL_3}{\phi_+\left(2D\tau_D+V^2\tau_M^2\right)\mathscr{D}} & \begin{pmatrix} \left(2-V^2\tau_M^2\phi_+^2\right)\phi_+\left(\phi_+^2-\varphi^2\right)I_0(r\phi_-)M_6 \\ -\left(2-V^2\tau_M^2\phi_-^2\right)\phi_+\left(\phi_+^2-\varphi^2\right)I_0(a\phi_-)F_6(r) \\ +\left(2-V^2\tau_M^2\phi_+^2\right)\phi_-\left(\varphi^2-\phi_-^2\right)I_1(c\phi_-)F_1(r) \end{pmatrix} \\
+\frac{(\tau_D+\tau_M)\left(b^2-c^2\right)}{2D\tau_DV^2\tau_M^2\phi_+\varphi\mathscr{D}} & \begin{pmatrix} -\left(2-V^2\tau_M^2\phi_+^2\right)\phi_+^2I_0(r\phi_-)\left(\varphi L_3M_7+\phi_+L_4M_6\right) \\ +\left(2-V^2\tau_M^2\phi_-^2\right)\phi_+^2I_0(a\phi_-)\left(\varphi L_3F_7(r)+\phi_+L_4F_6(r)\right) \\ +\left(2-V^2\tau_M^2\phi_+^2\right)\phi_-^2\left(\varphi I_0(c\phi_-)L_3+\phi_-I_1(c\phi_-)L_4\right)F_1(r) \end{pmatrix} \\
+\frac{(\tau_D+\tau_M)A}{2\phi_+\mathscr{D}} & \begin{pmatrix} \left(2-V^2\tau_M^2\phi_-^2\right)\phi_+\begin{pmatrix} -\phi_+\left(\phi_+^2-\varphi^2\right)L_3G_1(r) \\ +c\phi_-^2\left(\phi_+^2-\varphi^2\right)L_3F_6(r)N_7 \\ +c\phi_+\phi_-\left(\varphi^2-\phi_-^2\right)L_3F_7(r)N_6 \\ +c\phi_-\varphi\left(\phi_+^2-\phi_-^2\right)L_3F_6(r)N_6 \end{pmatrix} \\ -\left(2-V^2\tau_M^2\phi_+^2\right)\phi_-\begin{pmatrix} -\phi_-\left(\varphi^2-\phi_-^2\right)L_3F_1(r) \\ +c\phi_+\phi_-\left(\phi_+^2-\varphi^2\right)L_3M_6G_7(r) \\ +c\phi_+^2\left(\varphi^2-\phi_-^2\right)L_3M_7G_6(r) \\ +c\phi_+\varphi\left(\phi_+^2-\phi_-^2\right)L_3M_6G_6(r) \end{pmatrix} \end{pmatrix},
\end{aligned}
$$

$$t_{\mathbf{0}}^{out} = \frac{(\tau_D+\tau_M)\left(c^2-r^2+2b^2\ln\frac{r}{c}\right)}{2\left(2D\tau_D+V^2\tau_M^2\right)}$$

$$-\frac{(\tau_D+\tau_M)}{2K\tau_D\phi_+\varphi\mathscr{D}}\begin{pmatrix}-\left(2-V^2\tau_M^2\phi_-^2\right)\phi_+^2\varphi\left(\phi_+^2-\varphi^2\right)I_0(a\phi_-)L_3\\+\left(2-V^2\tau_M^2\phi_+^2\right)c\phi_+\phi_-^2\varphi\left(\phi_+^2-\varphi^2\right)I_0(c\phi_-)L_3M_6\\+\left(2-V^2\tau_M^2\phi_+^2\right)c\phi_+^2\phi_-\varphi\left(\varphi^2-\phi_-^2\right)I_1(c\phi_-)L_3M_7\\+\left(2-V^2\tau_M^2\phi_+^2\right)c\phi_+\phi_-\varphi^2\left(\phi_+^2-\phi_-^2\right)I_1(c\phi_-)L_4M_6\\+\frac{V^2\tau_M^2}{D\tau_D}\phi_+^2\phi_-\left(\phi_+^2-\phi_-^2\right)I_1(c\phi_-)H_4(r)\\+2\left(\phi_+^2-\phi_-^2\right)\left(\phi_+^2-\varphi^2\right)\left(\varphi I_0(c\phi_-)L_3+\phi_-I_1(c\phi_-)L_4\right)\end{pmatrix}$$

$$+\frac{(\tau_D+\tau_M)\left(2-V^2\tau_M^2\phi_+^2\right)}{2\phi_+\varphi\left(2D\tau_D+V^2\tau_M^2\right)\mathscr{D}}\begin{pmatrix}-\left(2-V^2\tau_M^2\phi_-^2\right)\varphi\left(\phi_+^2-\varphi^2\right)I_0(a\phi_-)L_3\\+\left(2-V^2\tau_M^2\phi_-^2\right)c\phi_+\varphi\left(\phi_+^2-\varphi^2\right)I_0(c\phi_-)L_3M_6\\+\left(2-V^2\tau_M^2\phi_+^2\right)c\phi_-\varphi\left(\varphi^2-\phi_-^2\right)I_1(c\phi_-)L_3M_7\\+\frac{V^2\tau_M^2}{D\tau_D}c\phi_+\phi_-\left(\phi_+^2-\phi_-^2\right)I_1(c\phi_-)\left(H_4(r)-L_4\right)M_6\end{pmatrix}$$

$$
-\frac{(\tau_D+\tau_M)\left(b^2-c^2\right)}{4c\phi_+\varphi\left(2D\tau_D+V^2\tau_M^2\right)\mathscr{D}}
\begin{pmatrix}
2\left(2-V^2\tau_M^2\phi_+^2\right)c\varphi^3\left(\phi_+^2-\phi_-^2\right)I_0(c\phi_-)L_3M_7 \\
+\left(2-V^2\tau_M^2\phi_-^2\right)\phi_+^2 I_0(a\phi_-)\begin{pmatrix}2\left(\phi_+^2-\varphi^2\right)L_4\\ +\dfrac{V^2\tau_M^2}{D\tau_D}\phi_+^2 H_4(r)\end{pmatrix} \\
+\left(2-V^2\tau_M^2\phi_+^2\right)c\phi_+^3 I_0(c\phi_-)\begin{pmatrix}2\left(\varphi^2-\phi_-^2\right)L_4\\ -\dfrac{V^2\tau_M^2}{D\tau_D}\phi_-^2 H_4(r)\end{pmatrix}M_6 \\
+\left(2-V^2\tau_M^2\phi_+^2\right)c\phi_-^3 I_1(c\phi_-)\begin{pmatrix}2\left(\phi_+^2-\varphi^2\right)L_4\\ +\dfrac{V^2\tau_M^2}{D\tau_D}\phi_+^2 H_4(r)\end{pmatrix}M_7
\end{pmatrix}
$$

$$
-\frac{(\tau_D+\tau_M)\left(\phi_+^2-\phi_-^2\right)A}{4\phi_+\varphi\mathscr{D}}
\begin{pmatrix}
\left(2-V^2\tau_M^2\phi_-^2\right)\begin{pmatrix}2\left(\phi_+^2-\varphi^2\right)(\varphi L_3N_7+\phi_-L_4N_6)\\ +\dfrac{V^2\tau_M^2}{D\tau_D}\phi_+^2\phi_- H_4(r)N_6\end{pmatrix} \\
+\left(2-V^2\tau_M^2\phi_+^2\right)\begin{pmatrix}2\left(\varphi^2-\phi_-^2\right)(\varphi L_3M_7+\phi_+L_4M_6)\\ -\dfrac{V^2\tau_M^2}{D\tau_D}\phi_+\phi_-^2 H_4(r)M_6\end{pmatrix}
\end{pmatrix},
$$

$$s^{out} = \tau_M + \frac{(\tau_D+\tau_M)\left(c^2-r^2+2b^2\ln\frac{r}{c}\right)}{2\left(2D\tau_D+V^2\tau_M^2\right)}$$

$$-\frac{(\tau_D+\tau_M)}{2K\tau_D\phi_+\varphi\mathscr{D}}\begin{pmatrix}-\left(2-V^2\tau_M^2\phi_-^2\right)\phi_+^2\varphi\left(\phi_+^2-\varphi^2\right)I_0(a\phi_-)L_3\\+\left(2-V^2\tau_M^2\phi_+^2\right)c\phi_+\phi_-^2\varphi\left(\phi_+^2-\varphi^2\right)I_0(c\phi_-)L_3M_6\\+\left(2-V^2\tau_M^2\phi_+^2\right)c\phi_+^2\phi_-\varphi\left(\varphi^2-\phi_-^2\right)I_1(c\phi_-)L_3M_7\\+\left(2-V^2\tau_M^2\phi_+^2\right)c\phi_+\phi_-\varphi^2\left(\phi_+^2-\phi_-^2\right)I_1(c\phi_-)L_4M_6\\-2\phi_+^2\phi_-\left(\phi_+^2-\phi_-^2\right)I_1(c\phi_-)H_4(r)\\+2\left(\phi_+^2-\phi_-^2\right)\left(\phi_+^2-\varphi^2\right)\left(\varphi I_0(c\phi_-)L_3+\phi_-I_1(c\phi_-)L_4\right)\end{pmatrix}$$

$$+\frac{(\tau_D+\tau_M)}{\phi_+\varphi\left(2D\tau_D+V^2\tau_M^2\right)\mathscr{D}}\begin{pmatrix}-\left(2-V^2\tau_M^2\phi_-^2\right)\varphi\left(\phi_+^2-\varphi^2\right)I_0(a\phi_-)L_3\\+\left(2-V^2\tau_M^2\phi_+^2\right)c\phi_+\varphi\left(\phi_+^2-\varphi^2\right)I_0(c\phi_-)L_3M_6\\+\left(2-V^2\tau_M^2\phi_+^2\right)c\phi_-\varphi\left(\varphi^2-\phi_-^2\right)I_1(c\phi_-)L_3M_7\\+\left(2-V^2\tau_M^2\phi_+^2\right)c\phi_+\phi_-\left(\phi_+^2-\phi_-^2\right)I_1(c\phi_-)H_4(r)M_6\\-\left(2-V^2\tau_M^2\phi_+^2\right)c\phi_+\phi_-\left(\phi_+^2-\phi_-^2\right)I_1(c\phi_-)L_4M_6\end{pmatrix}$$

$$-\frac{(\tau_D+\tau_M)\left(b^2-c^2\right)}{2c\phi_+\varphi\left(2D\tau_D+V^2\tau_M^2\right)\mathscr{D}}\begin{pmatrix}\left(2-V^2\tau_M^2\phi_+^2\right)c\varphi^3\left(\phi_+^2-\phi_-^2\right)I_0(c\phi_-)L_3M_7\\+\left(2-V^2\tau_M^2\phi_-^2\right)\phi_+^2I_0(a\phi_-)\left(\left(\phi_+^2-\varphi^2\right)L_4-\phi_+^2H_4(r)\right)\\+\left(2-V^2\tau_M^2\phi_+^2\right)c\phi_+^3I_0(c\phi_-)\left(\left(\varphi^2-\phi_-^2\right)L_4+\phi_-^2H_4(r)\right)M_6\\+\left(2-V^2\tau_M^2\phi_+^2\right)c\phi_-^3I_1(c\phi_-)\left(\left(\phi_+^2-\varphi^2\right)L_4-\phi_+^2H_4(r)\right)M_7\end{pmatrix}$$

$$-\frac{(\tau_D+\tau_M)\left(\phi_+^2-\phi_-^2\right)A}{2\phi_+\varphi\mathscr{D}}\begin{pmatrix}\left(2-V^2\tau_M^2\phi_-^2\right)\begin{pmatrix}\left(\phi_+^2-\varphi^2\right)(\varphi L_3N_7+\phi_-L_4N_6)\\-\phi_+^2\phi_-H_4(r)N_6\end{pmatrix}\\+\left(2-V^2\tau_M^2\phi_+^2\right)\begin{pmatrix}\left(\varphi^2-\phi_-^2\right)(\varphi L_3M_7+\phi_+L_4M_6)\\+\phi_+\phi_-^2H_4(r)M_6\end{pmatrix}\end{pmatrix},$$

where

$$\varphi=\sqrt{\frac{2D\tau_D+V^2\tau_M^2}{D\tau_DV^2\tau_M^2}},$$

$$\phi_\pm=\sqrt{\frac{2D\tau_D+V^2\tau_M^2+K\tau_DV^2\tau_M^2\pm\sqrt{\begin{matrix}V^2\tau_M^2\left(4D\tau_D+V^2\tau_M^2+2K\tau_DV^2\tau_M^2\right)\\+\tau_D^2\left(2D-KV^2\tau_M^2\right)^2\end{matrix}}}{2D\tau_DV^2\tau_M^2}},$$

$$L_3=I_1(b\varphi)K_1(c\varphi)-I_1(c\varphi)K_1(b\varphi),$$
$$L_4=I_1(b\varphi)K_0(c\varphi)+I_0(c\varphi)K_1(b\varphi),$$

$$M_5=I_1(c\phi_+)K_1(a\phi_+)-I_1(a\phi_+)K_1(c\phi_+),$$
$$M_6=I_1(c\phi_+)K_0(a\phi_+)+I_0(a\phi_+)K_1(c\phi_+),$$
$$M_7=I_0(c\phi_+)K_0(a\phi_+)-I_0(a\phi_+)K_0(c\phi_+),$$
$$M_8=I_0(c\phi_+)K_1(a\phi_+)+I_1(a\phi_+)K_0(c\phi_+),$$

$$N_5=I_1(c\phi_-)K_1(a\phi_-)-I_1(a\phi_-)K_1(c\phi_-),$$
$$N_6=I_1(c\phi_-)K_0(a\phi_-)+I_0(a\phi_-)K_1(c\phi_-),$$
$$N_7=I_0(c\phi_-)K_0(a\phi_-)-I_0(a\phi_-)K_0(c\phi_-),$$
$$N_8=I_0(c\phi_-)K_1(a\phi_-)+I_1(a\phi_-)K_0(c\phi_-),$$

$$F_1(r) = I_0(r\phi_+)K_0(a\phi_+) - I_0(a\phi_+)K_0(r\phi_+),$$
$$F_6(r) = I_1(c\phi_+)K_0(r\phi_+) + I_0(r\phi_+)K_1(c\phi_+),$$
$$F_7(r) = I_0(c\phi_+)K_0(r\phi_+) - I_0(r\phi_+)K_0(c\phi_+),$$

$$G_1(r) = I_0(r\phi_-)K_0(a\phi_-) - I_0(a\phi_-)K_0(r\phi_-),$$
$$G_6(r) = I_1(c\phi_-)K_0(r\phi_-) + I_0(r\phi_-)K_1(c\phi_-),$$
$$G_7(r) = I_0(c\phi_-)K_0(r\phi_-) - I_0(r\phi_-)K_0(c\phi_-),$$

$$H_4(r) = I_1(b\varphi)K_0(r\varphi) + I_0(r\varphi)K_1(b\varphi),$$

$$\mathscr{D} = \frac{1}{2}\begin{pmatrix} \left(2 - V^2\tau_M^2\phi_-^2\right)\phi_+\left(\phi_+^2 - \varphi^2\right)I_0(a\phi_-)L_3 \\ -\left(2 - V^2\tau_M^2\phi_+^2\right)c\phi_-^2\left(\phi_+^2 - \varphi^2\right)I_0(c\phi_-)L_3M_6 \\ -\left(2 - V^2\tau_M^2\phi_+^2\right)c\phi_+\phi_-\left(\varphi^2 - \phi_-^2\right)I_1(c\phi_-)L_3M_7 \\ -\left(2 - V^2\tau_M^2\phi_+^2\right)c\phi_-\varphi\left(\phi_+^2 - \phi_-^2\right)I_1(c\phi_-)L_4M_6 \end{pmatrix},$$

$$\mathscr{L} = \frac{1}{2}\left(\begin{array}{c} \left(2-V^2\tau_M^2\phi_-^2\right)\phi_+^2 \left(\begin{array}{c} \left(\phi_+^2-\varphi^2\right)L_3 \\ +ca\phi_-^2\left(\phi_+^2-\varphi^2\right)L_3M_5N_7 \\ +ca\phi_+\phi_-\left(\varphi^2-\phi_-^2\right)L_3M_8N_6 \\ +ca\phi_-\varphi\left(\phi_+^2-\phi_-^2\right)L_4M_5N_6 \end{array}\right) \\ -\left(2-V^2\tau_M^2\phi_+^2\right)\phi_-^2 \left(\begin{array}{c} \left(\varphi^2-\phi_-^2\right)L_3 \\ +ca\phi_+\phi_-\left(\phi_+^2-\varphi^2\right)L_3M_6N_8 \\ +ca\phi_+^2\left(\varphi^2-\phi_-^2\right)L_3M_7N_5 \\ +ca\phi_+\varphi\left(\phi_+^2-\phi_-^2\right)L_4M_6N_5 \end{array}\right) \end{array}\right) I_0\left(\frac{a\sqrt{2}}{V\tau_M}\right)$$
$$+ca\phi_+\phi_-\left(\phi_+^2-\phi_-^2\right)\left(\begin{array}{c} \phi_-\left(\phi_+^2-\varphi^2\right)L_3M_6N_7 \\ +\phi_+\left(\varphi^2-\phi_-^2\right)L_3M_7N_6 \\ +\varphi\left(\phi_+^2-\phi_-^2\right)L_4M_6N_6 \end{array}\right)\frac{V\tau_M}{\sqrt{2}}I_1\left(\frac{a\sqrt{2}}{V\tau_M}\right),$$

$$
\begin{aligned}
A = {} & \frac{cL_3}{\left(2D\tau_D + V^2\tau_M^2\right)\mathscr{L}} \left[\begin{pmatrix} \left(2 - V^2\tau_M^2\phi_+^2\right)\phi_- \left(\varphi^2 - \phi_-^2\right) I_1(c\phi_-) \\ + \left(2 - V^2\tau_M^2\phi_-^2\right) a\phi_+^2 \left(\phi_+^2 - \varphi^2\right) I_0(a\phi_-) M_5 \\ + \left(2 - V^2\tau_M^2\phi_+^2\right) a\phi_+\phi_- \left(\phi_+^2 - \varphi^2\right) I_1(a\phi_-) M_6 \end{pmatrix} I_0\left(\frac{a\sqrt{2}}{V\tau_M}\right) \right. \\
& \left. + a\sqrt{2}V\tau_M\phi_+ \left(\phi_+^2 - \phi_-^2\right)\left(\phi_+^2 - \varphi^2\right) I_0(a\phi_-) M_6 I_1\left(\frac{a\sqrt{2}}{V\tau_M}\right) \right] \\
& - \frac{\left(b^2 - c^2\right)}{2D\tau_D V^2\tau_M^2\varphi\mathscr{L}} \left[\begin{pmatrix} -\left(2 - V^2\tau_M^2\phi_+^2\right)\phi_-^2 \left(\varphi I_0(c\phi_-) L_3 + \phi_- I_1(c\phi_-) L_4\right) \\ + \left(2 - V^2\tau_M^2\phi_-^2\right) a\phi_+^3 I_0(a\phi_-) \left(\varphi L_3 M_8 + \phi_+ L_4 M_5\right) \\ + \left(2 - V^2\tau_M^2\phi_+^2\right) a\phi_+^2\phi_- I_1(a\phi_-) \left(\varphi L_3 M_7 + \phi_+ L_4 M_6\right) \end{pmatrix} I_0\left(\frac{a\sqrt{2}}{V\tau_M}\right) \right. \\
& \left. + a\sqrt{2}V\tau_M\phi_+^2 \left(\phi_+^2 - \phi_-^2\right) I_0(a\phi_-) \left(\varphi L_3 M_7 + \phi_+ L_4 M_6\right) I_1\left(\frac{a\sqrt{2}}{V\tau_M}\right) \right] \\
& - \frac{a\phi_+^2\phi_-}{K\tau_D\mathscr{L}} \left[\begin{pmatrix} \left(\phi_+^2 - \varphi^2\right) I_1(a\phi_-) L_3 \\ + c\phi_- \left(\phi_+^2 - \varphi^2\right) I_0(c\phi_-) L_3 M_5 \\ + c\phi_+ \left(\varphi^2 - \phi_-^2\right) I_1(c\phi_-) L_3 M_8 \\ + c\varphi \left(\phi_+^2 - \phi_-^2\right) I_1(c\phi_-) L_4 M_5 \end{pmatrix} I_0\left(\frac{a\sqrt{2}}{V\tau_M}\right) \right. \\
& \left. + \begin{pmatrix} -\phi_- \left(\phi_+^2 - \varphi^2\right) I_0(a\phi_-) L_3 \\ + c\phi_+\phi_- \left(\phi_+^2 - \varphi^2\right) I_0(c\phi_-) L_3 M_6 \\ + c\phi_+^2 \left(\varphi^2 - \phi_-^2\right) I_1(c\phi_-) L_3 M_7 \\ + c\phi_+\varphi \left(\phi_+^2 - \phi_-^2\right) I_1(c\phi_-) L_4 M_6 \end{pmatrix} \frac{V\tau_M}{\sqrt{2}} I_1\left(\frac{a\sqrt{2}}{V\tau_M}\right) \right].
\end{aligned}
$$

Appendix B.2 provides a comprehensive justification for all denominators remaining strictly nonzero.

Assuming the searcher starts in the detection phase, the mean detection time over the entire domain was calculated as follows:

$$t_m = \frac{1}{\pi b^2}\int_0^b\int_0^{2\pi} t_{\mathbf{0}} r d\theta_r dr = \frac{2}{b^2}\int_0^b t_{\mathbf{0}} r dr = \frac{2}{b^2}\int_0^a t_{\mathbf{0}}^{in} r dr + \frac{2}{b^2}\int_a^c t_{\mathbf{0}}^{mid} r dr + \frac{2}{b^2}\int_c^b t_{\mathbf{0}}^{out} r dr$$

$$t_m = \frac{(\tau_D+\tau_M)}{2b^2}\left(-\frac{\left(3-4\ln\frac{b}{c}\right)b^4-4b^2c^2+c^4}{2\left(2D\tau_D+V^2\tau_M^2\right)}+\gamma_1+\gamma_2+\gamma_3+\gamma_4\right) \tag{2.33}$$

where

$$\gamma_1 = \frac{\left(2-V^2\tau_M^2\phi_+^2\right)}{\phi_+^3\phi_-\varphi^2\left(2D\tau_D+V^2\tau_M^2\right)\mathscr{D}}$$

$$\cdot\left(\begin{array}{c}
\left(2-V^2\tau_M^2\phi_-^2\right)\phi_+^2\varphi^2\left(\phi_+^2-\varphi^2\right)L_3\left(\begin{array}{c} c\phi_+\left(\left(b^2-c^2\right)\phi_- I_0(c\phi_-)\right)M_6 \\ +2c\phi_+\left(cI_1(c\phi_-)-aI_1(a\phi_-)\right)M_6 \\ -\phi_- I_0(a\phi_-)\left(\left(b^2-c^2\right)+2caM_5\right)\end{array}\right) \\
+\left(2-V^2\tau_M^2\phi_+^2\right)c\phi_-^2\varphi^2\left(\varphi^2-\phi_-^2\right)I_1(c\phi_-)L_3\left(\left(b^2-c^2\right)\phi_+^2M_7-2\left(1-c\phi_+M_6\right)\right) \\
-\frac{V^2\tau_M^2}{D\tau_D}c\phi_+^3\phi_-^2\left(\phi_+^2-\phi_-^2\right)I_1(c\phi_-)\left(\left(b^2-c^2\right)\varphi L_4-2cL_3\right)M_6
\end{array}\right),$$

$$\gamma_2 = \frac{1}{K\tau_D\phi_+\phi_-\varphi^2\mathscr{D}}$$

$$\cdot \begin{pmatrix} \left(2-V^2\tau_M^2\phi_-^2\right)\phi_+^2\varphi^2\left(\phi_+^2-\varphi^2\right)L_3 \begin{pmatrix} \left(b^2-a^2\right)\phi_- I_0(a\phi_-) \\ -2cI_1(c\phi_-)+2aI_1(a\phi_-) \end{pmatrix} \\ -\left(2-V^2\tau_M^2\phi_+^2\right)c\phi_-^2\varphi^2 \begin{pmatrix} \left(b^2-a^2\right)\phi_+\phi_-\left(\phi_+^2-\varphi^2\right)I_0(c\phi_-)L_3M_6 \\ +\left(b^2-a^2\right)\phi_+^2\left(\varphi^2-\phi_-^2\right)I_1(c\phi_-)L_3M_7 \\ +\left(b^2-a^2\right)\phi_+\varphi\left(\phi_+^2-\phi_-^2\right)I_1(c\phi_-)L_4M_6 \\ -2a\phi_-\left(\phi_+^2-\varphi^2\right)I_0(c\phi_-)L_3M_5 \\ -2a\varphi\left(\phi_+^2-\phi_-^2\right)I_1(c\phi_-)L_4M_5 \\ +2\left(\varphi^2-\phi_-^2\right)I_1(c\phi_-)L_3\left(1-a\phi_+M_8\right) \end{pmatrix} \\ -2\phi_-\left(\phi_+^2-\phi_-^2\right) \begin{pmatrix} \left(b^2-c^2\right)\varphi^2\left(\phi_+^2-\varphi^2\right)I_0(c\phi_-)L_3 \\ +\left(b^2-c^2\right)\phi_-\varphi\left(\phi_+^2-\varphi^2\right)I_1(c\phi_-)L_4) \\ +\dfrac{V^2\tau_M^2}{D\tau_D}c\phi_+^2\phi_- I_1(c\phi_-)L_3 \end{pmatrix} \end{pmatrix},$$

$$\gamma_3 = -\frac{\left(b^2-c^2\right)}{c\phi_+^3\phi_-\varphi^2\left(2D\tau_D+V^2\tau_M^2\right)\mathscr{D}}$$

$$\cdot\left(\begin{array}{c}
\left(2-V^2\tau_M^2\phi_-^2\right)\phi_+^4\phi_- I_0\left(a\phi_-\right)\left(\begin{array}{c}\left(b^2-c^2\right)\varphi\left(\phi_+^2-\varphi\right)L_4\\ +\dfrac{V^2\tau_M^2}{D\tau_D}c\phi_+^2 L_3\end{array}\right)\\
+\left(2-V^2\tau_M^2\phi_+^2\right)c\phi_+^2\phi_-\left(\begin{array}{c}\left(b^2-c^2\right)\varphi^4\left(\phi_+^2-\phi_-^2\right)I_0(c\phi_-)L_3M_7\\ +\left(b^2-c^2\right)\phi_+^3\varphi\left(\varphi^2-\phi_-^2\right)I_0(c\phi_-)L_4M_6\\ +\left(b^2-c^2\right)\phi_-^3\varphi\left(\phi_+^2-\varphi^2\right)I_1(c\phi_-)L_4M_7\\ -\dfrac{V^2\tau_M^2}{D\tau_D}c\phi_+^3\phi_-^2 I_0(c\phi_-)L_3M_6\\ +\dfrac{V^2\tau_M^2}{D\tau_D}c\phi_+^2\phi_-^3 I_1(c\phi_-)L_3M_7\end{array}\right)\\
+\left(2-V^2\tau_M^2\phi_+^2\right)^2 c\phi_-^3\varphi^2\left(\varphi I_0(c\phi_-)L_3+\phi_- I_1(c\phi_-)L_4\right)\left(1-c\phi_+M_6\right)\\
+\left(2-V^2\tau_M^2\phi_+^2\right)\left(2-V^2\tau_M^2\phi_-^2\right)c\phi_+^2\varphi^3\left(\begin{array}{c}\phi_+^2\varphi\left(cI_1(c\phi_-)-aI_1(a\phi_-)\right)L_3M_7\\ +\phi_+^3\left(cI_1(c\phi_-)-aI_1(a\phi_-)\right)L_4M_6\\ +\phi_-\varphi I_0(a\phi_-)L_3\left(1-a\phi_+M_8\right)\\ -a\phi_+^2\phi_- I_0(a\phi_-)L_4M_5\end{array}\right)
\end{array}\right),$$

$$\gamma_4 = \frac{A}{\phi_+^3 \phi_-^2 \varphi^2 \mathscr{D}}$$

$$\left(\begin{array}{c}
-\left(2 - V^2\tau_M^2\phi_-^2\right)\phi_+^2\phi_-^2\left(\phi_+^2 - \phi_-^2\right)\left(\begin{array}{c} \left(b^2 - c^2\right)\varphi\left(\phi_+^2 - \varphi^2\right)\left(\varphi L_3 N_7 + \phi_- L_4 N_6\right) \\ + \dfrac{V^2\tau_M^2}{D\tau_D} c\phi_+^2 \phi_- L_3 N_6 \end{array} \right) \\
-\left(2 - V^2\tau_M^2\phi_+^2\right)\phi_+^2\phi_-^2\left(\phi_+^2 - \phi_-^2\right)\left(\begin{array}{c} \left(b^2 - c^2\right)\varphi\left(\varphi^2 - \phi_-^2\right)\left(\varphi L_3 M_7 + \phi_+ L_4 M_6\right) \\ - \dfrac{V^2\tau_M^2}{D\tau_D} c\phi_+\phi_-^2 L_3 M_6 \end{array} \right) \\
+\left(2 - V^2\tau_M^2\phi_-^2\right)^2\phi_+^4\varphi^2\left(\phi_+^2 - \varphi^2\right)L_3\left(1 - c\phi_- N_6\right) \\
-\left(2 - V^2\tau_M^2\phi_+^2\right)^2\phi_-^4\varphi^2\left(\varphi^2 - \phi_-^2\right)L_3\left(1 - c\phi_+ M_6\right) \\
+\left(2 - V^2\tau_M^2\phi_+^2\right)\left(2 - V^2\tau_M^2\phi_-^2\right)c\phi_+^2\phi_-^2\varphi^2 \left(\begin{array}{c}
a\phi_-^2\left(\phi_+^2 - \varphi^2\right)L_3 M_5 N_7 \\
-a\phi_+^2\left(\varphi^2 - \phi_-^2\right)L_3 M_7 N_5 \\
-\phi_-\left(\varphi^2 - \phi_-^2\right)L_3\left(1 - a\phi_+ M_8\right)N_6 \\
+\phi_+\left(\phi_+^2 - \varphi^2\right)L_3 M_6\left(1 - a\phi_- N_8\right) \\
+a\phi_-\varphi\left(\phi_+^2 - \varphi^2\right)L_4 M_5 N_6 \\
-a\phi_+\varphi\left(\phi_+^2 - \varphi^2\right)L_4 M_6 N_5
\end{array} \right)
\end{array} \right).$$

The objective of this section is to identify the intermittence criterion, i.e., to determine when an intermittent strategy yields a smaller mean search time than the diffusion-only model. We begin by examining how space affects the relative performance of the two strategies. In the original single-detection zone model, Loverdo et al. [4] reported that intermittence becomes favorable whenever $b \gg \frac{D}{V}$. We test whether an analogous spatial criterion holds for our extended model.

Fixing the baseline parameters $a = 1$, $c = 3$, $b = 10$ and $K = 1$, we perform a numerical sweep over diffusion and relocation parameters (D, V). Specifically, we consider all pairs (D, V) on a 9×9 grid with $D, V \in \{0.01, 0.05, 0.1, 0.5, 1, 5, 10, 50, 100\}$. For each pair, we

evaluate and compare the intermittence (Equation 2.33) and diffusion-only (Equation 2.23) mean search time formulas, recording which is smaller. Across the grid, we find that intermittence is favorable whenever $\frac{D}{V} \leq 0.1$. Since $b = 10$, these results are consistent with a spatial criterion of the form $b \gg \frac{D}{V}$ in our model as well.

We next investigate how the detection rate K affects the intermittence criterion. To ensure $b \gg \frac{D}{V}$, we fix the baseline parameters $a = 1, b = 10, D = 1$, and $V = 10$ and examine a range of (c, K) pairs with $c \in \{2,3,4,5,6,7,8,9\}$ and $K = \{10^{-7}, 10^{-6}, ..., 10^{6}, 10^{7}\}$. For each pair, we again evaluate and compare the the intermittence (Equation 2.33) and diffusion-only (Equation 2.23) mean search time formulas and record the smaller of the two. To evaluate the intermittent expression, we perform a numerical sweep over a 100×100 grid with uniform mesh on $[0, T_{diff}] \times [0, T_{diff}]$, where T_{diff} denotes the diffusion-only mean search time at (c, K).

The results are summarized in Table 2.4. As seen in the one-dimensional case, an entry **F** indicates that there exists at least one choice (τ_D, τ_M) for which intermittence outperforms diffusion alone, while **N** indicates that no such choice is found. Entries marked with **N*** correspond to parameter settings for which the numerical evaluation produces an overflow-related `RuntimeWarning` message; in these cases, intermittence may still be favorable, but the minimum may be obscured without additional analytical simplification of Equation (2.33).

Overall, the table indicates that non-favorability becomes more prevalent as c approaches b and that the largest values of K tend to suppress intermittence relative to the smallest values. However, the transition from favorability to non-favorability is not monotone in K: for certain pairs (c, K), multiple switches can occur as K increases. A more refined characterization of these non-monotone transitions appears to be not analytically manageable within the scope of this work.

Because the intermittence mean search time Equation (2.33) is too complex to dissect further, we turn to simplified limiting regimes. Since the model contains three spatial regions (the first detection zone, the second detection zone, and the exterior no-detection

Table 2.4: Results of comparing intermittence with diffusion-alone. F represents when intermittence is favorable and N represents when it is not.

	$c=2$	$c=3$	$c=4$	$c=5$	$c=6$	$c=7$	$c=8$	$c=9$
$K=10^{-7}$	F	F	F	F	F	F	F	F
$K=10^{-6}$	F	F	F	F	F	F	F	F
$K=10^{-5}$	F	F	F	F	F	F	F	F
$K=10^{-4}$	F	F	F	F	F	F	F	F
$K=10^{-3}$	F	F	F	F	F	F	F	F
$K=10^{-2}$	F	F	F	F	F	F	F	F
$K=10^{-1}$	F	F	N	N	N	N	N	N
$K=10^{0}$	F	F	F	F	N	N	N	N
$K=10^{1}$	F	F	F	F	F	F	F	N
$K=10^{2}$	F	F	F	F	F	F	F	F
$K=10^{3}$	F	F	F	F	F	F	F	F
$K=10^{4}$	F	F	F	F	F	F	N	N
$K=10^{5}$	F	N*	N	N	N	N	N	N
$K=10^{6}$	N*	N	N	N	N	N	N	N
$K=10^{7}$	N	N	N	N	N	N	N	N

region), we isolate their roles by considering limits in which one region is effectively removed. Specifically, we analyze the following:

1) $c \to a$

2) $a \to 0$

3) $b \to c$

Case 1: $c \to a$ During this case, the second detection zone vanishes, and the model simplifies to the original single-detection zone framework of Loverado et al. [4]. We verify this analytically by taking the limit $c \to a$ and by showing that our two-detection zone mean search time expression in Equation (2.33) simplifies to the original mean search time

in Equation (2.1). As a consequence, the intermittence criterion then coincides with that of the original model: intermittence is favorable whenever $b \gg \frac{D}{V}$.

Case 2: $a \to 0$ During this case, the first detection zone collapses to the point of the target, leaving only one detection zone with a fixed rate K of finding the target. To determine the intermittence criterion, we first start with approximating the diffusion-only formula in Equation (2.23). Using Taylor Expansion for the modified Bessel functions, we see that for small x,

$$I_0(x) \sim 1, \quad I_1(x) \sim \frac{x}{2}, \quad K_0(x) \sim -\ln\left(\frac{x}{2}\right) - \gamma, \quad K_1(x) \sim \frac{1}{x}, \tag{2.34}$$

where γ is the Euler-Mascheroni constant so that

$$\begin{aligned}
\lim_{a\to 0^+} \frac{J_1}{J_2} &= \lim_{a\to 0^+} \frac{I_0\left(c\sqrt{\frac{K}{D}}\right) K_0\left(a\sqrt{\frac{K}{D}}\right) - I_0\left(a\sqrt{\frac{K}{D}}\right) K_0\left(c\sqrt{\frac{K}{D}}\right)}{I_1\left(c\sqrt{\frac{K}{D}}\right) K_0\left(a\sqrt{\frac{K}{D}}\right) + I_0\left(a\sqrt{\frac{K}{D}}\right) K_1\left(c\sqrt{\frac{K}{D}}\right)} \\
&= \lim_{a\to 0^+} \frac{I_0\left(c\sqrt{\frac{K}{D}}\right)\left(-\ln\left(\frac{a}{2}\sqrt{\frac{K}{D}}\right) - \gamma\right) - K_0\left(c\sqrt{\frac{K}{D}}\right)}{I_1\left(c\sqrt{\frac{K}{D}}\right)\left(-\ln\left(\frac{a}{2}\sqrt{\frac{K}{D}}\right) - \gamma\right) + K_1\left(c\sqrt{\frac{K}{D}}\right)} \\
&= \lim_{a\to 0^+} \frac{I_0\left(c\sqrt{\frac{K}{D}}\right)\left(-\frac{1}{a}\right)}{I_1\left(c\sqrt{\frac{K}{D}}\right)\left(-\frac{1}{a}\right)} \quad \text{by L'Hôpital's rule} \\
&= \frac{I_0\left(c\sqrt{\frac{K}{D}}\right)}{I_1\left(c\sqrt{\frac{K}{D}}\right)}.
\end{aligned}$$

Using these, Equation (2.23) reduces to the following:

$$t_{diff} \approx -\frac{\left(3-4\ln\frac{b}{c}\right)b^4-4b^2c^2+c^4}{8b^2D}+\frac{1}{K}-\frac{(b^2-c^2)^2 I_0\left(c\sqrt{\frac{K}{D}}\right)}{2b^2cDI_1\left(c\sqrt{\frac{K}{D}}\right)}+\frac{b^2-c^2}{b^2\sqrt{KD}}. \quad (2.35)$$

We next determine the intermittence approximation. Using the modified Bessel approximations in Equation (2.34), we see that as $a \to 0^+$,

$$\mathscr{L} \sim \frac{1}{2}\left(\begin{array}{c} \left(2-V^2\tau_M^2\phi_-^2\right)\left(\begin{array}{c}\phi_+^2\left(\phi_+^2-\varphi^2\right)L_3\\ +c\phi_+\phi_-^2\left(\phi_+^2-\varphi^2\right)I_1(c\phi_+)L_3X_-\\ +c\phi_+^2\phi_-\left(\varphi^2-\phi_-^2\right)I_0(c\phi_+)L_3Y_-\\ +c\phi_+\phi_-\varphi\left(\phi_+^2-\phi_-^2\right)I_1(c\phi_+)L_4Y_-\end{array}\right)\\ -\left(2-V^2\tau_M^2\phi_+^2\right)\left(\begin{array}{c}\phi_-^2\left(\varphi^2-\phi_-^2\right)L_3\\ +c\phi_+\phi_-^2\left(\phi_+^2-\varphi^2\right)I_0(c\phi_-)L_3Y_+\\ +c\phi_+^2\phi_-\left(\varphi^2-\phi_-^2\right)I_1(c\phi_-)L_3X_+\\ +c\phi_+\phi_-\varphi\left(\phi_+^2-\phi_-^2\right)I_1(c\phi_-)L_4Y_+\end{array}\right)\end{array}\right) \xrightarrow{a\to 0^+} \infty$$

where

$$X_\pm = I_0(c\phi_\pm)K_0(a\phi_\pm)-K_0(c\phi_\pm), \qquad Y_\pm = I_1(c\phi_\pm)K_0(a\phi_\pm)+K_1(c\phi_\pm)$$

because

$$X_\pm \xrightarrow{a\to 0^+} \infty \qquad \text{and} \qquad Y_\pm \xrightarrow{a\to 0^+} \infty.$$

Consequently, this gives us that $\gamma_4 \to 0$ as $a \to 0^+$ since

$$A \sim \frac{1}{\mathscr{L}} \begin{bmatrix} \dfrac{cL_3}{(2D\tau_D + V^2\tau_M^2)} \begin{pmatrix} \left(2 - V^2\tau_M^2\phi_+^2\right)\phi_- \left(\varphi^2 - \phi_-^2\right) I_1(c\phi_-) \\ + \left(2 - V^2\tau_M^2\phi_-^2\right)\phi_+ \left(\phi_+^2 - \varphi^2\right) I_1(c\phi_+) \end{pmatrix} \\ -\dfrac{\left(b^2 - c^2\right)}{2D\tau_D V^2\tau_M^2\varphi} \begin{pmatrix} -\left(2 - V^2\tau_M^2\phi_+^2\right)\phi_-^2 \left(\varphi I_0(c\phi_-)L_3 + \phi_- I_1(c\phi_-)L_4\right) \\ + \left(2 - V^2\tau_M^2\phi_-^2\right)\phi_+^2 \left(\varphi I_0(c\phi_+)L_3 + \phi_+ I_1(c\phi_+)L_4\right) \end{pmatrix} \end{bmatrix} \to 0.$$

Additionally, since

$$\frac{M_6}{\mathscr{D}} \to -\frac{2I_1(c\phi_+)}{(2 - V^2\tau_M^2)c\phi_- D_1}, \quad \frac{M_7}{\mathscr{D}} \to -\frac{2I_0(c\phi_+)}{(2 - V^2\tau_M^2)c\phi_- D_1},$$

$$\frac{N_6}{\mathscr{D}} \to -\frac{2I_1(c\phi_-)}{(2 - V^2\tau_M^2)c\phi_- D_1}, \quad \frac{N_7}{\mathscr{D}} \to -\frac{2I_0(c\phi_-)}{(2 - V^2\tau_M^2)c\phi_- D_1},$$

where

$$D_1 = \begin{pmatrix} \phi_-(\phi_+^2 - \varphi^2) I_1(c\phi_+) I_0(c\phi_-) L_3 \\ +\phi_+(\varphi^2 - \phi_-^2) I_0(c\phi_+) I_1(c\phi_-) L_3 \\ +\varphi(\phi_+^2 - \phi_-^2) I_1(c\phi_+) I_1(c\phi_-) L_4 \end{pmatrix},$$

we can reduce the intermittence mean search time Equation (2.33) to the following:

$$t_m = \frac{(\tau_D + \tau_M)}{2b^2} \left(\frac{2b^2}{K\tau_D} - \frac{\left(3 - 4\ln\frac{b}{c}\right) b^4 - 4b^2c^2 + c^4}{2\left(2D\tau_D + V^2\tau_M^2\right)} + \tilde{\gamma}_1 + \tilde{\gamma}_2 + \tilde{\gamma}_3 \right), \tag{2.36}$$

where

$$\tilde{\gamma}_1 = \frac{2\left(b^2 - c^2\right)^2}{\left(2D\tau_D + V^2\tau_M^2\right) c\phi_+\phi_-\varphi D_1} \begin{pmatrix} \varphi^3\left(\phi_+^2 - \phi_-^2\right) I_0(c\phi_+) I_0(c\phi_-) L_3 \\ +\phi_+^3\left(\varphi^2 - \phi_-^2\right) I_1(c\phi_+) I_0(c\phi_-) L_4 \\ +\phi_-^3\left(\phi_+^2 - \varphi^2\right) I_0(c\phi_+) I_1(c\phi_-) L_4 \end{pmatrix},$$

$$\tilde{\gamma}_2 = \frac{2\left(b^2-c^2\right)D^2\tau_D^2V^4\tau_M^4}{K\tau_D\left(2D\tau_D+V^2\tau_M^2\right)^2D_1}\begin{pmatrix}\phi_-\left(\phi_+^2-\varphi^2\right)\left(\varphi^2\phi_-^2-\varphi^2\phi_+^2+\phi_+^2\phi_-^2\right)I_1(c\phi_+)I_0(c\phi_-)L_3\\+\phi_+\left(\phi_-^2-\varphi^2\right)\left(\varphi^2\phi_-^2-\varphi^2\phi_+^2-\phi_+^2\phi_-^2\right)I_0(c\phi_+)I_1(c\phi_-)L_3\\+\varphi\left(\phi_+^2-\phi_-^2\right)\left(\varphi^2\phi_-^2+\varphi^2\phi_+^2-\phi_+^2\phi_-^2\right)I_1(c\phi_+)I_1(c\phi_-)L_4\end{pmatrix},$$

$$\tilde{\gamma}_3 = -\frac{4cV^4\tau_M^4\left(\phi_+^2-\phi_-^2\right)I_1(c\phi_+)I_1(c\phi_-)L_3}{\left(2D\tau_D+V^2\tau_M^2\right)^2D_1}.$$

We next investigate the intermittence criterion. For an initial study, we fix the baseline parameters at $c = 1$ and $b = 10$. We then evaluate and compare the approximate mean search time formulas for intermittence (Equation 2.36) and diffusion alone (Equation 2.35) over all parameter triples (D,V,K) with $D,V,K \in \{0.001, 0.01, 0.1, 1, 10, 100, 1000\}$. This computational exploration indicates that the familiar spatial condition $b \gg \frac{D}{V}$ remains predictive: intermittence is favorable whenever $\frac{D}{V} \geq 0.1$. In addition, two features emerge. First, varying V produces no discernible change in the favorability boundary. Second, there appears to be a well-defined threshold in the detection rate K, depending solely on D, such that diffusion alone is favored for smaller K while intermittence becomes favorable once K is large enough. We now examine this threshold in more detail.

To ensure that we remain within the spatial regime, we fix $V = 100$ and vary $D\{0.5, 1.0, ..., 8.0, 8.5\}$. For each D, we determine the value of K at which intermittence first becomes favorable. Concretely, for each candidate $K \in \{0.01, 0.01, ..., 9.99, 10.00\}$, we evaluate the intermittent expression over a 100×100 uniform grid in (τ_D, τ_M) and compare its minimum to the diffusion-only prediction. The resulting K-threshold curve is shown in Figure 2.5.

As illustrated in the figure, the numerically estimated threshold is approximately linear in D. A least-squares fit yields $K(D) \approx 1.10995 - 0.04066D$. Consequently, for this case, the intermittence criterion is as follows:

$$b \gg \frac{D}{V}, \qquad K \geq 1.10995 - 0.04066D.$$

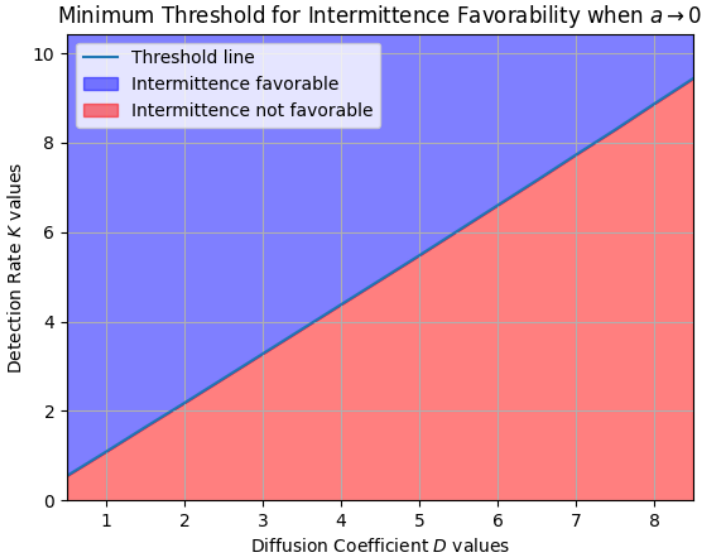

Figure 2.5: The line represents the minimum detection rate K threshold for intermittence favorability in the limit $a \to 0$.

Case 3: $b \to c$ During this case, the region outside any detection zone shrinks, so the searcher can detect the target from any location in the domain. Accordingly, taking this limit in the two-zone expression simplifies Equation (2.33) to yield the following:

$$\begin{aligned} t_m \approx & \frac{(\tau_D+\tau_M)\left((c^2-a^2)\phi_+ M_6 - 2aM_5\right)}{c^2 K \tau_D \phi_+ M_6} \\ & + \frac{(\tau_D+\tau_M) a^2 \phi_+ \left(\phi_+^2-\phi_-^2\right)\left(2-V^2\tau_M^2\phi_-^2\right)\left(\phi_- M_5 N_6 - \phi_+ M_6 N_5\right)}{c^2 K \tau_D M_6 \mathscr{L}_b} M_+ \end{aligned} \tag{2.37}$$

where

$$\mathscr{L}_b = \frac{1}{2} a\phi_+\phi_-\left(\phi_+^2-\phi_-^2\right)\begin{bmatrix} \begin{pmatrix} \left(2-V^2\tau_M^2\phi_-^2\right)\phi_+ M_5 N_6 \\ -\left(2-V^2\tau_M^2\phi_+^2\right)\phi_- M_6 N_5 \end{pmatrix} I_0\left(\frac{a\sqrt{2}}{V\tau_M}\right) \\ +2\left(\phi_+^2-\phi_-^2\right) M_6 N_6 \frac{V\tau_M}{\sqrt{2}} I_1\left(\frac{a\sqrt{2}}{V\tau_M}\right) \end{bmatrix},$$

$$M_+ = I_0\left(\frac{a\sqrt{2}}{V\tau_M}\right) M_5 + \frac{V\tau_M\phi_+}{\sqrt{2}} I_1\left(\frac{a\sqrt{2}}{V\tau_M}\right) M_6.$$

Additionally, in the diffusion-only setting, we take the limit $b \to c$ in Equation (2.23) to obtain the following expression:

$$t_{diff} \approx \frac{\left(c^2 - a^2\right) J_2 - 2aJ_3}{c^2 K J_2}, \tag{2.38}$$

where

$$J_2 = I_1\left(c\sqrt{\frac{K}{D}}\right) K_0\left(a\sqrt{\frac{K}{D}}\right) + I_0\left(a\sqrt{\frac{K}{D}}\right) K_1\left(c\sqrt{\frac{K}{D}}\right),$$
$$J_3 = I_1\left(c\sqrt{\frac{K}{D}}\right) K_1\left(a\sqrt{\frac{K}{D}}\right) - I_1\left(a\sqrt{\frac{K}{D}}\right) K_1\left(c\sqrt{\frac{K}{D}}\right).$$

A preliminary numerical comparison of the two mean search time approximations in Equation (2.37) and Equation (2.38) suggests that the parameter K exerts a substantially stronger influence on the predicted search times than either D or V. As a baseline, we fix

$$a = 1, \quad c = 10, \quad \tau_D = 10, \quad \tau_M = 10, \quad D = 1, \quad V = 1, \quad \text{and} \quad K = 1.$$

To assess parameter sensitivity, we vary each D, V, and K independently over the set $\{0.01, 0.1, 1, 10, 100\}$ while holding all remaining parameters are held at their baseline values. The resulting values, reported in Table 2.5, indicate that the mean search time approximations are significantly more sensitive to changes in K than to analogous changes in either D or V.

Table 2.5: Ranges of the mean search time approximations t_m in Equation (2.37) and t_{diff} in Equation (2.38) obtained by varying each of D, V, and K over the set $\{0.01, 0.1, 1, 10, 100\}$ (one parameter at a time), with all remaining parameters fixed at their baseline parameters.

Varying Parameter	t_m Ranges	t_{diff} Ranges
D	$(0.857, 1.974)$	$(0.934, 0.969)$
V	$(1.919, 1.923)$	$(0.961, 0.961)$
K	$(0.0198, 73.543)$	$(0.010, 93.391)$

Additionally, when $K > 1$, intermittence appears to be unfavorable. This behavior is consistent with the interpretation of K as a Poisson rate. In this case, the time to detect

the target is exponentially distributed with mean $\frac{1}{K}$, implying that a significant probability of detection occurs on a timescale shorter than $\frac{1}{K}$. When $K > 1$, the mean detection time satisfies $\frac{1}{K} < 1$, indicating that detection is almost immediate throughout the domain without the need for intermittence.

Conversely, intermittence must become favorable below some critical rate whenever $K \ll 1$. Indeed, as $K \to 0^+$, the searcher within second detection zone effectively ceases to be able to detect, and the model reverts to the single-detection zone setting of the original article [4]. Since intermittence is known to be advantageous in that model, it follows that there must exist a threshold value of K below which intermittence again becomes favorable.

We begin by analyzing the diffusion-only expression. In the asymptotic regime $K \ll 1$ with

$$a\sqrt{\frac{K}{D}} < c\sqrt{\frac{K}{D}} \ll 1, \tag{2.39}$$

a Taylor expansion of the required modified Bessel equations are as follows:

$$I_0\left(a\sqrt{\frac{K}{D}}\right) \approx 1, \qquad I_1\left(a\sqrt{\frac{K}{D}}\right) \approx \frac{a}{2}\sqrt{\frac{K}{D}}, \qquad I_1\left(c\sqrt{\frac{K}{D}}\right) \approx \frac{c}{2}\sqrt{\frac{K}{D}},$$

$$K_0\left(a\sqrt{\frac{K}{D}}\right) \approx -\ln\left(a\sqrt{\frac{K}{D}}\right) - (\gamma - \ln 2),$$

$$K_1\left(a\sqrt{\frac{K}{D}}\right) \approx \frac{1}{a}\sqrt{\frac{D}{K}}, \qquad K_1\left(c\sqrt{\frac{K}{D}}\right) \approx \frac{1}{c}\sqrt{\frac{D}{K}},$$

where γ is the Euler-Mascheroni constant so that

$$J_2 \approx -\frac{c}{2}\sqrt{\frac{K}{D}}\ln\left(a\sqrt{\frac{K}{D}}\right) - (\gamma - \ln 2)\frac{c}{2}\sqrt{\frac{K}{D}} + \frac{1}{c}\sqrt{\frac{K}{D}} \approx \frac{1}{c}\sqrt{\frac{K}{D}}$$

$$J_3 \approx \frac{c^2 - a^2}{2ca}$$

since $\frac{1}{c}\sqrt{\frac{K}{D}}$ is the dominant term in J_2. Substituting these approximations into Equation (2.38) yields the following equation:

$$t_{diff} \approx \frac{\left(c^2 - a^2\right)}{c^2 K}\left(1 - \sqrt{\frac{K}{D}}\right). \tag{2.40}$$

We next consider the approximation for the intermittence equation. Again, in the asymptotic regime $K \ll 1$ with

$$\frac{2K\tau_D V^2 \tau_M^2 \left(V^2\tau_M^2 - 2D\tau_D\right)}{\left(2D\tau_D + V^2\tau_M^2\right)^2} \ll 1, \tag{2.41}$$

we approximate $\phi_\pm$ with

$$\phi_\pm \approx \sqrt{\frac{\left(2D\tau_D + V^2\tau_M^2 + K\tau_D V^2\tau_M^2\right) \pm \left(2D\tau_D + V^2\tau_M^2\right)\left(1 + \frac{K\tau_D V^2\tau_M^2\left(V^2\tau_M^2 - 2D\tau_D\right)}{\left(2D\tau_D + V^2\tau_M^2\right)^2}\right)}{2D\tau_D V^2\tau_M^2}}$$

since for small x

$$\sqrt{1+x} \approx 1 + \frac{1}{2}x$$

Further simplification gives us the following:

$$\phi_- \approx \sqrt{\frac{2K\tau_D}{2D\tau_D + V^2\tau_M^2}} \tag{2.42}$$

and

$$\phi_+ \approx \sqrt{\frac{\left(2D\tau_D + V^2\tau_M^2\right)^2 + K\tau_D V^4\tau_M^4}{D\tau_D V^2\tau_M^2\left(2D\tau_D + V^2\tau_M^2\right)}}. \tag{2.43}$$

Since the approximation for ϕ_- in Equation (2.42) is dependent on K, we consider $K \ll 1$ such that

$$a\phi_- < c\phi_- \ll 1, \tag{2.44}$$

giving us the following Taylor expansions

$$I_0(a\phi_-) \approx 1 + \frac{a^2\phi_-^2}{4}, \qquad I_1(a\phi_-) \approx \frac{a\phi_-}{2} + \frac{a^3\phi_-^3}{16}, \qquad I_1(c\phi_-) \approx \frac{c\phi_-}{2} + \frac{c^3\phi_-^3}{16},$$

$$K_0(a\phi_-) \approx -\ln\left(\frac{a\phi_-}{2}\right) - \gamma + \frac{a^2\phi_-^2}{4}\left(1-\gamma-\ln\left(\frac{a\phi_-}{2}\right)\right),$$

where γ is the Euler-Mascheroni constant so that

$$N_5 \approx \frac{K\tau_D\left(c^4-a^4-4c^2a^2\ln\frac{c}{a}\right)}{8ca\left(2D\tau_D+V^2\tau_M^2\right)} + \frac{c^2-a^2}{2ca}$$
$$N_6 \approx -\frac{\sqrt{K\tau_D}\left(c^2-a^2-2c^2\ln\frac{c}{a}\right)}{2c\sqrt{2\left(2D\tau_D+V^2\tau_M^2\right)}} + \frac{\sqrt{2D\tau_D+V^2\tau_M^2}}{c\sqrt{2K\tau_D}}.$$

For ϕ_+, we see in Equation (2.43) that minimizing K does not make ϕ_+ less than 1 since

$$\phi_+ \approx \varphi\sqrt{1+\frac{K\tau_D V^4\tau_M^4}{\left(2D\tau_D+V^2\tau_M^2\right)^2}}$$

where all parameters are positive and

$$\varphi = \sqrt{\frac{2D\tau_D+V^2\tau_M^2}{D\tau_D V^2\tau_M^2}}.$$

As such, assuming $K \ll 1$ such that

$$\frac{K\tau_D V^4\tau_M^4}{\left(2D\tau_D+V^2\tau_M^2\right)^2} \ll 1, \tag{2.45}$$

we can simplify ϕ_+ to get the following

$$\phi_+ \approx \varphi + \frac{K\tau_D V^3\tau_M^3}{2\sqrt{D\tau_D}\left(2D\tau_D+V^2\tau_M^2\right)^{3/2}}$$

using the Taylor expansion for $\sqrt{1+x}$ once again. Thus, linearizing the required modified Bessel functions yield the following:

$$
\begin{aligned}
I_0(a\phi_+) &\approx \frac{K\tau_D V^3 \tau_M^3 a I_1(a\varphi)}{2\sqrt{D\tau_D}\left(2D\tau_D + V^2\tau_M^2\right)^{3/2}} + I_0(a\varphi) \\
I_1(a\phi_+) &= \frac{K\tau_D V^3 \tau_M^3 \left(a\sqrt{2D\tau_D + V^2\tau_M^2} I_0(a\varphi) - V\tau_M\sqrt{D\tau_D} I_1(a\varphi)\right)}{2\sqrt{D\tau_D}\left(2D\tau_D + V^2\tau_M^2\right)^2} + I_1(a\varphi) \\
I_1(c\phi_+) &= \frac{K\tau_D V^3 \tau_M^3 \left(c\sqrt{2D\tau_D + V^2\tau_M^2} I_0(c\varphi) - V\tau_M\sqrt{D\tau_D} I_1(c\varphi)\right)}{2\sqrt{D\tau_D}\left(2D\tau_D + V^2\tau_M^2\right)^2} + I_1(c\varphi) \\
K_0(a\phi_+) &\approx -\frac{K\tau_D V^3 \tau_M^3 a K_1(a\varphi)}{2\sqrt{D\tau_D}\left(2D\tau_D + V^2\tau_M^2\right)^{3/2}} + K_0(a\varphi) \\
K_1(a\phi_+) &\approx -\frac{K\tau_D V^3 \tau_M^3 \left(a\sqrt{2D\tau_D + V^2\tau_M^2} K_0(a\varphi) + V\tau_M\sqrt{D\tau_D} K_1(a\varphi)\right)}{2\sqrt{D\tau_D}\left(2D\tau_D + V^2\tau_M^2\right)^{3/2}} + K_1(a\varphi) \\
K_1(c\phi_+) &\approx -\frac{K\tau_D V^3 \tau_M^3 \left(c\sqrt{2D\tau_D + V^2\tau_M^2} K_0(c\varphi) + V\tau_M\sqrt{D\tau_D} K_1(c\varphi)\right)}{2\sqrt{D\tau_D}\left(2D\tau_D + V^2\tau_M^2\right)^{3/2}} + K_1(c\varphi)
\end{aligned}
$$

so that

$$
\begin{aligned}
M_5 \approx\ & \frac{K^2\tau_D V^6 \tau_M^6 \begin{pmatrix} V\tau_M\sqrt{D\tau_D(2D\tau_D + V^2\tau_M^2)}(aL_6 - cL_8) \\ +D\tau_D V^2 \tau_M^2 L_5 - ca(2D\tau_D + V^2\tau_M^2)L_7 \end{pmatrix}}{4D\left(2D\tau_D + V^2\tau_M^2\right)^4} \\
& - \frac{KV^3\tau_M^3 \left(2D\tau_D V\tau_M L_5 + (aL_6 - cL_8)\sqrt{D\tau_D(2D\tau_D + V^2\tau_M^2)}\right)}{2D\left(2D\tau_D + V^2\tau_M^2\right)^2} + L_5 \\
M_6 \approx\ & \frac{K^2\tau_D V^6 \tau_M^6 a \left(V\tau_M\sqrt{D\tau_D} L_5 - c\sqrt{2D\tau_D + V^2\tau_M^2} L_8\right)}{4D\left(2D\tau_D + V^2\tau_M^2\right)^{7/2}} \\
& - \frac{K\tau_D V^3 \tau_M^3 \left(V\tau_M\sqrt{D\tau_D} L_6 + (aL_5 - cL_7)\sqrt{2D\tau_D + V^2\tau_M^2}\right)}{2\sqrt{D\tau_D}\left(2D\tau_D + V^2\tau_M^2\right)^2} + L_6
\end{aligned}
$$

where

$$L_5 = I_1(c\varphi)K_1(a\varphi) - I_1(a\varphi)K_1(c\varphi), \qquad L_6 = I_1(c\varphi)K_0(a\varphi) + I_0(a\varphi)K_1(c\varphi),$$
$$L_7 = I_0(c\varphi)K_0(a\varphi) - I_0(a\varphi)K_0(c\varphi), \qquad L_8 = I_0(c\varphi)K_1(a\varphi) + I_1(a\varphi)K_0(c\varphi).$$

We then use these approximations into the intermittence formula in Equation (2.37) and use the inequality $t_m < t_{diff}$ representing when intermittence is favorable to arrive at the following inequality:

$$\begin{aligned}
&-4a(\tau_D+\tau_M)(\phi_+^2-\phi_-^2)I_0\left(\frac{a\sqrt{2}}{V\tau_M}\right)M_5N_5 \\
&+\left(\begin{array}{c}\left(\tau_M+\sqrt{\frac{K}{D}}\tau_D\right)(c^2-a^2)\phi_+^2\phi_-\left(2-V^2\tau_M^2\phi_-^2\right)I_0\left(\frac{a\sqrt{2}}{V\tau_M}\right) \\ +2(\tau_D+\tau_M)a\phi_-^3\left(2-V^2\tau_M^2\phi_+^2\right)\frac{V\tau_M}{\sqrt{2}}I_1\left(\frac{a\sqrt{2}}{V\tau_M}\right)\end{array}\right)M_5N_6 \\
&-\left(\begin{array}{c}\left(\tau_M+\sqrt{\frac{K}{D}}\tau_D\right)(c^2-a^2)\phi_+\phi_-^2\left(2-V^2\tau_M^2\phi_+^2\right)I_0\left(\frac{a\sqrt{2}}{V\tau_M}\right) \\ +2(\tau_D+\tau_M)a\phi_+^3\left(2-V^2\tau_M^2\phi_-^2\right)\frac{V\tau_M}{\sqrt{2}}I_1\left(\frac{a\sqrt{2}}{V\tau_M}\right)\end{array}\right)M_6N_5 \\
&+2(c^2-a^2)\phi_+\phi_-(\phi_+^2-\phi_-^2)\left(\tau_M+\sqrt{\frac{K}{D}}\tau_D\right)\frac{V\tau_M}{\sqrt{2}}I_1\left(\frac{a\sqrt{2}}{V\tau_M}\right)M_6N_6 < 0
\end{aligned} \tag{2.46}$$

Therefore, our threshold for $K \ll 1$ exists whenever Equations (2.41), (2.45), and (2.46) hold. We confirm this numerically by using various choices for the parameters and varying K with the set $\{0.001, 0.0001, 0.00001, 0.000001, 0.0000001\}$. In every case where the conditions held, while the other conditions discussed (i.e., Equations (2.39), and (2.44)) made no difference to favoraing intermittence, we do see that intermittence is favorable whenever Equation (2.46) hold, and intermittence is unfavorable whenever Equation (2.46) does not hold. As an example, intermittence holds despite Equations (2.39) and (2.44) being false with the following parameters:

$$a = 1, \quad c = 100, \quad \tau_D = 0.5, \quad V = 0.5, \quad K = 0.0001, \quad \tau_D = 10, \quad \text{and} \quad \tau_M = 1$$

so that

$$t_m = 8269.239 < t_{diff} = 9857.593.$$

Conversely, we see that intermittence does not hold when all conditions are met except the inequality condition in Equation (2.46) for the following parameters:

$$a = 1, \quad c = 100, \quad D = 0.5, \quad ,V = 0.01, \quad K = 0.00001 \quad \tau_D = 10, \quad \text{and} \quad \tau_M = 60$$

so that

$$t_m = 186842.861 > t_{diff} = 99542.831.$$

This confirms that Equations (2.41), (2.45), and (2.46) are important for the intermittence criterion, with Equation (2.46) possibly being the most important.

2.2.3 Summary for Chapter 2

In this chapter, we derived and solved the equations for the diffusion-only model and the intermittent strategy within one-dimensional and two-dimensional disks. We then averaged the resulting expressions over the entire domain to obtain the corresponding mean search times formulas. From these formulas, we identified a spatial region that was not in the intermittence criterion: namely, that intermittence was never favorable whenever the domain radius $b \leq \frac{D}{V}$ in both dimensions.

We further showed that the detection rate K substantially modifies the intermittence criterion in the one-dimensional model. In particular, increasing K reduces and ultimately removes any benefit of intermittence, whereas decreasing K makes intermittence increasingly important for improving the mean search time. This dependence is amplified by the spatial size of the second detection zone: as the outer radius c increases toward the domain boundary, the more that K eliminated options for intermittence favorability.

To further uncover how the three spatial regions (first detection zone, second detection zone, and the exterior no-detection region) interact with intermittence, we analyzed three limiting cases in which one region is effectively removed. In the limit $c \to a$, the second detection zone vanishes and the model reduces to that of the original authors [4] with a single, instantaneous detection zone. This case then recovers the intermittence criterion of $b > \frac{D}{V}$. In the limit $a \to 0$, the model again has a single detection zone, but now

governed by a detection rate K; despite this reduced detectability relative to the original setting, the intermittence criterion remains $b > \frac{D}{V}$ in the one-dimensional case. However, in the two-dimensional model, the intermittence criterion has an additional condition of $K \geq 1.10995 - 0.04066D$. Finally, in the limit $b \to c$, the exterior no-detection region disappears. In this case, we showed that intermittence is not favorable whenever $c \leq \frac{D}{V}$, and that an intermittent advantage requires a sufficiently small detection rate $K \ll 1$ that satisfy three inequality conditions.

Several directions for future work remain open. One natural extension is to determine the optimal switching times (τ_D, τ_M) that minimize the mean search time where intermittence is favorable. Another is to replace the fixed speed with a nontrivial speed distribution (as we did in Chapter 1.2) and/or allow biased left-right direction. Finally, rather than taking the detection rate K to be constant within the second zone, it may be more realistic to let K to vary spatially - for example, increasing K as the searcher approaches the first detection zone.

Chapter 3

Modeling Opioid Use Disorder using Stochastic Networking

3.1 Background

Opioid-related mortality has steadily been on the rise for the past three decades, with over 806,000 overdose deaths recorded since 1991 [25]. In response to the growing crisis, the U.S. Department of Health and Human Services declared a nationwide public health emergency in 2017 [26], a declaration that has been renewed every 90 days and remains in effect as of the most recent extension on March 16, 2026 [27]. This ongoing emergency highlights the importance of understanding how the epidemic developed, which is widely recognized as having progressed in three distinct waves [25].

Starting in the late 1990s, the first wave saw an increase in prescription opioid use, which can be identified by the introduction of OxyContin [28, 29]. Released in 1996, OxyContin is a slow-release formulation of oxycodone designed to deliver pain relief gradually over a twelve hours [30]. The manufacturer, Purdue Pharma, extensively promoted the seemingly safe drug to physicians for prescribing the drug as an initial treatment for all manner of pain, including moderate non-cancer pain [31, 32]. This "aggressive" marketing campaign resulted in a shocking increase in the number of prescriptions treating for non-cancer pain with OxyContin, rising from about 670,000 in 1997 to around 6.2 million in 2002 [32]. While this increase ideally should not have posed a problem, patients soon discovered that by consuming a crushed form of the tablet via injection or inhalation, they could bypass the slow-release mechanism, producing a rapid and intense euphoric high [30]. OxyContin misuse began to escalate, with lifetime nonmedical use rising from 1.9 million individuals in 2002 to 3.1 million in 2004, including 615,000 new users obtaining the drug without a medical prescription in 2004 [32]. Consequently, the spike in prescription opioid misuse was accompanied by a dramatic rise in overdose deaths, increasing from 3,442 fatalities in 1999 to 17,029 in 2017 [33]. In response to the widespread misuse of their product, the manufacturer of OxyContin eventually realized how harmful their product was, and made some changes that would inadvertently usher in the next wave of the opioid crisis.

The second wave commenced with the reformulation of OxyContin and the rise of heroin use [30, 25, 34]. In early August 2010, Purdue Pharma pulled the existing OxyContin from stores and replaced with a reformulation variant [30, 35]. Instead of a fine powder, the new formula when crushed would turn into a gummy substance, making injection or inhalation more difficult [30]. At the same time, the illegal opioid heroin was becoming cheaper, resulting in many abusers of prescription opioids to "graduate" or transition to heroin [34, 36]. Thus, while prescription opioid overdose deaths became to stagnate from 2010 to 2013, heroin-related morality nearly tripled during the same period, reaching approximately 8,600 deaths in 2013 [37, 38, 39]. However, a far deadlier contender was poised to overtake heroin, heralding the most lethal wave of the opioid crisis to date.

Beginning in 2013, the third and current wave was marked by the introduction of synthetic opioids into the illicit, black-market heroin supply [25, 40]. Unlike natural opioids which are derived from organic substances such as morphine and codeine found in poppy plants, synthetic opioids are entirely manufactured through chemical processes in laboratories, the most prevalent being fentanyl [25, 41]. Fentanyl is extremely potent (about 50 times stronger than heroin and 100 times stronger than morphine), is inexpensive to produce, and closely resembles other drugs in its powdered form [42, 43]. Consequently, to reduce production costs and increase profits, fentanyl has often been mixed with heroin or pressed into counterfeit pills masquerading as prescription opioids [42, 44]. Since 2013, deaths from synthetic opioids* have increased annually by over 2300% reaching to 72,776 deaths† in 2023 [47]. With the scale and persistence of the opioid crisis, researchers have turned to mathematical modeling in the hopes of formulating intervention strategies.

*This statistic excludes methadone, a pharmacotherapy treatment for heroin use disorder [45].

†Numbers are age-adjusted using the direct method by applying age-specific rates to a standardized age distribution [46].

3.1.1 Previous Models

Multiple models have been created to address this opioid crisis. Most models find their basis in a 2007 paper by Emma White and Catherine Comiskey modeling heroin use in the Irish population [48]. White and Comiskey categorized the demographic into three drug classes: susceptibles[‡], drug users not in treatment, and drug users in treatment. In the model, susceptibles, who are not drug users, could transition into drug users not in treatment, however drug users in general were only able to switch between the treatment and no treatment classes. Their analysis concluded that preventing susceptibles from becoming drug users was significantly more effective in controlling the spread of drug use in Ireland than treating individuals who were already drug users. This fundamental work was one of many compartmental models that categorize populations into distinct groups, or "compartments", to capture the dynamics of opioid use.

While various approaches have been used to model the opioid crisis, compartmental models remain the most prevalent, with three notable examples demonstrating their versatility in depicting different facets of opioid use and treatment [49]. To begin with, Junli Liu and Tailei Zhang adapted White and Comiskey's model to a Chinese population by incorporating a reversion delay effect, enabling consideration for the various temporal, social, and physical factors that influence relapse in drug users [50]. Their conclusions reinforced those of their predecessor that prevention is more effective than treatment. As another example, Nicholas Battista, Leigh Pearcy, and W. Christopher Strickland developed a model that focused on various pathways through which individuals using prescription opioids could develop a substance use disorder[§] [52]. As a result, they introduced a distinct "prescribed" class that could both directly develop an OUD and indirectly contribute to others' development of an OUD through unsecured or unused prescriptions [52]. They determined that effective strategies for addressing the opioid crisis would be reducing

[‡]Susceptibles are individuals who are not currently using opioids and have never needed treatment for opioid misuse.

[§]We will be using the term "substance use disorder" (SUD) rather than "addiction" as a more rigorous and less volatile definition found in the Diagnostic and Statistical Manual of Mental Disorders (DSM-5) [51].

the number and duration of medically prescribed painkillers, improving treatment success rates, and enhancing the accessibility, convenience, and motivation for individuals with OUD to seek treatment. Rounding out these examples, the model by Sandra Cole and Stephen Wirkus focused exclusively on illicit opioid use disorder (OUD)[¶] and incorporated a "recovered" class whose members cannot become susceptibles again [53]. When comparing the ways an individual with illicit OUD would seek treatment, their sensitivity analysis concluded that voluntarily entering treatment was more important than seeking treatment through interactions with others. Although many compartmental models have been developed to study the opioid crisis, the most foundational and relevant to our work is by Tricia Phillips, Suzanne Lenhart, and W. Christopher Strickland [5].

The model by Phillips et al. focused on the interrelationship between prescription-based OUD and heroin/fentanyl OUD. This model underpins my work and also serves as the starting point for the two extended models discussed later, which together inform the model I develop. The model consisted of five drug classes: susceptibles (S), prescribed opioid users (P), prescription-based OUD (A), heroin/fentanyl-based OUD (H), and stably recovered individuals (R). While susceptibles and prescribed opioid users could transition into either OUD class, once in the OUD classes, individuals could only ever transition between the recovery and two OUD classes. The model and its transition pathways were depicted in Figure 3.1, with arrows indicating the direction of movement between classes. Each drug class was considered a proportion of the entire population. The population size was maintained through the parameter μ, representing both the natural death rate across classes and the incoming "birth" rate for the susceptible class. To understand the behavior of the drug class transitions, we highlight the main aspects of the model's parameterization.

While a full description of parameters is not required for our purposes, we must emphasize the two types of rates: linear and nonlinear. To start, the linear rates consisted of parameters multiplied solely by the proportion of the current drug class. For example, using Figure 3.1, αS from the S class, γP from the P class, and ζA from the A class were all

[¶]"Illicit opioid use disorder" (IOUD) model describes the role that black market opioids such as heroin, fentanyl, and other synthetic opioids play in the current opioid epidemic [53].

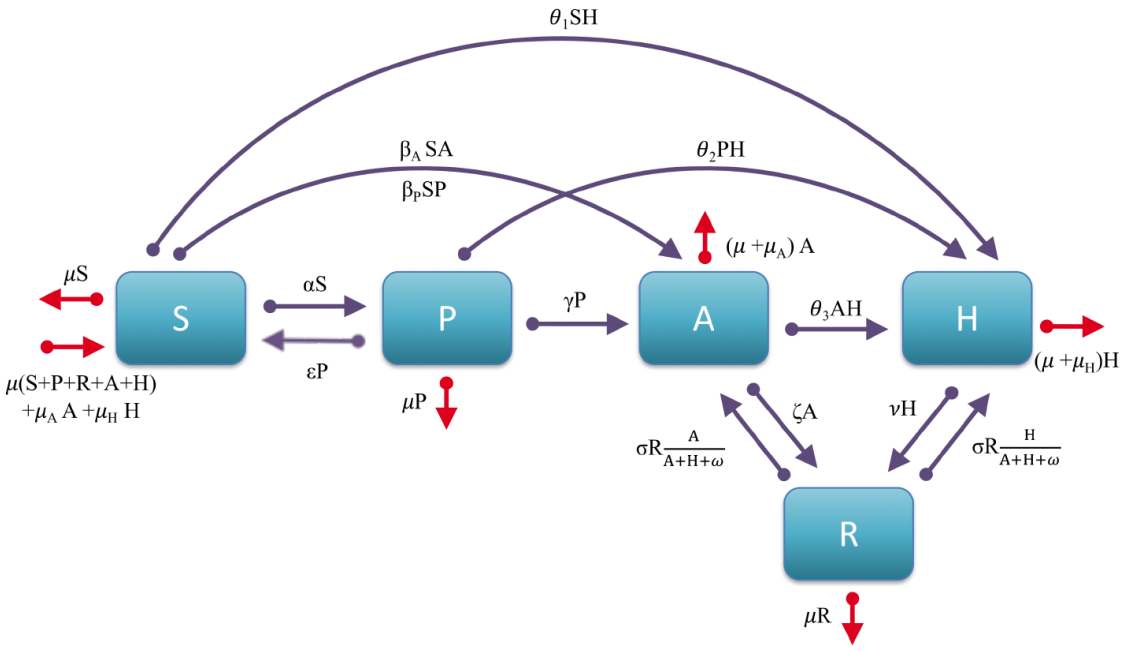

Figure 3.1: Flow diagram by Phillips et al. [5] illustrating the transitions between drug classes of individuals and ultimately visualizing a system of ordinary differential equations (ODEs).

examples of linear rates. Next, most of the nonlinear rates were assumed to be proportional to the proportion of the population with whom individuals were in contact. As such, the rates were scaled by the proportion of individuals in the corresponding contact drug class. For example, from the susceptible S class, the three nonlinear rates ($\beta_A SA$, $\beta_P SP$, and $\theta_1 SH$) denoted interactions of susceptibles with the prescription-based OUD A class, the prescribed P class, and heroin/fentanyl-based OUD H class, respectively. However, there was a specific nonlinear rate that worked a little differently: the relapse rates. These rates $\sigma R\frac{A}{A+H+\omega}$ and $\sigma R\frac{H}{A+H+\omega}$ represented the transition of stably recovered R individuals back to the prescription-based A and heroin/fentanyl-based H OUD classes, respectively. While these expressions are nonlinear, the fractions described the proportions of each OUD class within the at-risk population, meaning the rates could be interpreted as average per-capita rates. Thus, the relapse rates were approximately linear. In the case where $A = H = 0$, a small perturbation term ω was added to the denominator to avoid division by zero. Having

outlined the model structure and several key rate types, we are positioned to evaluate the author's conclusions.

After completing analysis using data from Tennessee between 2013 and 2018, Phillips et al. made a several insights. They predicted an increase in heroin and fentanyl use disorders for 2020-2022 with a corresponding increase in overall overdose mortality. Additionally, their analysis found that the most effective approach for controlling the spread of drug use in Tennessee would be to focus on treatment of individuals with OUD as well as monitoring stably recovered individuals. Building on this groundwork, two additional models were later developed, a stochastic agent-based model and an community-subcommunity ordinary differential equation (ODE) model. Both of these models serve as the foundation for our current research.

The first model discussed is an agent-based model, developed by Leigh Pearcy [6]. Agent-based modeling examines individual behaviors along with their interactions with one another and the environment to gain insight into system-level dynamics [54]. Of the models developed to address the opioid crisis, the least employed are agent-based models [49]. Pearcy's model builds on the concepts from Phillips et al. [5] by incorporating individual interactions. The model consisted of a network of nodes and edges, where each node represented an individual in the community and the edges between nodes represented preexisting social connections between the individuals. Any two connected nodes by an edge were considered neighbors. To build on this foundation, we next examine how the network was generated and how individuals could move between drug classes within the model.

The network of nodes and edges were formed by using common generating algorithms. While Pearcy used three, the most relevant was the Erdös-Réyni (ER) method, where each distinct pair of nodes had an independent probability p of developing an edge, resulting in a simple random sample of edges across the network. Any node generated without edges are reintroduced under the same procedure until at least one edge is established. During network setup, each node was assigned a drug class according to the initial population proportions determined by Phillips et al. [5]. Consequently, the drug classes were presented

not as proportions but as the actual number of individuals in each class. After generating the network, Pearcy ran her model for some time, where at each time step, every individuals had a chance of changing drug classes.

Following the dynamics described by Phillips et al. [5] and illustrated in Figure 3.1, transitions between drug classes occurred through a two-step process. In the first, the model evaluated whether a transition would take place. Considering the two types of rates (linear and nonlinear), we discuss how each created a Poisson process. Since linear rates represented the total expected number of individuals that makes the transition per year, individuals transitioning through a linear rate underwent a Poisson process with the respective rate parameter. For example, since the expected number of susceptibles S transitioning to prescribed P class were αS, susceptibles underwent a Poisson process with rate parameter α. Nonlinear rates, on the other hand, represented individuals by contact with another drug class. In Pearcy's model, this was captured by the density of all neighbors in the relevant contact class, resulting in a Poisson process with the respective rate parameter proportional to the density. For example, if node k transitioned from susceptible S class to prescribed-based OUD A class through contact with A individuals, the individual underwent a Poisson process with rate parameter $\beta_A \frac{A_k}{N_k}$, where A_k was the number of prescribed-based OUD A neighbors and N_k was the total neighbors. Lastly, relapse rates considered the fraction to be global scaling factor, again resulting in a Poisson process with rate $\sigma \frac{A}{A+H+\omega}$ or $\sigma \frac{H}{A+H+\omega}$ to prescribed-based A or heroin/fentanyl-based H OUD class, respectively. Putting these all together, at each time step Δt, the probability of transitioning was given by

$$P(\text{transition in } (t, t+\Delta t]) = 1 - e^{-\lambda \Delta t},$$

where the sum λ of all transition rates out of the current class defined the Poisson process. For example, if a node k would leave the S class, then using Figure 3.1,

$$\lambda = \alpha + \mu + \beta_A \frac{A_k}{N_k} + \beta_P \frac{P_k}{N_k} + \theta_1 \frac{H_k}{N_k},$$

where A_k, P_k, H_k represented the number of neighbors node k has in each representative class and N_k denoted the total number of neighbors. The probability was then compared with a uniform random number to determine whether a change of class would occur. If so, the model proceeded to the second step of the process.

The second step identified the specific drug class to which the node would shift. Each transition rate was normalized by λ and treated as a probability. Again, if node k was determined to leave the S class, then Pearcy defined the probability of transitioning to P by α/λ, A by $\left(\beta_A \frac{A_k}{N_k} + \beta_P \frac{P_k}{N_k}\right)/\lambda$, H by $\theta_1 \frac{H_k}{N_k}/\lambda$, and S by μ/λ, as the node would die and be "reborn" as a susceptible. Consequently, when a node dies, all prior connections are removed, and the individual is reintroduced using the same network initialization algorithm. If the removal leaves any neighboring nodes isolated, those nodes are likewise reintroduced under the same procedure. Having shown how a compartmental framework can be translated into a network-based model, we now present the underlying compartmental model that motivates our study.

The second model directly relevant to our research is a community-subcommunity model developed by Kimberlyn Eversman [1]. Basing off the model by Phillips et al. [5], Eversman introduced a design of two interacting systems: a broader community and a focal subcommunity of interest situated within the larger population. The model considered the community population to consist of five subgroups (S_C, P_C, A_C, F_C, R_C) and the subcommunity population to consist of six subgroups (S_V, S_H, P_V, A_V, F_V, R_V). Descriptions of the drug subgroups are given in Table 3.1. The model and its pathways were described by the system of ODEs describing the community and subcommunity models are provided in Equations (3.1) and (3.2), respectively. Visual representations of the community and subcommunity models along with all pathways directed by arrows are shown in Figure 3.2. Each subgroup was measured as proportion of the community and subcommunity populations, respectively, at any given time. With the model described, we now focus on three key parameters that significantly change, while a fuller description of the remaining parameters and assumptions are found in [1].

Table 3.1: Definition of each drug class as described by Eversman [1].

Drug Classes	Explanation
Susceptibles (S_C, S_V, S_H)	Individuals that are not currently taking any form of opioids and have never suffered from an opioid use disorder. The susceptible class in the subcommunity was divided into two subclasses: the susceptibles without chronic pain (S_V) and those with chronic pain S_H.
Prescription opioid users (P_C, P_V)	Individuals that are currently taking prescribed opioids but have not developed an opioid use disorder.
Prescription-based OUD (A_C, A_V)	Individuals that are taking prescription opioids and have an opioid use disorder. However, these individuals are not taking any illicit opioids such as fentanyl or heroin. Opioids taken need not have been prescribed to the individual.
Illicit-based OUD (F_C, F_V)	Individuals that are taking illicit opioids, such as fentanyl or heroin, and have an opioid use disorder. Individuals can also be taking prescribed opioids.
Stably Recovered (R_C, R_V)	Individuals who had an opioid use disorder, and are no longer taking opioids and/or have completed treatment for the disorder. Individuals also have not relapsed for at least 4 weeks.

$$
\begin{cases}
\dfrac{dS_C}{dt} = -\alpha_C S_C - \beta_{CA} S_C A_C - \beta_{CP} S_C P_C - \theta_{S_C} S_C F_C + \varepsilon_C P_C + \mu(P_C + A_C + F_C + R_C) \\
\qquad + \mu_A A_C + \mu_F F_C \\
\dfrac{dP_C}{dt} = -\varepsilon_C P_C - \mu P_C - \gamma P_C - \theta_P P_C F_C + \alpha_C S_C \\
\dfrac{dA_C}{dt} = -\zeta A_C - \theta_A A_C F_C - (\mu + \mu_A) A_C + \beta_{CA} S_C A_C + \beta_{CP} S_C P_C + \gamma P_C \\
\qquad + \sigma R_C \dfrac{\lambda_A A_C + (1-\lambda_F) F_C}{A_C + F_C + \omega} \\
\dfrac{dF_C}{dt} = -\nu F_C - (\mu + \mu_F) F_C + \theta_{S_C} S_C F_C + \theta_P P_C F_C + \theta_A A_C F_C \\
\qquad + \sigma R_C \dfrac{(1-\lambda_A) A_C + \lambda_F F_C}{A_C + F_C + \omega} \\
\dfrac{dR_C}{dt} = -\sigma R_C \dfrac{\lambda_A A_C + (1-\lambda_F) F_C}{A_C + F_C + \omega} - \sigma R_C \dfrac{(1-\lambda_A) A_C + \lambda_F F_C}{A_C + F_C + \omega} - \mu R_C + \zeta A_C + \nu F_C
\end{cases}
\tag{3.1}
$$

System of equations modeling drug transitions among members of the population.

$$
\begin{cases}
\dfrac{dS_V}{dt} = -[kF_C + (1-k)F_V]\theta_{S_V} S_V - \rho_V S_V - [kA_C + (1-k)A_V]\beta_{VA} S_V \\
\qquad - [kP_C + (1-k)P_V]\beta_{VP} S_V - \alpha_V S_V + \rho_H S_H + \varepsilon_V P_V \\
\qquad + \mu(S_H + P_V + A_V + F_V + R_V) + \mu_A A_V + \mu_F F_V \\
\dfrac{dS_H}{dt} = -[kA_C + (1-k)A_V]\beta_{HA} S_H - [kP_C + (1-k)P_V]\beta_{HP} S_H \\
\qquad - \rho_H S_H - \alpha_H S_H - [kF_C + (1-k)F_V]\theta_{S_H} S_H - \mu S_H + \rho_V S_V + \varepsilon_H P_V \\
\dfrac{dP_V}{dt} = -\varepsilon_V P_V - \varepsilon_H P_V - \gamma P_V - [kF_C + (1-k)F_V]\theta_P P_V - \mu P_V + \alpha_H S_H + \alpha_V S_V \\
\dfrac{dA_V}{dt} = -[kF_C + (1-k)F_V]\theta_A A_V - \zeta A_V - (\mu + \mu_A) A_V + [kA_C + (1-k)A_V]\beta_{VA} S_V \\
\qquad + [kP_C + (1-k)P_V]\beta_{VP} S_V + [kA_C + (1-k)A_V]\beta_{HA} S_H \\
\qquad + [kP_C + (1-k)P_V]\beta_{HP} S_H + \gamma P_V + \sigma R_V \dfrac{\lambda_A A_C + (1-\lambda_F) F_C}{A_C + F_C + \omega} \\
\dfrac{dF_V}{dt} = -\nu F_V - (\mu + \mu_F) F_V + [kF_C + (1-k)F_V]\theta_{S_V} S_V + [kF_C + (1-k)F_V]\theta_{S_H} S_H \\
\qquad + [kF_C + (1-k)F_V]\theta_P P_V + [kF_C + (1-k)F_V]\theta_A A_V + \sigma R_V \dfrac{(1-\lambda_A) A_C + \lambda_F F_C}{A_C + F_C + \omega} \\
\dfrac{dR_V}{dt} = -\sigma R_V \dfrac{\lambda_A A_C + (1-\lambda_F) F_C}{A_C + F_C + \omega} - \sigma R_V \dfrac{(1-\lambda_A) A_C + \lambda_F F_C}{A_C + F_C + \omega} - \mu R_V + \zeta A_V + \nu F_V
\end{cases}
\tag{3.2}
$$

System of equations representing drug transitions among members of the focal community.

As seen in Phillips et al. [5], to keep each population size consistent, μ represented both the total natural death rate of any class as well as the incoming "birth" rate for the susceptible class. This parameter μ was the same in both the community and subcommunity. Additionally, in the subcommunity, the "birth" rate occurred in the susceptible S_V class without chronic pain.

Social influence played a significant role in the development of an opioid use disorder (OUD) in Eversman's model, reflecting known mechanisms implicated in the spread of the problematic drug use behaviors [1]. The two key parameters that captured these effects were β for developing prescription-based OUD and θ for developing an illicit-based OUD. In the community model, this social interaction was represented by multiplying by the proportion of said interaction subgroup in the community. For example, $\theta_{S_C} S_C F_C$ represented the rate at which susceptible individuals develop fentanyl/heroin use disorder by illicit purchases or interaction with individuals who have fentanyl/heroin use disorder. A similar idea applied to the subcommunity model with a slight difference. The author assumed that members within a subcommunity might have more influence over its members than those outside the subcommunity. To highlight this, instead of multiplying by the proportion of the interaction subgroup in the community, each interaction term was replaced with a term representing this in-group bias. For example, corresponding term in the subcommunity was changed from $\theta_{S_V} S_V F_C$ to $(kF_C + (1-k)F_V)\theta_{S_V} S_V$, where $k \in [0,1]$ described the extent of segregation. The subcommunity was considered completely segregated if $k = 0$ and had no intergroup preference if $k = 1$.

Lastly, Eversman introduced new parameters to the relapse rates to more precisely direct relapse toward either OUD class. The population fractions incorporate parameters $\lambda_A, \lambda_F \in [0,1]$ which skews relapses toward the prescription-based OUD A or the illicit-based OUD F, respectively. Accordingly, the community relapse rates are expressed as

$$\sigma R_C \frac{\lambda_A A_C + (1-\lambda_F) F_C}{A_C + F_C + \omega}, \qquad \sigma R_C \frac{(1-\lambda_A) A_C + \lambda_F F_C}{A_C + F_C + \omega}.$$

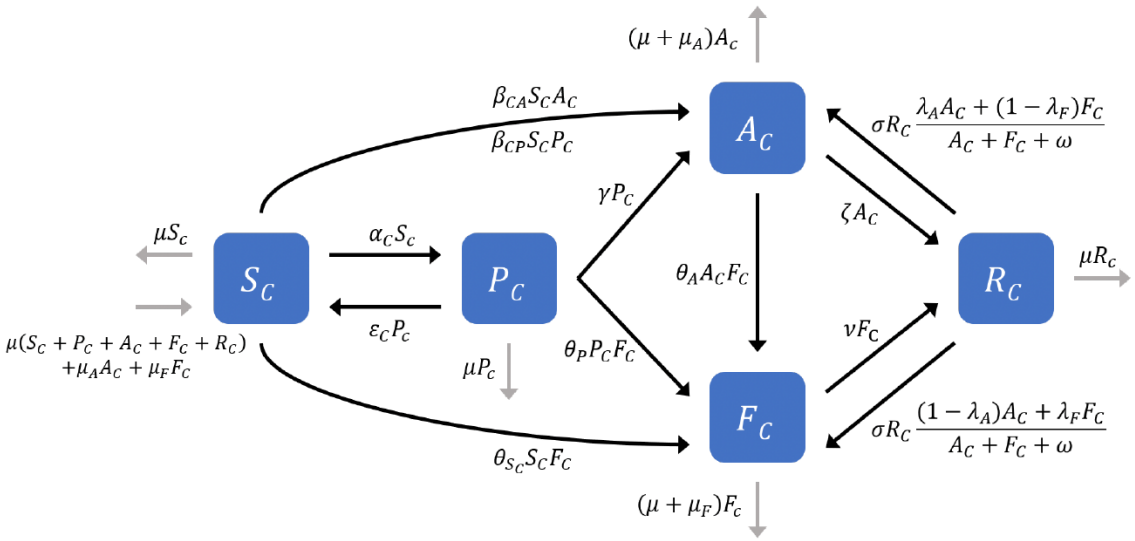

(a) Flow diagram illustrating drug class transitions for the entire community as described by Equation (3.1).

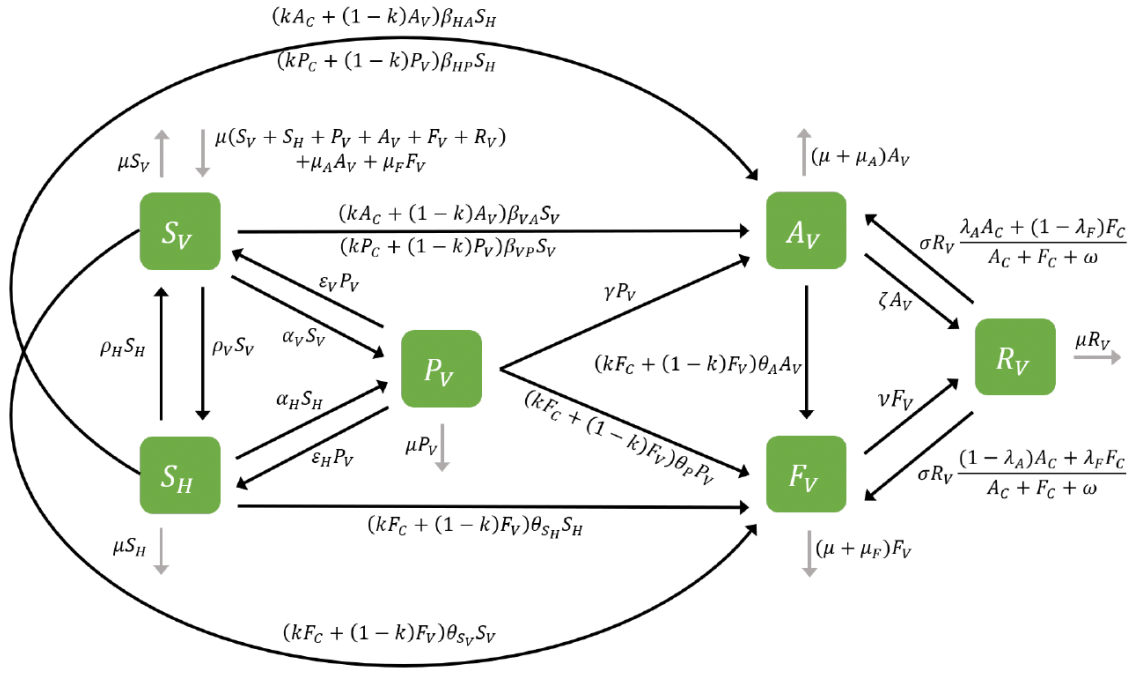

(b) Flow diagram illustrating drug class transitions for the subcommunity as described by Equation (3.2).

Figure 3.2: Visual representations of how individuals from both the community in Figure 3.2a and subcommunity in Figure 3.2b. These diagrams were created by Eversman [1].

Similar formulations applied to the subcommunity relapse rates. Having outlined the model structure and some key parameters, we move on to review Eversman's findings.

Her analysis indicated that the susceptible and prescribed classes could essentially exist as a separate system from the OUD and recovery classes. Eversman's findings ultimately cooperated with Phillips et al. [5] in that the most effective approach for reducing overall overdose mortality would be focusing on treatment for individuals with established OUD and closely monitoring stably recovered individuals. In particular, she suggested focusing on the prevention of illicit opioids. Additionally, she determined that term k for assigning the extent of the subcommunity segregation had minimal impact on any class sizes.

3.1.2 Our Model

Our individual-based model is derived from the population dynamics of Eversman's compartmental model [1], with one notable deviation. Eversman utilized a community/subcommunity structure, where the dynamics of a focal subcommunity was focused on within the entire community. However, applying this framework to our model would result in ambiguity, as assigning individuals solely to the focal subcommunity or the broader community fails to meaningfully distinguish those outside the focal subcommunity. To address this limitation, we adopt Eversman's definition of the non-subcommunity, which encompasses all members not belonging to the focal subcommunity. This adjustment allows for a clear distinction between individuals within and outside the focal subcommunity. Consequently, the compartmental model underpinning our individual-based approach employs a subcommunity/non-subcommunity framework inspired by Eversman's model. With this deviation from Eversman's model established, we now turn to key features of Pearcy's OUD agent-based model [6] that have been integrated into our design.

Our individual-based model adopts its methodology from Pearcy, differing in three key aspects. The first concerns the network structure: Pearcy's model was a static network, in which all connections were fixed at initialization and remained unchanged throughout the process. However, real-world relationships exhibit a level of relational mobility, reflecting

the ease with which individuals can form new connections and abandon existing ones [55, 56]. Thus, our model incorporates a dynamic network. New connections are more likely to form between individuals who belong to the same drug class, while existing connections are severed based on an assigned mobility level (strong or weak), with strong connections being more prone to dissolution.

A second key distinction from Pearcy's design is the incorporation of varying levels of social influence across connections in our model. This feature allows certain relationships to exert stronger effects on individuals' transitions between drug-use classes. For the purposes of this analysis, social influence is defined as the capacity of an individual's connections to induce changes in their drug-use classifications [57]. Previous research has demonstrated that relationships such as family and peers can significantly influence the initiation of either medically prescribed or recreational opioid use [58, 59, 60]. In our model, social influence is implemented by assigning each edge an influence level, categorized as strong or weak, with strongly-influenced edges exerting a greater impact on drug class transitions.

The third difference from Pearcy's opioid model involves incorporating social isolation into the pathways for developing OUD. While further research is needed, existing studies have identified an association between social isolation and elevated risks of developing OUD [61, 62, 63]. Accordingly, we incorporate this idea by converting the OUD-development and relapse rates into negated sigmoid functions. This methodology comes from the work of Leigh Pearcy, who developed both a system of ODEs and a subsequent individual-based model to study alcohol use disorder (AUD) [6].

In her model, Pearcy had two specific isolation terms, one of which being the rate β_i of susceptibles initiating heavy drinking, with a subscript i used to identify parameters related specifically to isolation. To incorporate population-level parameter β_i from her ODE model, then the corresponding individual-level isolation parameter was given by the degree-dependent function $\beta_i(n)$:

$$\hat{\beta}_i(n) = -\frac{L}{1+e^{-k(n-m)}} + C,$$

where k controlled the slope, m was the midpoint, L was the amplitude and C was the vertical shift of the curve. Using the boundary conditions

$$\hat{\beta}_i(0) = r\beta_i, \qquad \hat{\beta}_i(N-1) = \beta_i$$

for some scaling factor $r > 1$, where N represented the total population size, Pearcy solved L and C to yield

$$\hat{\beta}_i(n) = \frac{-L}{1+e^{-k(n-m)}} + \frac{L}{1+e^{-k(N-1-m)}} + \beta_i,$$

where

$$L = \frac{\beta_i(r-1)\left(1+e^{-k(N-1-m)}\right)\left(1+e^{km}\right)}{e^{km}\left(1-e^{-k(N-1)}\right)}.$$

The effects of how the shaping parameters r, m, and k affect the isolation function is visualized in Figure 3.3.

Motivated by her work, we likewise develop a stochastic analogue based on a deviation of the ODE introduced by Eversman [1]. While our model follows Pearcy's methodology, [6] the interactions between individuals are informed by a deviation of Eversman's model. Our central objective is to quantify how individual-level social connections aggregate to population-level dynamics, with a particular emphasis on how

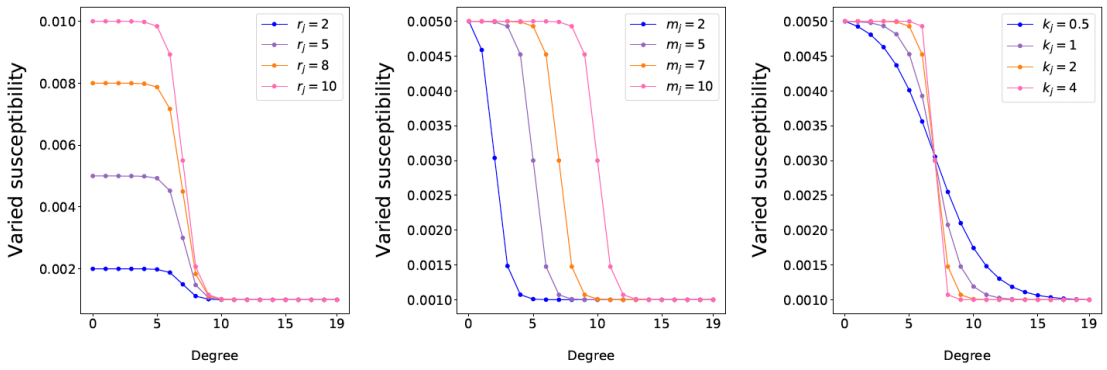

Figure 3.3: Graphs by Pearcy [6] illustrating $\hat{\beta}_i(n)$ for varying shaping parameters r, m, and k. Subscripts here simply determined which isolation function was being considered; here, it is $\hat{\beta}_i(n)$. Each graph was generated with $\beta_i = 0.001$ on a network size of $N = 20$. As shown, r scaled the maximum susceptibility of isolated individuals, m shifted the midpoint of the curve, and k adjusted the steepness of the declining slope.

relationship restructure affects the development of OUD within the population. The remainder of this chapter presents the model formulation, simulation procedure, and analysis.

3.2 Methods

The stochastic network model we developed is an individual-based model that uses the population dynamics of the community/out-community deviation of the ODE model created by Eversman [1]. As such, many premises and parameters in the ODE model are retained in ours. Hereafter, we will label our model as the "SN model" and the deviation as the "ODE model." We also redefine the structure of individuals as follows: the general population (G) is partitioned into a focal community (C) and out-community (O), consisting of individuals "outside" the community. Although Pearcy [6] converted a general-population-only ODE model into an static individual-based model (with edges remaining fixed over time), we extend her methods and procedures to our community/out-community ODE deviation to construct a dynamic model (with edges forming and dissolving over time).

The fundamental structure of the SN model can be described in graph theory terms, where individuals correspond to vertices and individual relationships are represented by edges. Let $\mathbb{G}$ be a graph of N individuals, where $V = \{V_k\}_{k=1}^{N}$ denotes the set of *vertices*, and E denotes the set of *edges* in graph $\mathbb{G}$ such that E is the subset of the set of all possible edges, i.e., $E \subseteq \big\{\{V_k, V_j\} \mid 1 \leq k < j \leq N\big\}$. Each vertex V_k signifies an individual in our community, and each edge $\{V_k, V_j\}$ denotes a connection between two individuals V_k and V_j. All edges are unordered and undirected, meaning all edges are symmetrical $\{V_k, V_j\} = \{V_j, V_k\}$ and all relationships are mutual, respectively. If there is no edge between two vertices, then there is no connection between the individuals. However, if there is an edge $\{V_k, V_j\}$, we say that V_k and V_j are *neighbors*. The *neighborhood* $\mathscr{N}(V_k)$ of vertex V_k is the set of all vertices that share an edge with V_k, i.e., $\mathscr{N}(V_k) = \big\{V_j : \{V_k, V_j\} \in \mathbb{G}\big\}$. The

number of neighbors $|\mathcal{N}(V_k)|$ in a neighborhood of vertex V_k is called the *degree* of V_k, or $\deg(V_k)$.

Each vertex in the network is assigned a drug class, a process detailed in the forthcoming Chapter 3.2.1. The general population has five drug classes (S_G, P_G, A_G, F_G, R_G). The focal community consists of six drug classes (S_C, S_H, P_C, A_C, F_C, R_C) and the out-community consists of five (S_O, P_O, A_O, F_O, R_O). Definitions of these drug classes are found in Table 3.2.

As the model progresses through time, vertices transition between drug classes based on the ODE model developed by Eversman[1]. To enhance clarity and reduce potential confusion, we present the equations again using our new notation in Equations (3.4) and (3.5), which correspond to the focal community and the out-community, respectively. Additionally, we provide a visual representation of the model using the updated notation in Figure 3.4.

Each drug class in the general population can be written as a weighted sum of the respective classes in the community and out-community. For example, the illicit-based OUD (IOUD) general population class can be converted as such:

$$F_G = q_C F_C + q_O F_O, \tag{3.3}$$

where q_C and q_O are the fixed proportions partitioned between the focal community and out-community, respectively, so that $q_C + q_O = 1$. We use this relationship to reformulate the relapse and social contact terms from Everman's model.

As our ODE model is a community/out-community model, we must convert the terms containing general population classes from Eversman's population/community model. Firstly, the population fractions in the relapse terms from Everman's model are converted as such:

$$\Lambda_A = \frac{\lambda_A A_G + (1-\lambda_F) F_G}{A_G + F_G + \omega} = \frac{\lambda_A \left[q_C A_C + q_O A_O\right] + (1-\lambda_F)\left[q_C F_C + q_O F_O\right]}{\left[q_C A_C + q_O A_O\right] + \left[q_C F_C + q_O F_O\right] + \omega}$$

Table 3.2: Definition of the drug classes from the general population G, the focal community C, and the out-community O.

Drug Classes	Explanation
Susceptibles (S_G, S_C, S_H, S_O)	Individuals that are not currently taking any form of opioids and have never suffered from an opioid use disorder. The susceptible class in the focal community was divided into two subclasses: the susceptibles with acute-to-little pain (S_C) and those with chronic pain (S_H) as they are "hurt".
Prescription opioid users (P_G, P_C, P_O)	Individuals that are currently taking prescribed opioids but have not developed an opioid use disorder.
Prescription-based OUD (POUD) (A_G, A_C, A_O)	Individuals that are taking prescription opioids and have an opioid use disorder. However, these individuals are not taking any illicit opioids such as fentanyl or heroin. Opioids taken need not have been prescribed to the individual.
Illicit-based OUD (IOUD) (F_G, F_C, F_O)	Individuals that are taking illicit opioids, such as fentanyl or heroin, and have an opioid use disorder. Individuals can also be taking prescribed opioids.
Stably Recovered (R_G, R_C, R_O)	Individuals who had an opioid use disorder, and are no longer taking opioids and/or have completed treatment for the disorder. Individuals also have not relapsed for at least 4 weeks.

$$
\begin{cases}
\frac{dS_C}{dt} = & -\theta_{S_C} S_C[(1-\kappa q_O)F_C + \kappa q_O F_O] - \rho_C S_C - \beta_{CP} S_C[(1-\kappa q_O)P_C + \kappa q_O P_O] \\
& -\beta_{CA} S_C[(1-\kappa q_O)A_C + \kappa q_O A_O] - \alpha_C S_C + \rho_H S_H + \varepsilon_C P_C \\
& +\mu(S_H + P_C + A_C + F_C + R_C) + \mu_A A_C + \mu_F F_C \\
\frac{dS_H}{dt} = & -\beta_{HP} S_H[(1-\kappa q_O)P_C + \kappa q_O P_O] - \beta_{HA} S_H[(1-\kappa q_O)A_C + \kappa q_O A_O] \\
& -\rho_H S_H - \alpha_H S_H - \theta_{S_H} S_H[(1-\kappa q_O)F_C + \kappa q_O F_O] - \mu S_H + \rho_C S_C + \varepsilon_H P_C \\
\frac{dP_C}{dt} = & -\varepsilon_C P_C - \varepsilon_H P_C - \gamma P_C - \theta_P P_C[(1-\kappa q_O)F_C + \kappa q_O F_O] - \mu P_C + \alpha_H S_H + \alpha_C S_C \\
\frac{dA_C}{dt} = & -\theta_A A_C[(1-\kappa q_O)F_C + \kappa q_O F_O] - \zeta A_C - (\mu + \mu_A)A_C \\
& +\beta_{CP} S_C[(1-\kappa q_O)P_C + \kappa q_O P_O] + \beta_{CA} S_C[(1-\kappa q_O)A_C + \kappa q_O A_O] \\
& +\beta_{HP} S_H[(1-\kappa q_O)P_C + \kappa q_O P_O] + \beta_{HA} S_H[(1-\kappa q_O)A_C + \kappa q_O A_O] \\
& +\gamma P_C + \sigma R_C \Lambda_A \\
\frac{dF_C}{dt} = & -\nu F_C - (\mu + \mu_F) F_C + \theta_{S_C} S_C[(1-\kappa q_O)F_C + \kappa q_O F_O] \\
& +\theta_{S_H} S_H[(1-\kappa q_O)F_C + \kappa q_O F_O] + \theta_P P_C[(1-\kappa q_O)F_C + \kappa q_O F_O] \\
& +\theta_A A_C[(1-\kappa q_O)F_C + \kappa q_O F_O] + \sigma R_C \Lambda_F \\
\frac{dR_C}{dt} = & -\sigma R_C \Lambda_A - \sigma R_C \Lambda_F - \mu R_C + \zeta A_C + \nu F_C
\end{cases}
\tag{3.4}
$$

System of equations describing the focal community as developed by Eversman [1]..

$$
\begin{cases}
\frac{dS_O}{dt} = & -\alpha_O S_O - \beta_{OP} S_O(q_C P_C + q_O P_O) - \beta_{OA} S_O(q_C A_C + q_O A_O) \\
& -\theta_{S_O} S_O(q_C F_C + q_O F_O) + \varepsilon_O P_O + \mu(P_O + A_O + F_O + R_O) + \mu_A A_O + \mu_F F_O \\
\frac{dP_O}{dt} = & -\varepsilon_O P_O - \mu P_O - \gamma P_O - \theta_P P_O(q_C F_C + q_O F_O) + \alpha_O S_O \\
\frac{dA_O}{dt} = & -\zeta A_O - \theta_A A_O F_C - (\mu + \mu_A) A_O + \beta_{OA} S_O(q_C A_C + q_O A_O) \\
& +\beta_{OP} S_O(q_C P_C + q_O P_O) + \gamma P_O + \sigma R_O \Lambda_A \\
\frac{dF_O}{dt} = & -\nu F_O - (\mu + \mu_F) F_O + \theta_{S_O} S_O(q_C F_C + q_O F_O) + \theta_P P_O(q_C F_C + q_O F_O) \\
& +\theta_A A_O(q_C F_C + q_O F_O) + \sigma R_O \Lambda_F \\
\frac{dR_O}{dt} = & -\sigma R_O \Lambda_A - \sigma R_O \Lambda_F - \mu R_O + \zeta A_O + \nu F_O
\end{cases}
\tag{3.5}
$$

System of equations describing the out-community as developed by Eversman [1].

and

$$\Lambda_F = \frac{(1-\lambda_A)A_G + \lambda_F F_G}{A_G + F_G + \omega} = \frac{(1-\lambda_A)\left[q_C A_C + q_O A_O\right] + \lambda_F \left[q_C F_C + q_O F_O\right]}{\left[q_C A_C + q_O A_O\right] + \left[q_C F_C + q_O F_O\right] + \omega}.$$

The social contact terms are converted similarly; for example, when susceptibles S_H with chronic pain in the focal community develop IOUD by interacting with IOUD users, we use the drug class relationship in Equation (3.3) and the fact that q_C and q_O are partitioned proportions to convert Eversman's population/community term as such:

$$\begin{aligned}\theta_{S_H} S_H \left[\kappa F_G + (1-\kappa)F_C\right] &= \theta_{S_H} S_H \left[\kappa(q_C F_C + q_O F_O) + F_C - \kappa(q_C + q_O)F_C\right] \\ &= \theta_{S_H} S_H \left[(1-\kappa q_O)F_C + \kappa q_O F_O\right].\end{aligned}$$

This reformulation extends to the other social contact terms developing either illicit-based OUD (IOUD) or prescription-based OUD (POUD). We change the symbol for the segregation levels in Eversman's model to κ from k, as k is already in use.

3.2.1 Establishing the initial graph

With the outline of our SN model's basic structure, we now turn to the construction of the initial state of the graph. The graph $\mathbb{G}$ is generated using the Erdös-Réyni algorithm, one of the simplest to construct [64, 65]. After determining the set of vertices V, each distinct pair of vertices $\{V_k, V_j\}$ has an independent and identical probability p of developing an edge. From this algorithm, there are two consequences we must consider.

The first consequence is the possibility of individuals initially being disconnected, represented by vertices without any edges. This scenario is permissible within the context of our dynamic network. Since the potential for connection exists at each time step, isolated individuals are regarded as temporary.

The second consequence concerns to the reduced connectivity within the network. While the ODE model operates under the well-mixed assumption, which presumes a fully-connected network, our network exhibits sparsity that may influence the resulting dynamics. In Chapter 3.3, we compare the outcomes of our SN model with those of the ODE model and demonstrate that, under specific conditions, the differences are minimal.

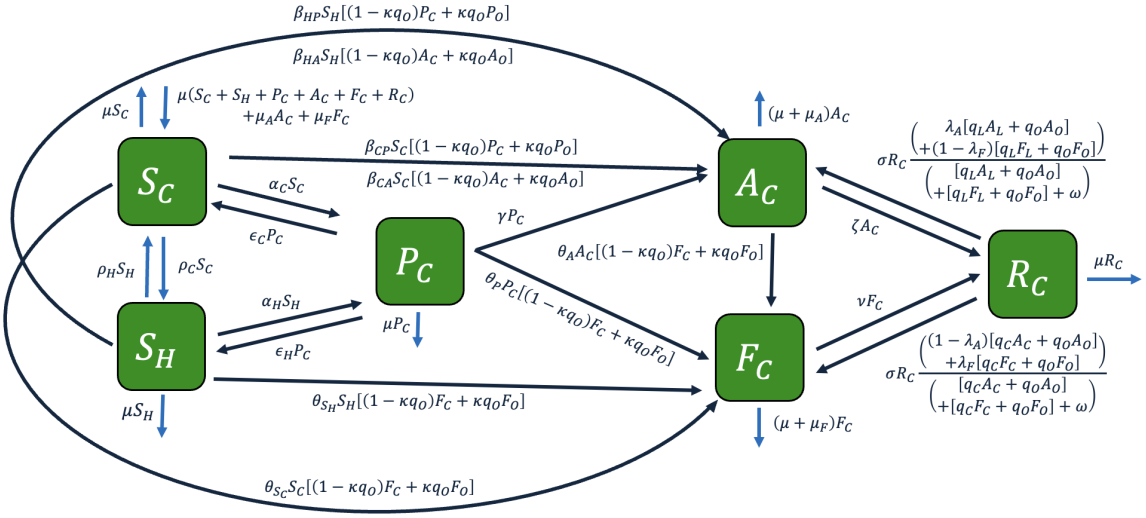

(a) Flow diagram illustrating drug class transitions for the focal community as described by Equation (3.4).

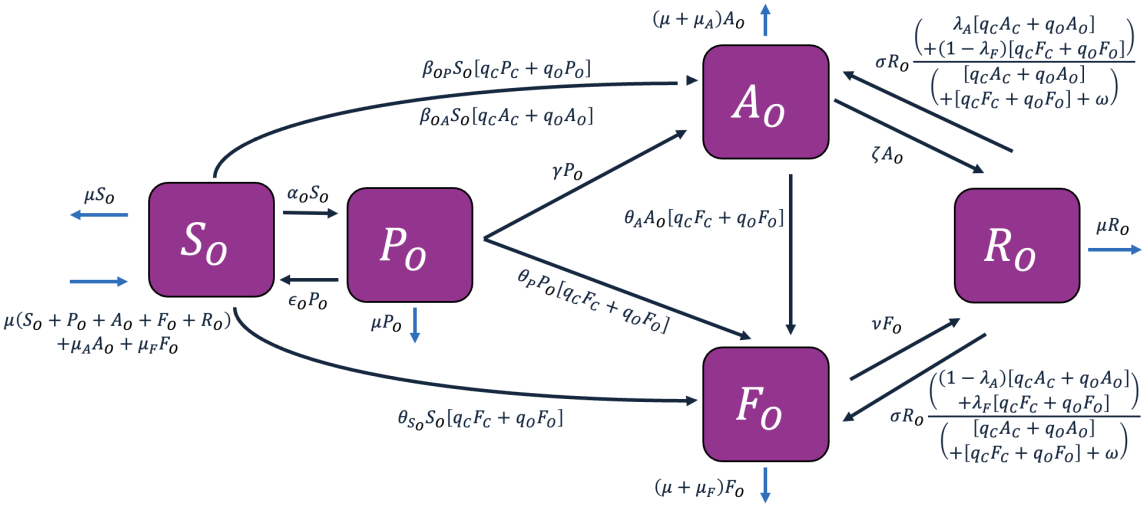

(b) Flow diagram illustrating drug class transitions for the out-community as described by Equation (3.5).

Figure 3.4: Visual representations of how individuals from both the focal community in Figure 3.4a and out-community in Figure 3.4b.

After defining the network structure, edges are assigned two independent attributes: social influence level and relational mobility level. The social influence level can take one of two values: 1, representing weak influence, or a prespecified constant $\ell_i \in \mathbb{N}$, greater than 1, representing strong influence. Similarly, the relational mobility level is either 1, indicating weak mobility, or another prespecified constant $\ell_m \in \mathbb{N}$, greater than 1, indicating strong mobility. As we detail in the upcoming Chapter 3.2.2, strong influence levels correspond with an increased likelihood of affecting each individual's drug state. In contrast, strong mobility levels are associated with an increased probability of severing connections. The proportions of edges with strong influence and strong mobility are predetermined and denoted by p_{is} and p_{im}, respectively. Consequently, the proportions of edges with weak influence and weak mobility are given by $1 - p_{is}$ and $1 - p_{im}$.

To assign the influence and mobility levels within the network, we begin by considering the total number of edges, denoted $e = |E|$. A number of edges $p_{is}e$ rounded to the nearest integer is randomly selected without replacement from a complete list of edges in the network and designated with the strong influence level ℓ_i. The remaining edges are assigned the weak influence level of 1. Similarly, another independent random selection without replace is performed to assign strong mobility levels. Specifically, $p_{im}e$ edges, rounded to the nearest integer, are labeled with the strong mobility level ℓ_m, while the remaining edges are given the weak mobility level 1. By this designation process, edges can exhibit varying combinations of influence and mobility levels. We demonstrate further how these edge attributes play crucial roles in modeling individual behavior within the network in the upcoming Chapter 3.2.2. Once all edges have been labeled with their respective influence and mobility attributes, drug classes are then assigned to the vertices in the network.

We partition the total population of N vertices into the two groups: the focal community and the out-community, with fixed proportions q_C and $q_O = 1 - q_C$, respectively. The focal community consists of $N_C = \texttt{round}(q_C N)$ vertices, rounded to the nearest integer. To determine the number of vertices in each drug class within the focal community, we scale the initial conditions of the ODE model by N_C. For instance, the number of vertices labeled S_H is calculated as $S_H(0)N_C$, rounded to the nearest integer. The number of vertices

labeled as P_C, A_C, F_C, and R_C are determined similarly. Any remaining vertices in the focal community are assigned to the S_C drug class. The number of drug class labels in the out-community, consisting of $N_O = N - N_C$ total vertices, are determined using a comparable process. A list containing these labels is then constructed, randomly shuffled, and distributed to the vertices.

Consequently, while the ODE model represents drug classes as proportions within each subgroup, the SN model expresses the drug classes as discrete counts of individuals in each class such that

$$S_C + S_H + P_C + A_C + F_C + R_C = N_C \qquad \text{and} \qquad S_O + P_O + A_O + F_O + R_O = N_O.$$

Furthermore, a proportional drug class in the ODE model can be approximated in the SN model by dividing the number of vertices in a given class by the total number of vertices in the corresponding subgroup. For example,

$$A_C \text{ in ODE model } \approx \frac{\text{\# of vertices in SN model labeled } A_C}{N_C}.$$

Once the vertices are labeled with their respective drug classes, each vertex is randomly assigned a unique set of transition parameters to account for individual variability. The parameters in the ODE model (Equations 3.4 and 3.5) represent population-level averages of individual transition rates. To ensure consistency between the ODE and SN models, individual vertices must be assigned transition rates that collectively average to the population-level parameters specified in the ODE model.

For each parameter, we construct a truncated normal distribution centered at a mean equal to the corresponding population parameter with a standard deviation set to 10% of the mean. This distribution is symmetrically truncated around the mean to exclude negative values. By setting the standard deviation to 10% of the mean, zero lies exactly 10 standard deviations below the mean, ensuring that truncation has negligible impact on the overall distribution while maintaining biological validity. Individual transition rates are then independently sampled from these distributions and assigned to each vertex.

For example, Eversman estimated the recovery rate for POUD as $\zeta = 0.0536$ per year [1]. Based on this estimate, each vertex V_k is assigned an individual recovery rate $\zeta^{(k)}$, sampled from a truncated normal distribution with a mean of 0.0536 and a standard deviation of 0.00536, excluding negative values. This procedure is repeated for every parameter, resulting in each vertex being assigned a complete set of individualized transition rates that reflect both variability and alignment with population-level averages.

While most population parameters are constant and can be determined prior to running the model, the prescribing rate is time-dependent, and must be continuously updated during the simulation. For example, at each time step, the prescribing rate of susceptibles in the out-community, denoted α_O, is calculated using the linear relationship:

$$\alpha_O = \tilde{m}_O t + \tilde{b}_O.$$

This value is then utilized to randomly assign individuals α_O rates from the corresponding truncated normal distribution. The same process is applied to prescribing rates α_C and α_H within the focal community. This approach ensures that time-dependent variations in prescribing behavior are accurately reflected in the model while maintaining consistency with population-level dynamics.

3.2.2 Running the model

Having established the methodology for constructing the initial state of the vertices and edges in the SN model, we now focus on describing how the model evolves over time. Once the initial network is generated, the model is simulated over a specified duration T (measured in years). At each predetermined time step Δt, the network undergoes potential changes through two key processes: a drug transition process, where individuals may switch between drug classes and an edge reconfiguration, where edges may restructure by either forming new connections or severing existing ones.

The drug transition event enables each individual to be reclassified into a different drug class, implemented through a two-step method previously developed by Pearcy [6]. The first step assesses whether a transition occurs, and only if a transition is confirmed does

the second step identify the new drug class for the individual. In the initial step, the mean transition rates out of a given class are added together as the mean waiting time λ in a Poisson process, consistent with Pearcy's method. However, our model introduces two key modifications.

The first modification incorporates social influence by weighing neighborhoods based on the influence levels of their edges. Specially, the total neighbors $N^{(k)}$ of a vertex V_k weighted by influence is calculated as the sum of influence levels of all edges to V_k, expressed as follows:

$$N^{(k)} = \sum_{j=1}^{\deg(V_k)} I_{k_j}, \qquad I_{k_j} = \begin{cases} 1, & \text{if edge } \{V_k, V_{k_j}\} \text{ has weak influence,} \\ \ell_i, & \text{if edge } \{V_k, V_{k_j}\} \text{ has strong influence,} \end{cases}$$

This adjustment ensures that the influence of an individual's social connections is appropriately accounted for when determining transition probabilities.

The second modification entails adjusting the OUD development rates to reflect isolation as a heightened risk factor for OUD progression. This methodology aligns with the approach introduced in the AUD model by Pearcy [6]. While Pearcy had completely separate isolation terms, we incorporate the idea of isolation into our social contact rates. To illustrate this process, we examine the parameter β_{CP}, which denotes the rate at which susceptible individuals within the focal community develop POUD.

Our goal is to construct a function where fewer connections correspond with higher rates. To achieve this, we employ the negated sigmoid function $\hat{\beta}_{CP}(n_k)$, which depends on the degree n_k of a vertex V_k and replaces the isolation parameter β_{CP} in the SN model. In a network with N individuals, a fully connected vertex has $N-1$ connections, defining the boundary condition $\hat{\beta}_{CP}(N-1) = \beta_{CP}$ as the minimum baseline case. Conversely, the maximum boundary condition occurs when the vertex has no neighbors, resulting in $\hat{\beta}_{CP}(0) = r\beta_{CP}$ for a scaling factor $r > 1$. Enforcing these conditions yields the following function:

$$\hat{\beta}_{CP}(n_k) = \frac{L}{1+e^{-s(N-1-m)}} - \frac{L}{1+e^{-s(n_k-m)}} + \beta_{CP},$$

where

$$L = \frac{\beta_{CP}(r-1)\left(1+e^{-s(N-1-m)}\right)(1+e^{-sm})}{1-e^{-s(N-1-m)}}.$$

In this formulation, $s > 0$ determines the slope of the curve, $m > 0$ specifies the midpoint, and L represents the amplitude. For a clearer understanding of how these shaping parameters impact the function, refer to Figure 3.3; however, the figure uses the label k in place of our shaping parameter s. This construction is applied to the POUD development rates $(\beta_{CP}, \beta_{CA}, \beta_{HP}, \beta_{HA}, \beta_{OP}, \beta_{OA})$, the IOUD development rates $(\theta_{S_C}, \theta_{S_H}, \theta_{S_O}, \theta_P, \theta_A)$, and the relapse rates σ. Having established these modifications, we next outline the procedure for determining whether an individual transitions between drug classes.

Drug transitions are modeled as Poisson processes with the rate parameters λ determined by the sum of two distinct categories of transition terms: social contact terms and autonomous terms. For example, when a vertex V_k is considered for transitioning out of the S_C class (refer to Figure 3.4a), the autonomous terms are $\rho_C^{(k)}$, $\alpha_C^{(k)}$, and $\mu^{(k)}$.

The social contact terms require conversion. Consider the rate β_{CP} associated with developing POUD through social contact with prescribed individuals. We first substitute the negated sigmoid function $\hat{\beta}_{CP}$ previously discussed. Now, we consider the social component. Labeling the number of individuals in the community and out-community are denoted by $N_C = q_C N$ and $N_O = q_O N$, respectively, the coefficient in the ODE rate undergoes conversion to align with the SN model as follows:

$$\begin{aligned}
[(1-\kappa q_O)P_C + \kappa q_O P_O] &= \left[\left(1-\kappa\frac{N_O^{(k)}}{N^{(k)}}\right)\frac{P_C^{(k)}}{N_C^{(k)}} + \kappa\frac{N_O^{(k)}}{N^{(k)}}\frac{P_O^{(k)}}{N_O^{(k)}}\right] \\
&= \left[\left(N_C^{(k)} + (1-\kappa)N_O^{(k)}\right)\frac{P_C^{(k)}}{N_C^{(k)}} + \kappa P_O^{(k)}\right]/N^{(k)},
\end{aligned}$$

where $P_C^{(k)}$ and $P_O^{(k)}$ denote the number of P_C and P_O neighbors, respectively, while $N_C^{(k)}$, $N_O^{(k)}$, and $N^{(k)}$ represent the number of community, out-community, and total neighbors, respectively, associated with vertex V_k. Each of these neighbor counts is weighted by the

influence level of edges. Other social contact terms in the ODE model undergo similar conversions within our SN model. Consequently, the total transition rate out of the S_C class is expressed as

$$\lambda = \rho_C^{(k)} + \alpha_C^{(k)} + \mu^{(k)} + \hat{\beta}_{CP}\frac{\left[\left(N_C^{(k)} + (1-\kappa)N_O^{(k)}\right)P_C^{(k)}/N_C^{(k)} + \kappa P_O^{(k)}\right]}{N^{(k)}}$$
$$+ \hat{\beta}_{CA}\frac{\left[\left(N_C^{(k)} + (1-\kappa)N_O^{(k)}\right)A_C^{(k)}/N_C^{(k)} + \kappa A_O^{(k)}\right]}{N^{(k)}}$$
$$+ \hat{\theta}_{S_C}\frac{\left[\left(N_C^{(k)} + (1-\kappa)N_O^{(k)}\right)F_C^{(k)}/N_C^{(k)} + \kappa F_O^{(k)}\right]}{N^{(k)}}.$$

Since drug transitions follow a Poisson process with rate λ, mean waiting times are exponentially distributed. At each time step Δt, the probability of a transition occurring within the interval $(t, t+\Delta t]$ is given by

$$P(\text{transition in } (t, t+\Delta t]) = 1 - e^{-\lambda \Delta t}.$$

A transition is triggered whenever this probability exceeds a uniformly distributed random number selected from $[0,1]$. Once a drug transition occurs, the process advances to the subsequent step.

The second step of the two-step process identifies the specific drug class to which the vertex transitions. The possible outcomes including transitioning to another drug class or death. If the individual is determined to have died, the vertex is "reborn" as a susceptible in the same subgroup as the deceased vertex - S_C for vertices in the focal community and S_O for those in the out-community. Following this reclassification, all connections associated with the vertex are severed, and the vertex undergoes the same Erdös-Réyni process described in Chapter 3.2.1, where each remaining vertex has a probability p of forming a connection with the "reborn" vertex. Realistically, this process models an individual aging into the population, effectively replacing the deceased vertex while maintaining the network's structure and dynamics.

Each transition rate is normalized by λ and treated as a probability. For example, when a vertex V_k leaves the S_C drug class, the probability of transitioning to S_H is given by $\rho_C^{(k)}/\lambda$, to P_C by $\alpha_C^{(k)}/\lambda$, to A_C by

$$\left[\begin{array}{l} \hat{\beta}_{CP}\dfrac{\left(N_C^{(k)}+(1-\kappa)N_O^{(k)}\right)P_C^{(k)}/N_C^{(k)}+\kappa P_O^{(k)}}{N^{(k)}} \\ +\hat{\beta}_{CA}\dfrac{\left(N_C^{(k)}+(1-\kappa)N_O^{(k)}\right)A_C^{(k)}/N_C^{(k)}+\kappa A_O^{(k)}}{N^{(k)}} \end{array}\right]/\lambda,$$

to F_C by $\hat{\theta}_{S_C}\dfrac{\left(N_C^{(k)}+(1-\kappa)N_O^{(k)}\right)F_C^{(k)}/N_C^{(k)}+\kappa F_O^{(k)}}{N^{(k)}}/\lambda$, and finally to S_C by μ/λ. Again, in the final case, the individual would die and be "reborn" as a susceptible S_C without chronic pain.

The drug class is selected by sampling from a cumulative distribution defined by these probabilities. Specifically, a uniform random number $r \in [0,1]$ is compared to the cumulative probabilities: if $r < \rho_C^{(k)}/\lambda$, the new class is S_H; if $r \in \left(\rho_C^{(k)}/\lambda,\ \rho_C^{(k)}/\lambda + \alpha_C^{(k)}/\lambda\right)$, the class is P_C, and so forth. Once the drug class update process is complete, we proceed to examine the mechanisms governing connection modifications within the network.

The edge reconfiguration event encompasses both the formation and severance of edges within the network. For edge formation, the model reflects the tendency of individuals to establish connections under similar circumstances. To implement this behavior computationally, newly formed edges are assumed to be more likely between individuals belonging to the same drug class, regardless of subgroup affiliation. Each pair of disconnected vertices is assigned a forming rate that depends on their respective drug classes. Letting ι_{add} denote the baseline forming rate, the weighted forming rate for two disconnected vertices establishing an edge is expressed as ι_{add}/a_d, where a_d represents the compatibility level defined as:

$$a_d = \begin{cases} \ell_a, & \text{if drug classes are the same} \\ 1, & \text{if drug classes are different,} \end{cases}$$

where $\ell_a \leq 1$ is a predetermined constant. This formulation ensures that vertices with compatible drug classes are ℓ_a times more likely to form a connection.

For edge dissolution, each connected edge is assigned a severing rate based on its mobility level. Letting ι_{cut} represent the baseline severing rate, the weighted severing rate for an edge is given by ι_{cut}/m_e, where m_e denotes the mobility level of the edge and is defined as:

$$m_e = \begin{cases} 1, & \text{for weak mobility edge} \\ \ell_m, & \text{for strong mobility edge.} \end{cases}$$

Since $\ell_m \leq 1$, this formulation ensures that edges with higher mobility levels are $\ell_m \leq 1$ times more likely to be severed.

Each edge reconfiguration event is modeled as a Poisson process with rate $\hat{\lambda}$, defined as:

$$\hat{\lambda} = \begin{cases} \iota_{add} a_d, & \text{if edge does not exist within the network} \\ \iota_{cut}/m_e, & \text{if edge does exist within the network.} \end{cases} \tag{3.6}$$

Given that mean waiting times in Poisson processes follow an exponential distribution, the probability of an edge reconfiguration occurring within the interval $(t, t+\Delta t]$ for each time step Δt is expressed as follows:

$$P(\text{reconfiguration in } (t, t+\Delta t]) = 1 - e^{-\hat{\lambda}\Delta t}.$$

If this probability exceeds a uniformly distributed random number drawn from $[0,1]$, a reconfiguration event occurs. Specifically, if the edge previously existed, it is severed; otherwise, the edge is formed.

3.2.3 Model with Connection Preferences

Building on the basic model previously outlined, we now examine its enhanced form, which incorporates grouping preferences. As discussed earlier, individuals in the focal community are assumed to be more strongly influenced by members within their own community compared to those outside it. This concept is further extended by introducing a

preference for all individuals to form connections with others in their same community, reflecting the tendency of individuals to prioritize relationships within their immediate social group.

When initializing the network, we incorporate the degree of connectivity both within and between communities. To quantify this, we define $\xi_{com} \in [0,1]$ as the community segregation level. A value of $\xi_{com} = 0$ represents complete segregation, where no connections are formed between the two communities. Conversely, $\xi_{com} = 1$ signifies no preference, with connections being equally likely to form both within and between communities.

However, individuals can be categorized using multiple metrics, such as race, gender, geographic location, and other distinguishing factors. To enhance the model's ability to account for these additional dimensions of classification, we introduce a new categorization referred to as a "cluster." This categorization represents one of these supplementary metrics, allowing for a more nuanced partitioning of the population.

To integrate this layer of classification into the model, individuals are organized into K clusters within the network. These clusters are independent of the predefined communities and are characterized by proportions denoted as $\{q_j\}_{j=1}^{K}$, which satisfy the condition $\sum_{j=1}^{K} q_j = 1$. Furthermore, we define $\xi_{clu} \in [0,1]$ as the clustering segregation level, which parallels the community segregation level ξ_{com}. We assume that ξ_{clu} governs all clusters uniformly, without showing favoritism toward any specific cluster. This parameter governs the degree of connectivity between individuals belonging to different clusters. Next, we explore how this concept is integrated into our model.

Given an Erdös-Rényi connection probability p, Table 3.3 summarizes how the segregation levels ξ_{com} and ξ_{clu} influence the likelihood of connections concerning both community and cluster groupings. For any two vertices, an edge is formed if the corresponding likelihood exceeds a randomly selected value from a uniform distribution over the interval $[0,1]$. Having described how this process operates during network initialization, we next highlight three key components of the model that are directly influence by these segregation dynamics.

Table 3.3: Descriptions of the likelihood of any two vertices forming an edge respect to their community and their cluster.

Connection Terms	Explanation
p	Likelihood that two individuals from the same community and same cluster form a connection.
$p\xi_{com}$	Likelihood that one individual from the focal community and another from the out-community form a connection within the same cluster.
$p\xi_{clu}$	Likelihood that two individuals, either both from the focal community or both from the out-community, form a connection across different clusters.
$p\xi_{com}\xi_{clu}$	Likelihood that one individual from the focal community and another from the out-community form a connection across different clusters.

The first component concerns "reborn" vertices. These vertices not only retain their original community but also preserve their assigned cluster. Additionally, the formation of connections involving these vertices adheres to the same procedure utilized during the network's initialization, ensuring consistency in edge assignment.

The second component involves refining the edge reconfiguration event during the model's runtime. Since the severing of edges is solely dependent on the edges' mobility levels, the primary adjustment pertains to the formation of new connections. Thus, the edge reconfiguration from Equation 3.6 updates to the following:

$$\hat{\lambda} = \begin{cases} \iota_{add} a_d f_{com} f_{clu}, & \text{if edge does not exist within the network} \\ \dfrac{\iota_{cut}}{m_e}, & \text{if edge does exist within the network,} \end{cases}$$

where

$$f_{com} = \begin{cases} 1, & \text{if the vertices belong to the same community} \\ \xi_{com}, & \text{if the vertices belong to different communities} \end{cases}$$

and

$$f_{clus} = \begin{cases} 1, & \text{if the vertices belong to the same cluster} \\ \xi_{clu}, & \text{if the vertices belong to different clusters.} \end{cases}$$

This refinement ensures that both community and cluster segregation dynamics are incorporated into the edge reconfiguration process, allowing for a more nuanced representation of network evolution.

Additionally, to ensure a consistent degree throughout time, we must have the expected number of added edges to equal that of the removed ones. To this end, we introduce a scaling parameter X_{scale} governing the edge-removal probability. Since $\hat{\lambda}$ is the rate of a Poisson process, the removal time of an edge is exponentially distributed; hence, the probability that a given edge is removed by time T is $1-\exp\left(\hat{\lambda}T\right)$. In particular, for weakly mobile and strongly mobile connections with removal rates, the corresponding removal probabilities p_w and p_s, respectively, by time T are the following:

$$p_w = 1-\exp\left(-\iota_{cut}X_{scale}T\Delta t\right), \qquad p_s = 1-\exp\left(-\frac{\iota_{cut}}{\ell_m}X_{scale}T\Delta t\right),$$

where ι_{cut} is the baseline severing rate, $\ell_m \leq 1$ is the degree predetermined , and Δt is the simulated time step. In addition, the probability that a new edge is formed by time T between two individuals in the same drug class (p_{same}) or in different drug classes (p_{diff}) by time T is given by

$$p_{same} = 1-\exp\left(-\iota_{add}\ell_a f_{com}f_{clu}T\Delta t\right), \qquad p_{diff} = 1-\exp\left(-\iota_{add}f_{com}f_{clu}T\Delta t\right).$$

We assign n_w and n_s as the number of edges with weak and strong mobility, respectively, and n_{same} and n_{diff} as the number of edges potential edges between two individuals with the same drug class and different drug classes, respectively. Thus, the desired expected values are as follows:

$$\mathbb{E}[\#\text{ of removed edges}] = n_1 p_1 + n_2 p_2, \quad \mathbb{E}[\#\text{ of added edges}] = n_{same} p_{same} + n_{diff} p_{diff}.$$

Since

$$1 - e^{-x} \approx x$$

for small x, we can approximate the following probabilities

$$p_w \approx \iota_{cut} X_{scale} T \Delta t, \qquad p_s = \frac{\iota_{cut}}{\ell_m} X_{scale} T \Delta t,$$

$$p_{same} \approx \iota_{add} \ell_a f_{com} f_{clu} T \Delta t, \qquad p_{diff} \approx \iota_{add} f_{com} f_{clu} T \Delta t.$$

Equating the two expected values allows us to solve for X_{scale}:

$$X_{scale} = \frac{\left(n_{same} \ell_a + n_{diff}\right) \ell_m \iota_{add} f_{com} f_{clu}}{\iota_{cut} \left(n_w \ell_m + m_s\right)}.$$

This leaves us with Poisson removal and addition rate of

$$\hat{\lambda} = \begin{cases} \iota_{add} a_d f_{com} f_{clu}, & \text{if edge does not exist within the network} \\ \dfrac{\iota_{cut}}{m_e} X_{scale}, & \text{if edge does exist within the network,} \end{cases}$$

Lastly, the third component pertains to the average degree of vertices within the network. In the basic model with N individuals, the Erdös-Réyni algorithm establishes connections between vertices with a probability p. Since each vertex can potentially connect to the remaining $N-1$ vertices, the average degree of a vertex is given by $(N-1)p$.

With the introduction of the community segregation level ξ_{com} and the cluster segregation level ξ_{clu}, the probability of forming connections becomes further constrained. To quantity these effects, we now calculate the new average degree within the network. Let N represent the total number of individuals in the network, and let $N_C = \texttt{round}(q_C N)$ denote the number of individuals in the focal community, where q_C is the fixed proportion of focal community members. Also, $N_O = N - N_C$ represents the number of individuals in the out-community. For $j \in \{1, ..., K-1\}$, let $N_j = \texttt{round}(q_j N)$ denote the number of

individuals in cluster j, where q_j is the fixed proportion of members in cluster j. Within each cluster j, let $C_j = \texttt{round}\left(q_j N_C\right)$ represent the number of community members, and let $O_j = N_j - C_j$ represent the number of out-community members. For the final cluster K, we define its size and composition as follows:

$$N_K = N - \sum_{j=1}^{K-1} N_j, \qquad C_K = N_C - \sum_{j=1}^{K-1} C_j, \qquad O_K = N - N_C - \sum_{j=1}^{K-1} O_j.$$

This methodology ensures that the following relationships hold:

$$N_C + N_O = N, \quad \sum_{j=1}^{K} N_j = N, \quad \sum_{j=1}^{K} C_j = N_C, \quad \sum_{j=1}^{K} O_j = N_O \quad C_j + O_j = N_j$$

for $j \in \{1, ..., K\}$. To maintain consistency with the general population structure, each cluster is proportionally divided into community and out-community members based on their respective proportions in the overall population. This ensures that the distribution of individuals across clusters reflects both community membership and overall network composition.

To calculate the average degree, we begin by considering an individual in the focal community C and within cluster j for some $j \in \{1, ..., K\}$, denoted $V_{C,j}$. Among the remaining $C - 1$ members of the focal community and cluster j, each has a probability p of forming a connection with vertex $V_{C,j}$, resulting in an average number of connections within the same community and cluster as $(C_j - 1)p$. For out-community member in the same cluster O_j, the average number of connections is $O_j p \xi_{com}$. Next, for other clusters (i.e., not j), there are $N_C - C_j$ individuals in the focal community and $N_O - O_j$ individuals in the out-community, resulting in an average number of connections as $(N_C - C_j)p\xi_{clu}$ for focal community members and $(N_O - O_j)p\xi_{com}\xi_{clu}$ for out-community members in different clusters.

By summing these contributions, we obtain a comprehensive formula for the expected degree of vertex $V_{C,j}$ in the focal community and cluster j is given by

$$\mathbb{E}[\deg(V_{C,j})] = (C_j - 1)p + O_j p\xi_{com} + (N_C - C_j)p\xi_{clu} + (N_O - O_j)p\xi_{com}\xi_{clu}.$$

Using a similar argument, the expected degree of a vertex $V_{O,j}$ in the out-community and cluster j is

$$\mathbb{E}[\deg(V_{O,j})] = (O_j - 1)p + C_j p\xi_{com} + (N_O - O_j)p\xi_{clu} + (N_C - C_j)p\xi_{com}\xi_{clu}.$$

Given that the network consists of N vertices with C_j focal community members and O_j out-community members in j, the total expected degree of the network is calculated as

$$\mathbb{E}[\deg(V)] = \frac{1}{N}\sum_{j=1}^{K}\left(C_j\mathbb{E}[\deg(V_{C,j})] + O_j\mathbb{E}[\deg(V_{O,j})]\right).$$

Simplifying this formula yields

$$\mathbb{E}[\deg(V)] = p\frac{1}{N}\sum_{j=1}^{K}\begin{bmatrix} N_j\left(N_j - 1 + (N - N_j)\xi_{clu}\right) \\ -\left(2C_jO_j(1-\xi_{clu}) + (N_CO_j + N_OC_j)\xi_{clu}\right)(1-\xi_{com})\end{bmatrix}. \quad (3.7)$$

We demonstrate that the average degree in Equation (3.7) is at most that of the basic Erdős–Rényi model, i.e., $(N-1)p$. Since $\xi_{com}, \xi_{clu} \leq 1$, it follows that $-(1-\xi_{com}) \leq 0$. Therefore,

$$\mathbb{E}[\deg(V)] \leq p\frac{1}{N}\sum_{j=1}^{K} N_j\left(N_j - 1 + (N - N_j)\right) = p(N-1)\frac{1}{N}\sum_{j=1}^{K} N_j = p(N-1).$$

This result establishes that the average degree is bounded above by $(N-1)p$, consistent with the Erdös-Réyni model when no segregation levels are applied. Consequently, when conducting simulations, it is essential to account for the effects of segregation levels ξ_{com} and ξ_{clu} and adjust the values of p accordingly to maintain desired network properties. This means that the code needs inputs for the expected degree $\mathbb{E}[\deg(V)]$ as well as ξ_{com}, ξ_{clu} and computes p using the variation to Equation (3.7):

$$p = \frac{\mathbb{E}[\deg(V)]N}{\sum_{j=1}^{K}\begin{bmatrix} N_j\left(N_j - 1 + (N - N_j)\xi_{clu}\right) \\ -\left(2C_jO_j(1-\xi_{clu}) + (N_CO_j + N_OC_j)\xi_{clu}\right)(1-\xi_{com})\end{bmatrix}}.$$

We now must determine the parameters for our ODE model.

3.2.4 Parameter Estimation

We begin by utilizing the estimates established by Eversman [1] for both universal and focal-community-specific parameters, as detailed in Tables 3.4 and 3.6. For the out-community-specific parameters, we rely on Eversman's decomposition of the population parameters into their respective community and out-community components. Our analysis begins with an examination of the initial conditions for the drug state proportions of the out-community.

The initial conditions for the prescribed (P), POUD (A), IOUD (F), and recovery (R) drug state proportions are identical in both the general population and the focal community as seen in Tables 3.5 and 3.6. Consequently, the corresponding proportions in the out-community are also equal. We demonstrate this equivalence using the drug class relationship defined in Equation (3.3) with the P classes as follows:

$$\begin{aligned} P_{G_0} &= P_{C_0} q_C + P_{O_0} q_O \\ P_{O_0} q_O &= P_{G_0}(1 - q_C), && \text{since } P_{C_0} = P_{G_0} \\ P_{O_0} q_O &= P_{G_0} q_O, && \text{since } q_C + q_O = 1 \\ P_{O_0} &= P_{G_0}. \end{aligned}$$

For the susceptible S classes, the sum of the focal community proportions S_{C_0} and S_{H_0} equals the general population proportion S_{G_0}. Therefore, the out-community susceptible proportion S_{O_0} is also equal to S_{G_0}, shown as follows:

$$S_{G_0} = (S_{C_0} + S_{H_0}) q_C + S_{O_0} q_O = S_{G_0} q_C + S_{O_0} q_O$$

$$S_{O_0} q_O = S_{G_0}(1 - q_C) = S_{G_0} q_O$$

$$S_{O_0} = S_{G_0}.$$

The initial values for all out-community parameters are summarized in Table 3.7. With these initial conditions established, we now turn to determining the parameter terms for the out-community. The ODE model incorporates two types of terms: social contact and autonomous.

For a social contact example, consider the terms involving susceptibles developing an IOUD through social interaction. In the model developed by Eversman [1], the general population term is expressed as $\theta_{S_G} S_G F_G$, while the community terms are $\theta_{S_C} S_C[\kappa F_G + (1-\kappa)F_C]$ and $\theta_{S_H} S_H[\kappa F_G + (1-\kappa)F_C]$, and the out-community term is $\theta_{S_O} S_O F_G$. As before, the population term can be decomposed as follows:

Table 3.4: Estimations for universal parameters involved in general population, focal community, and out-community, determined by Eversman [1].

Parameters	Estimated Value	Units
θ_P	0.0101	$\frac{1}{\text{year}}$
θ_A	48.9	$\frac{1}{\text{year}}$
γ	1.16×10^{-5}	$\frac{1}{\text{year}}$
ζ	0.0536	$\frac{1}{\text{year}}$
ν	0.00319	$\frac{1}{\text{year}}$
σ	0.97	$\frac{1}{\text{year}}$
λ_A	0.00633	$\frac{1}{\text{year}}$
λ_F	1.0	$\frac{1}{\text{year}}$
μ	0.0143	$\frac{1}{\text{year}}$
μ_A	0.0471	$\frac{1}{\text{year}}$
μ_F	0.471	$\frac{1}{\text{year}}$

Table 3.5: Parameter estimations specific for the general population determined by Eversman [1].

Parameters	Estimated Value	Units
$\tilde{m}_G$	-0.0288	$\frac{1}{\text{year}}$
$\tilde{b}_G$	0.332	$\frac{1}{\text{year}}$
β_{GA}	0.001	$\frac{1}{\text{year}}$
β_{GP}	0.0001	$\frac{1}{\text{year}}$
θ_{S_G}	0.00111	$\frac{1}{\text{year}}$
ε_G	7.0	$\frac{1}{\text{year}}$
S_{G_0}	0.953493	dimensionless
P_{G_0}	0.0432	dimensionless
A_{G_0}	0.00246	dimensionless
F_{G_0}	0.000339	dimensionless
R_{G_0}	0.000508	dimensionless

Table 3.6: Parameter estimations specific for focal community parameters determined by Eversman [1].

Parameters	Estimated Value	Units
$\tilde{m}_C$	-0.03456	$\frac{1}{\text{year}}$
$\tilde{b}_C$	0.3154	$\frac{1}{\text{year}}$
$\tilde{m}_H$	-0.00576	$\frac{1}{\text{year}}$
$\tilde{b}_H$	0.3984	$\frac{1}{\text{year}}$
ρ_C	0.1	$\frac{1}{\text{year}}$
ρ_H	0.4	$\frac{1}{\text{year}}$
β_{CA}	0.0008	$\frac{1}{\text{year}}$
β_{CP}	8.0×10^{-5}	$\frac{1}{\text{year}}$
β_{HA}	0.0002	$\frac{1}{\text{year}}$
β_{HP}	2.0×10^{-5}	$\frac{1}{\text{year}}$
θ_{S_C}	0.000891	$\frac{1}{\text{year}}$
θ_{S_H}	0.000223	$\frac{1}{\text{year}}$
ε_C	5.603	$\frac{1}{\text{year}}$
ε_H	1.401	$\frac{1}{\text{year}}$
κ	1.0	dimensionless
S_{C_0}	0.762493	dimensionless
S_{H_0}	0.191	dimensionless
P_{C_0}	0.0432	dimensionless
A_{C_0}	0.00246	dimensionless
F_{C_0}	0.000339	dimensionless
R_{C_0}	0.000508	dimensionless

Table 3.7: The estimations of the parameters used in the out-community.

Parameters	Estimated Value	Units
$\tilde{m}_O$	-0.02858	$\frac{1}{\text{year}}$
$\tilde{b}_O$	0.3326	$\frac{1}{\text{year}}$
β_{OA}	0.0011	$\frac{1}{\text{year}}$
β_{OP}	0.00011	$\frac{1}{\text{year}}$
θ_{S_O}	0.001253	$\frac{1}{\text{year}}$
ε_O	6.998	$\frac{1}{\text{year}}$
S_{O_0}	0.953493	dimensionless
P_{O_0}	0.0432	dimensionless
A_{O_0}	0.00246	dimensionless
F_{O_0}	0.000339	dimensionless
R_{O_0}	0.000508	dimensionless

$$\theta_{S_G} S_G F_G = [\kappa F_G + (1-\kappa) F_C] (\theta_{S_C} S_C + \theta_{S_H} S_H) q_C + \theta_{S_O} S_O F_G q_O.$$

By isolating θ_{S_O}, we obtain

$$\theta_{S_O} = \frac{\theta_{S_G} S_G F_G - [\kappa F_G + (1-\kappa) F_C] (\theta_{S_C} S_C + \theta_{S_H} S_H) q_C}{q_O S_O F_G}. \tag{3.8}$$

This construction is also applied to the POUD development rates β_{OP} and β_{OA}. Having explained the social contact terms, we next move to the autonomous terms.

There are only two autonomous terms distinct with the out-community: ε_O and α_O. We first consider ε_O, which is the involving individuals completing their prescriptions. The corresponding terms for the general population, focal community, and out-community are $\varepsilon_G S_G$, $(\varepsilon_C + \varepsilon_H) P_C$, and $\varepsilon_O P_O$, respectively. Recall that individuals in the focal community who complete their prescriptions may either retain chronic pain (transitioning to S_H) or recover without chronic pain (transitioning to S_C). This distinction explains why the community term is express as $(\varepsilon_C + \varepsilon_H) P_C$. Given that the proportions of community and out-community members are denoted by q_C and q_O, respectively, the decomposition of the population term can be derived as follows:

$$\varepsilon_G P_G = (\varepsilon_C + \varepsilon_H) P_C q_C + \varepsilon_O P_O q_O$$

which, when isolating ε_O, results in

$$\varepsilon_O = \frac{\varepsilon_G P_G - (\varepsilon_C + \varepsilon_H) P_C q_C}{P_O q_O}. \tag{3.9}$$

With ε_O now established, we proceed to examine α_O, the prescribing rate within the out-community.

Recall that α_O is a linear term in time defined as follows:

$$\alpha_O = \tilde{m}_O t + \tilde{b}_O.$$

Similarly, the prescribing rates for the community groups S_C and S_H as well as the general population S_G, follow the same linear formulation. Consequently, we establish the following relationship:

$$\alpha_G S_G = (\alpha_C S_C + \alpha_H S_H) q_C + \alpha_O S_O q_O$$

$$\left(\tilde{m}_G t + \tilde{b}_G\right) S_G = \left[\left(\tilde{m}_C t + \tilde{b}_C\right) S_C + \left(\tilde{m}_H t + \tilde{b}_H\right) S_H\right] q_C + \left(\tilde{m}_O t + \tilde{b}_O\right) S_O q_O,$$

which results in the following two equations:

$$\tilde{m}_O = \frac{\tilde{m}_G S_G - (\tilde{m}_C S_C + \tilde{m}_H S_H) q_C}{S_O q_O}, \tag{3.10}$$

$$\tilde{b}_O = \frac{\tilde{b}_G S_G - \left(\tilde{b}_C S_C + \tilde{b}_H S_H\right) q_C}{S_O q_O}. \tag{3.11}$$

Having outlined the process for determining the out-community parameters, we now address the initial issues associated with this framework we have established.

Since each drug-state proportion varies over time, the corresponding out-community parameters are inherently time-dependent. However, for the purposes of the ODE model, these parameters must be treated as constants. To resolve this discrepancy, we solve the ODE model developed by Eversman [1], extracting these parameters at each time step and subsequently averaging the results to derive fixed parameter estimates.

A complication arises from the fact that Eversman's ODE system did not explicitly include the out-community drug-state proportions in the formulations. To overcome this, we reformulate the out-community parameter expressions by leveraging the relationships among the three collective groups (general population, focal community, and out-community). For example, applying the identity $P_G = P_C q_C + P_O q_O$ allows us to rewrite Equation (3.9) as

$$\varepsilon_O = \frac{\varepsilon_G P_G - (\varepsilon_C + \varepsilon_H) P_C q_C}{P_G - P_C q_C}.$$

Similarly, using $S_G = (S_C + S_H) q_C + S_O q_O$, we can also reformulate Equation (3.8) as

$$\theta_{S_O} = \frac{\theta_{S_G} S_G F_G - [\kappa F_G + (1-\kappa) F_C] \left(\theta_{S_C} S_C + \theta_{S_H} S_H\right) q_C}{[S_G - (S_C + S_H) q_C] F_G},$$

Equation (3.10) as

$$\tilde{m}_O = \frac{\tilde{m}_G S_G - (\tilde{m}_C S_C + \tilde{m}_H S_H)\, q_C}{S_G - (S_C + S_H) q_C},$$

and Equation (3.11) as

$$\tilde{b}_O = \frac{\tilde{b}_G S_G - (\tilde{b}_C S_C + \tilde{b}_H S_H)\, q_C}{S_G - (S_C + S_H) q_C}.$$

To compute these parameters, we employ `solve_ivp` to integrate Eversman's ODE model over the interval $t = 0$ to $t = 4$, using a time step of $1/100$, which corresponds to 3.65 days per step. Once the system is solved, the drug-state proportions at each time point are used to calculate the corresponding out-community parameters. The resulting averages are presented in Table 3.7, providing fixed values for use in the ODE model. With the out-community parameters now established, our next step is to determine the isolation parameters r and s.

The slope parameter s governs the transformation of negated sigmoid functions into step-like functions as the value increases. For simplicity, we set $s = 1$ across all relevant functions, including those modeling POUD development rates, IOUD development rates, and relapse rates.

Now, we consider the scaling parameter r, which plays a role in converting OUD development rates and relapse rates into negated sigmoid functions. We define two distinct values of r: one corresponding to OUD development (r_{OUD}) and another for relapse (r_σ).

To establish the scaling value r_{OUD} for OUD development rates, an ideal approach would involve identifying a study that empirically examines the number of social connections an individual has and compares how frequently they develop OUD. However, such data is not readily available. Consequently, we must infer the impact of reduced social relationships through alternative measures.

One such measure is an individual's difficulty participating in social activities. It is reasonable to assume that individuals who experience greater discomfort in social settings are likely to have fewer relationships. The findings in "Opioid use disorder and its association with self-reported difficulties participating in social activities" [66] provides valuable insights in this arena.

Using data from the 2008–2017 National Survey on Drug Use and Health (NSDUH), the authors analyzed responses from a sample of 398,962 individuals aged 18 years and older. Two assessments from this study were particularly relevant to our research. The first assessment diagnosed individuals with OUD based off ten yes/no questions aligned with the DSM-IV criteria for heroin and prescription opioid use disorder. The second assessment categorized responses as "none" or "severe" to the following question: "During that one month when your emotions, nerves, or mental health interfered most with your daily activities, how much difficulty did you have participating in social activities, like visiting friends or going to parties?"

The study revealed that individuals who reported experiencing "severe" difficulty were 4.10 times more likely to have an OUD compared to those who reported "none." Based on this information, we set $r_{OUD} = 4.10$ as the scaling factor for the negated sigmoid functions governing the POUD development rates $\left(\hat{\beta}_{CP}, \hat{\beta}_{CA}, \hat{\beta}_{HP}, \hat{\beta}_{HA}, \hat{\beta}_{OP}, \hat{\beta}_{OA}\right)$ and IOUD development rates $\left(\hat{\theta}_{S_C}, \hat{\theta}_{S_H}, \hat{\theta}_{S_O}, \hat{\theta}_P, \hat{\theta}_A\right)$. We next must determine the scaling parameter r_σ for relapse rates σ.

The scaling parameter r_σ is a defining feature of the function $\hat{\sigma}$ dependent on the number of connections an individual has. Direct determination of this value is challenging, so an alternative approach involves inferring the parameter through surveys that assess loneliness levels. The study "Loneliness and Illicit Opioid Use Among Methadone Maintenance Treatment Patients" [2] examined the relationship between loneliness and opioid use in the past month. Adult patients enrolled in methadone maintenance treatment were surveyed. Specifically, participants were asked: "Which best describes your illegal opioid use (heroin or non-prescription pain killers) during the past four weeks?" The response options included: *every day*, *at least once a week*, *once a month*, and *did not use*. To measure loneliness, patients were asked how frequently they experienced the following: (a) lacked companionship, (b) felt left out, and (c) felt isolated from others. Responses for each question were scaled as follows: 1 = *hardly ever*, 2 = *some of the time*, and 3 = *often*. Summed scores across these questions were categorized into three levels: little or

no loneliness (scores of $3-4$), moderate loneliness (scores of $5-6$), and severe loneliness (scores of $7-9$).

The original study reported data separately by sex and presented results as percentages. For our purposes, we aggregated the sexes, and converted to the data into counts of individuals, as shown in Table 3.8. Among individuals experiencing severe loneliness, the proportion who recently used opioids was $p_{severe} = 33/97 \approx 0.340$. In contrast, for individuals with little or no loneliness, the proportion was $p_{none} = 43/153 \approx 0.281$. These observations suggest that individuals with fewer social connections are approximately $p_{severe}/p_{none} \approx 1.2105$ times more likely to relapse compared to those experiencing little or no loneliness. Based on this inference, we set $r_\sigma = 1.2105$ as the scaling parameter for the negated sigmoid function $\hat{\sigma}$ governing OUD relapse terms. Having established the parameters for the negated sigmoid functions, we next establish values for the baseline forming ι_{add} and severing ι_{cut} rates.

We next must determine the rates at which individuals form new connections and sever old ones. In "Turnover in close friendships" [3], the authors analyzed mobile phone records collected over a three-year period from January 2007 to December 2009. Data from $644,170$ consistent users and $1,143,718$ unique links between them were included in the study. The total number of incoming and outgoing calls was ranked in decreasing order for each of the 36 months and averaged on a yearly basis. During the mid-to-late $2000s$, text messaging was less prevalent, making this method an effective way to identify an individual's closest relationships. Only links between users mutually ranked within the top five positions in each other's networks during 2007 and 2009 were considered. This approach allowed the authors to investigate the formation and decay of close relationships. Although the original data was separated by multiple categories, for the purposes of this analysis, the data was aggregated, as shown in Table 3.9.

Among the $155,503$ total links analyzed, an average of 7860 connections formed over the three years. To calculate the continuous-time relationship-formation rate ι_{add}, we let $E_0 = 155,503$ represent the number of connections at the start of the year. Since there would be $E = 155,503 + 7860 = 163,363$ connections at the end of $t = 3$ years, ι_{add} can

Table 3.8: The distribution of individuals by loneliness levels and their reported use of heroin or nonprescription opioids in the past month. These values were calculated based on percentages provided by Polenick et al. [2].

Loneliness Level	Used opioids	No opioids	Total
Little or none	43	110	153
Moderate	43	78	121
Severe	33	64	97
Total	119	252	371

Table 3.9: The distribution of individuals by age over a three-year period, calculated based on percentages provided by Roy et al. [3]. Data was collected, aggregated, and converted into counts from Supplementary Tables 1–4. Due to the presence of connections that neither formed nor decayed, the overall connection count in each column exceeds the sum of connections formed and decayed.

	Young-adult	Adult	Middle-aged	Sum of Connections
Connections Formed	879	4891	2090	7860
Connections Decayed	870	6666	1695	9231
Overall Connection Count	11,954	106,171	37,378	1,555,503

be determined using the following equation:

$$E = E_0 \exp(\iota_{add} t),$$

resulting in $\iota_{add} \approx 0.016437$.

Similarly, among the $155,503$ total links analyzed, an average of 9231 connections were severed over the three years. We next calculate the continuous-time relationship-severing rate ι_{cut}. Since there would be $E = 155,503 - 9231 = 146,272$ connections at the end of $t = 3$ years when starting with $E_0 = 155,503$ connections at the beginning of the year, we can determine ι_{cut} using the following equation:

$$E = E_0 \exp(-\iota_{cut} t),$$

resulting in $\iota_{cut} \approx 0.020399$.

3.3 Results

Our objective is to quantify how individual-level social structures shape population-level dynamics, particularly how interpersonal connections influence the proportion of individuals who develop OUD. We isolate two distinct mechanisms by which network structure can affect an individual's drug class: (i) the formation of new ties within the same drug class and (ii) the influence arising from the most close, trusted relationships.

During the edge reconfiguration step, individuals may form new connections or sever existing ones. To model a people's preference for connecting with like-minded people, we include a parameter $\ell_a \geq 1$ that scales the relative tendency to form edges with individuals in the same drug class versus a different class. Since transitions into OUD states depend on an individual's exposure to OUD neighbors through the ratio of OUD neighbors to total neighbors, increasing ℓ_a can reduce cross-class exposure (i.e., between susceptible and OUD individuals). This potentially decreases the probability of more individuals developing OUD. Moreover, stronger associations with fellow POUD individuals may prevent the progression from prescription-based OUD to illicit-based OUD.

A second mechanism concerns the strength of interpersonal influence. When evaluating drug transitions into an OUD class, we scale the development rate by a weighted neighbor

ratio, in which weak influence contributes weight 1 and strong influence contributes weight $\ell_i \geq 1$. Consequently, increasing ℓ_i certainly increases the effective exposure to neighbors even when the unweighted neighbor proportions remain unchanged. If most strong connections have are within the OUD class, this would increase the likelihood of developing OUD. However, likewise, if most strong connections are from the susceptible or prescribed classes, increasing ℓ_i could actually decrease the likelihood of developing OUD.

For each mechanism, we run independent simulations for each tested value of ℓ_a and ℓ_i. Because each run uses the same initial conditions, our primary interest lies in the distribution of terminal outcomes across runs. We therefore record, at the final time the terminal proportions of individuals in each community drug class. To compare outcomes under each tested parameter value against the baseline case $\ell_a = \ell_i = 1$ (representing no adding preference or differential influence), we test whether the resulting terminal-outcome distributions differ. We use the two-sample Kolmogorov-Smirnov (KS) test as a nonparametric tool for comparing these pair of distributions.

The two-sample KS test compares two continuous distributions by measuring the maximum difference between their empirical cumulative distribution functions (ECDFs) [67, 68]. If $X_1, ..., X_n$ and $Y_1, ..., Y_m$ are independent samples from continuous distributions with CDFs F and G respectively, then their corresponding ECDFs are

$$F_n(x) = \frac{\text{number of } X \text{ elements } \leq x}{n}, \qquad G_m(x) = \frac{\text{number of } Y \text{ elements } \leq x}{n},$$

respectively.

At significance level $\alpha = 0.05$, the two-sided KS test for equality of the population distributions is

$$H_0 : F(x) = G(x) \text{ for every } x$$
$$H_1 : F(x) \neq G(x) \text{ for some } x$$

where the test statistic is defined by the following:

$$D_{n,m} = \sup_x |F_n(x) - G_m(x)| .$$

Although the two-sided KS test detects *any* distributional discrepancy, our present study is primarily concerned with directional effects relative to the baseline: namely, whether changing a network parameter shifts the terminal outcome distribution toward systematically smaller or larger values. Accordingly, we emphasize the one-sided two-sample KS tests, which addresses the question "does one empirical CDF tend to lie above the other?" The one-sided hypotheses can be written as follows:

$$\begin{aligned} H_0 &: F(x) \geq G(x) \text{ for every } x \\ H_1 &: F(x) < G(x) \text{ for some } x \end{aligned} \tag{3.12}$$

and

$$\begin{aligned} H_0 &: F(x) \leq G(x) \text{ for every } x \\ H_1 &: F(x) > G(x) \text{ for some } x \end{aligned} \tag{3.13}$$

Under Equation (3.12), rejecting H_0 provides evidence that F accumulates probability faster at some point than G, which would mean that F tends to produce smaller values than G. Alternatively, when rejecting the null hypothesis of the Hypothesis Test (3.13), we can conclude that G tends to produce smaller values than F.

With the testing methodology in place, we proceed to evaluate each mechanism separately.

3.3.1 Testing ℓ_a values

We vary the single parameter $\ell_a \in \{1, 2, 3, 5, 8, 10, 15\}$ that governs the likelihood of forming new connections with individuals in the same drug class. The case $\ell_a = 1$ serves as the baseline (no forming preference) on a dynamically rewriting network. For each value of ℓ_a, we run 100 independent simulations and record the community-level proportion in each drug class at the final observational time.

To implement the one-sided two-sample KS tests, the first task is to determine which directional alternative hypothesis H_1 is appropriate for each comparison relative to the

baseline $\ell_a = 1$. Let the baseline outcomes have population CDF F (with ECDF F_n) and let the outcomes under a tested value of ℓ_a have the CDF G (with ECDF G_m). Using `scipy.stats.ks_2samp`, we rely on the returned `statistic_sign` to determine the sign of the extremal ECDF separation in the direction $F_n - G_m$. Table 3.10 reports these signs, where a "+" indicates that the one-sided statistic

$$D^{+}_{n,m} = \sup_x (F_n(x) - G_m(x)) > 0,$$

whereas a "−" indicates that the opposite direction, i.e.,

$$D^{-}_{n,m} = \sup_x (F_n(x) - G_m(x)) < 0.$$

Accordingly, comparisons with "+" are tested using Equation (3.13), while those with "−" are tested using Equation (3.12). The resulting p-values for each baseline-versus-test comparison are reported in Table 3.11.

Among the comparisons, only the S_C outcome at $\ell_a = 10$ yields a rejection of H_0 in the one-sided test with alternative $H_1 : F(x) > G(x)$ for some x. Equivalently, there exists a threshold x^* such that $F(x^*) > G(x^*)$, meaning that the baseline distribution $\ell_a = 1$ assigns a larger probability mass to values $\leq x^*$ than the $\ell_a = 10$ distribution. This behavior is illustrated in Figure 3.5. We can confidently conclude that strengthening the likelihood of forming new connections with individuals in the same drug class by 10 results in the terminal S_C proportions being stochastically larger.

In contrast, three comparisons (S_H with $\ell_a = 3$, S_H with $\ell_a = 10$, and A_C with $\ell_a = 8$) reject H_0 under the opposite one-sided alternative $H_1 : F(x) < G(x)$ for some x. This is consistent with the corresponding test-case distributions being shifted toward smaller values relative to the baseline. The associated histogram overlays are shown in Figure 3.6.

Having examined how individual preferences for forming new connections with the same drug class affect the population-level drug-class propositions, we now turn to the second mechanistic test.

Table 3.10: Directional sign of the one-sided two-sample KS test statistic when comparing the baseline $\ell_a = 1$ against each tested ℓ_a. "+" indicates the comparison is evaluated using Equation (3.13) and "−" means it is evaluated using Equation (3.12).

Drug Class	$\ell_a = 2$	$\ell_a = 3$	$\ell_a = 5$	$\ell_a = 8$	$\ell_a = 10$	$\ell_a = 15$
S_C	+	+	+	+	+	+
S_H	−	−	−	−	−	−
P_C	+	+	−	+	−	+
A_C	−	−	−	−	−	−
F_C	+	+	+	+	+	+
R_C	+	−	−	+	+	+

Table 3.11: P-values of the one-sided two-sample KS tests using significance level $\alpha = 0.05$ for comparisons of the baseline case $\ell_a = 1$ against each tested ℓ_a.

Drug Class	$\ell_a = 2$	$\ell_a = 3$	$\ell_a = 5$	$\ell_a = 8$	$\ell_a = 10$	$\ell_a = 15$
S_C	0.0556	0.0775	0.0775	0.2378	**0.0011**	0.1057
S_H	0.1057	**0.0270**	0.0556	0.2378	**0.0019**	0.0556
P_C	0.2993	0.5286	0.3691	0.2378	0.1057	0.6139
A_C	0.2993	0.3691	0.6988	**0.0031**	0.1057	0.4462
F_C	0.6139	0.2993	0.7797	0.1413	0.2378	0.9143
R_C	0.8528	0.9901	0.9901	0.7797	0.8528	0.6988

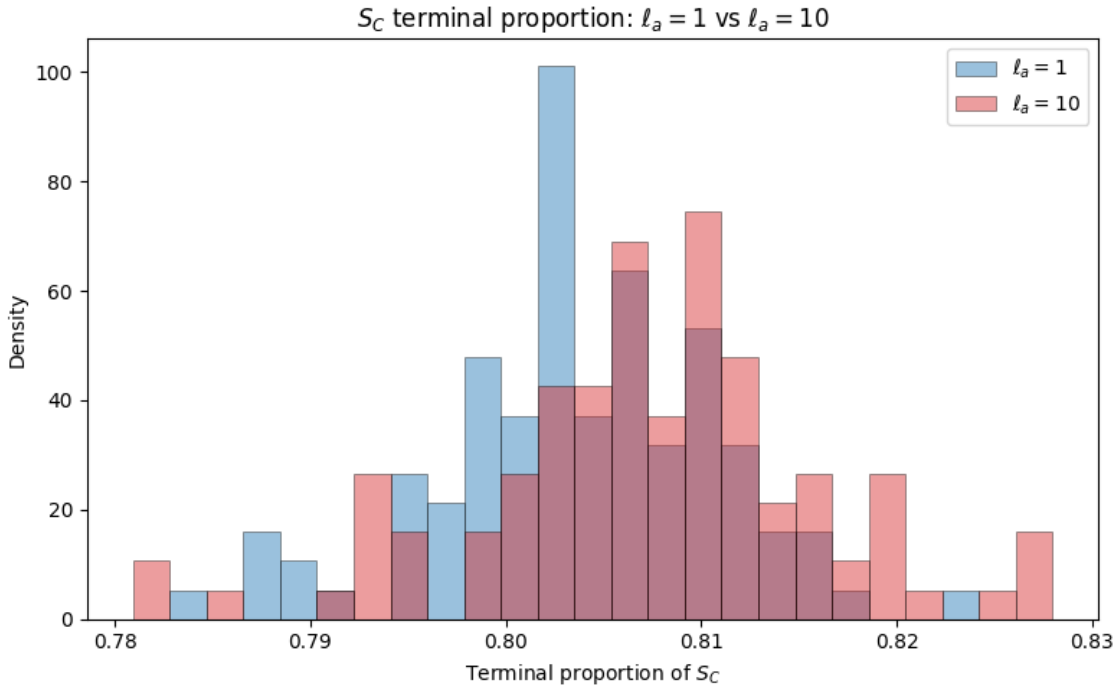

Figure 3.5: Overlapping histograms of the sampled outcomes. The values for $\ell_a = 10$ are stochastically larger than those of $\ell_a = 1$.

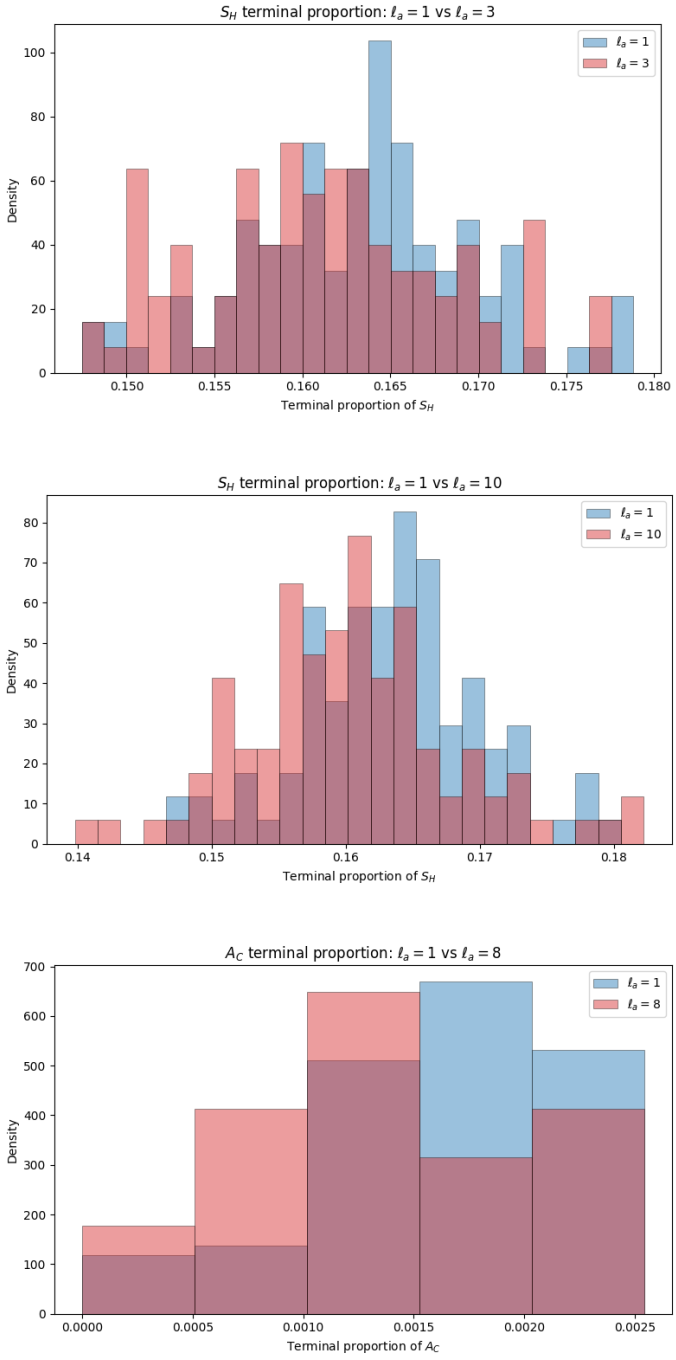

Figure 3.6: Overlapping histograms of the sampled outcomes for all outcomes that reject H_0 whenever $H_1 : F(x) < G(x)$ for some x.

3.3.2 Testing ℓ_i values

Recall that ℓ_i denotes the weight assigned to *strong* influential social ties when computing an individual's possibility of transitioning into an OUD class. We vary this single parameter $\ell_i \in \{1,2,3,5,8,10,15\}$, where $\ell_i = 1$ serves as the baseline case in which weak and strong connections contribute equally. For each value of ℓ_i, we perform 500 independent simulations and record the community drug proportions at the final observation time. The objective is to quantify how the distribution of these terminal proportions changes as ℓ_i increases.

As in the previous analysis, for each comparison of the tested ℓ_i against the baseline $\ell_i = 1$, we first determine which one-sided two-sample KS alternative is appropriate; the resulting direction assignments are summarized in Table 3.12. We then apply the corresponding one-sided two-sample KS test using `scipy.stats.ks_2samp` and report the resulting p-values from the returned `pvalue` in Table 3.13.

Three comparisons (S_C with $\ell_i = 5$, S_C with $\ell_i = 10$, and A_C with $\ell_i = 10$) reject H_0 under the one-sided alternative hypothesis $H_1 : F(x) > G(x)$ for some x. As seen in Figure 3.7, these tested cases ℓ_i result in terminal proportions shifted toward stochastically larger values relative to the baseline. Conversely, two comparisons (S_H with $\ell_i = 5$ and F_C with $\ell_i = 10$) reject H_0 under the opposite alternative hypothesis $H_1 : F(x) < G(x)$ for some x. This indicates that these test cases ℓ_i is stochastically shifted toward smaller values relative to the baseline $\ell_i = 1$, as seen in Figure 3.8.

3.4 Conclusion

In this chapter, we developed an individual-based model that adappted the class-transition mechanisms proposed by Eversman [1] and Pearcy [6]. In addition to the focal community structure, we introduced a second population partition, referred to as *clusters*, to capture intersectionality within the population. Each community and cluster was assigned

Table 3.12: Directional sign of the one-sided two-sample KS test statistic when comparing the baseline $\ell_i = 1$ against each tested ℓ_i. "+" indicates the comparison is evaluated using Equation (3.13) and "−" means it is evaluated using Equation (3.12).

Drug Class	$\ell_i = 2$	$\ell_i = 3$	$\ell_i = 5$	$\ell_i = 8$	$\ell_i = 10$	$\ell_i = 15$
S_C	+	+	+	+	+	+
S_H	−	−	−	−	−	−
P_C	+	+	−	−	−	+
A_C	+	+	+	+	+	+
F_C	−	−	−	−	−	−
R_C	+	−	−	−	−	−

Table 3.13: P-values of the one-sided two-sample KS tests using significance level $\alpha = 0.05$ for comparisons of the baseline case $\ell_i = 1$ against each tested ℓ_i.

Drug Class	$\ell_i = 2$	$\ell_i = 3$	$\ell_i = 5$	$\ell_i = 8$	$\ell_i = 10$	$\ell_i = 15$
S_C	0.0863	0.2086	**0.0347**	0.3801	**0.0293**	0.2867
S_H	0.0647	0.1291	**0.0477**	0.2086	0.0647	0.1654
P_C	0.1654	0.4142	0.5996	0.4860	0.4860	0.3801
A_C	0.7500	0.2329	0.2589	0.3801	**0.0248**	0.0863
F_C	0.5613	0.6759	0.5996	0.4860	**0.0293**	0.5613
R_C	0.8800	0.9513	0.1464	0.6759	0.9822	0.2589

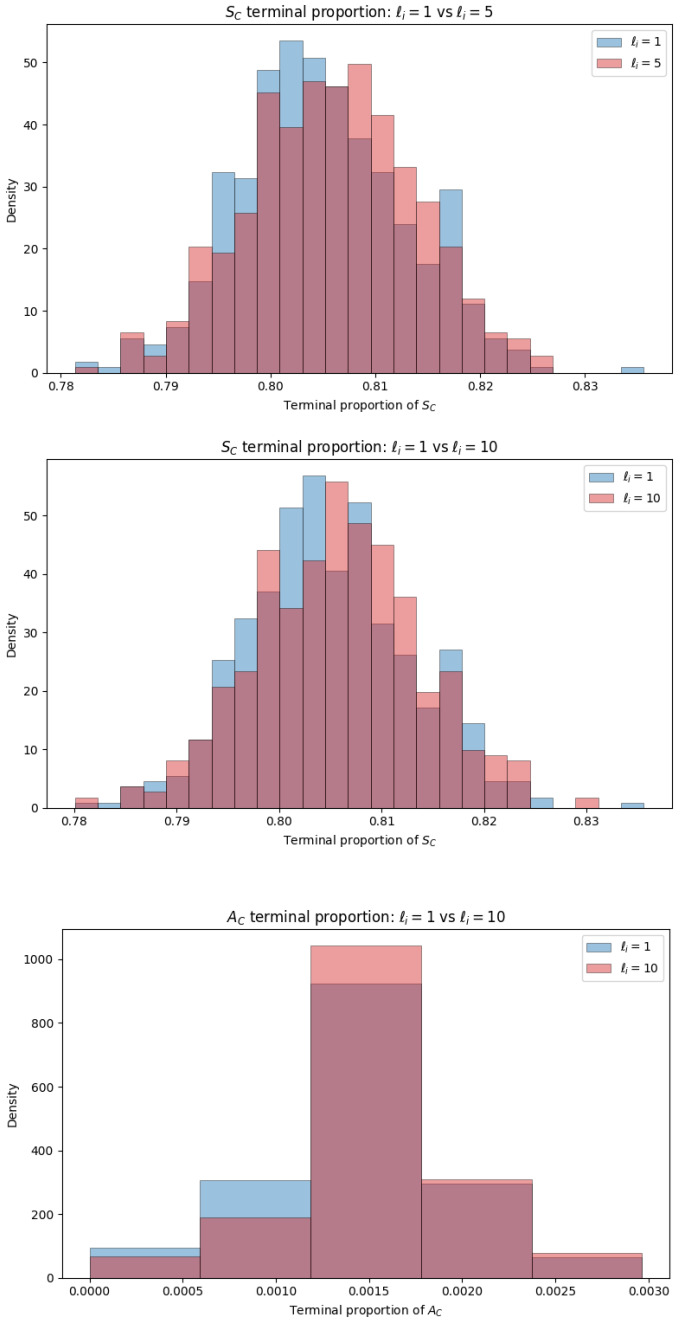

Figure 3.7: Overlapping histograms of the sampled outcomes for all outcomes that reject H_0 whenever $H_1 : F(x) > G(x)$ for some x.

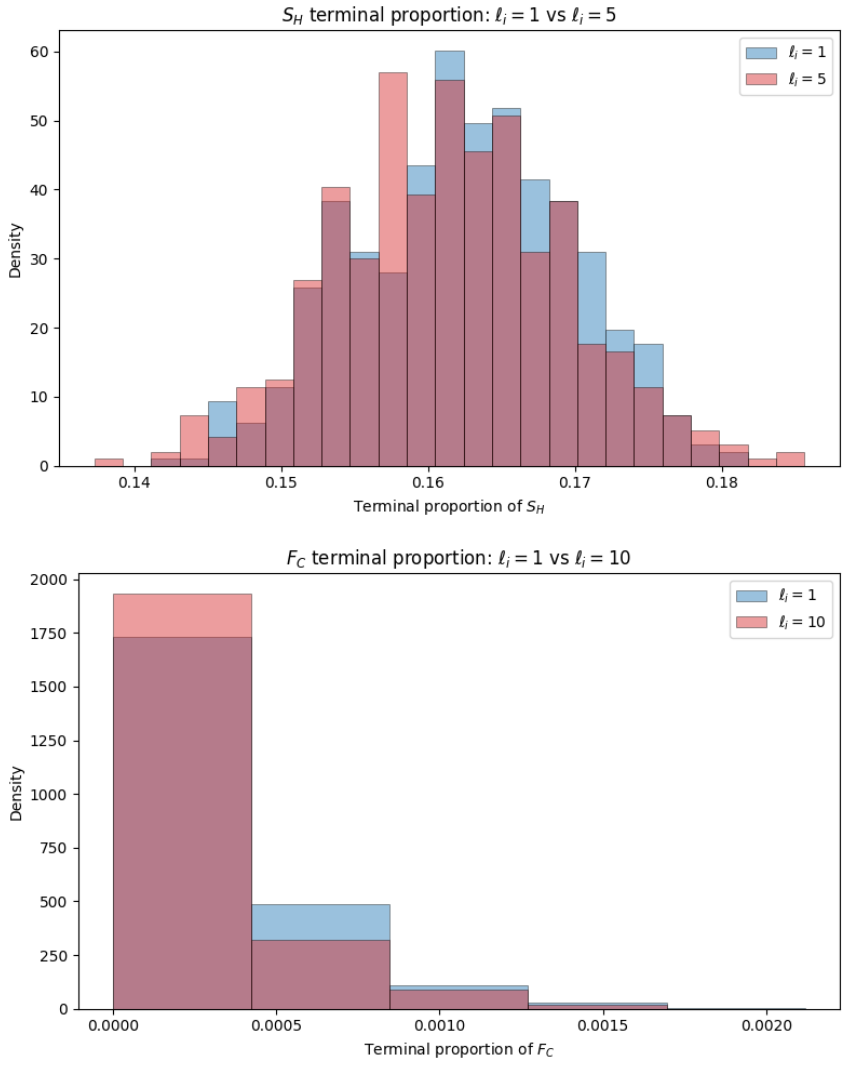

Figure 3.8: Overlapping histograms of the sampled outcomes for all outcomes that reject H_0 whenever $H_1 : F(x) < G(x)$ for some x.

a segregation level, which parametrized the degree of social isolation experienced by that subgroup and thereby shaped the frequency and makeup of potential social contacts.

The model allowed individuals to transition between drug classes and allowed dyads to form or sever social connections. Importantly, the model permitted OUD development among isolated individuals as well as among sociable individuals with OUD neighbors, thereby allowing for social exposure and isolation as pathways into OUD. We determined the parameter values for the out-community from the population and community data reported by Eversman [1], while most of the remaining parameters were estimated from the literature.

We then studied two mechanisms by which individual-level social structure could influence population-level class proportions: (i) increasing the strength of preference for individuals forming connections with same drug classes and (ii) increasing the weight assigned to highly influential connections when computing the probability of transition into an OUD class. In both investigations, we found that amplifying these effects could shift the terminal proportions in the susceptible and OUD classes. At the same time, among the cases that did exhibit measurable differences, the changes were not uniformly "beneficial" from a public-health perspective (e.g., some modifications had a decreased likelihood of terminal susceptible proportion or increased likelihood of OUD proportion). Moreover, the majority of parameter variations did not yield changes large enough to be distinguished from the baseline simulation output. These observations indicated that while network-level effects could be consequential, they were highly context dependent. Further calibration and validation are required before the model can be used reliably for intervention assessment.

Future work could include applying the model to additional locations and time periods, particularly high-risk settings for OUD progression. Given major changes in data collection and the evolving nature of the opioid crisis since 2020, an important next step would also be to recalibrate and evaluate the model using more recent data. Moreover, a natural extension is to incorporate individual-specific data, allowing the model to assign person-specific parameter values instead of relying solely on population averaged estimates.

Bibliography

[1] Kimberlyn Eversman. *Modeling the Opioid Epidemic in Vulnerable Subpopulations and a Multiscale Mixed Modeling Approach to Parasitoid Wasp Dispersal with Host Interaction*. PhD diss., University of Tennessee, Knoxville, 2025. ix, x, xii, 126, 127, 129, 130, 131, 133, 134, 135, 137, 142, 154, 155, 156, 157, 160, 172, 176

[2] Courtney A. Polenick, Brandi Parker Cotton, William C. Bryson, and Kira S. Birditt. Loneliness and illicit opioid use among methadone maintenance treatment patients. *Substance Use & Misuse*, page 2089–2098, 2019. x, 162, 164

[3] Chandreyee Roy, Kunal Bhattacharya, Robin I. M. Dunbar, and Kimmo Kaski. Turnover in close friendships. *Scientific Reports*, June 2022. x, 163, 164

[4] C. Loverdo, O. Bénichou, M. Moreau, and R. Voituriez. Robustness of optimal intermittent search strategies in one, two, and three dimensions. *Physical Review E*, 80, September 2009. xi, xii, 5, 6, 8, 10, 12, 13, 46, 47, 48, 56, 72, 73, 74, 77, 102, 104, 111, 116

[5] Tricia Phillips, Suzanne Lenhart, and W. Christopher Strickland. A data-driven mathematical model of the heroin and fentanyl epidemic in tennessee. *Bulletin of Mathematical Biology*, 83:1–27, 2021. xii, 122, 123, 124, 125, 126, 129, 131

[6] Leigh Pearcy. *Modeling Substance Use Disorder using Deterministic and Stochastic Approaches and A Bayesian Model of Sudden Death*. PhD diss., University of Tennessee, Knoxville, 2023. xii, 124, 131, 132, 133, 134, 142, 143, 172

[7] Richard P Heitz. The speed-accuracy tradeoff: history, physiology, methodology, and behavior. *Frontiers in Neuroscience*, 8, June 2014. 2

[8] M. Chupeau, O. Bénichou, and S. Redner. Search in patchy media: Exploitation-exploration tradeoff. *Physical Review E*, 95, 2017. 2

[9] Henri Weimerskirch, André Ancel, Michel Caloin, Alexandre Zahariev, Jérôme Spagiari, Marcel Kersten, and Olivier Chastel. Foraging efficiency and adjustment of energy expenditure in a pelagic seabird provisioning its chick. *Journal of Animal Ecology*, 72:500–508, May 2003. 2

[10] Karl Pearson. The problem of the random walk. *Nature*, 72:294, July 1905. 2

[11] G. M. Viswanathan, V. Afanasyevt, S. V. Buldyrev, E. J. Murphy, P.A. Prince, and H. E. Stanley. Lévy flight search patterns of wandering albatrosses. *Nature*, May 1996. 3

[12] G. M. Viswanathan, Sergey V. Buldyrev, Shlomo Havlin, M. G. E. da Luzk, E. P. Raposok, and H. Eugene Stanley. Optimizing the success of random searches. *Nature*, October 1999. 3

[13] Gabriel Ramos-Fernández, José L. Mateos, Octavio Miramontes, Germinal Cocho, Hernán Larralde, and Bárbara Ayala-Orozco. Lévy walk patterns in the foraging movements of spider monkeys (ateles geoffroyi). *Behavioral Ecology and Sociobiology*, 2004. 3

[14] David A. Raichlen, Brian M. Wood, Adam D. Gordon, Audax Z. P. Mabullad, Frank W. Marlowe, and Herman Pontzer. Evidence of lévy walk foraging patterns in human hunter–gatherers. *PNAS*, page 728–733, January 2014. 3

[15] Vladimir V. Palyulin, Aleksei V. Chechkin, and Ralf Metzler. Lévy flights do not always optimize random blind search for sparse targets. *Biophysics and Computational Biology*, 111:2931–2936, February 2014. 3

[16] Andrew M. Edwards, Richard A. Phillips, Nicholas W. Watkins, Mervyn P. Freeman, Eugene J. Murphy, Vsevolod Afanasyev, Sergey V. Buldyrev, M. G. E. da Luz, E. P. Raposo, H. Eugene Stanley, and Gandhimohan M. Viswanathan. Revisiting lévy flight search patterns of wandering albatrosses, bumblebees and deer. *Nature*, 449(7165):1044–1048, 2007. 3

[17] Monique de Jager, Frederic Bartumeus, Andrea Kölzsch, Franz J. Weissing, Geerten M. Hengeveld, Bart A. Nolet, Peter M. J. Herman, and Johan van de Koppel. How superdiffusion gets arrested: ecological encounters explain shift from lévy to brownian movement. *Proceedings of the Royal Society B: Biological Sciences*, 281, January 2014. 3

[18] John Ellis, Natalia Petrovskaya, and Sergei Petrovskii. Effect of density-dependent individual movement on emerging spatial population distribution: Brownian motion vs levy flights. *Journal of Theoretical Biology*, 464:159–178, 2019. 3

[19] O. Bénichou, M. Coppey, M. Moreau, P.H. Suet, and R. Voituriez. A stochastic model for intermittent search strategies. *Journal of Physics: Condensed Matter*, 17(49), November 2005. 3

[20] O. Bénichou, C. Loverdo, M. Moreau, and R. Voituriez. Intermittent search strategies. *Rev. Mod. Phys.*, 83:81–129, Mar 2011. 3, 4, 14, 19, 43, 46, 50

[21] O. Bénichou, C. Loverdo, M. Moreau, and R. Voituriez. A minimal model of intermittent search in dimension two. *Journal of Physics: Condensed Matter*, 19(6), Jan 2007. 9, 48, 49, 86

[22] C.W. Gardiner. *Handbook of Stochastic Methods for Physics, Chemistry and the Natural Sciences*. Springer-Verlag, 1985. 17

[23] Sidney Redner. *A Guide to First-Passage Processes*. Cambridge University Press, 2001. 17

[24] O. Bénichou, C. Loverdo, M. Moreau, and R. Voituriez. Two-dimensional intermittent search processes: An alternative to lévy flight strategies. *Physical Review E*, 74, August 2006. 22

[25] U.S. Centers for Disease Control and Prevention, Overdose Prevention. Understanding the opioid overdose epidemic. https://www.cdc.gov/overdose-prevention/about/understanding-the-opioid-overdose-epidemic.html, June 2025. Accessed on April 29, 2026. 119, 120

[26] Administration for Strategic Preparedness and Response (ASPR), U.S. Department of Health and Human Services (HHS). Renewal of determination that a public health emergency exists. https://aspr.hhs.gov/legal/PHE/Pages/opioids.aspx, 2017. Accessed on April 29, 2026. 119

[27] Administration for Strategic Preparedness and Response (ASPR), U.S. Department of Health and Human Services (HHS). Renewal of determination that a public health emergency exists. https://aspr.hhs.gov/legal/PHE/Pages/Opioid-Renewal-16Mar2026.aspx, March 2026. Accessed on April 29, 2026. 119

[28] Leonard J. Paulozzi, Christopher M. Jones, Karin A. Mack, and Rose A. Rudd. Vital signs: overdoses of prescription opioid pain relievers—united states, 1999–2008. *Morbidity and Mortality Weekly Report (MMWR)*, 60:1487–1492, November 2011. 119

[29] Abby E. Alpert, William N. Evans, Ethan M. J. Lieber, and David Powell. Origins of the opioid crisis and its enduring impacts. Working Paper 26500, National Bureau of Economic Research, 2019. Accessed on April 29, 2026. 119

[30] William N. Evans, Ethan Lieber, and Patrick Power. How the reformulation of oxycontin ignited the heroin epidemic. Technical Report Working Paper No. 24475, National Bureau of Economic Research, April 2018. 119, 120

[31] U.S. Government Accountability Office. Oxycontin abuse and diversion and efforts to address the problem. Technical Report GAO-03-620, U.S. Government Accountability Office, December 2003. Accessed on April 29, 2026. 119

[32] Art V. Zee. The promotion and marketing of oxycontin: Commercial triumph, public health tragedy. *American Journal of Public Health*, 99:221–227, February 2009. Accessed on April 29, 2026. 119

[33] National Institute on Drug Abuse. Drug overdose deaths: Facts and figures. https://nida.nih.gov/research-topics/trends-statistics/overdose-death-rates, August 2024. Accessed on April 29, 2026. 119

[34] Congressional Research Service. The opioid crisis in the united states: A brief history. In focus, Congressional Research Service, December 2022. 120

[35] Daniel C. Beachler, Kelsey Hall, Renu Garg, Geetanjoli Banerjee, Ling Li, Luke Boulanger, Huseyin Yuce, and Alexander M. Walker. An evaluation of the effect of the oxycontin feformulation on unintentional fatal and nonfatal overdose. *Clinical Journal of Pain*, 38:396–404, June 2022. 120

[36] Theodore J. Cicero, Matthew S. Ellis, Hilary L. Surratt, and Steven P. Kurtz. The changing face of heroin use in the united states: A retrospective analysis of the past 50 years. *JAMA Psychiatry*, 71, July 2014. 120

[37] Richard C. Dart, Hilary L. Surratt, Theodore J. Cicero, Mark W. Parrino, S. Geoff Severtson, Becki Bucher-Bartelson, and Jody L. Green. Trends in opioid analgesic abuse and mortality in the united states. *The New England Jounral of Medicine*, 372, January 2015. 120

[38] U.S. Centers for Disease Control and Prevention. Quickstats: Rates of deaths from drug poisoning and drug poisoning involving opioid analgesics — united states, 1999–2013. *Morbidity and Mortality Weekly Report (MMWR)*, January 2015. 120

[39] Drug Enforcement Administration. National heroin threat assessment summary. Technical report, U.S. Department of Justice, Drug Enforcement Administration, April 2015. Accessed on April 29, 2026. 120

[40] Daniel Ciccarone. The triple wave epidemic: Supply and demand drivers of the us opioid overdose crisis. *International Journal of Drug Policy*, 71:183–188, September 2019. 120

[41] Drug Enforcement Administration. Synthetic opioids. Technical report, U.S. Department of Justice, Drug Enforcement Administration, April 2020. Accessed on April 29, 2026. 120

[42] U.S. Centers for Disease Control and Prevention. Fentanyl facts, April 2024. Accessed on April 29, 2026. 120

[43] U.S. Drug Enforcement Administration. Facts about fentanyl. Accessed on April 29, 2026. 120

[44] Sarah G. Mars, Daniel Rosenblum, and Daniel Ciccarone. Illicit fentanyls in the opioid street market: desired or imposed? *Addiction*, 114:774–780, May 2019. 120

[45] Mary Jeanne Kreek, Lisa Borg, Elizabeth Ducat, and Brenda Ray. Pharmacotherapy in the treatment of addiction: methadone. *Journal of Addictive Diseases*, 29:200–216, April 2010. 120

[46] National Center for Health Sciences, U.S. Centers for Disease Control and Prevention. Age adjustment. https://www.cdc.gov/nchs/hus/sources-definitions/age-adjustment.htm, December 2024. Accessed on April 29, 2026. 120

[47] Matthew F. Garnett and Arialdi M. Miniño. Drug overdose deaths in the united states, 2003-2023. Technical report, National Center for Health Statistics, U.S. Department of Health and Human Services, December 2024. Accessed on April 29, 2026. 120

[48] Emma White and Catherine Comiskey. Heroin epidemics, treatment and ode modeling. *Mathematical Biosciences*, 208:312–324, 2007. 121

[49] Magdalena Cerdá, Mohammad S. Jalali, Ava D. Hamilton, Catherine DiGennaro, Ayaz Hyder, Julian Santaella-Tenorio, Navdep Kaur, Christina Wang, and Katherine M. Keyes. A systematic review of simulation models to track and address the opioid crisis. *Epidemiologic Reviews*, 43:147–165, November 2021. 121, 124

[50] Junli Liu and Tailei Zhang. Global behaviour of a heroin epidemic model with distributed delays. *Applied Mathematics Letters*, 24:1685–1692, October 2011. 121

[51] American Psychiatric Association. *Diagnostic and Statistical Manual of Mental Disorders: DSM-5-TR*. American Psychiatric Association Publishing, Washington, DC, 5th, text revision edition, 2022. 121

[52] Nicholas A. Battista, Leigh B. Pearcy, and W. Christopher Strickland. Modeling the prescription opioid epidemic. *Bulletin of Mathematical Biology*, 81:2258–2289, April 2019. 121

[53] Sandra Cole and Stephen Wirkus. Modeling the dynamics of heroin and illicit opioid use disorder, treatment, and recovery. *Bulletin of Mathematical Biology*, 84, March 2022. 122

[54] Yan Li, Mark A. Lawley, David S. Siscovick, Donglan Zhang, and José A. Pagán. Agent-based modeling of chronic diseases: a narrative review and future research directions. *Preventing Chronic Disease, U.S. Centers for Disease Control and Prevention*, 13, May 2016. 124

[55] Masaki Yuki, Joanna Schug, Hiroshi Horikawa, Kosuke Takemura, Kaori Sato, Kazuhiro Yokota, and Koichi Kamaya. Development of a scale to measure

perceptions of relational mobility in society. Center for Experimental Research in Social Sciences (CERSS) Working Paper 75, Hokkaido University, Center for Experimental Research in Social Sciences, December 2007. 132

[56] Liman Man Wai Li, Shengyuan Wang, and Ying Lin. The casual effect of relational mobility on integration of social networks: an agent-based modeling approach. *Current Psychology*, 42:21900–21916, June 2022. 132

[57] Robert H. Gass. Social influence, sociology of. In James D. Wright, editor, *International Encyclopedia of the Social & Behavioral Sciences (Second Edition)*, pages 348–354. Elsevier, 2015. 132

[58] Mathijs de Vaana and Toby Stuart. Does intra-household contagion cause an increase in prescription opioid use? *American Sociological Review*, 84:577–608, 2019. 132

[59] Shoshana Eitan, Michael A. Emery, M. L. Shawn Bates, and Christopher Horrax. Opioid addiction: Who are your real friends? *Neuroscience and Biobehavioral Reviews*, 83:697–712, December 2017. 132

[60] Mohammad S. Jalali, Michael Botticelli, Rachael C. Hwang, Howard K. Koh, and R. Kathryn McHugh. The opioid crisis: a contextual, social-ecological framework. *Health Research Policy and Systems*, 18, August 2020. 132

[61] Nina C. Christie. The role of social isolation in opioid addiction. *Social Cognitive and Affective Neuroscience*, 16:645–656, July 2021. 132

[62] Tse-Chuan Yang, Carla Shoff, Seulki Kim, and Benjamin A. Shaw. County social isolation and opioid use disorder among older adults: A longitudinal analysis of medicare data, 2013-2018. *Social Science and Medicine*, 301, May 2022. 132

[63] Guro Løseth, Marie Eikemo, and Siri Leknes. Opioid regulation of social homeostasis: Connecting loneliness to addiction. *Bioligical Psychiatry*, 97:971–981, May 2025. 132

[64] P. Erdös and A. Rényi. On random graphs. i. *Publicationes Mathematicae*, page 290–297, 1959. 138

[65] M. E. J. Newman, D. J. Watts, and S. H. Strogatz. Random graph models of social networks. *Proceedings of the National Academy of Sciences*, 99:2566–2572, 2002. 138

[66] Lisham Ashrafioun, Nicholas P. Allan, and Tracy A. Stecker. Opioid use disorder and its association with self-reported difficulties participating in social activities. *American Journal on Addictions*, Jan 2022. 161

[67] E. L. Lehmann and Joseph P. Romano. *Testing Statistical Hypotheses*. Springer, 3rd edition, 2005. 166

[68] Myles Hollander, Douglas A. Wolfe, and Eric Chicken. *Nonparametric statistical methods*. Wiley, 3rd edition, 2013. 166

[69] Richard Hamming. *Numerical Methods for Scientists and Engineers*. Dover Publications, 1973. 191

[70] M. Abramowitz and I. A. Stegun. *Handbook of Mathematical Functions with Formulas, Graphs, and Mathematical Tables*. Dover, New York, June 1964. 195

Appendix

A Appendices for Chapter 1

A.1 Further Details on the Solutions for Chapter 1.4.1

In this section, we demonstrate that all expressions appearing in the denominators of the solutions for the three-dimensional arbitrarily-distributed velocities model are strictly nonzero. Firstly, we assume that the search process occurs whenever the target is *not* on top of the target. As such, we assume $r > 0$. Now, the parameters K, τ_D, and τ_M are all positive real numbers and the lengths a and b are ordered to satisfy $0 < a < b$. Additionally, because $V > 0$ for $V \in [R_1, R_2]$ for $0 < R_1 < R_2$, we know that $\mathbb{E}\left[V^2\right] > 0$. We have one remaining term.

We claim $-\sinh\alpha + \alpha\cosh\alpha > 0$ when

$$\alpha = a\sqrt{\frac{3K\tau_D}{\mathbb{E}\left[V^2\right]\tau_M^2(1+K\tau_D)}}.$$

We see that $\alpha > 0$. Then

$$-\sinh\alpha + \alpha\cosh\alpha = (-\tanh\alpha + \alpha)\cosh\alpha = h(\alpha)\cosh\alpha.$$

Since $\cosh\alpha > 0$ for every α, we must determine the sign of h. Considering the derivative

$$h'(\alpha) = -\operatorname{sech}^2\alpha + 1 = \tanh^2\alpha > 0$$

for $\alpha > 0$, meaning that h is strictly increasing. Since $h(0) = 0$, we know that $h(\alpha) > h(0) = 0$ for $\alpha > 0$. Therefore, we have proven that no expressions in denominators are zero.

In this section, we verify that every term appearing in the denominators of the solutions for the three-dimensional model with arbitrarily distributed velocities is strictly nonzero. We assume the search process only occurs whenever the searcher is not at the target; hence, we assume $r > 0$. The parameters K, τ_D, and τ_M are taken to be strictly positive. Moreover, since $V \in [R_1, R_2]$ with $0 < R_1 < R_2$ so that $V > 0$, we have $\mathbb{E}\left[V^2\right] > 0$. We have one remaining term to consider.

We claim that $-\sinh\alpha + \alpha\cosh\alpha > 0$ whenever

$$\alpha = a\sqrt{\frac{3K\tau_D}{\mathbb{E}[V^2]\,\tau_M^2(1+K\tau_D)}}.$$

Under the assumptions above, $\alpha > 0$. Then

$$-\sinh\alpha + \alpha\cosh\alpha = (-\tanh\alpha + \alpha)\cosh\alpha = h(\alpha)\cosh\alpha.$$

Since $\cosh\alpha > 0$ for every α, we must show that $h(\alpha) > 0$ for $\alpha > 0$. Taking the derivative yields

$$h'(\alpha) = -\operatorname{sech}^2\alpha + 1 = \tanh^2\alpha > 0$$

for $\alpha > 0$ so that h is strictly increasing on $(0,\infty)$. Because $h(0) = 0$, we know that $h(\alpha) > 0$ for $\alpha > 0$.

Therefore, we have proven that no expressions in denominators are zero.

B Appendices for Chapter 2

B.1 Further Details on the Solutions for Chapter 2.2.1

In this section, we demonstrate that all expressions appearing in the denominators of the solutions for the one-dimensional second detection zone model are strictly nonzero. We assume that the parameters D, V, K, τ_D, and τ_M are all positive real numbers and that the lengths a, b, and c are ordered to satisfy $0 < a < c < b$. This assumption immediately yields that

$$\varphi = \sqrt{\frac{D\tau_D + V^2\tau_M^2}{D\tau_D V^2\tau_M^2}} > 0,$$

and

$$\begin{aligned}\phi_+ &= \sqrt{\frac{D\tau_D + V^2\tau_M^2 + K\tau_D V^2\tau_M^2 + \sqrt{\begin{array}{c}V^4\tau_M^4 + 2D\tau_D V^2\tau_M^2 + 2K\tau_D V^4\tau_M^4 \\ +(D - KV^2\tau_M^2)^2\tau_D^2\end{array}}}{2D\tau_D V^2\tau_M^2}} \\ &\geq \sqrt{\frac{D\tau_D + V^2\tau_M^2 + K\tau_D V^2\tau_M^2}{2D\tau_D V^2\tau_M^2}} \\ &> 0,\end{aligned}$$

and

$$\begin{aligned}\phi_- &= \sqrt{\frac{D\tau_D + V^2\tau_M^2 + K\tau_D V^2\tau_M^2 - \sqrt{\begin{array}{c}V^4\tau_M^4 + 2D\tau_D V^2\tau_M^2 + 2K\tau_D V^4\tau_M^4 \\ +(D - KV^2\tau_M^2)^2\tau_D^2\end{array}}}{2D\tau_D V^2\tau_M^2}} \\ &= \sqrt{\frac{D\tau_D + V^2\tau_M^2 + K\tau_D V^2\tau_M^2 - \sqrt{\left(D\tau_D + V^2\tau_M^2 + K\tau_D V^2\tau_M^2\right)^2 - 4KD\tau_D^2 V^2\tau_M^2}}{2D\tau_D V^2\tau_M^2}} \\ &> \sqrt{\frac{D\tau_D + V^2\tau_M^2 + K\tau_D V^2\tau_M^2 - \sqrt{\left(D\tau_D + V^2\tau_M^2 + K\tau_D V^2\tau_M^2\right)^2}}{2D\tau_D V^2\tau_M^2}} \\ &= 0.\end{aligned}$$

Furthermore, by definition, the inequality $\phi_+^2 - \phi_-^2 > 0$ holds. Thus, the only remaining requirements are to confirm that L and $\mathscr{D}$ are nonzero.

Proposition .1. $L \neq 0$.

Proof. We begin by considering

$$L = \left(K\tau_D - D\tau_D\phi_-^2\right)\cosh\left(\phi_+(c-a)\right) - \left(K\tau_D - D\tau_D\phi_+^2\right)\cosh\left(\phi_-(c-a)\right).$$

Since $\cosh(x) > 0$ for all real x, we focus on determining the signs of the coefficients preceding each hyperbolic cosine term. First, we observe that $K\tau_D - D\tau_D\phi_-^2 > 0$, as demonstrated as follows:

$$-4K\tau_D V^4\tau_M^4 < 0$$

$$\left(D\tau_D + V^2\tau_M^2 - K\tau_D V^2\tau_M^2\right)^2 < V^4\tau_M^4 + 2D\tau_D V^2\tau_M^2 + 2K\tau_D V^4\tau_M^4 + (D - KV^2\tau_M^2)^2\tau_D^2$$

$$-\frac{D\tau_D + V^2\tau_M^2 - K\tau_D V^2\tau_M^2 - \sqrt{\begin{array}{c} V^4\tau_M^4 + 2D\tau_D V^2\tau_M^2 + 2K\tau_D V^4\tau_M^4 \\ +(D - KV^2\tau_M^2)^2\tau_D^2 \end{array}}}{2V^2\tau_M^2} > 0$$

$$K\tau_D - D\tau_D\phi_-^2 > 0$$

Next, we analyze the sign of $K\tau_D - D\tau_D\phi_+^2$. We establish the following inequality:

$$K\tau_D - D\tau_D\phi_+^2 = \frac{-D\tau_D - V^2\tau_M^2 + K\tau_D V^2\tau_M^2 - \sqrt{\begin{array}{c} V^4\tau_M^4 + 2D\tau_D V^2\tau_M^2 + 2K\tau_D V^4\tau_M^4 \\ +(D - KV^2\tau_M^2)^2\tau_D^2 \end{array}}}{2V^2\tau_M^2}$$

$$< \frac{-V^2\tau_M^2 - \left(D - KV^2\tau_M^2\right)\tau_D - \left|D - KV^2\tau_M^2\right|\tau_D}{2V^2\tau_M^2}.$$

If $D \geq KV^2\tau_M^2$, then

$$-V^2\tau_M^2 - \left(D - KV^2\tau_M^2\right)\tau_D - \left|D - KV^2\tau_M^2\right|\tau_D = -V^2\tau_M^2 - 2\left(D - KV^2\tau_M^2\right)\tau_D < 0.$$

Otherwise, if $D < KV^2\tau_M^2$, then

$$-V^2\tau_M^2 - \left(D - KV^2\tau_M^2\right)\tau_D - \left|D - KV^2\tau_M^2\right|\tau_D = V^2\tau_M^2 < 0.$$

In either case, we conclude that $K\tau_D - D\tau_D\phi_+^2 < 0$. Therefore,

$$L = \left(K\tau_D - D\tau_D\phi_-^2\right)\cosh\left(\phi_+(c-a)\right) - \left(K\tau_D - D\tau_D\phi_+^2\right)\cosh\left(\phi_-(c-a)\right) > 0,$$

meaning that we have proven $L \neq 0$. □

Proposition .2. $\mathscr{D} \neq 0$.

Proof. Assume by way of contradiction that $\mathscr{D} = 0$. We observe that $\mathscr{D}$ is written as a linear combination of hyperbolic sine and cosine functions evaluated at $\varphi(b-c)$. Using the identities

$$\cosh(\alpha) = \frac{e^{\alpha} + e^{-\alpha}}{2} \qquad \text{and} \qquad \sinh(\alpha) = \frac{e^{\alpha} - e^{-\alpha}}{2},$$

we can rewrite $\mathscr{D}$ as a linear combination of the distinct set $\left\{e^{-\varphi(b-c)}, e^{\varphi(b-c)}\right\}$:

$$\begin{aligned}\mathscr{D} = &\left(A_1 + D^2\tau_D^2\phi_+\phi_-\varphi\left(\phi_+^2 - \phi_-^2\right)A_2\right)e^{\varphi(b-c)} \\ &- \left(A_1 - D^2\tau_D^2\phi_+\phi_-\varphi\left(\phi_+^2 - \phi_-^2\right)A_2\right)e^{-\varphi(b-c)},\end{aligned}$$

where

$$\begin{aligned}A_1 = \phi_+\phi_-&\begin{pmatrix}\left(K\tau_D - D\tau_D\phi_+^2\right)\left(1 + K\tau_D - D\tau_D\phi_-^2\right)\left(K\tau_D + D\tau_D(\varphi^2 - \phi_+^2)\right) \\ + \left(K\tau_D - D\tau_D\phi_-^2\right)\left(1 + K\tau_D - D\tau_D\phi_+^2\right)\left(K\tau_D + D\tau_D(\varphi^2 - \phi_-^2)\right)\end{pmatrix} \\ &+ \phi_-^2\left(K\tau_D - D\tau_D\phi_+^2\right)\left(1 + K\tau_D - D\tau_D\phi_-^2\right) \\ &\qquad \cdot \left(K\tau_D + D\tau_D(\varphi^2 - \phi_-^2)\right)\sinh(\phi_-(c-a))\sinh(\phi_+(c-a)) \\ &+ \phi_+^2\left(K\tau_D - D\tau_D\phi_-^2\right)\left(1 + K\tau_D - D\tau_D\phi_+^2\right) \\ &\qquad \cdot \left(K\tau_D + D\tau_D(\varphi^2 - \phi_+^2)\right)\sinh(\phi_-(c-a))\sinh(\phi_+(c-a)) \\ &- \phi_+\phi_-\left(K\tau_D - D\tau_D\phi_+^2\right)\left(1 + K\tau_D - D\tau_D\phi_+^2\right) \\ &\qquad \cdot \left(K\tau_D + D\tau_D(\varphi^2 - \phi_-^2)\right)\cosh(\phi_-(c-a))\cosh(\phi_+(c-a)) \\ &- \phi_+\phi_-\left(K\tau_D - D\tau_D\phi_-^2\right)\left(1 + K\tau_D - D\tau_D\phi_-^2\right) \\ &\qquad \cdot \left(K\tau_D + D\tau_D(\varphi^2 - \phi_+^2)\right)\cosh(\phi_-(c-a))\cosh(\phi_+(c-a)) \\ &+ \frac{D\tau_D}{V\tau_M}\phi_-\left(\phi_+^2 - \phi_-^2\right)\tanh\left(\frac{a}{V\tau_M}\right)\left(K\tau_D - D\tau_D\phi_+^2\right) \\ &\qquad \cdot \left(K\tau_D + D\tau_D(\varphi^2 - \phi_-^2)\right)\cosh(\phi_-(c-a))\sinh(\phi_+(c-a)) \\ &- \frac{D\tau_D}{V\tau_M}\phi_+\left(\phi_+^2 - \phi_-^2\right)\tanh\left(\frac{a}{V\tau_M}\right)\left(K\tau_D - D\tau_D\phi_-^2\right) \\ &\qquad \cdot \left(K\tau_D + D\tau_D(\varphi^2 - \phi_+^2)\right)\sinh(\phi_-(c-a))\cosh(\phi_+(c-a))\end{aligned}$$

and

$$A_2 = \begin{pmatrix} \phi_+\left(1+K\tau_D - D\tau_D\phi_+^2\right)\cosh\left(\phi_-(c-a)\right)\sinh\left(\phi_+(c-a)\right) \\ -\phi_-\left(1+K\tau_D - D\tau_D\phi_-^2\right)\sinh\left(\phi_-(c-a)\right)\cosh\left(\phi_+(c-a)\right) \\ -\dfrac{D\tau_D}{V\tau_M}\left(\phi_+^2-\phi_-^2\right)\tanh\left(\dfrac{a}{V\tau_M}\right)\cosh\left(\phi_-(c-a)\right)\cosh\left(\phi_+(c-a)\right) \end{pmatrix}.$$

Since the distinct set of exponential functions is linearly independent [69, Chapter 39.2], $\mathscr{D}$ can only be zero whenever each coefficient is zero. In particular,

$$A_1 + D^2\tau_D^2\phi_+\phi_-\varphi\left(\phi_+^2-\phi_-^2\right)A_2 = 0 \rightarrow A_1 = -D^2\tau_D^2\phi_+\phi_-\varphi\left(\phi_+^2-\phi_-^2\right)A_2$$

and

$$A_1 - D^2\tau_D^2\phi_+\phi_-\varphi\left(\phi_+^2-\phi_-^2\right)A_2 = 0 \rightarrow A_1 = D^2\tau_D^2\phi_+\phi_-\varphi\left(\phi_+^2-\phi_-^2\right)A_2$$

so that

$$D^2\tau_D^2\phi_+\phi_-\varphi\left(\phi_+^2-\phi_-^2\right)A_2 = -D^2\tau_D^2\phi_+\phi_-\varphi\left(\phi_+^2-\phi_-^2\right)A_2$$
$$2D^2\tau_D^2\phi_+\phi_-\varphi\left(\phi_+^2-\phi_-^2\right)A_2 = 0$$
$$A_2 = 0.$$

Since A_2 is a linear combination involving the hyperbolic sine and cosine functions evaluated at $\phi_+(c-a)$ and $\phi_-(c-a)$, we can rewrite A_2 as a linear combination of the following distinct set:

$$\left\{e^{(\phi_++\phi_-)(c-a)}, e^{(\phi_+-\phi_-)(c-a)}, e^{-(\phi_++\phi_-)(c-a)}, e^{-(\phi_+-\phi_-)(c-a)}\right\}.$$

Once again, since the set of distinct exponential functions is linearly independent, each coefficient must equal zero. We see that the coefficients of $e^{(\phi_++\phi_-)(c-a)}$ and $e^{(\phi_+-\phi_-)(c-a)}$

are

$$\begin{pmatrix} \phi_+\left(1+K\tau_D-D\tau_D\phi_+^2\right) \\ -\phi_-\left(1+K\tau_D-D\tau_D\phi_-^2\right) \\ -\dfrac{D\tau_D}{V\tau_M}\left(\phi_+^2-\phi_-^2\right)\tanh\left(\dfrac{a}{V\tau_M}\right) \end{pmatrix} \quad \text{and} \quad \begin{pmatrix} \phi_+\left(1+K\tau_D-D\tau_D\phi_+^2\right) \\ +\phi_-\left(1+K\tau_D-D\tau_D\phi_-^2\right) \\ -\dfrac{D\tau_D}{V\tau_M}\left(\phi_+^2-\phi_-^2\right)\tanh\left(\dfrac{a}{V\tau_M}\right) \end{pmatrix},$$

respectively. Since these coefficients must equal 0, this means

$$\phi_-\left(1+K\tau_D-D\tau_D\phi_-^2\right)=0.$$

However, this is impossible since $\phi_- > 0$ and $\left(1+K\tau_D-D\tau_D\phi_-^2\right) > 1 > 0$. Therefore, we have proven that $\mathscr{D} \neq 0$. □

We have shown that all terms in the denominator of the solutions are nonzero.

B.2 Further Details on the Solutions for Chapter 2.2.2

We plan to establish that all expressions in the denominators of all solutions for the two-dimensional second detection zone model are strictly nonzero. Recall that the parameters D, V, K, τ_D, and τ_M are all positive real numbers and that the inequalities $b > c > a > 0$ hold. This assumption directly implies the following:

$$\varphi = \sqrt{\frac{2D\tau_D+V^2\tau_M^2}{D\tau_D V^2\tau_M^2}} > 0$$

and

$$\begin{aligned}
\phi_- &= \sqrt{\frac{2D\tau_D + V^2\tau_M^2 + K\tau_D V^2\tau_M^2 - \sqrt{\begin{array}{c} V^2\tau_M^2\left(4D\tau_D + V^2\tau_M^2 + 2K\tau_D V^2\tau_M^2\right) \\ +\tau_D^2\left(2D - KV^2\tau_M^2\right)^2 \end{array}}}{2D\tau_D V^2\tau_M^2}} \\
&= \sqrt{\frac{2D\tau_D + V^2\tau_M^2 + K\tau_D V^2\tau_M^2 - \sqrt{\left(2D\tau_D + V^2\tau_M^2 + K\tau_D V^2\tau_M^2\right)^2 - 8KD\tau_S^2 V^2\tau_M^2}}{2D\tau_D V^2\tau_M^2}} \\
&> \sqrt{\frac{2D\tau_D + V^2\tau_M^2 + K\tau_D V^2\tau_M^2 - \sqrt{\left(2D\tau_D + V^2\tau_M^2 + K\tau_D V^2\tau_M^2\right)^2}}{2D\tau_D V^2\tau_M^2}} \\
&= 0
\end{aligned}$$

and

$$\begin{aligned}
\phi_+ &= \sqrt{\frac{2D\tau_D + V^2\tau_M^2 + K\tau_D V^2\tau_M^2 + \sqrt{\begin{array}{c} V^2\tau_M^2\left(4D\tau_D + V^2\tau_M^2 + 2K\tau_D V^2\tau_M^2\right) \\ +\tau_D^2\left(2D - KV^2\tau_M^2\right)^2 \end{array}}}{2D\tau_D V^2\tau_M^2}} \\
&\geq \sqrt{\frac{2D\tau_D + V^2\tau_M^2 + K\tau_D V^2\tau_M^2}{2D\tau_D V^2\tau_M^2}} \\
&> 0.
\end{aligned}$$

The only conditions left to check are that $\mathscr{D}$ and $\mathscr{L}$ are nonzero, specifically since $\mathscr{L}$ appears in the denominator of the constant A.

Proposition .3. $\mathscr{D} = 0$.

Proof. Assume by way of contradiction that $\mathscr{D} = 0$. We can rewrite $\mathscr{D}$ as a linear combination of $I_1(b\varphi)$ and $K_1(b\varphi)$:

$$0 = \mathscr{D} = \frac{1}{2}\left[\begin{array}{c} -\left(2-V^2\tau_M^2\phi_+^2\right)c\phi_-\varphi\left(\phi_+^2-\phi_-^2\right)I_1(c\phi_-)M_6\,K_0(c\varphi) \\ +\left(\begin{array}{c} \left(2-V^2\tau_M^2\phi_-^2\right)\phi_+\left(\phi_+^2-\varphi^2\right)I_0(a\phi_-) \\ -\left(2-V^2\tau_M^2\phi_+^2\right)c\phi_-^2\left(\phi_+^2-\varphi^2\right)I_0(c\phi_-)M_6 \\ -\left(2-V^2\tau_M^2\phi_+^2\right)c\phi_+\phi_-\left(\varphi^2-\phi_-^2\right)I_1(c\phi_-)M_7 \end{array}\right)K_1(c\varphi) \end{array}\right]I_1(b\varphi)$$
$$+\frac{1}{2}\left[\begin{array}{c} -\left(2-V^2\tau_M^2\phi_+^2\right)c\phi_-\varphi\left(\phi_+^2-\phi_-^2\right)I_1(c\phi_-)M_6\,I_0(c\varphi) \\ +\left(\begin{array}{c} -\left(2-V^2\tau_M^2\phi_-^2\right)\phi_+\left(\phi_+^2-\varphi^2\right)I_0(a\phi_-) \\ +\left(2-V^2\tau_M^2\phi_+^2\right)c\phi_-^2\left(\phi_+^2-\varphi^2\right)I_0(c\phi_-)M_6 \\ +\left(2-V^2\tau_M^2\phi_+^2\right)c\phi_+\phi_-\left(\varphi^2-\phi_-^2\right)I_1(c\phi_-)M_7 \end{array}\right)I_1(c\varphi) \end{array}\right]K_1(b\varphi).$$

Since $I_1(b\varphi)$ and $K_1(b\varphi)$ are linearly independent, this implies that each coefficient is zero, specifically the coefficient of $K_1(b\varphi)$, which can be rewritten as a linear combination of the set $\{I_0(c\varphi), I_1(c\varphi)\}$ so that

$$-\left(2-V^2\tau_M^2\phi_+^2\right)c\phi_-\varphi\left(\phi_+^2-\phi_-^2\right)I_1(c\phi_-)M_6\,I_0(c\varphi)$$
$$+\left(\begin{array}{c} -\left(2-V^2\tau_M^2\phi_-^2\right)\phi_+\left(\phi_+^2-\varphi^2\right)I_0(a\phi_-) \\ +\left(2-V^2\tau_M^2\phi_+^2\right)c\phi_-^2\left(\phi_+^2-\varphi^2\right)I_0(c\phi_-)M_6 \\ +\left(2-V^2\tau_M^2\phi_+^2\right)c\phi_+\phi_-\left(\varphi^2-\phi_-^2\right)I_1(c\phi_-)M_7 \end{array}\right)I_1(c\varphi) = 0.$$

We must prove a lemma before continuing.

Lemma .0.1. *$\{I_0(x), I_1(x)\}$ is linearly independent.*

Proof. Suppose that
$$A_0 I_0(x) + A_1 I_1(x) = 0$$

for some arbitrary $A_0, A_1 \in \mathbb{R}$. We use a summation identity (9.6.10) found in "Handbook of Mathematical Functions with Formulas, Graphs, and Mathematical Tables" by Milton Abramowitz and Irene Stegun [70]:

$$\begin{aligned} 0 = A_0 I_0(x) + A_1 I_1(x) &= A_0 \sum_{k=0}^{\infty} \frac{\left(\frac{1}{4}x^2\right)^k}{k!\,\Gamma(k+1)} + A_1 \left(\frac{1}{2}x\right) \sum_{k=0}^{\infty} \frac{\left(\frac{1}{4}x^2\right)^k}{k!\,\Gamma(k+2)} \\ &= \sum_{k=0}^{\infty} \frac{A_0}{2^{2k} k!\,\Gamma(k+1)} x^{2k} + \sum_{k=0}^{\infty} \frac{A_1}{2^{2k+1} k!\,\Gamma(k+2)} x^{2k+1} \\ &= \sum_{k=0}^{\infty} C_k x^k \end{aligned}$$

for constants C_k. Since the power series is linearly independent, $C_k = 0$ for every $k \in \mathbb{N} \cup \{0\}$. For $k = 0$, we see that

$$0 = C_0 = \frac{A_0}{\Gamma(1)} = A_0.$$

For $k = 1$, we observe that

$$0 = C_1 = \frac{A_1}{2\Gamma(2)} \qquad \rightarrow \qquad A_1 = 0.$$

Thus, we have shown that $\{I_0(x), I_1(x)\}$ is linearly independent. □

We now continue with the proof for the proposition. Since $\{I_0(c\varphi), I_1(c\varphi)\}$ is linearly independent, the coefficients are zero, namely,

$$-\left(2 - V^2 \tau_M^2 \phi_+^2\right) c\phi_- \varphi \left(\phi_+^2 - \phi_-^2\right) I_1(c\phi_-) M_6 = 0.$$

Because the terms $c\phi_-$, $c\phi_+$, and $a\phi_+$ are all strictly positive, we see that

$$I_1(c\phi_-) > 0 \qquad \text{and} \qquad M_6 = I_1(c\phi_+) K_0(a\phi_+) + I_0(a\phi_+) K_1(c\phi_+) > 0.$$

Because $c\phi_{-}\varphi\left(\phi_{+}^{2}-\phi_{-}^{2}\right)>0$, this leaves us with the following:

$$2-V^{2}\tau_{M}^{2}\phi_{+}^{2}=0$$

$$\frac{2D\tau_{D}-V^{2}\tau_{M}^{2}-K\tau_{D}V^{2}\tau_{M}^{2}-\sqrt{\begin{array}{c}V^{2}\tau_{M}^{2}\left(4D\tau_{D}+V^{2}\tau_{M}^{2}+2K\tau_{D}V^{2}\tau_{M}^{2}\right)\\+\tau_{D}^{2}\left(2D-KV^{2}\tau_{M}^{2}\right)^{2}\end{array}}}{2D\tau_{D}}=0$$

$$\left(2D\tau_{D}-V^{2}\tau_{M}^{2}-K\tau_{D}V^{2}\tau_{M}^{2}\right)^{2}=\left(\begin{array}{c}V^{2}\tau_{M}^{2}\left(4D\tau_{D}+V^{2}\tau_{M}^{2}+2K\tau_{D}V^{2}\tau_{M}^{2}\right)\\+\tau_{D}^{2}\left(2D-KV^{2}\tau_{M}^{2}\right)^{2}\end{array}\right)$$

$$-8D\tau_{D}V^{2}\tau_{M}^{2}=0.$$

However, this contradicts the fact that each parameter is strictly positive. Therefore, we have proven $\mathscr{D}\neq 0$. □

Proposition .4. $\mathscr{L}\neq 0$.

Proof. Assume by way of contradiction that $\mathscr{L}=0$. We see that $\mathscr{L}$ is a linear combination of the set $\left\{I_{0}\left(\frac{a\sqrt{2}}{V\tau_{M}}\right),I_{1}\left(\frac{a\sqrt{2}}{V\tau_{M}}\right)\right\}$. As shown in Lemma .0.1, each coefficient must equal 0, specifically

$$\begin{pmatrix}\phi_{-}\left(\phi_{+}^{2}-\varphi^{2}\right)M_{6}N_{7}K_{1}(c\varphi)\\+\phi_{+}\left(\varphi^{2}-\phi_{-}^{2}\right)M_{7}N_{6}K_{1}(c\varphi)\\+\varphi\left(\phi_{+}^{2}-\phi_{-}^{2}\right)M_{6}N_{6}K_{0}(c\varphi)\end{pmatrix}I_{1}(b\varphi)+\begin{pmatrix}-\left(\phi_{-}\left(\phi_{+}^{2}-\varphi^{2}\right)M_{6}N_{7}+\phi_{+}\left(\varphi^{2}-\phi_{-}^{2}\right)M_{7}N_{6}\right)I_{1}(c\varphi)\\+\varphi\left(\phi_{+}^{2}-\phi_{-}^{2}\right)M_{6}N_{6}I_{0}(c\varphi)\end{pmatrix}K_{1}(b\varphi)=0 \tag{14}$$

and

$$ca\phi_+\phi_-\left(\phi_+^2-\phi_-^2\right)\begin{pmatrix}\phi_-\left(\phi_+^2-\varphi^2\right)L_3M_6N_7\\ +\phi_+\left(\varphi^2-\phi_-^2\right)L_3M_7N_6\\ +\varphi\left(\phi_+^2-\phi_-^2\right)L_4M_6N_6\end{pmatrix}\frac{V\tau_M}{\sqrt{2}}=0.$$

Since $\{I_1(b\varphi),K_1(b\varphi)\}$ is linearly independent, once again, each coefficient is 0, specifically the coefficient of $K_1(b\varphi)$ in Equation 14:

$$\begin{pmatrix}-\left(\phi_-\left(\phi_+^2-\varphi^2\right)M_6N_7+\phi_+\left(\varphi^2-\phi_-^2\right)M_7N_6\right)I_1(c\varphi)\\ +\varphi\left(\phi_+^2-\phi_-^2\right)M_6N_6I_0(c\varphi)\end{pmatrix}=0.$$

Since this is another linear combination of two modified Bessel functions of the first kind $I_0(c\varphi)$ and $I_1(c\varphi)$, each coefficient must be zero so that

$$\varphi\left(\phi_+^2-\phi_-^2\right)M_6N_6=0.$$

However, each of these terms is strictly positive, causing a contradiction. Therefore, we have proven that $\mathscr{L}=0$. □

Hence, we have proven that all terms in the denominator of the solutions are nonzero.

Vita

Ryan Neil Campbell was born in Columbia, South Carolina, and raised by his parents, Billy and Lisa Campbell, alongside his brother, Jonathan. He graduated from Chapin High School in 2008. In 2012, he earned a Bachelor of Arts in Spanish and a Bachelor of Science in Mathematics with a concentration in Pure Mathematics from Wofford College. As an undergraduate, his interest in mathematics deepened through a research project modeling a variation of the Tower of Hanoi graphs, including formulas describing vertices, edges, and degree of vertices.

He pursued graduate study at the University of Tennessee, Knoxville, receiving the Master of Science in Mathematics in 2015 with the thesis titled *Injective Modules and Divisible Groups*. Following completing of the graduate degree, he remained in the Knoxville area and taught mathematics at Roane State Community College for five years. In 2020, after renewed interest in differential equations, he returned to the University of Tennessee as a full-time graduate student.

During this period, Ryan built a strong community at his church where he met his wife, Jackie. They married while he was in graduate school and had their first child, a daughter named Hazel.

In the final years of his graduate program, he held a research assistantship sponsored by Oak Ridge National Laboratory and the Department of Veteran Affairs. He completed his graduate work in spring 2026.